TESIS DE LA UNIVERSIDAD DE ZARAGOZA

2024 419

David Campillo Pérez

Study of the Reactivity of Organometallic Platinum and Palladium Complexes with Basic Properties Towards Electrophilic Species
ANEXO

Director/es
Martín Tello, Antonio Jesús

ISSN 2254-7606

Prensas de la Universidad Universidad Zaragoza

Universidad de Zaragoza
Servicio de Publicaciones

ISSN 2254-7606

Universidad Zaragoza
1542

Tesis Doctoral

STUDY OF THE REACTIVITY OF ORGANOMETALLIC PLATINUM AND PALLADIUM COMPLEXES WITH BASIC PROPERTIES TOWARDS ELECTROPHILIC SPECIES
ANEXO

Autor

David Campillo Pérez

Director/es

Martín Tello, Antonio Jesús

UNIVERSIDAD DE ZARAGOZA
Escuela de Doctorado

Programa de Doctorado en Química Inorgánica

2022

Supporting Information

Doctoral Thesis

Study of the Reactivity of Organometallic Platinum and Palladium Complexes with Basic Properties Towards Electrophilic Species

David Campillo Pérez

2022

Supporting Information

for

Chapter 1. Organometallic complexes with M-M' bonds as intermediates for bimetallic catalysis.

1. Crystal data and structural refinement

Crystal data and other details of the structure analyses are presented in Tables S1.1 and S1.2. Suitable crystals for X-Ray diffraction studies were obtained by slow diffusion of *n*-hexane into concentrated solutions of the complexes in 3 mL of CH_2Cl_2, $CHCl_3$ or acetone. Crystals were mounted at the end of a quartz fibre. The radiation used in all cases was graphite monochromated Mo-K_α (λ = 71.073 pm). X-Ray intensity data were collected on an Oxford Diffraction Xcalibur diffractometer. The diffraction frames were integrated and corrected from absorption by using the CrysAlis RED program.[1] The structures were solved by Patterson and Fourier methods and refined by full-matrix least squares on F^2 with SHELXL.[2] All atoms were assigned anisotropic displacement parameters and refined without positional constraints. The positions of the H atoms were constrained to idealized geometries and assigned isotropic displacement parameters equal to 1.2 or 1.5 times the U_{iso} values of their respective parent atoms. Full-matrix least-squares refinement of the models against F^2 converged to final residual indices given in Tables S1.1 and S1.2.

X-Ray structure determination of complex [Ag(PPh$_3$)$_2$](ClO$_4$) (AgP2). Figure S1.1 shows the structure of **AgP2**, and the caption lists the relevant structural parameters. Crystal data and other details of the structure analyses are presented in Table S1.1. Colourless suitable crystals for X-Ray diffraction studies were obtained by slow diffusion of *n*-hexane into concentrated solutions of **10*** in 3 mL of CH_2Cl_2. A crystal was mounted at the end of a quartz fibre. The radiation used in was graphite monochromated $Mo_{K\alpha}$ (λ = 0.71073 Å). X-Ray intensity data were collected on an Oxford Diffraction Xcalibur diffractometer. The diffraction frames were integrated and corrected from absorption by using the CrysAlis RED program.[1] The structures was solved by Patterson and Fourier methods and refined by full-matrix least squares on F^2 with SHELXL-97.[2] All non-hydrogen atoms were assigned anisotropic displacement parameters and refined without positional constraints, except as noted below. All hydrogen atoms were constrained to idealized geometries and assigned isotropic displacement parameters equal to 1.2 times the U_{iso} values of their attached parent atoms. Full-matrix least-squares refinement of this models against F^2 converged to final residual indices given in Table S1.1.

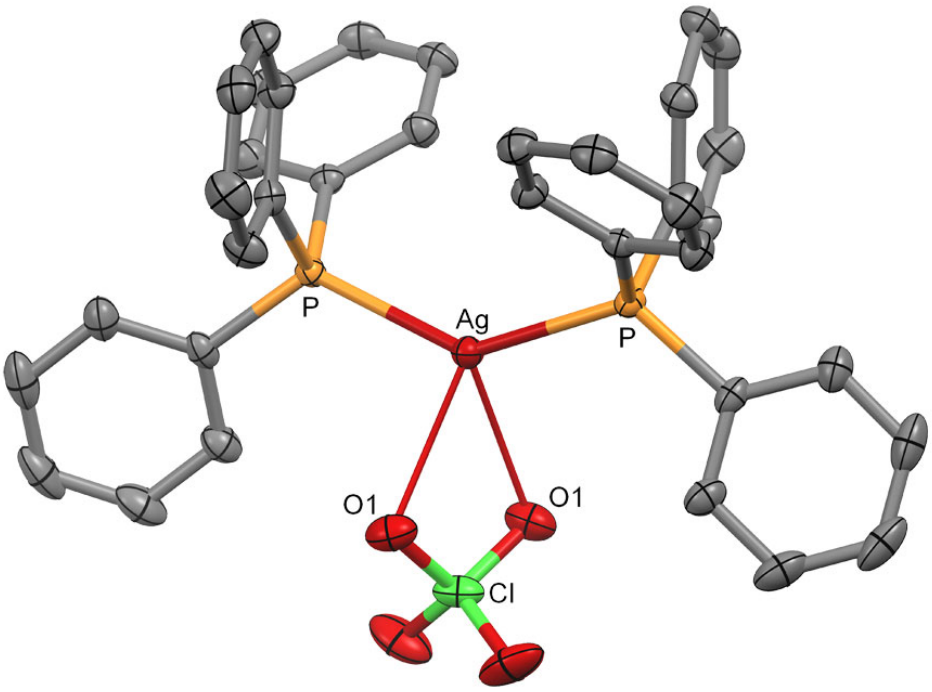

Figure S1.1. Crystal structure of the complex $[Ag(PPh_3)_2](ClO_4)$ (**AgP2**). Relevant bond distances (Å), angles (º): Ag–P 2.4054(4), Ag–O(1) 2.5987(13). P'–Ag–P 137.783(19), P'–Ag–O(1') 122.14(3), P–Ag–O(1') 96.36(3), O(1)–Ag–O(1') 53.67(5). Symmetry transformations used to generate equivalent atoms: –x+1/2, y, –z+1.

Table S1.1. Crystal data and structure refinement for complexes [(CNC)(PPh_3)PtAu(PPh_3)](ClO_4) (**4**), [{Pt(CNC)(PPh_3)}$_2$Au](ClO_4)·0.5Me_2CO·0.5*n*-C_6H_{14} (**6**·0.5Me_2CO·0.5*n*-C_6H_{14}), [{Pt(CNC)(PPh_3)}$_2$Ag](ClO_4)·3$CHCl_3$ (**8**·3$CHCl_3$), and [Ag(PPh_3)$_2$](ClO_4) (**AgP2**).

	4	**6**·0.5Me_2CO·0.5*n*-C_6H_{14}	**8**·3$CHCl_3$	**AgP2**
Formula	$C_{53}H_{41}AuClNO_4P_2Pt$	$C_{70}H_{52}AuClN_2O_4P_2Pt$ ·0.5Me_2CO·0.5*n*-C_6H_{14}	$C_{70}H_{52}AgClN_2O_4P_2Pt$ ·3$CHCl_3$	$C_{36}H_{30}AgClO_4P_2$
M_t	1245.31	1741.80	1938.68	731.86
Crystal system	orthorhombic	triclinic	monoclinic	monoclinic
Space group	*Pna*2$_1$	*P*-1	*P2$_1$*/c	*I*2/*a*
a/Å	16.6765(2)	14.1516(2)	23.6417(3)	14.9083(3)
b/Å	13.1713(1)	14.2469(2)	18.9314(2)	9.5290(2)
c/Å	20.8357(2)	17.2010(2)	15.7338(2)	22.6955(5)
a/º	90	88.413(1)	90	90
β/º	90	83.236(1)	92.558(1)	100.688(2)
γ/º	90	71.894(1)	90	90
V/Å^3	4576.59(8)	3273.19(8)	7034.94(14)	3168.22(11)
Z	4	2	4	4
D_c/g cm^{-3}	1.807	1.767	1.830	1.534
T/K	100(1)	100(1)	80(1)	100(1)
μ/mm^{-1}	6.431	6.641	4.719	0.861

$F(000)$	2408	1682	3768	1488
2θ range/^{o}	8.8-57.6	8.4-59.6	8.4-59.6	6.6-58.7
Collected reflections	26496	70706	87001	17872
Unique reflections	10324	17073	18492	3931
R_{int}	0.0249	0.0281	0.0312	0.0332
R_1, wR_2[a] ($I > 2\sigma(I)$)	0.0191, 0.0415	0.0242, 0.0541	0.0289, 0.0606	0.0240, 0.0559
R_1, wR_2[a] (all data)	0.0202, 0.0420	0.0297, 0.0565	0.0373, 0.0641	0.0278, 0.0574
GOF (F^2)[b]	1.060	1.062	1.085	1.037
Abs. struct. par.	-0.006(3)	-	-	-

[a] $R_1 = \sum(|F_o| - |F_c|) / \sum |F_o|$. $wR_2 = [\sum w (F_o^2 - F_c^2)^2 / \sum w(F_o^2)^2]^{1/2}$. [b] Goodness-of-fit = $[\sum w (F_o^2 - F_c^2)^2 / (n_{obs} - n_{param})]^{1/2}$.

Table S1.2. Crystal data and structure refinement for complexes [Pd(CNC)(PPh_3)] (**2**), [Pd(CNC-H)Cl(PPh_3)] (**3**·1.5CH_2Cl_2), [(CNC)(PPh_3)PdAu(PPh_3)](ClO_4) (**5**·3CH_2Cl_2), [{Pd(CNC)(PPh_3)}$_2$Au](ClO_4)·1.9CH_2Cl_2 (**7**·1.9CH_2Cl_2), [{Pd(CNC)(PPh_3)}$_2$Ag](ClO_4) (**9**·CH_2Cl_2).

	2	**3**·1.5CH_2Cl_2	**5**·3CH_2Cl_2	**7**·1.9CH_2Cl_2	**9**·CH_2Cl_2
Formula	$C_{35}H_{26}NPPd$	$C_{35}H_{27}ClNPPd$ ·1.5CH_2Cl_2	$C_{56}H_{47}AuCl_7NO_4P_2Pd$ ·3CH_2Cl_2	$C_{70}H_{52}AuClN_2O_4P_2Pd_2$ ·1.9CH_2Cl_2	$C_{70}H_{52}AgClN_2O4P_2Pd_2$ ·CH_2Cl_2
M_t	597.94	761.78	1411.40	1653.65	1488.12
Crystal system	monoclinic	monoclinic	monoclinic	monoclinic	triclinic
Space group	*P2$_1$/c*	*I2/a*	*P2$_1$/n*	*I2/a*	*P-1*
a/Å	13.96167(2)	22.1187(3)	17.21447(2)	17.5256(3)	14.0983(3)
b/Å	9.43318(1)	12.02149(1)	16.3255(2)	16.9649(2)	14.6782(3)
c/Å	20.5922(2)	25.0247(3)	20.2005(2)	23.6574(4)	16.5030(3)
a/º	90	90	90	90	64.1658(2)
β/º	95.6222(1)	104.3641(1)	100.7889(1)	99.3584(2)	89.3190(1)
γ/º	90	90	90	90	74.0900(5)
V/Å^3	2699.01(6)	6446.02(1)	5576.68(1)	6940.23(2)	2933.14(1)
Z	4	8	4	4	2
D_c/g cm^{-3}	1.472	1.570	1.681	1.583	1.685
T/K	100(2)	100(2)	150(2)	100(2)	100(2)
μ/mm^{-1}	0.772	0.985	3.389	2.900	1.183
F(000)	1216	3080	2784	3263	1492

2θ range/^{o}	6.7-60.5	6.7-64.9	6.5-58.8	4.7-56.7	6.5-58.9
Collected reflections	34864	53190	61933	68049	64746
Unique reflections	7401	10987	13616	15159	14514
R_{int}	0.0313	0.0203	0.0346	0.0458	0.0304
R_1, wR_2[a] ($I > 2\sigma(I)$)	0.0244, 0.0613	0.0372, 0.1074	0.0308, 0.0691	0.0425, 0.1061	0.0303, 0.0707
R_1, wR_2[a] (all data)	0.0281, 0.0638	0.0396, 0.1093	0.0385, 0.0728	0.0600, 0.1156	0.0367, 0.0743
GOF (F^2)[b]	1.029	1.012	1.019	1.055	1.034

[a] $R_1 = \sum(|F_o| - |F_c|) / \sum |F_o|$. $wR_2 = [\sum w (F_o^2 - F_c^2)^2 / \sum w(F_o^2)^2]^{1/2}$. [b] Goodness-of-fit = $[\sum w (F_o^2 - F_c^2)^2 / (n_{obs} - n_{param})]^{1/2}$.

2. IR, NMR and MS spectra of complexes

2.1. Spectra of complex [Pd(CNC)(PPh$_3$)] (2).

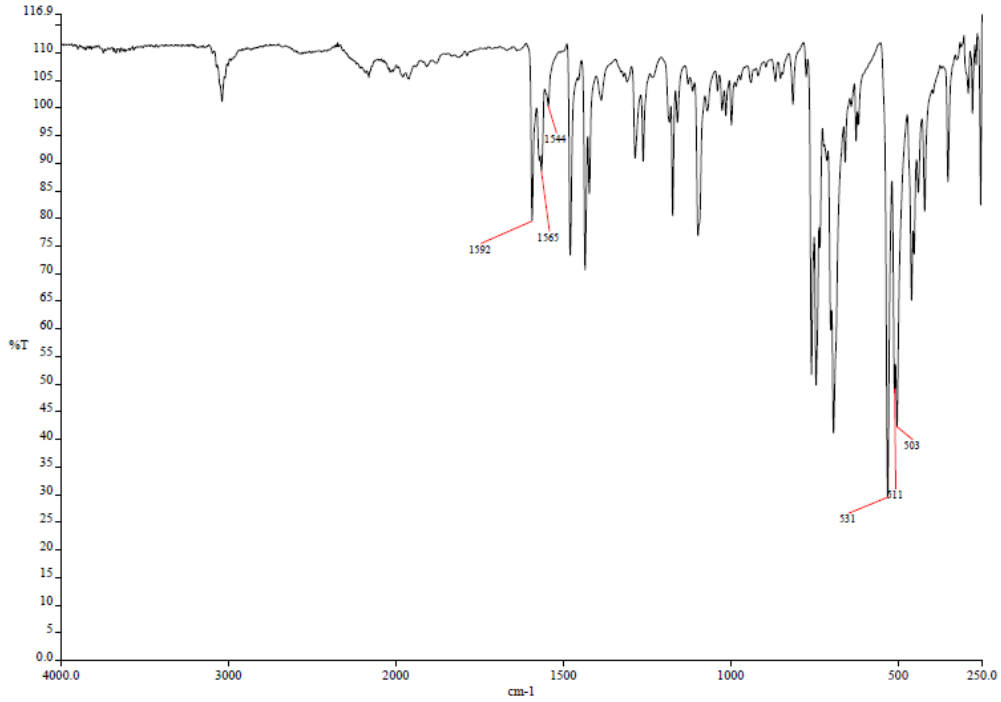

Figure S1.2. IR spectrum (CD_2Cl_2, RT) of complex [Pd(CNC)(PPh$_3$)] (**2**).

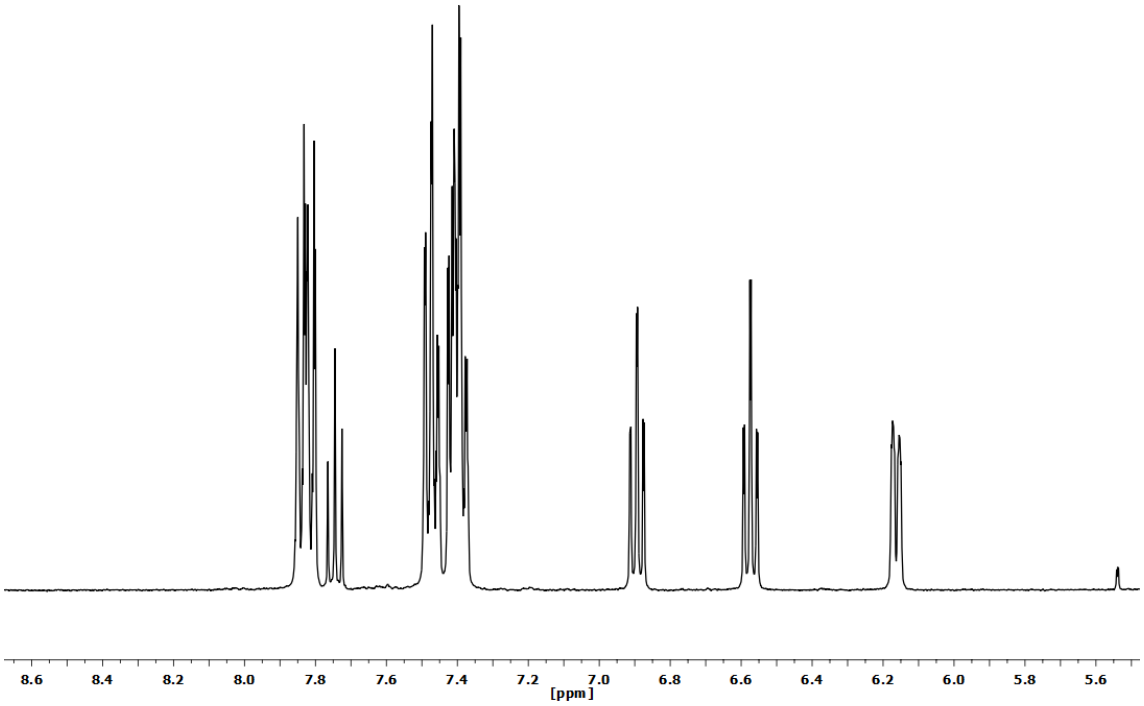

Figure S1.3. ^{1}H NMR spectrum (CD_2Cl_2, RT) of complex [Pd(CNC)(PPh_3)] (**2**).

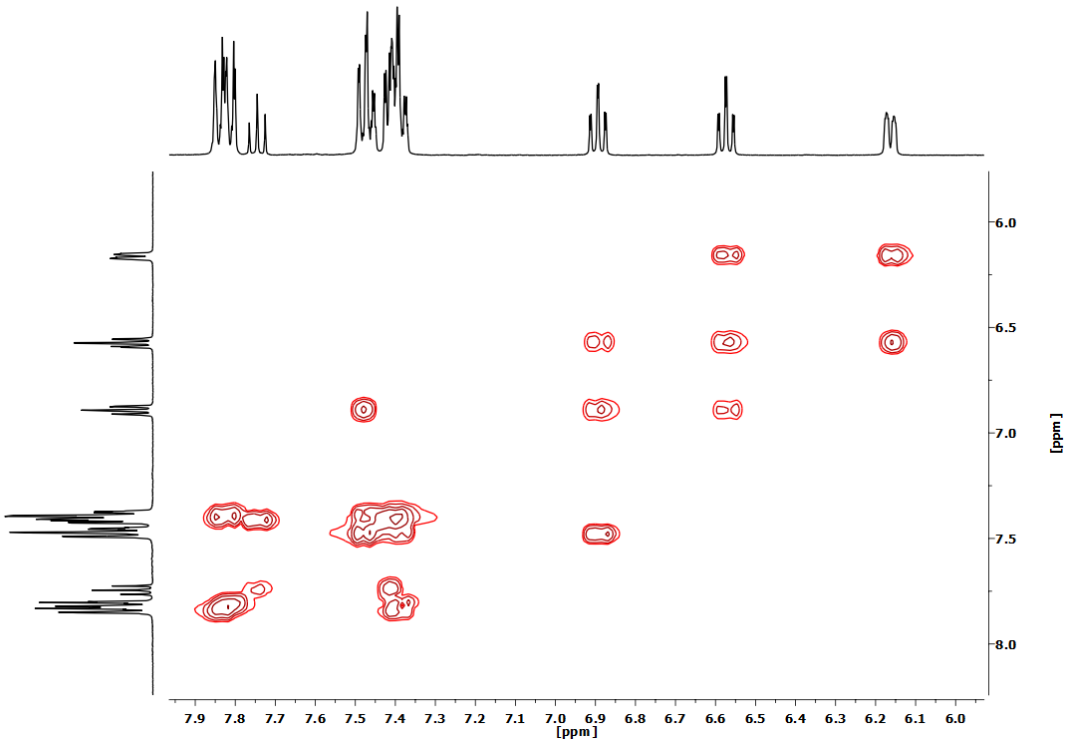

Figure S1.4. ^{1}H-^{1}H COSY NMR spectrum (CD_2Cl_2, RT) of complex [Pd(CNC)(PPh_3)] (**2**).

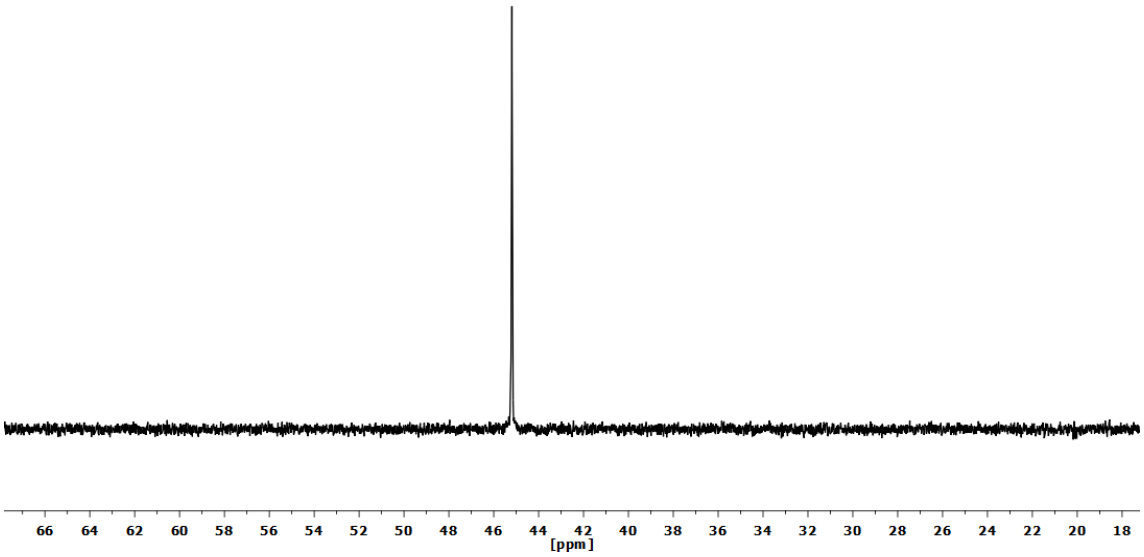

Figure S1.5. $^{31}P\{^{1}H\}$ NMR spectrum (CD_2Cl_2, RT) of complex [Pd(CNC)(PPh_3)] (**2**).

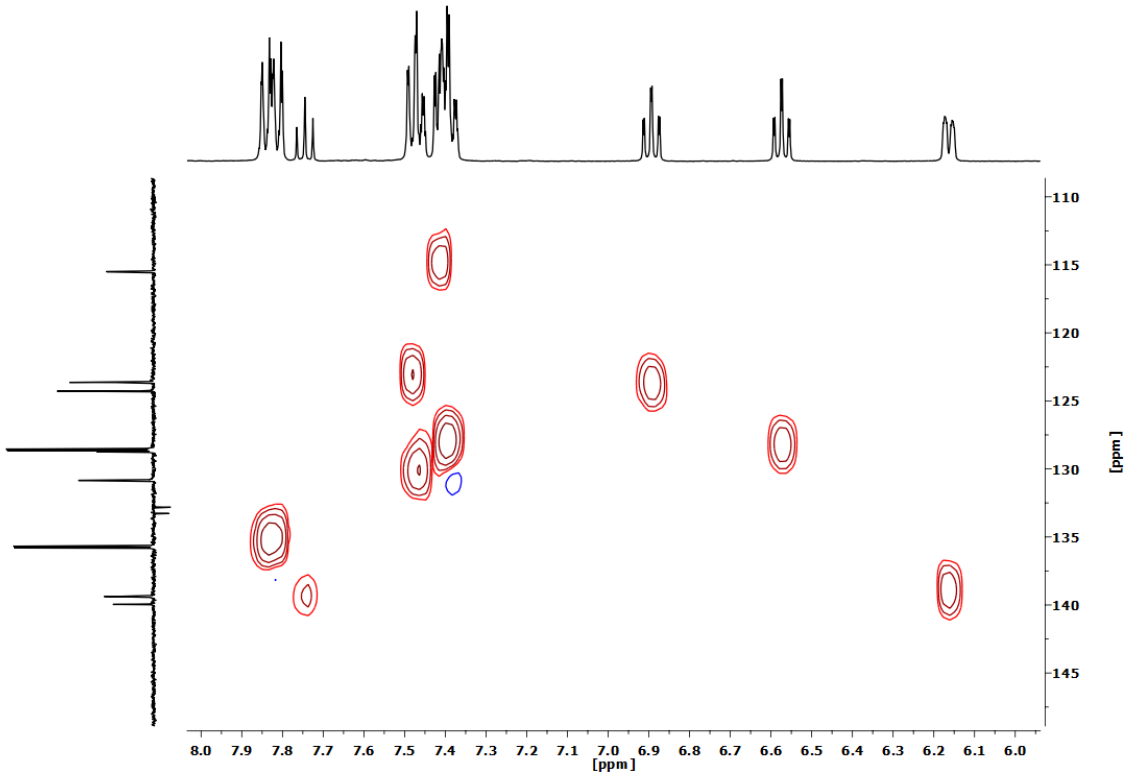

Figure S1.6. ^{1}H-^{13}C HSQC NMR (CD_2Cl_2, RT) spectrum of complex [Pd(CNC)(PPh_3)] (**2**).

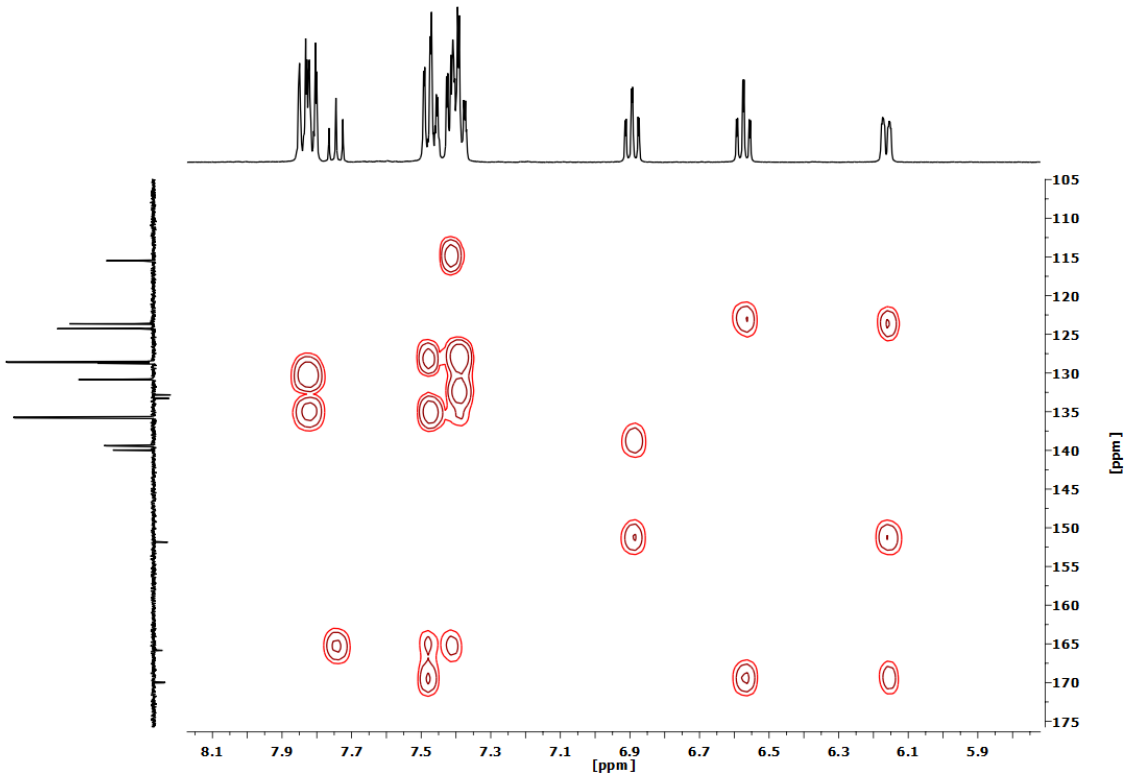

Figure S1.7. ^{1}H-^{13}C HMBC NMR spectrum (CD_2Cl_2, RT) of complex [Pd(CNC)(PPh_3)] (**2**).

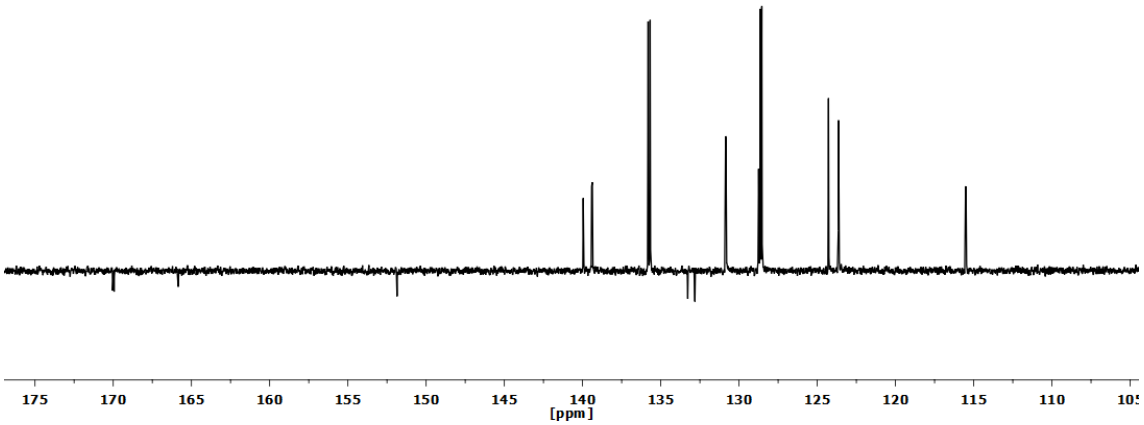

Figure S1.8. APT $^{13}C\{^{1}H\}$ NMR spectrum (CD_2Cl_2, RT) of complex [Pd(CNC)(PPh_3)] (**2**).

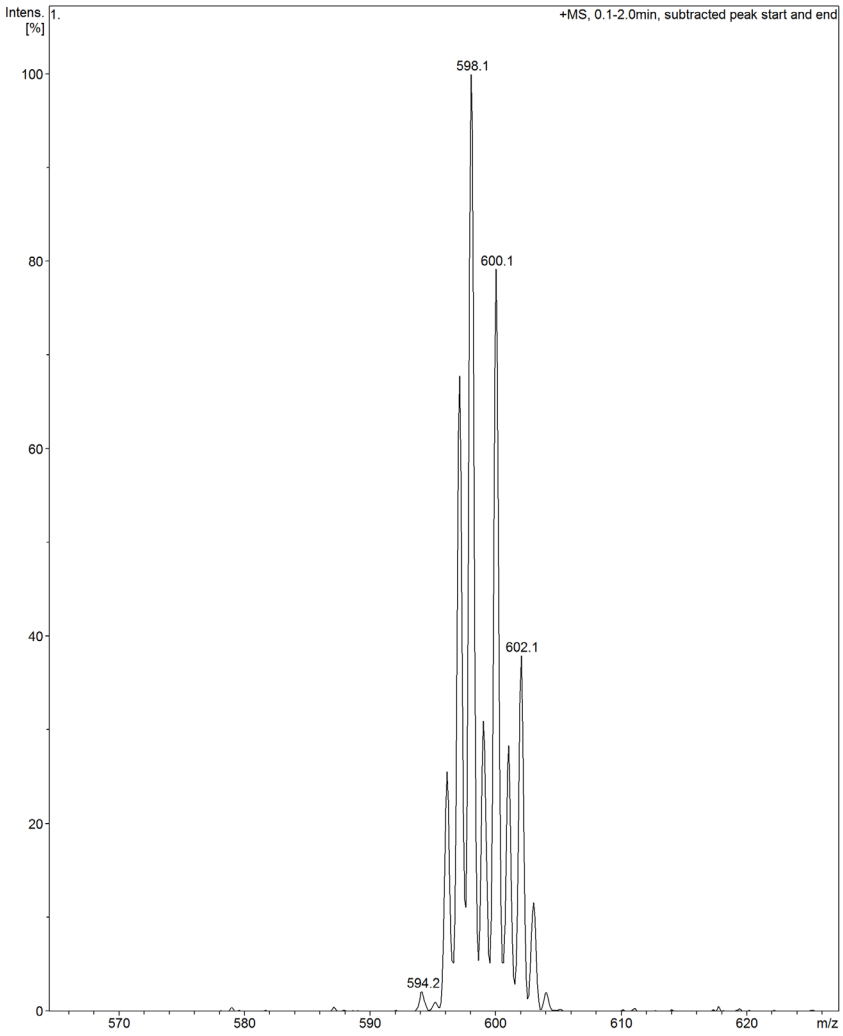

Figure S1.9. MS (MALDI+ DCTB) molecular peak of complex [Pd(CNC)(PPh_3)] (**2**).

2.2. Spectra of complex [Pd(CNC-H)Cl(PPh$_3$)] (3).

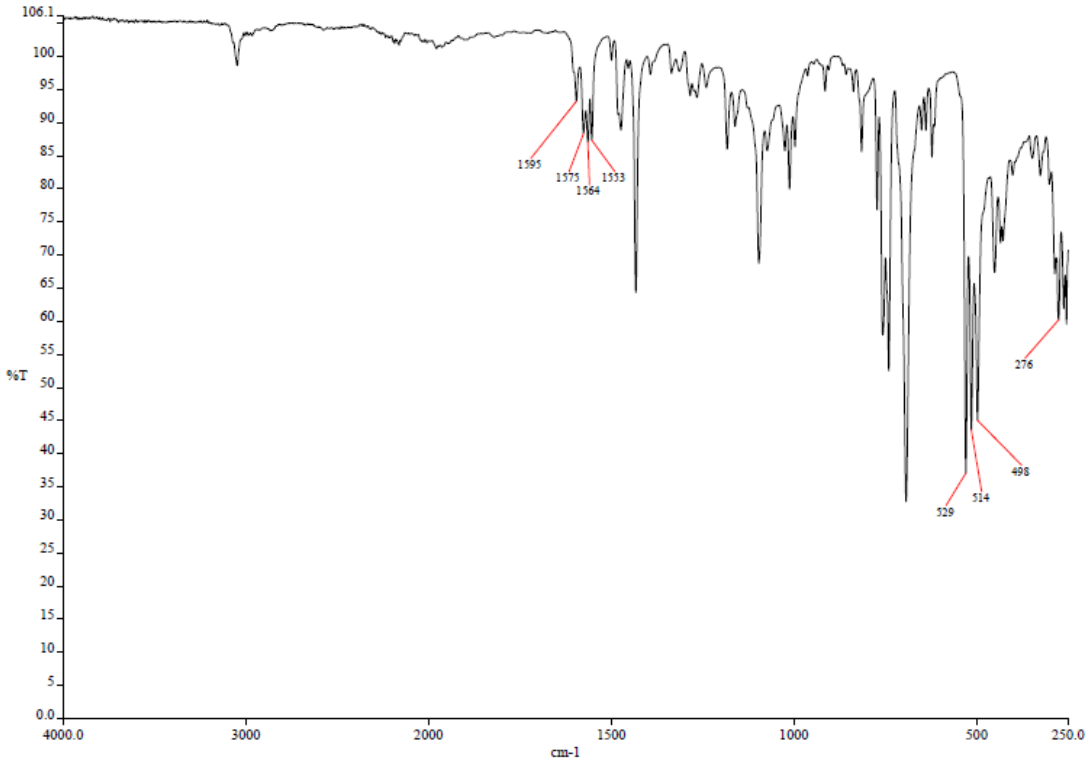

Figure S1.10. IR spectrum of complex [Pd(CNC-H)Cl(PPh$_3$)] (**3**).

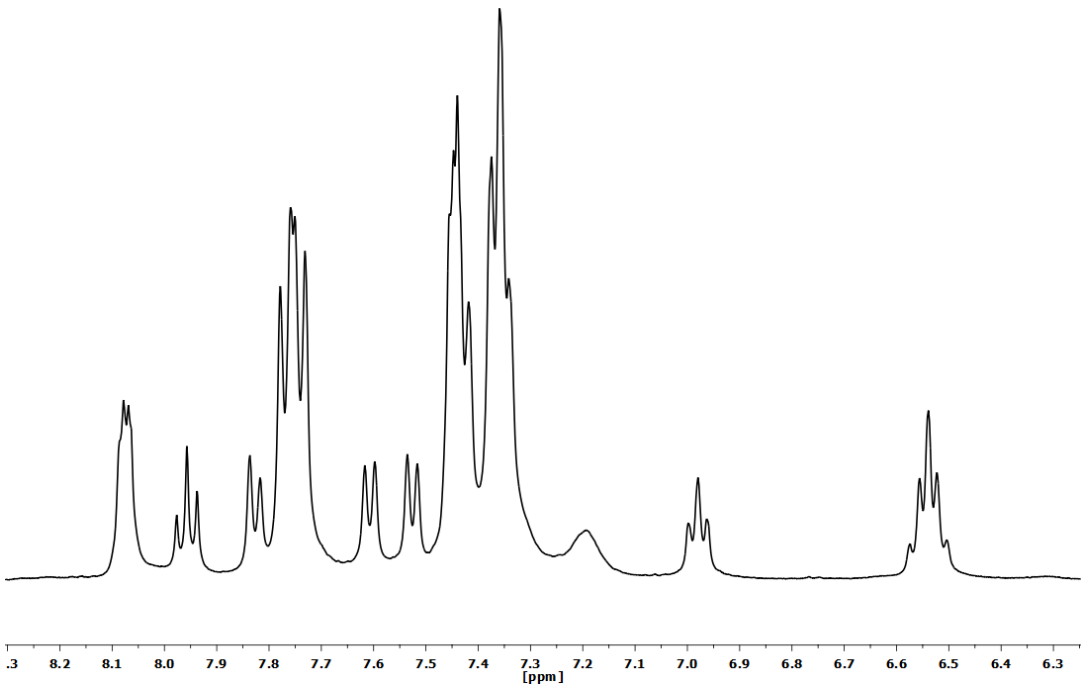

Figure S1.11. ^{1}H NMR spectrum (CD_2Cl_2, RT) of complex [Pd(CNC-H)Cl(PPh$_3$)] (**3**).

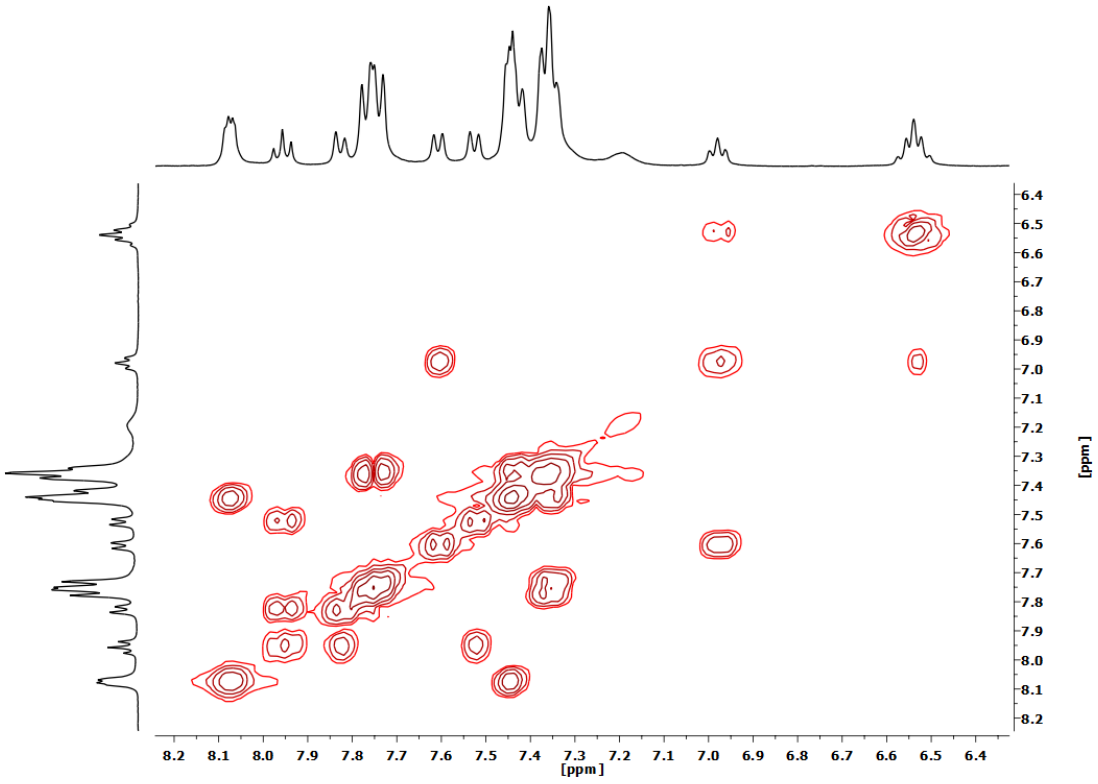

Figure S1.12. ^{1}H-^{1}H COSY NMR spectrum (CD_2Cl_2, RT) of complex [Pd(CNC-H)Cl(PPh_3)] (**3**).

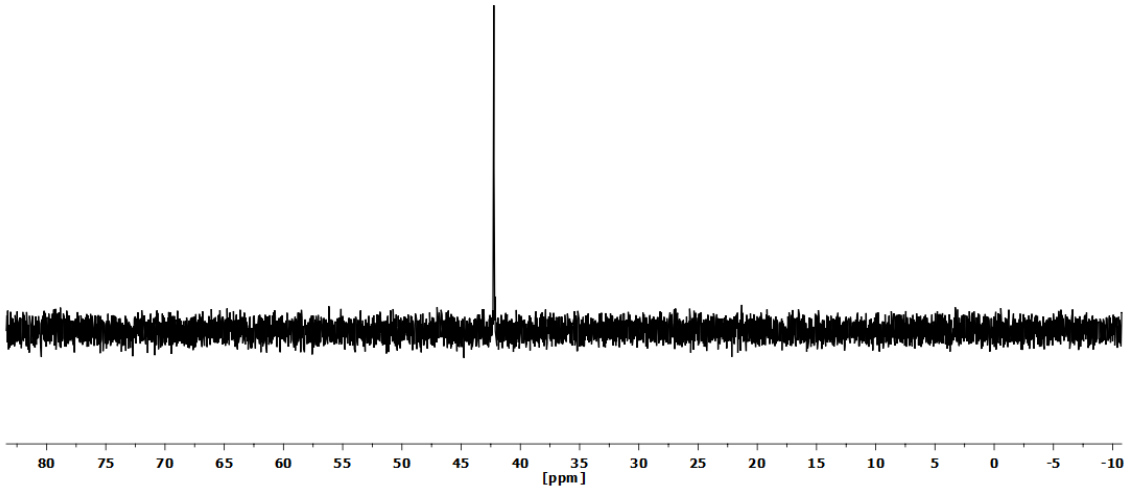

Figure S1.13. $^{31}P\{^{1}H\}$ NMR spectrum (CD_2Cl_2, RT) of complex [Pd(CNC-H)Cl(PPh_3)] (**3**).

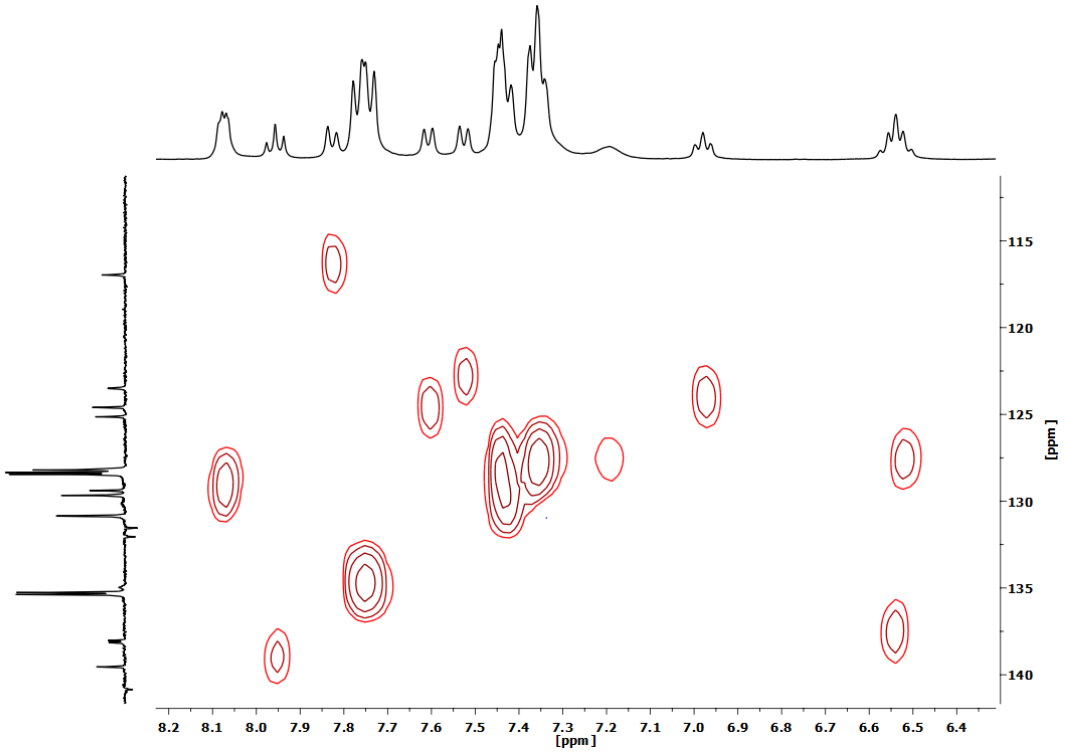

Figure S1.14. ^{1}H-^{13}C HSQC NMR spectrum (CD_2Cl_2, RT) of complex [Pd(CNC-H)Cl(PPh_3)] (**3**).

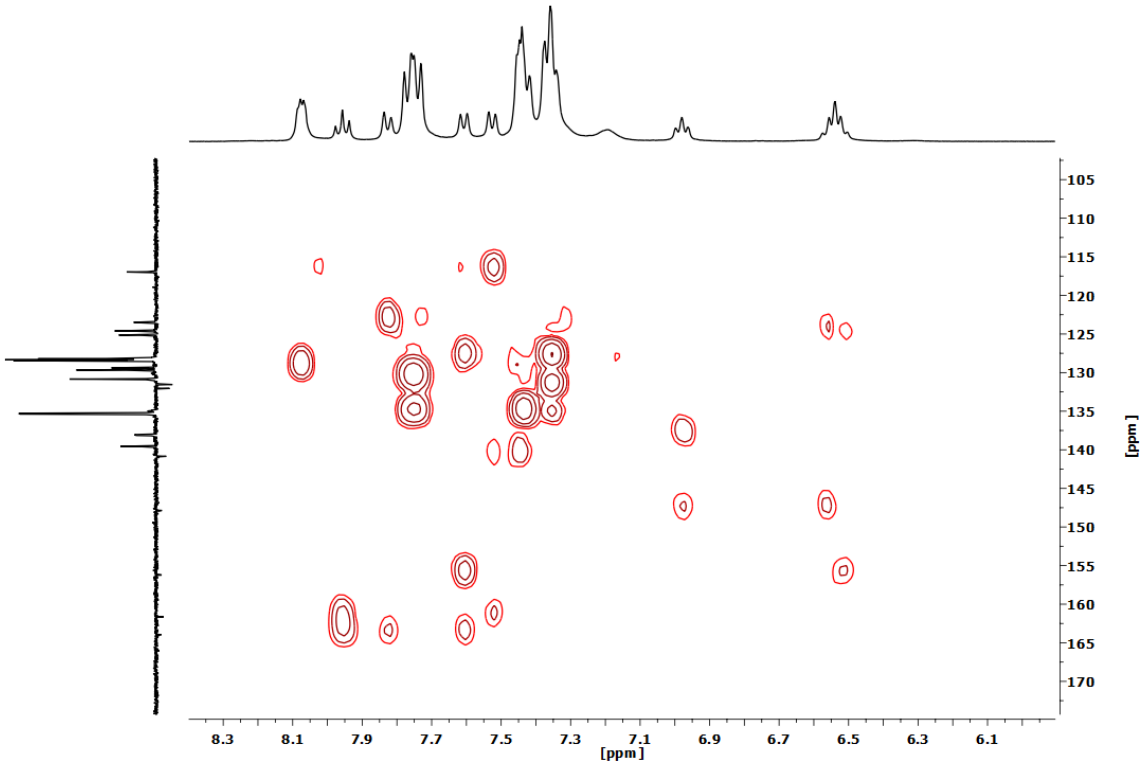

Figure S1.15. ^{1}H-^{13}C HMBC NMR spectrum (CD_2Cl_2, RT) of complex [Pd(CNC-H)Cl(PPh_3)] (**3**).

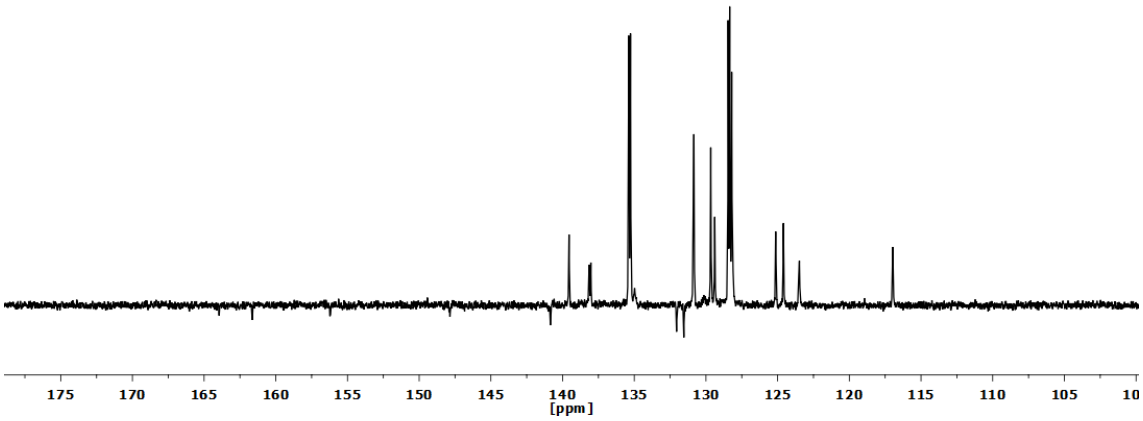

Figure S1.16. APT $^{13}C\{^{1}H\}$ NMR spectrum (CD_2Cl_2, RT) of complex [Pd(CNC-H)Cl(PPh_3)] (**3**).

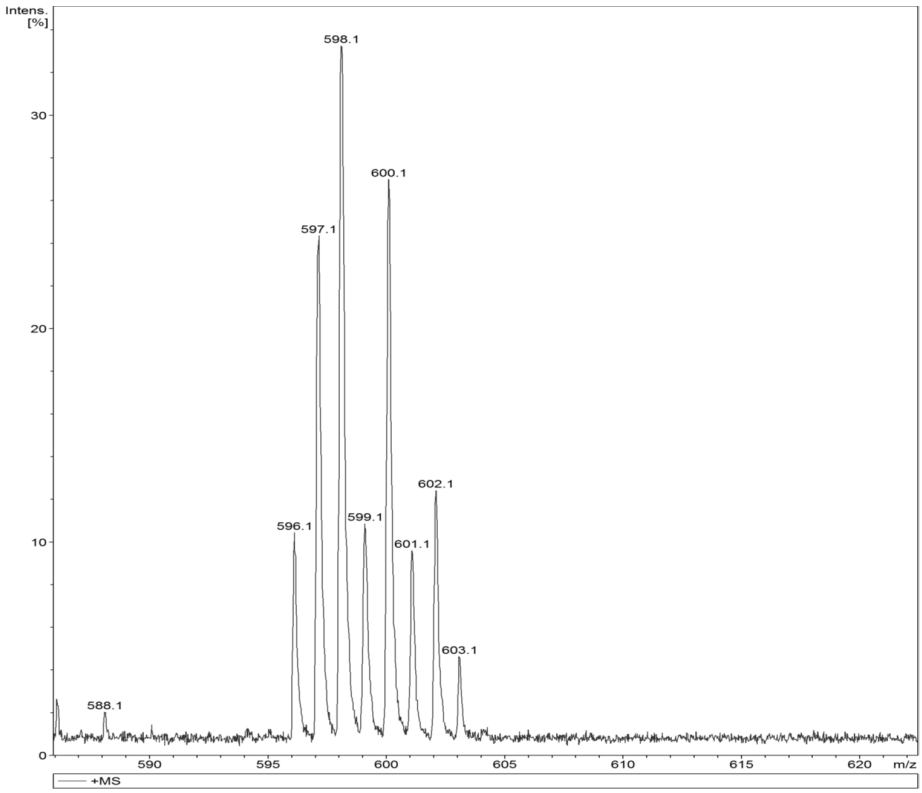

Figure S1.17. MS (MALDI+ DCTB) molecular peak of complex [Pd(CNC-H)Cl(PPh_3)] (**3**).

2.3. Spectra of complex [(CNC)(PPh$_3$)PtAu(PPh$_3$)](ClO$_4$) (4).

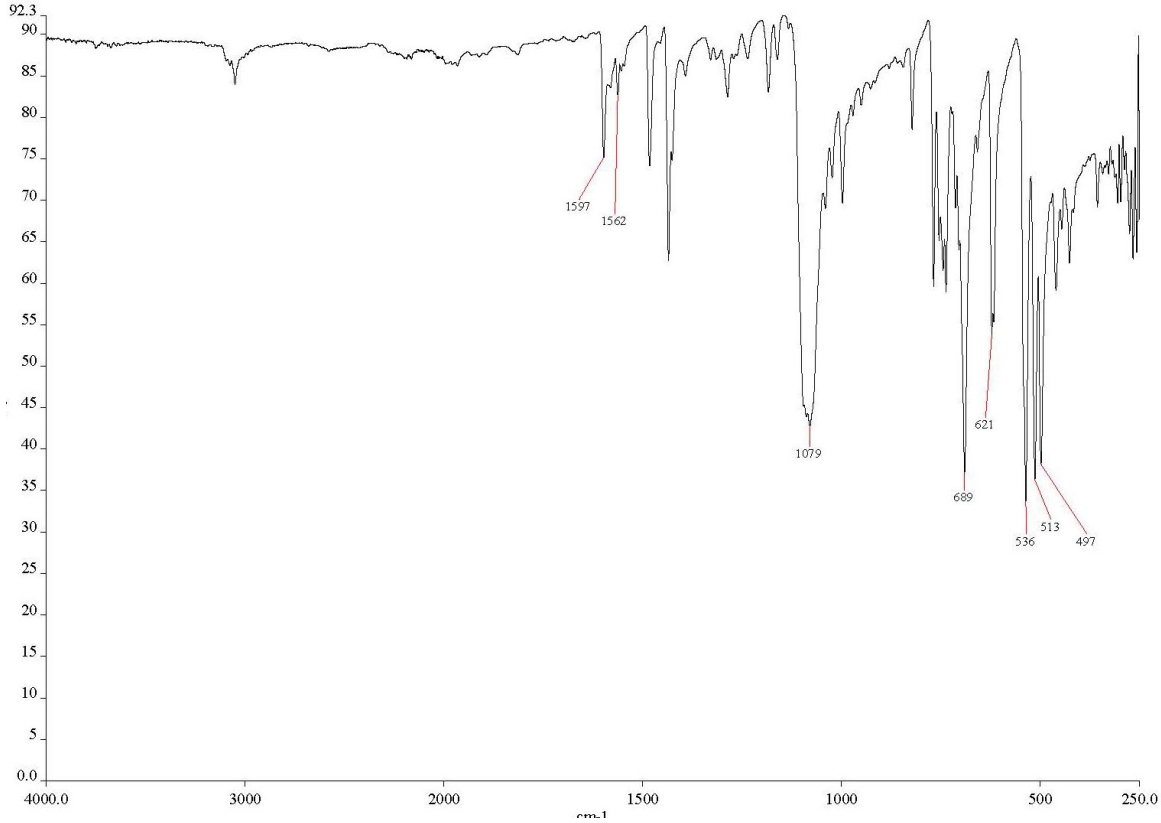

Figure S1.18. IR spectrum of complex [(CNC)(PPh$_3$)PtAu(PPh$_3$)](ClO$_4$) (**4**).

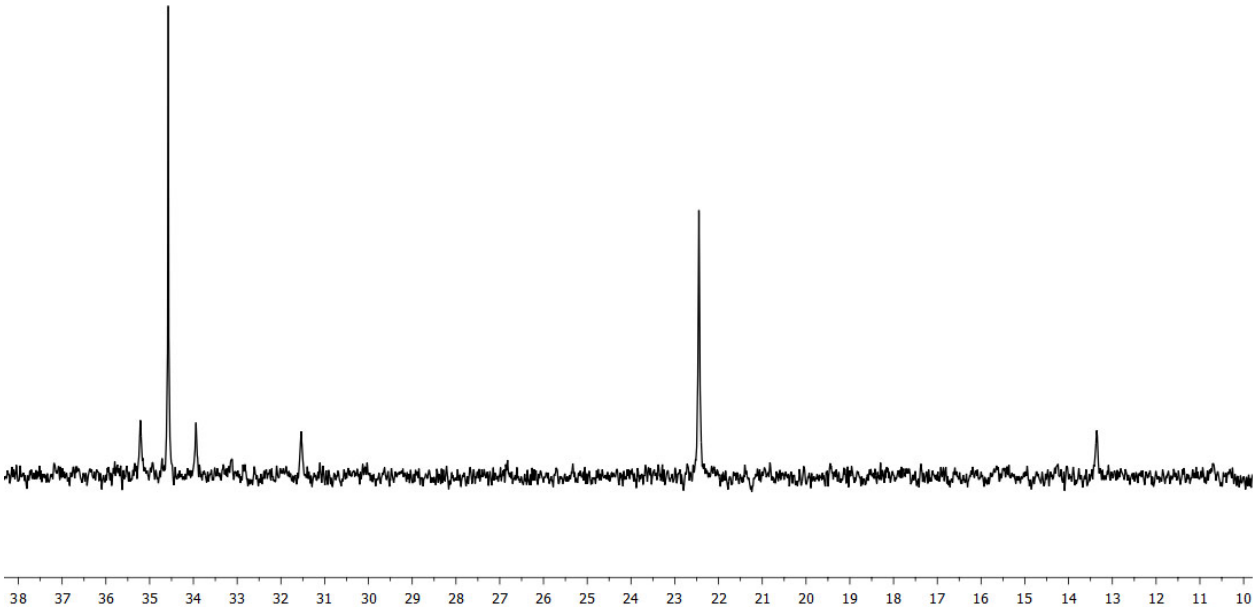

Figure S1.19. $^{31}P\{^{1}H\}$ NMR spectrum (CD_2Cl_2, RT) of complex [(CNC)(PPh$_3$)PtAu(PPh$_3$)](ClO$_4$) (**4**).

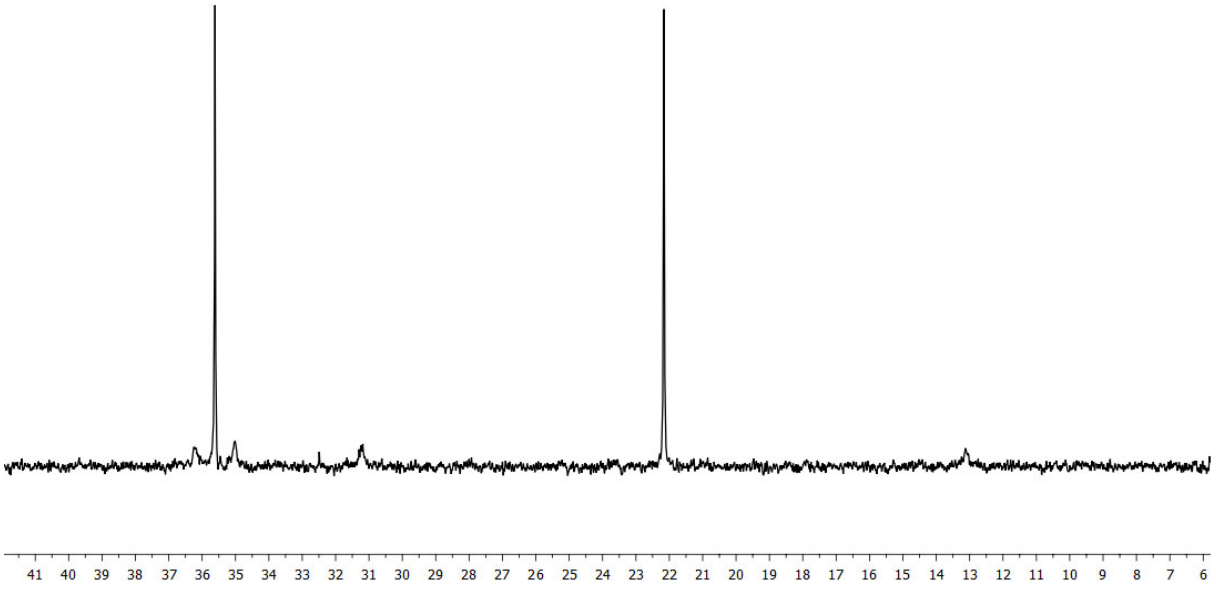

Figure S1.20. $^{31}P\{^{1}H\}$ NMR spectrum (CD_2Cl_2, 193K) of complex [(CNC)(PPh_3)PtAu(PPh_3)](ClO_4) (**4**).

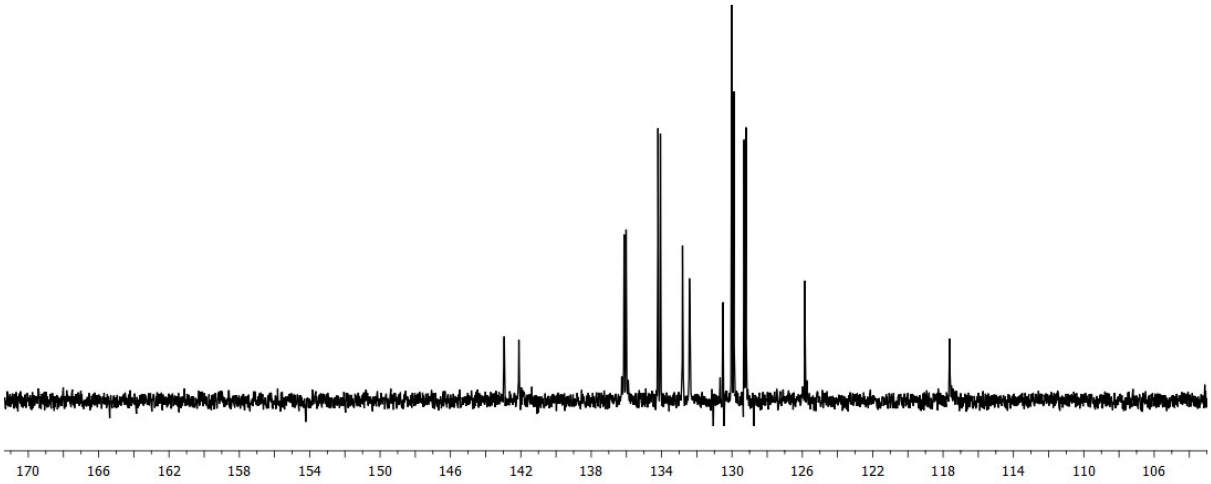

Figure S1.21. APT $^{13}C\{^{1}H\}$ NMR spectrum (CD_2Cl_2, 293K) of complex [(CNC)(PPh_3)PtAu(PPh_3)](ClO_4) (**4**).

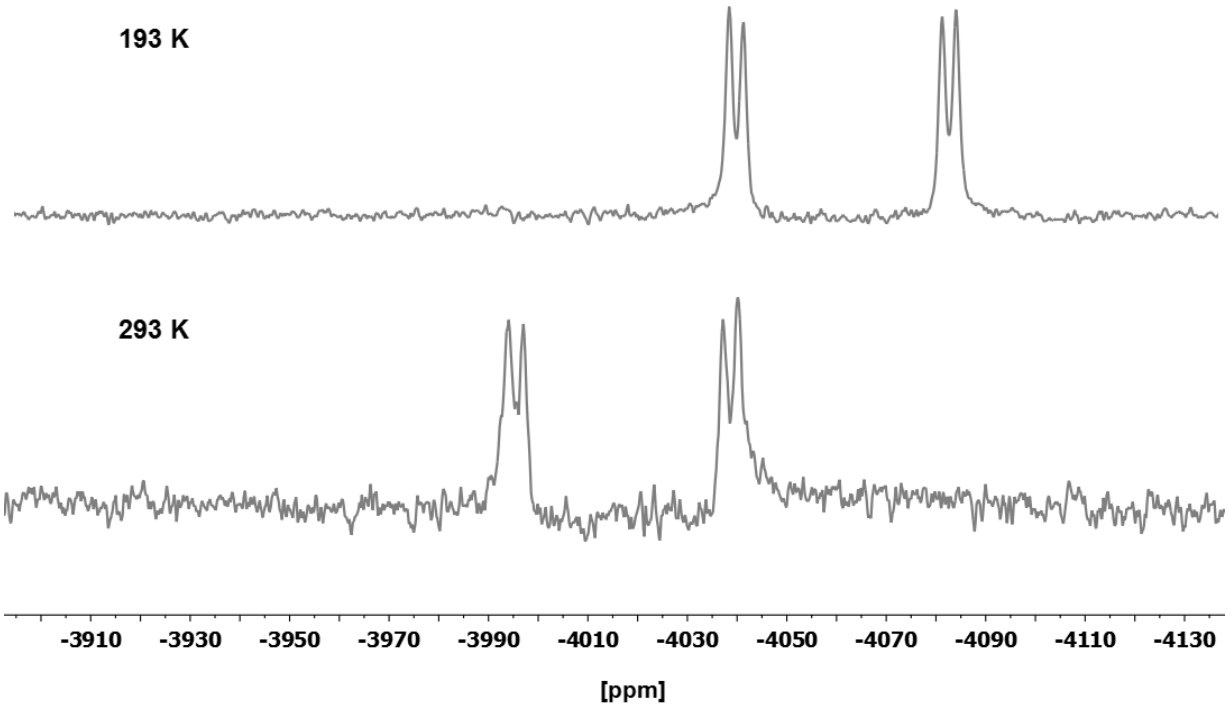

Figure S1.22. $^{195}Pt\{^{1}H\}$ NMR spectra (CD_2Cl_2, 193K top and 293K bottom) of complex $[(CNC)(PPh_3)PtAu(PPh_3)](ClO_4)$ (**4**).

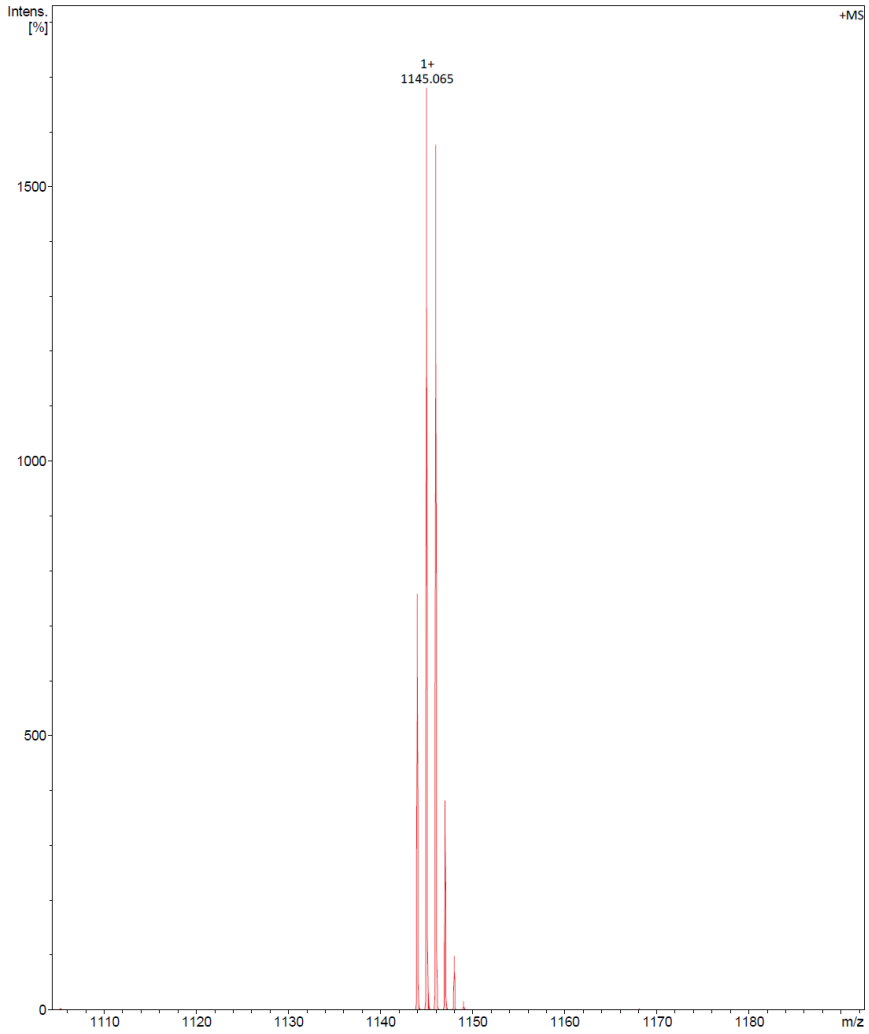

Figure S1.23. MS (MALDI+ DCTB) molecular peak of complex [(CNC)(PPh_3)PtAu(PPh_3)](ClO_4) (**4**).

2.4. Spectra of complex [(CNC)(PPh$_3$)PdAu(PPh$_3$)](ClO$_4$) (5).

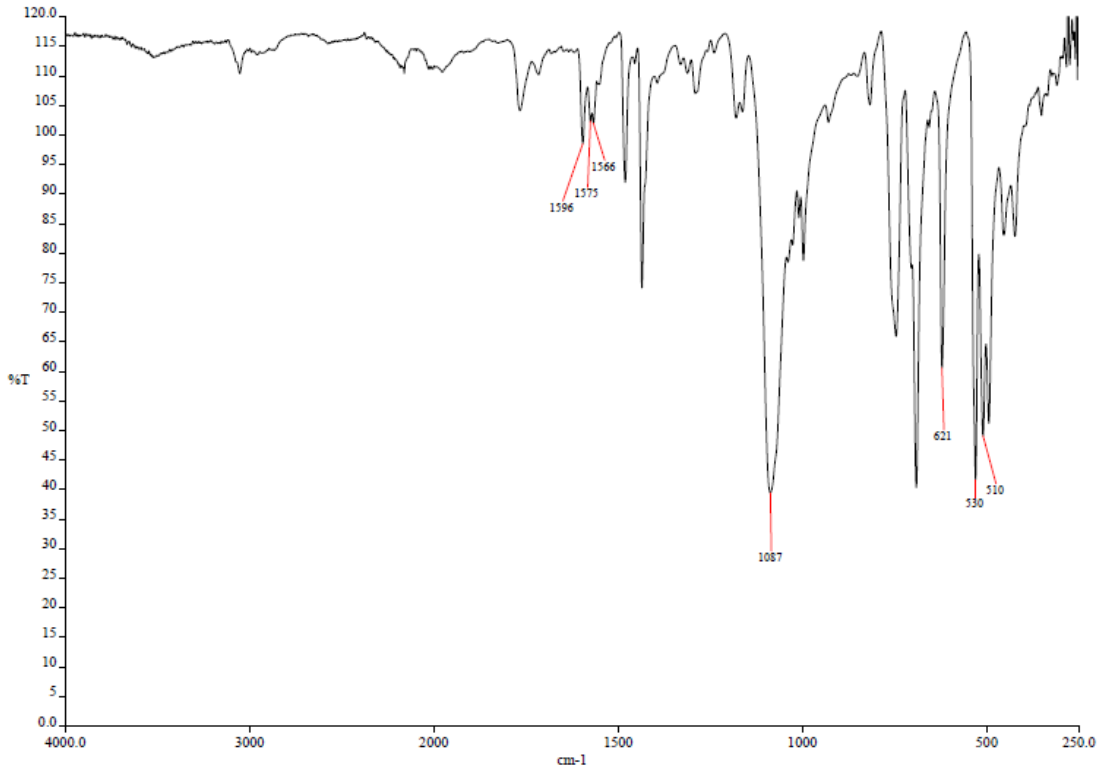

Figure S1.24. IR spectrum of complex [(CNC)(PPh$_3$)PdAu(PPh$_3$)](ClO$_4$) (**5**).

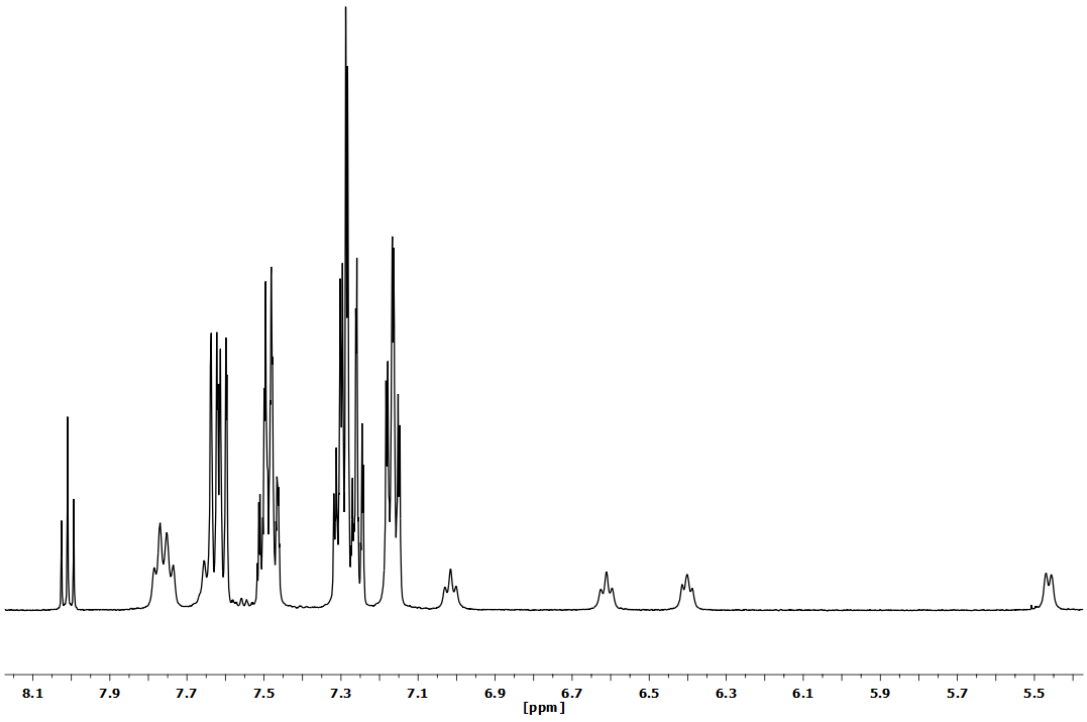

Figure S1.25. ^{1}H NMR spectrum (CD_2Cl_2, RT) of complex [(CNC)(PPh$_3$)PdAu(PPh$_3$)](ClO$_4$) (**5**).

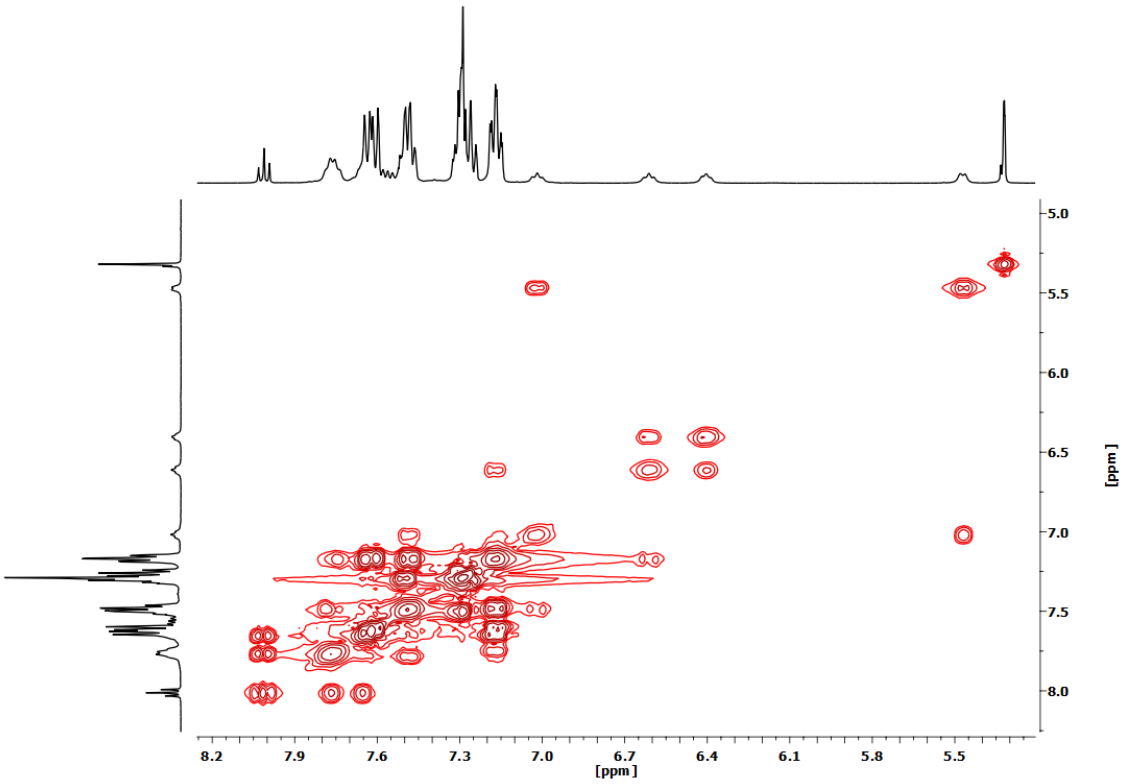

Figure S1.26. ^{1}H-^{1}H COSY NMR spectrum (CD_2Cl_2, RT) of complex [(CNC)(PPh_3)PdAu(PPh_3)](ClO_4) (**5**).

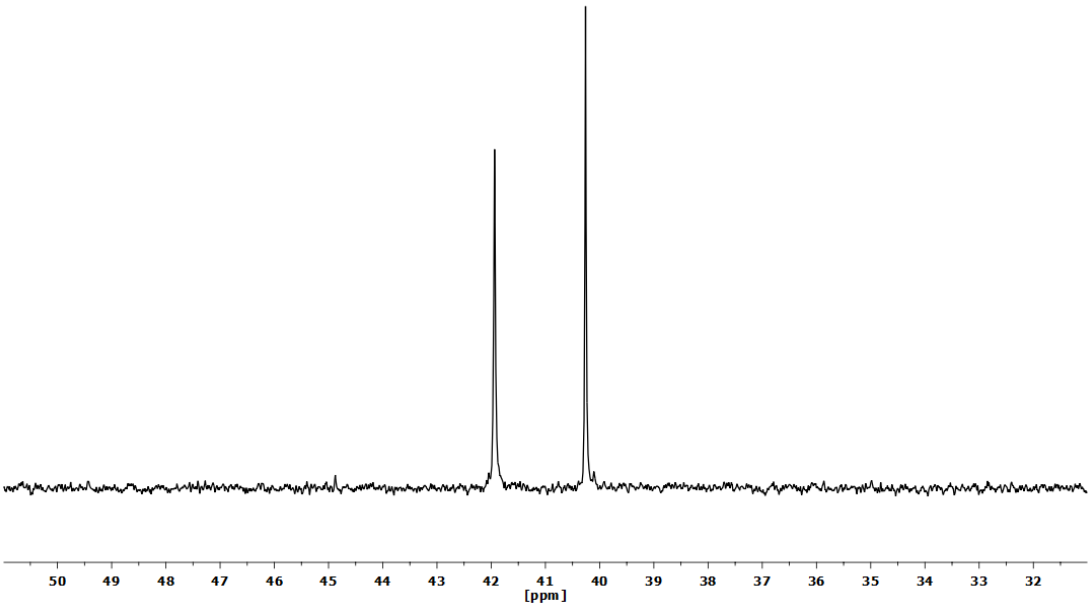

Figure S1.27. $^{31}P\{^{1}H\}$ NMR spectrum (CD_2Cl_2, RT) of complex [(CNC)(PPh_3)PdAu(PPh_3)](ClO_4) (**5**).

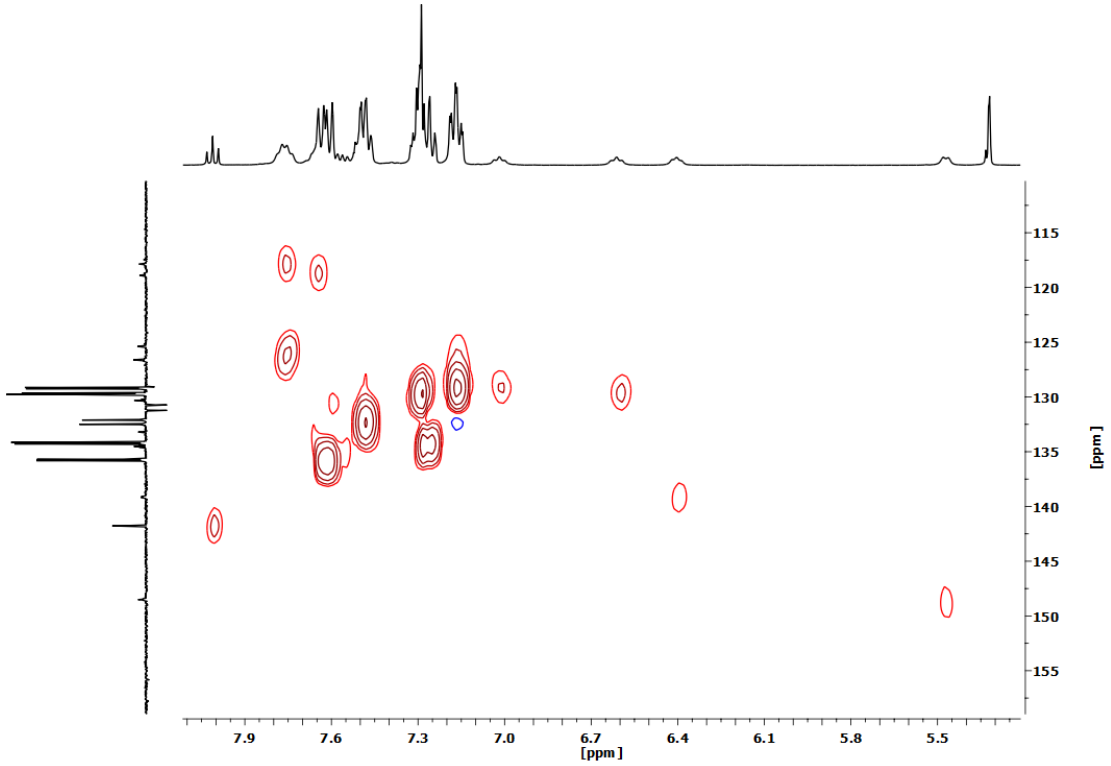

Figure S1.28. ^{1}H-^{13}C HSQC NMR spectrum (CD_2Cl_2, RT) of complex [(CNC)(PPh_3)PdAu(PPh_3)](ClO_4) (**5**).

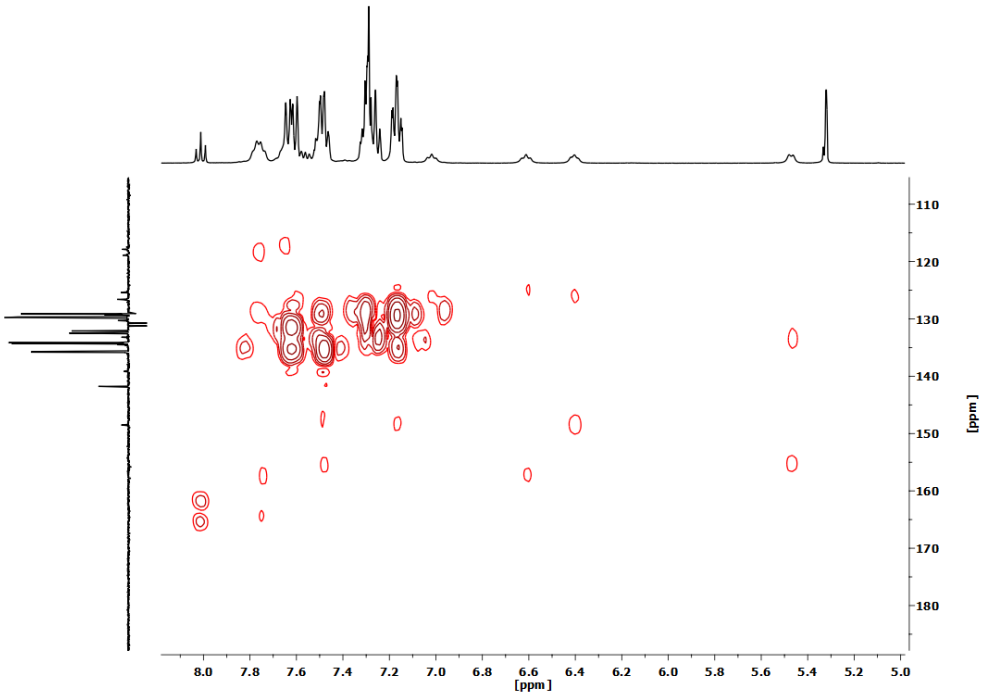

Figure S1.29. ^{1}H-^{13}C HMBC NMR spectrum (CD_2Cl_2, RT) of complex [(CNC)(PPh_3)PdAu(PPh_3)](ClO_4) (**5**).

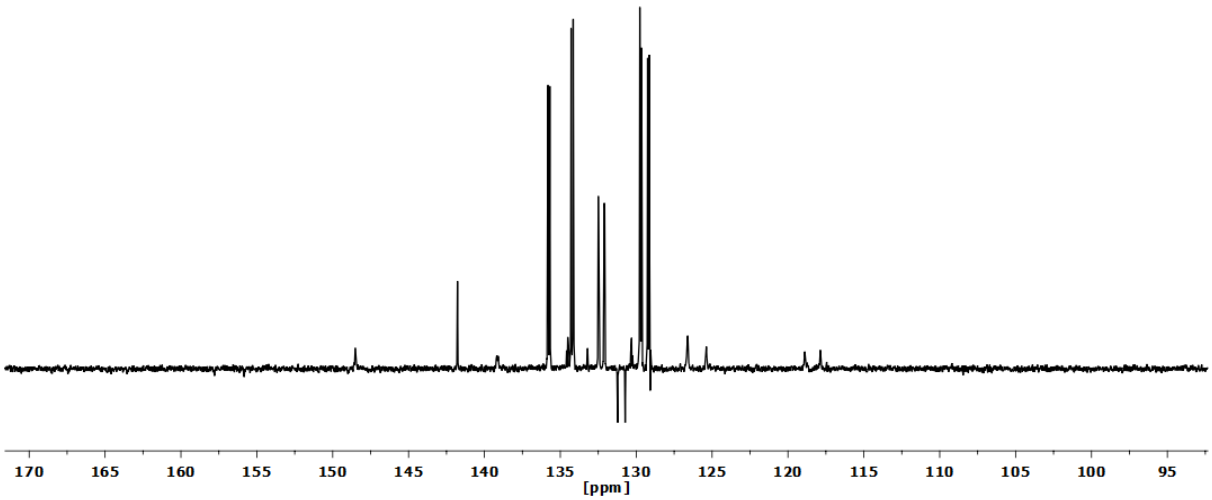

Figure S1.30. APT $^{13}C\{^{1}H\}$ NMR spectrum (CD_2Cl_2, RT) of complex [(CNC)(PPh_3)PdAu(PPh_3)](ClO_4) (**5**).

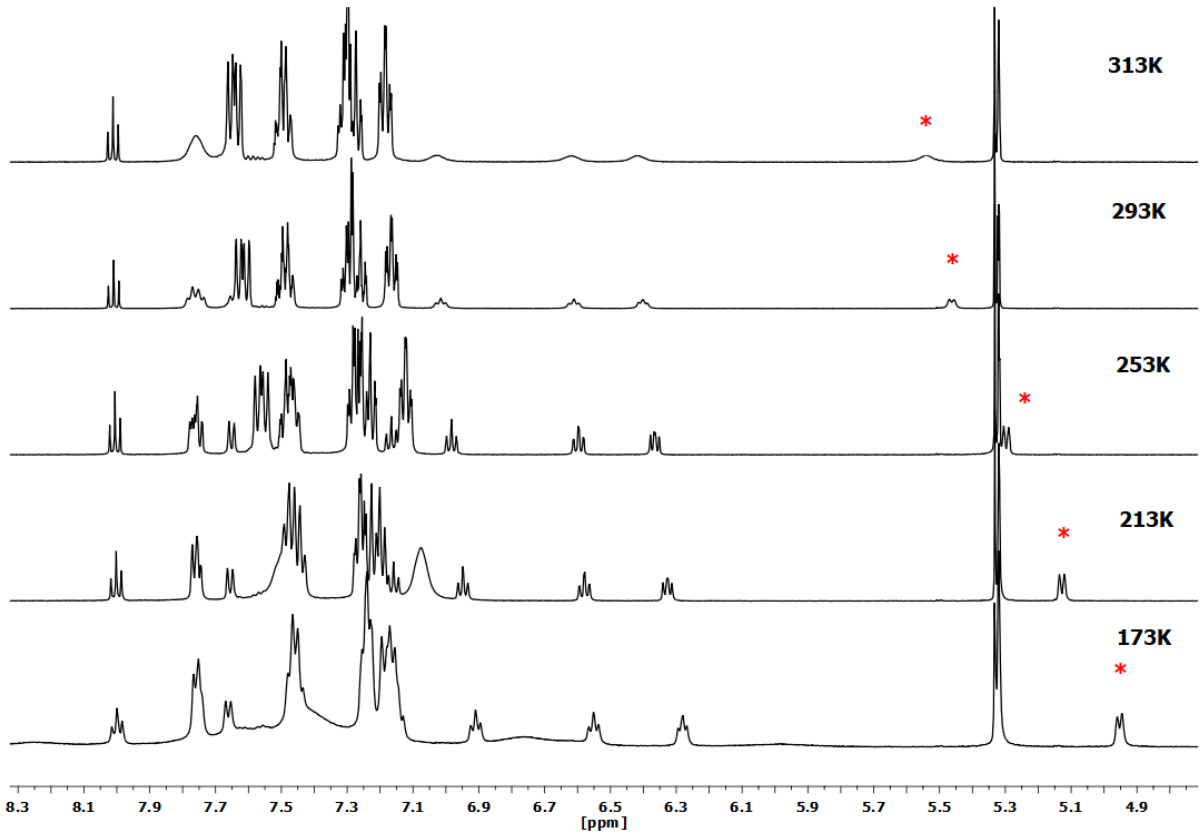

Figure S1.31. ^{1}H VT NMR spectra (CD_2Cl_2) of complex [(CNC)(PPh_3)PdAu(PPh_3)](ClO_4) (**5**).

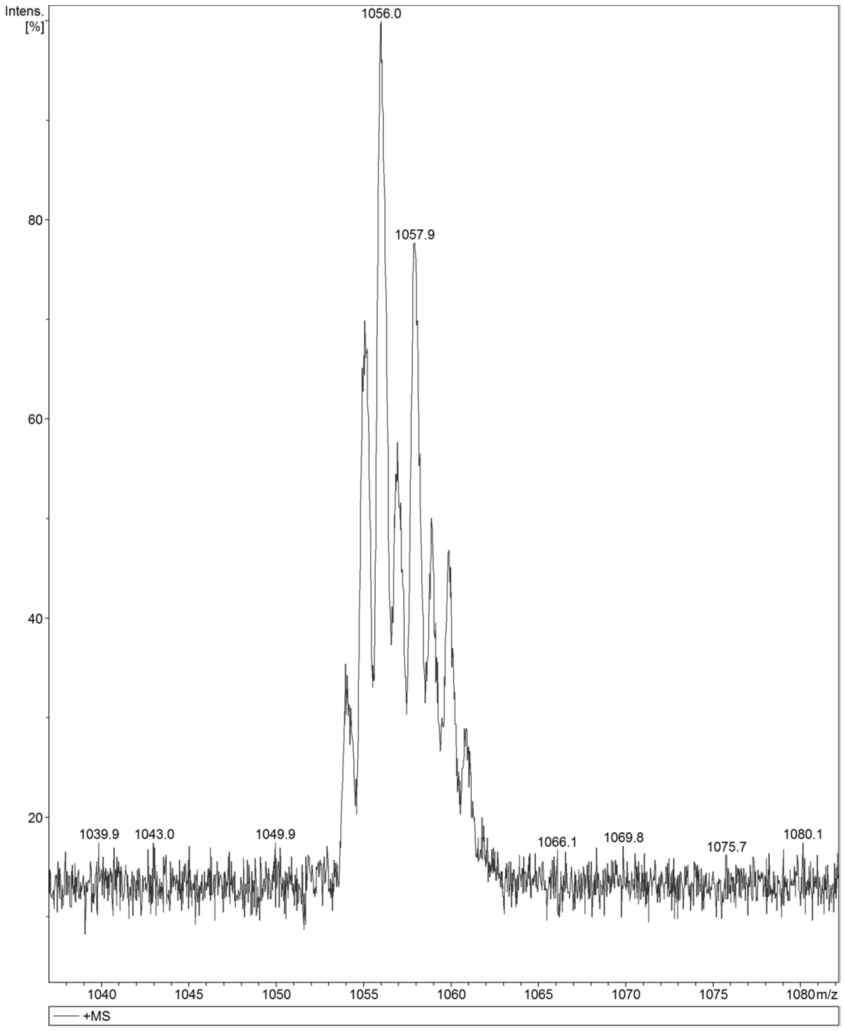

Figure S1.32. MS (MALDI+ DCTB) molecular peak of complex $[(CNC)(PPh_3)PdAu(PPh_3)](ClO_4)$ (**5**).

2.5. Spectra of complex [{Pt(CNC)(PPh$_3$)}$_2$Au](ClO$_4$) (6).

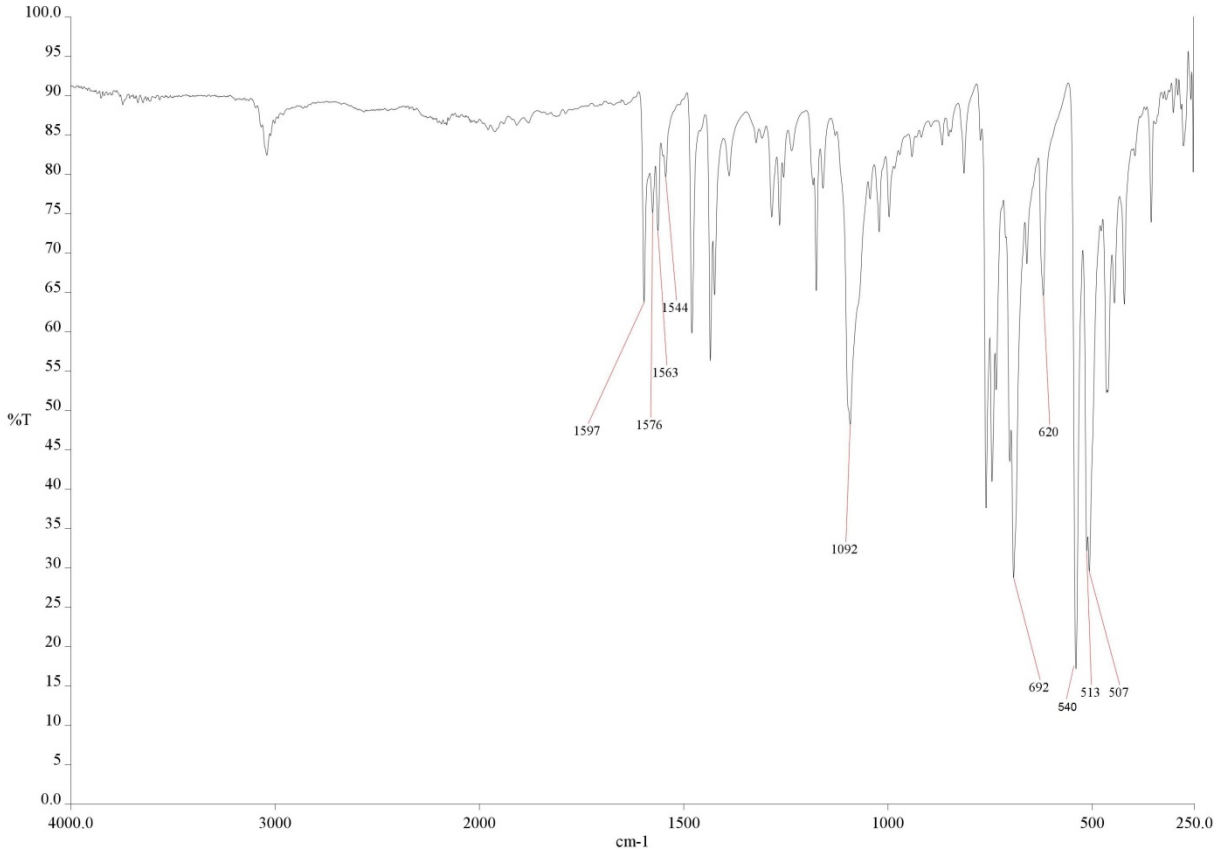

Figure S1.33. IR spectrum of complex [{Pt(CNC)(PPh$_3$)}$_2$Au](ClO$_4$) (**6**).

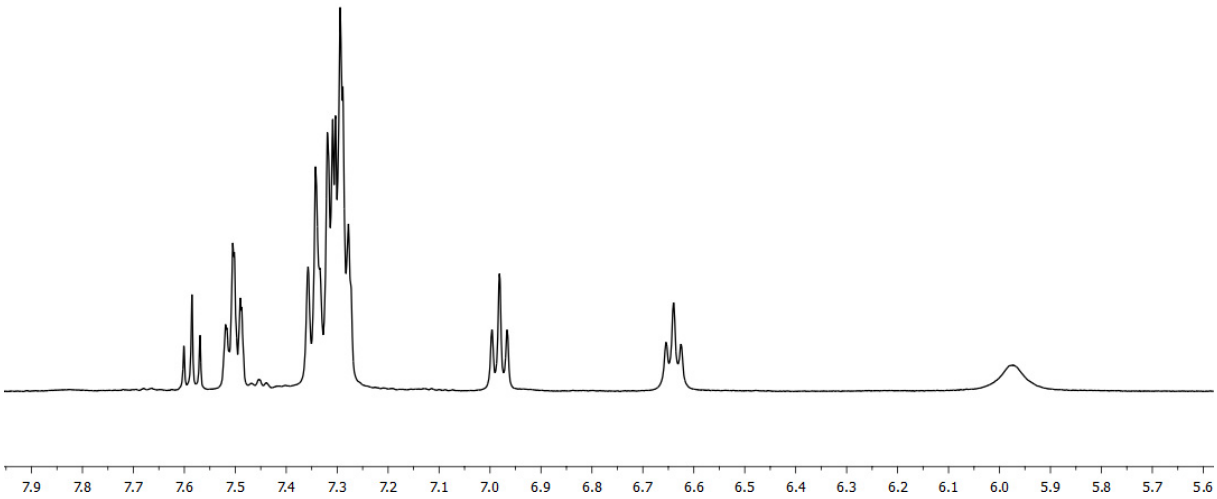

Figure S1.34. ^{1}H NMR spectrum (CD_2Cl_2, RT) of complex [{Pt(CNC)(PPh$_3$)}$_2$Au](ClO$_4$) (**6**).

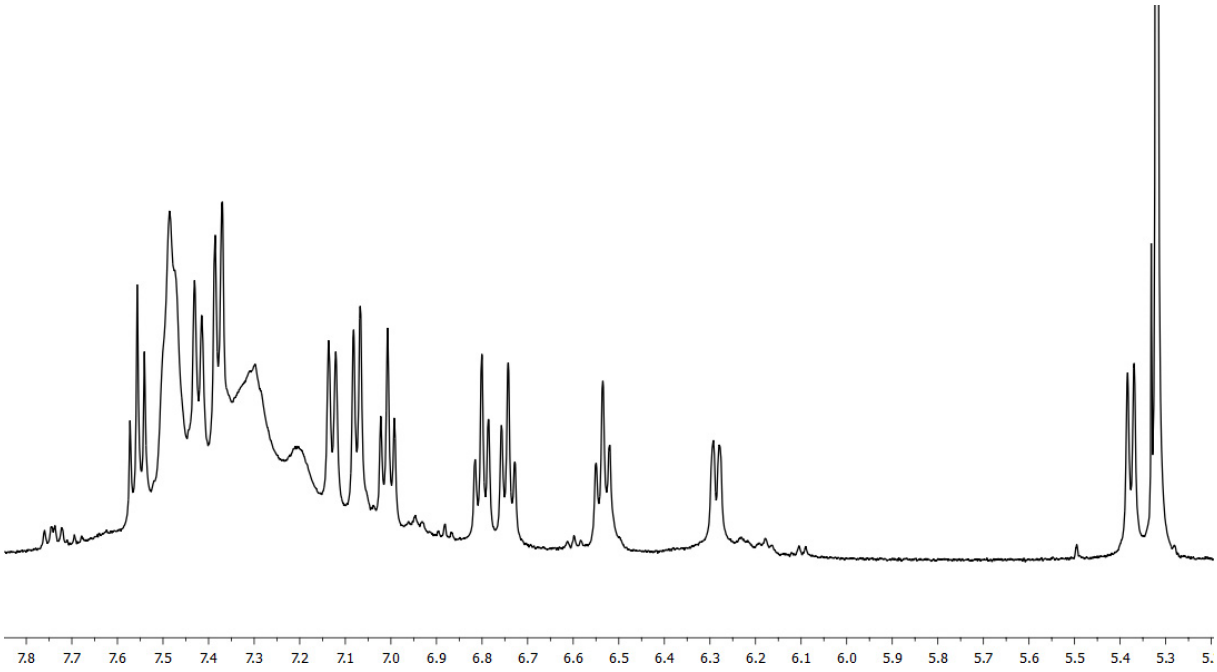

Figure S1.35. ^{1}H NMR spectrum (CD_2Cl_2, 193K) of complex [{Pt(CNC)(PPh_3)}$_2$Au](ClO_4) (**6**).

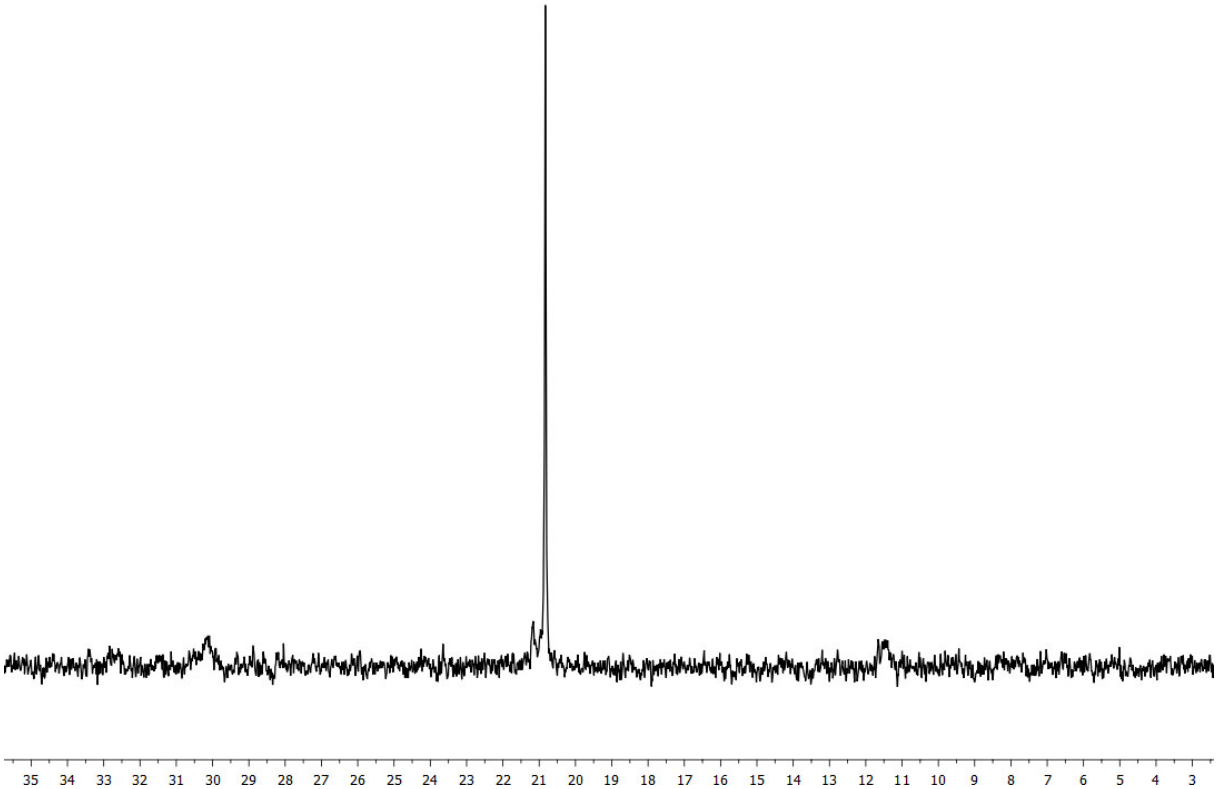

Figure S1.36. $^{31}P\{^{1}H\}$ NMR spectrum (CD_2Cl_2, 203K) of complex [{Pt(CNC)(PPh_3)}$_2$Au](ClO_4) (**6**).

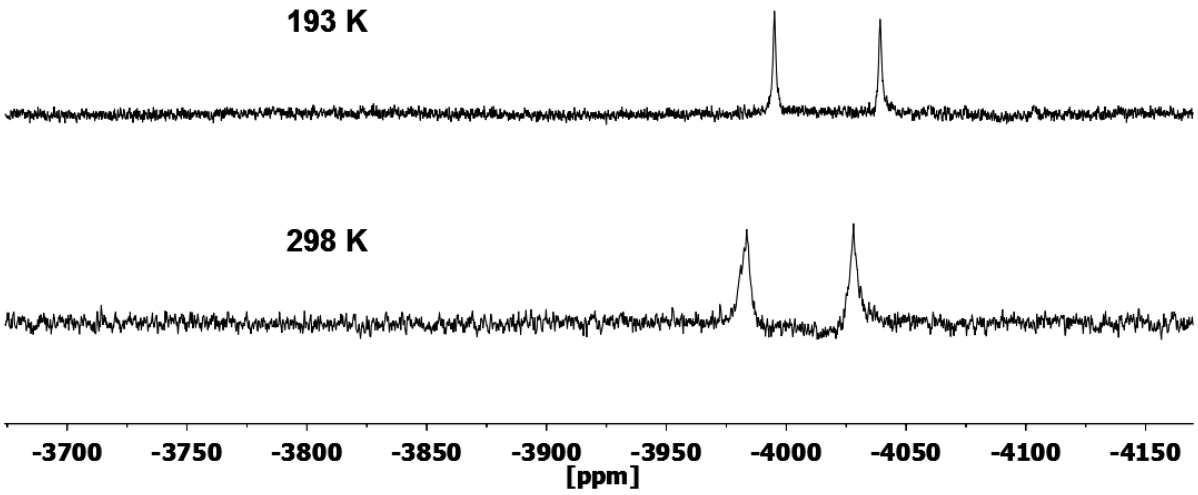

Figure S1.37. $^{195}Pt\{^{1}H\}$ NMR spectra (CD_2Cl_2, 193K top, 298K bottom, CD_2Cl_2) of complex $[\{Pt(CNC)(PPh_3)\}_2Au](ClO_4)$ (**6**).

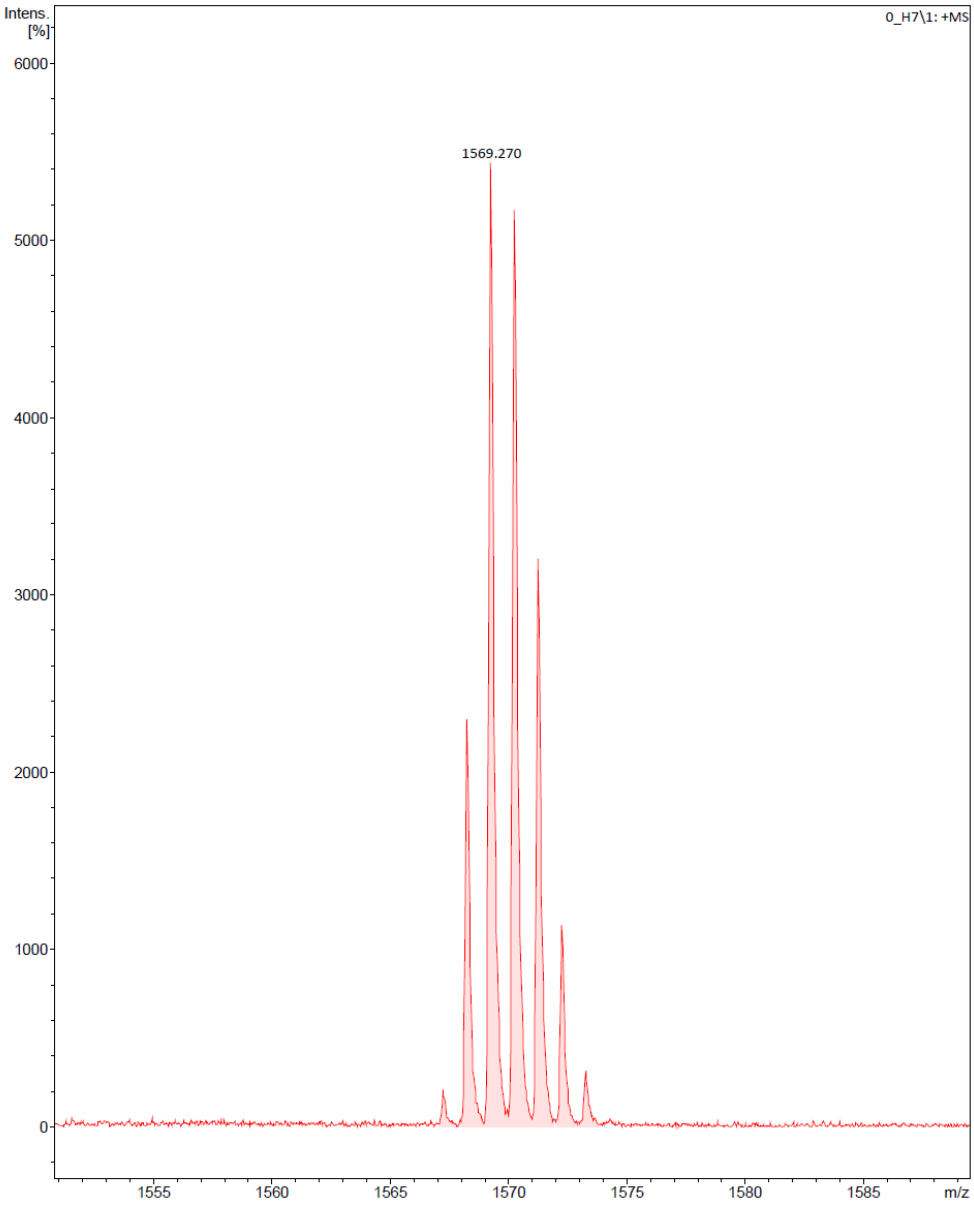

Figure S1.38. MS (MALDI+ DCTB) molecular peak of complex [{Pt(CNC)(PPh_3)}$_2$Au](ClO_4) (**6**).

2.6. Spectra of complex [{Pd(CNC)(PPh$_3$)}$_2$Au](ClO$_4$) (7).

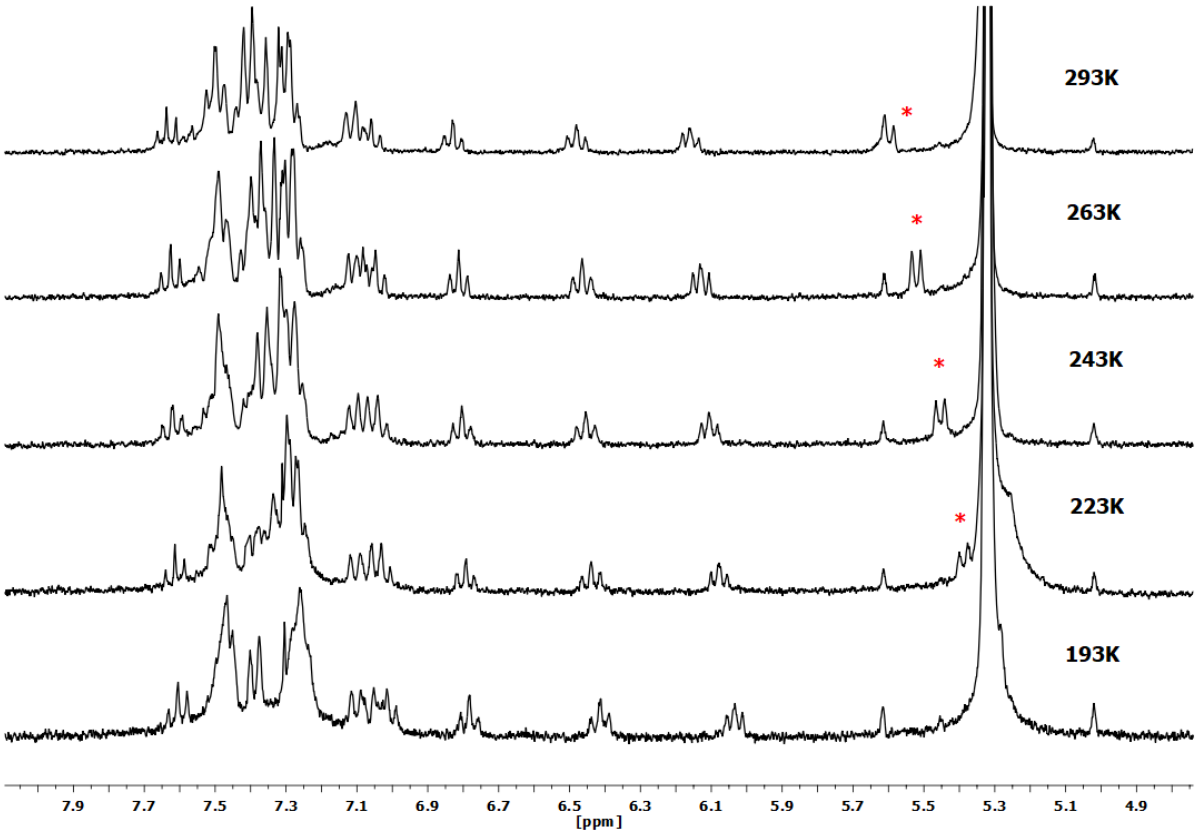

Figure S1.39. ^{1}H VT NMR spectra (CD_2Cl_2) of complex [{Pd(CNC)(PPh$_3$)}$_2$Au](ClO$_4$) (**7**).

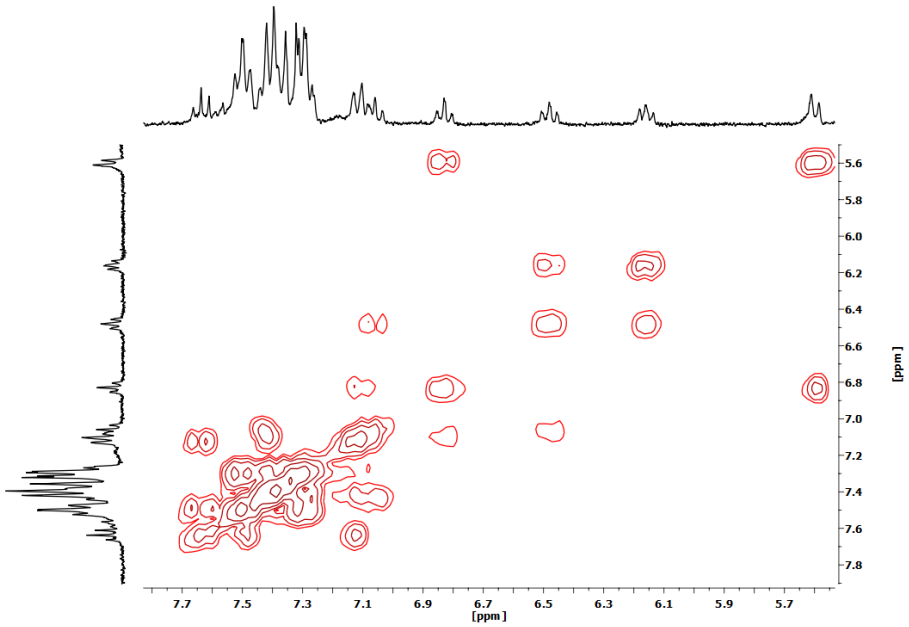

Figure S1.40. ^{1}H-^{1}H COSY NMR spectrum (CD_2Cl_2, RT) of complex [{Pd(CNC)(PPh$_3$)}$_2$Au](ClO$_4$) (**7**).

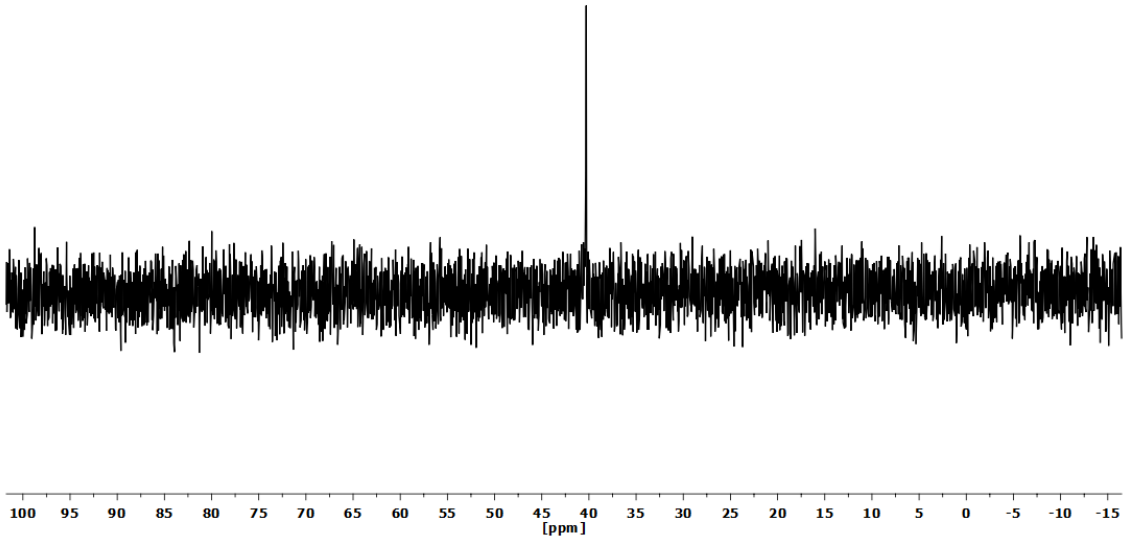

Figure S1.41. $^{31}P\{^{1}H\}$ NMR spectrum (CD_2Cl_2, RT) of complex [{Pd(CNC)(PPh_3)}$_2$Au](ClO_4) (**7**).

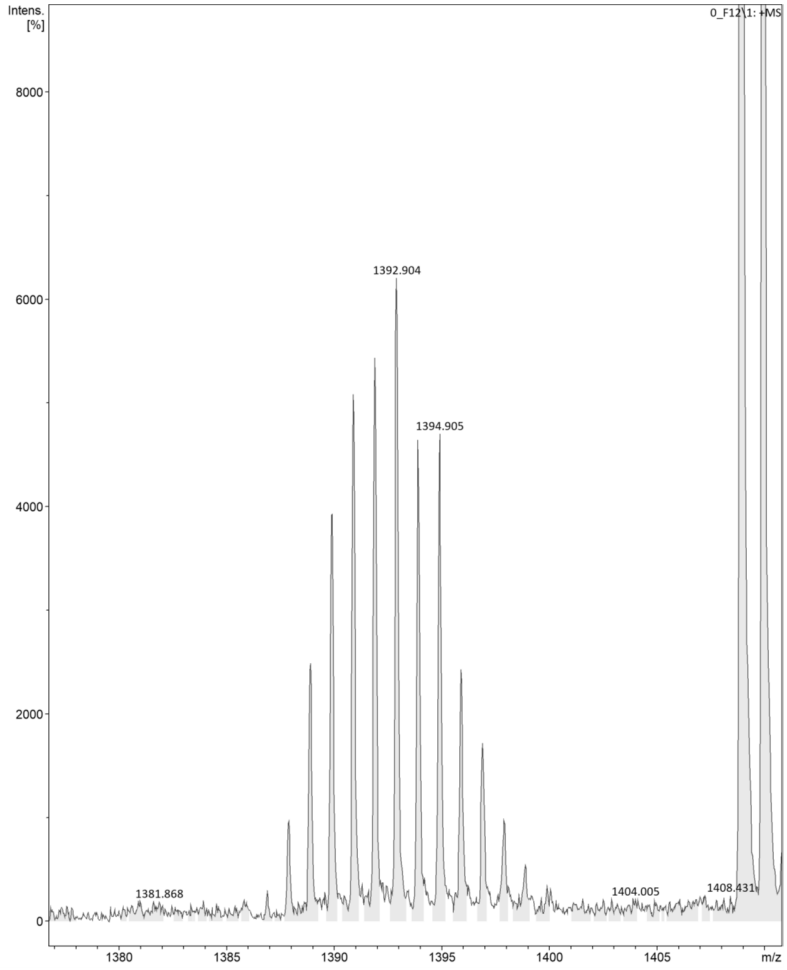

Figure S1.42. MS (MALDI+ DCTB) molecular peak of complex [{Pd(CNC)(PPh_3)}$_2$Au](ClO_4) (**7**).

2.7. Spectra of complex [{Pt(CNC)(PPh$_3$)}$_2$Ag](ClO$_4$) (8).

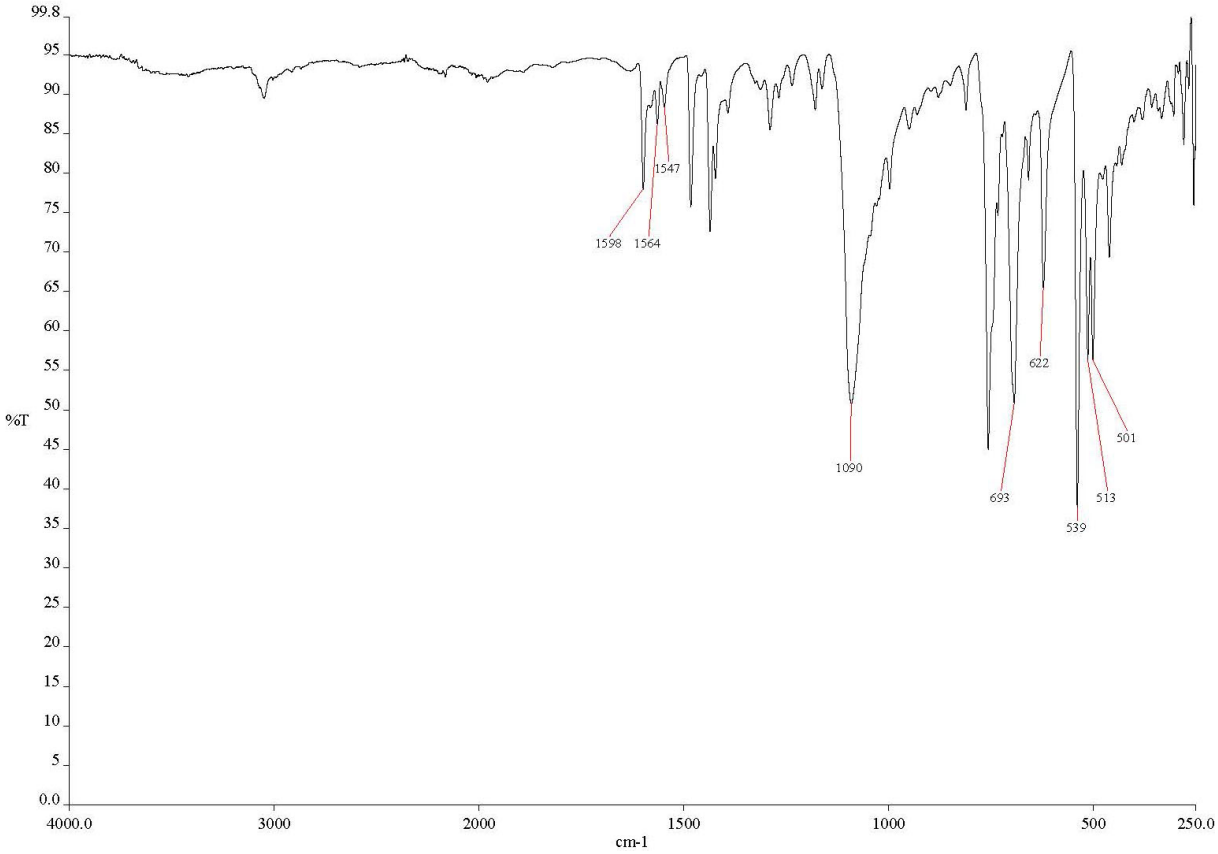

Figure S1.43. IR spectrum of complex [{Pt(CNC)(PPh$_3$)}$_2$Ag](ClO$_4$) (**8**).

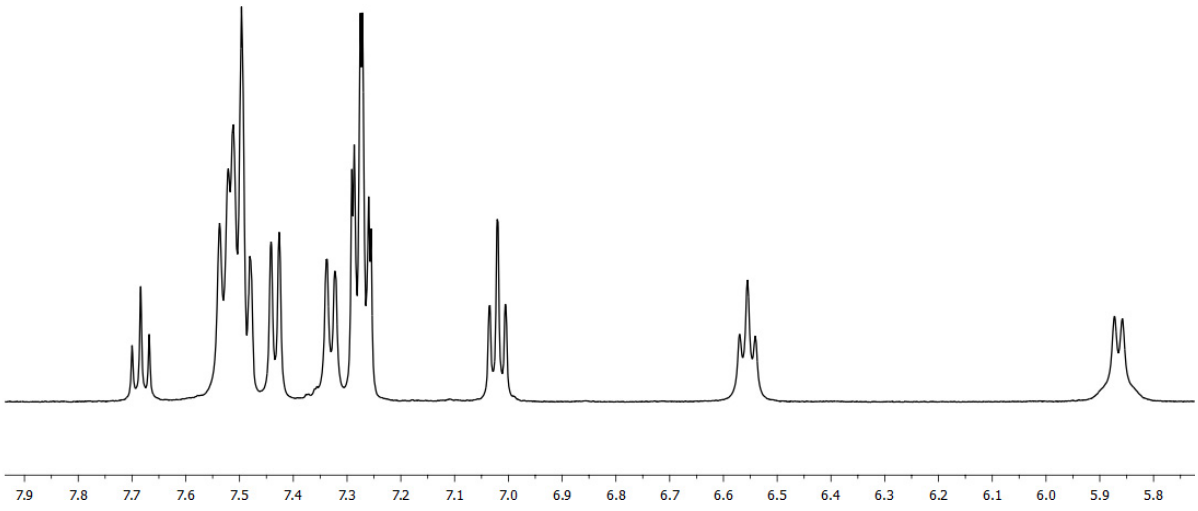

Figure S1.44. ^{1}H NMR spectrum (CD_2Cl_2, RT) of complex [{Pt(CNC)(PPh$_3$)}$_2$Ag](ClO$_4$) (**8**).

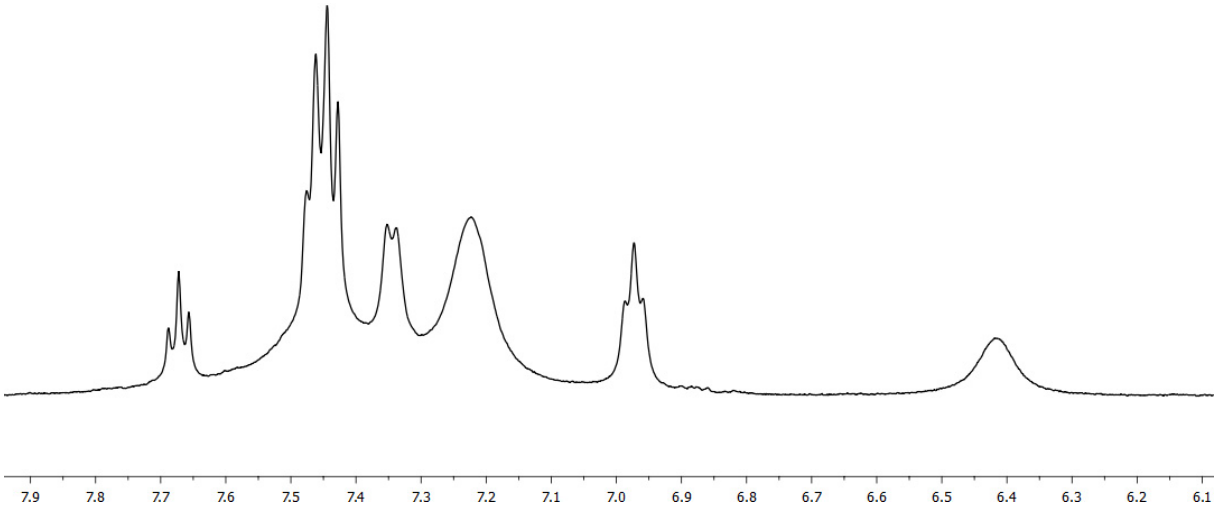

Figure S1.45. ^{1}H NMR spectrum (CD_2Cl_2, 193K) of complex [{Pt(CNC)(PPh_3)}$_2$Ag](ClO_4) (**8**).

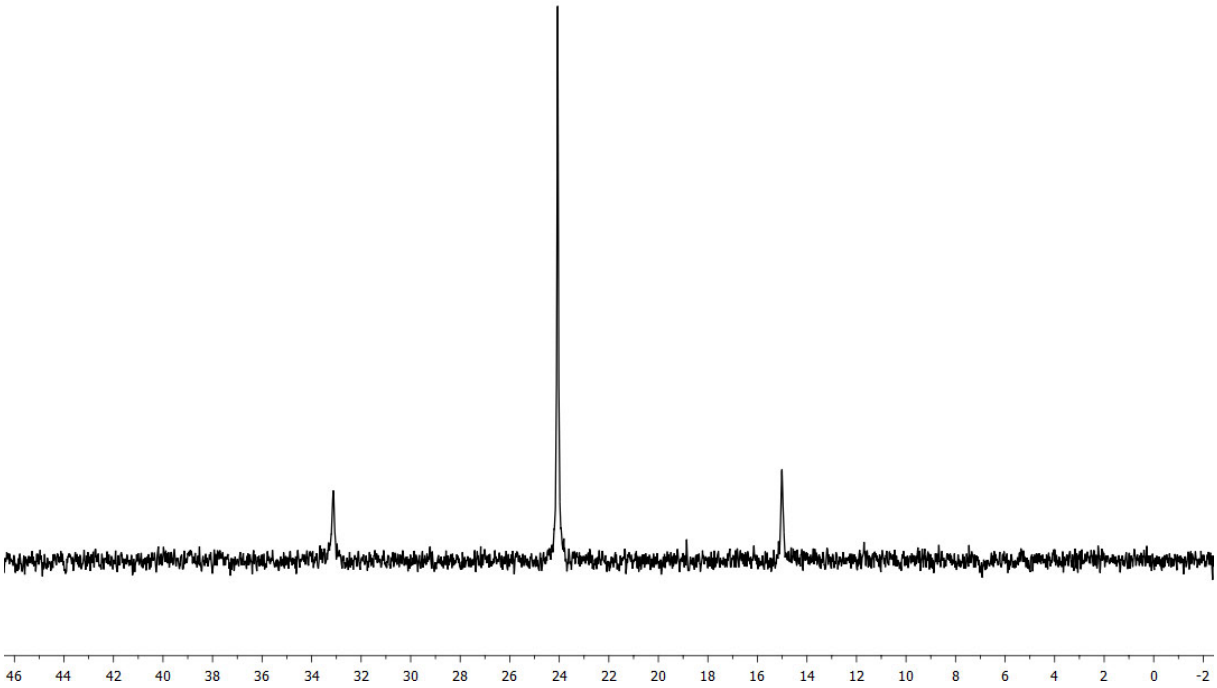

Figure S1.46. $^{31}P\{^{1}H\}$ NMR spectrum (CD_2Cl_2, 293K) of complex [{Pt(CNC)(PPh_3)}$_2$Ag](ClO_4) (**8**).

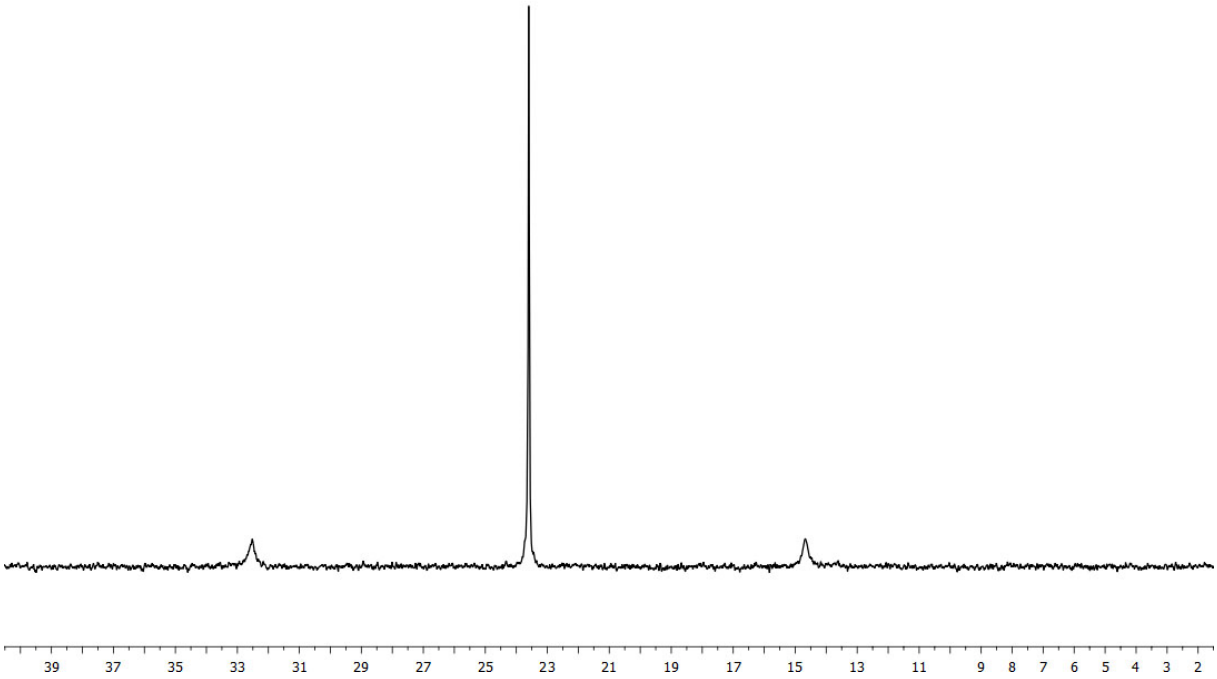

Figure S1.47. $^{31}P\{^{1}H\}$ NMR spectrum (CD_2Cl_2, 193K) of complex [{Pt(CNC)(PPh_3)}$_2$Ag](ClO_4) (**8**).

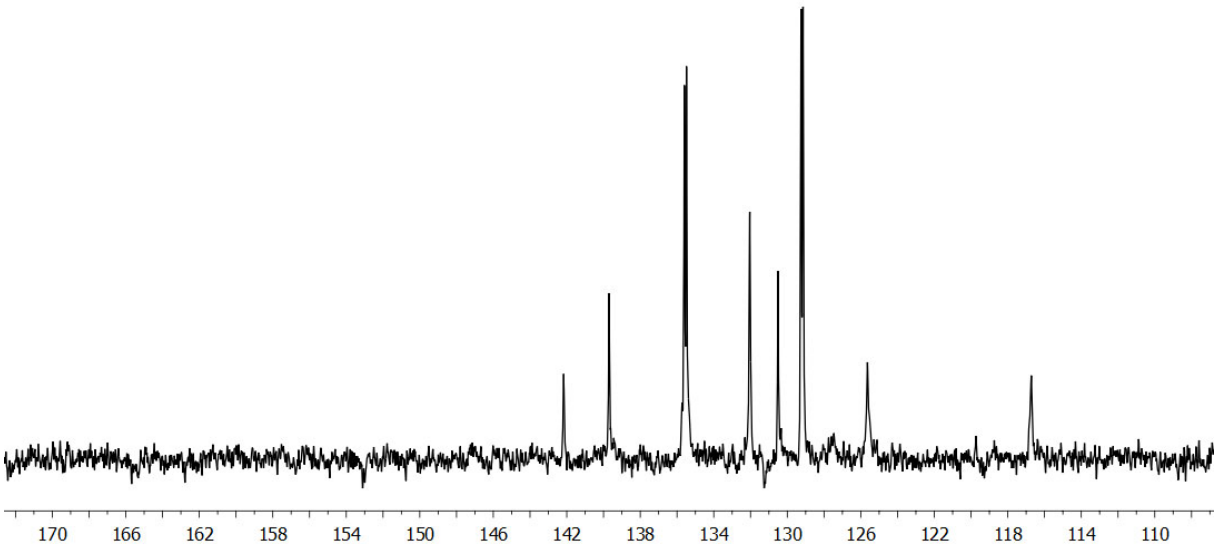

Figure S1.48. APT $^{13}C\{^{1}H\}$ NMR (CD_2Cl_2, 293K). spectrum of complex [{Pt(CNC)(PPh_3)}$_2$Ag](ClO_4) (**8**).

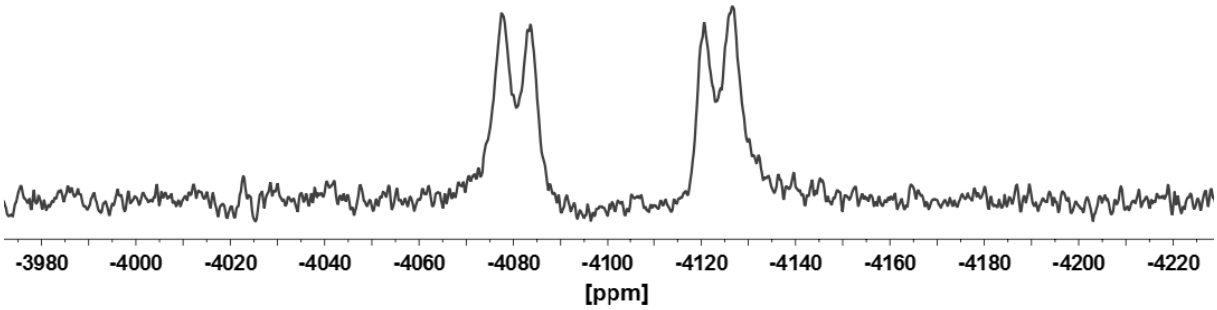

Figure S1.49. $^{195}Pt\{^{1}H\}$ NMR spectrum (CD_2Cl_2, 293K) of complex $[\{Pt(CNC)(PPh_3)\}_2Ag](ClO_4)$ (**8**).

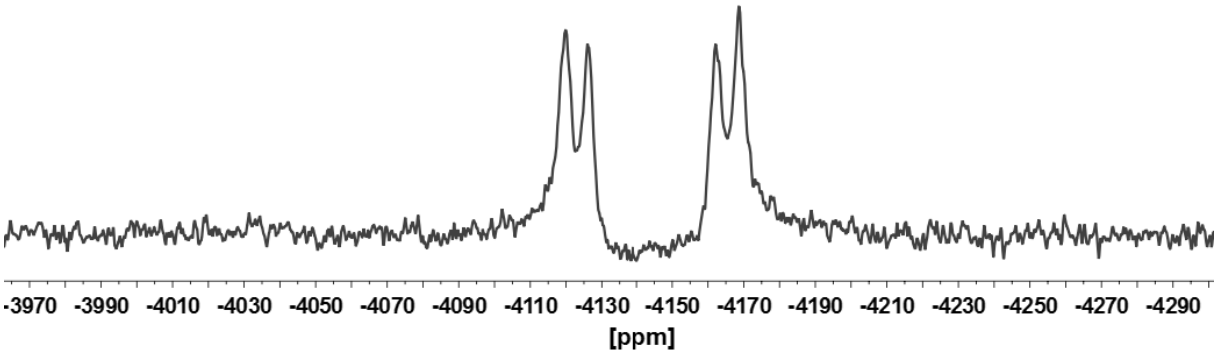

Figure S1.50. $^{195}Pt\{^{1}H\}$ NMR spectrum (CD_2Cl_2, 193K) of complex $[\{Pt(CNC)(PPh_3)\}_2Ag](ClO_4)$ (**8**).

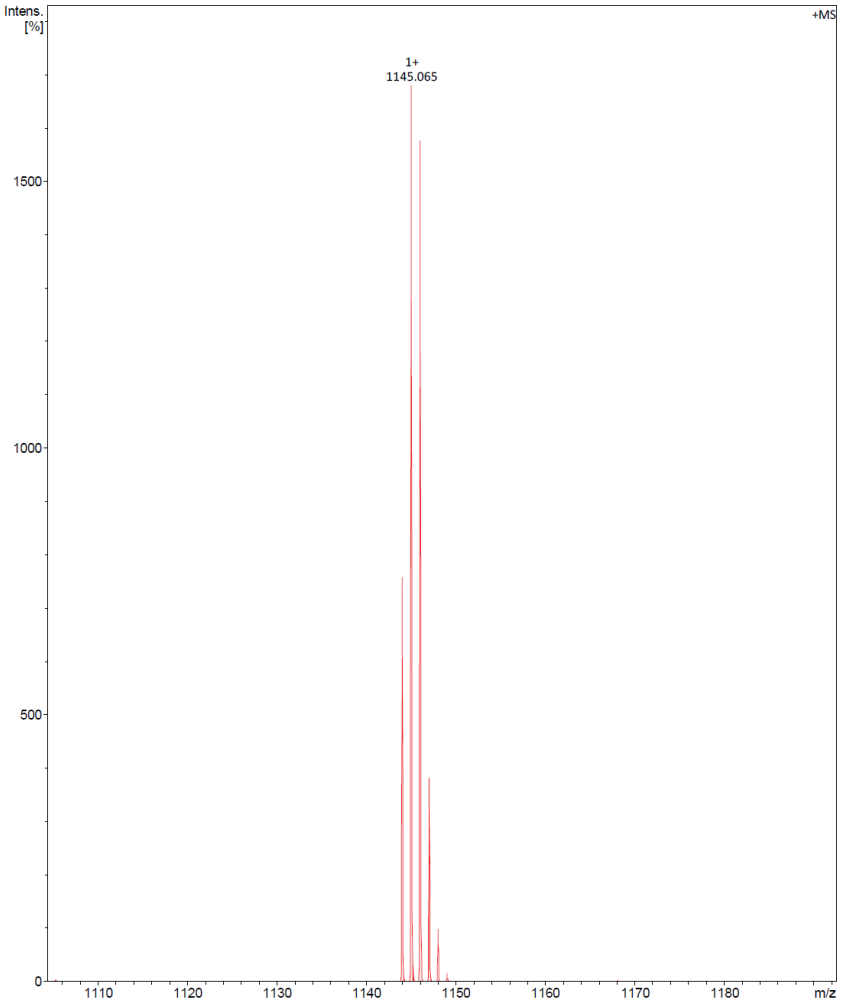

Figure S1.51. MS (MALDI+ DCTB) molecular peak of complex [{Pt(CNC)(PPh_3)}$_2$Ag](ClO_4) (**8**).

2.8. Spectra of complex [{Pd(CNC)(PPh$_3$)}$_2$Ag](ClO$_4$) (9).

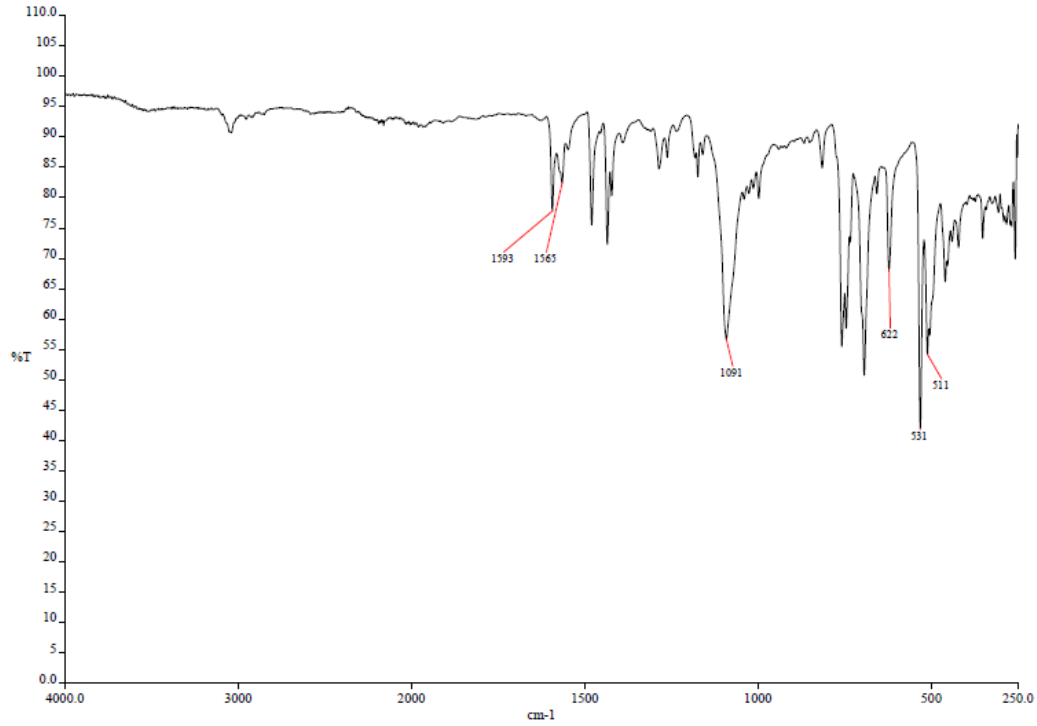

Figure S1.52. IR spectrum of complex [{Pd(CNC)(PPh$_3$)}$_2$Ag](ClO$_4$) (**9**).

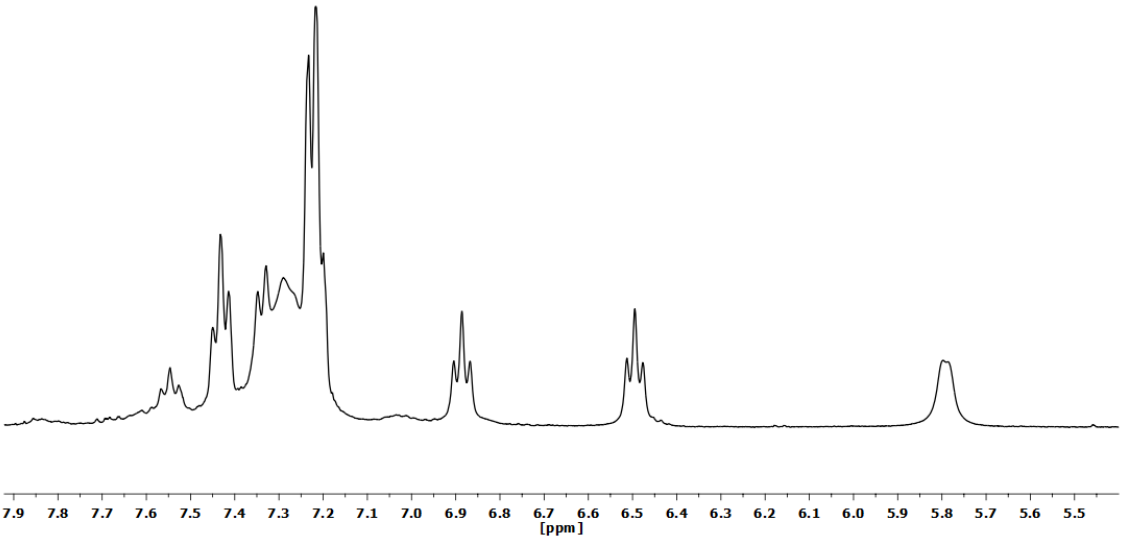

Figure S1.53. ^{1}H NMR spectrum (CD_2Cl_2, RT) of complex [{Pd(CNC)(PPh$_3$)}$_2$Ag](ClO$_4$) (**9**).

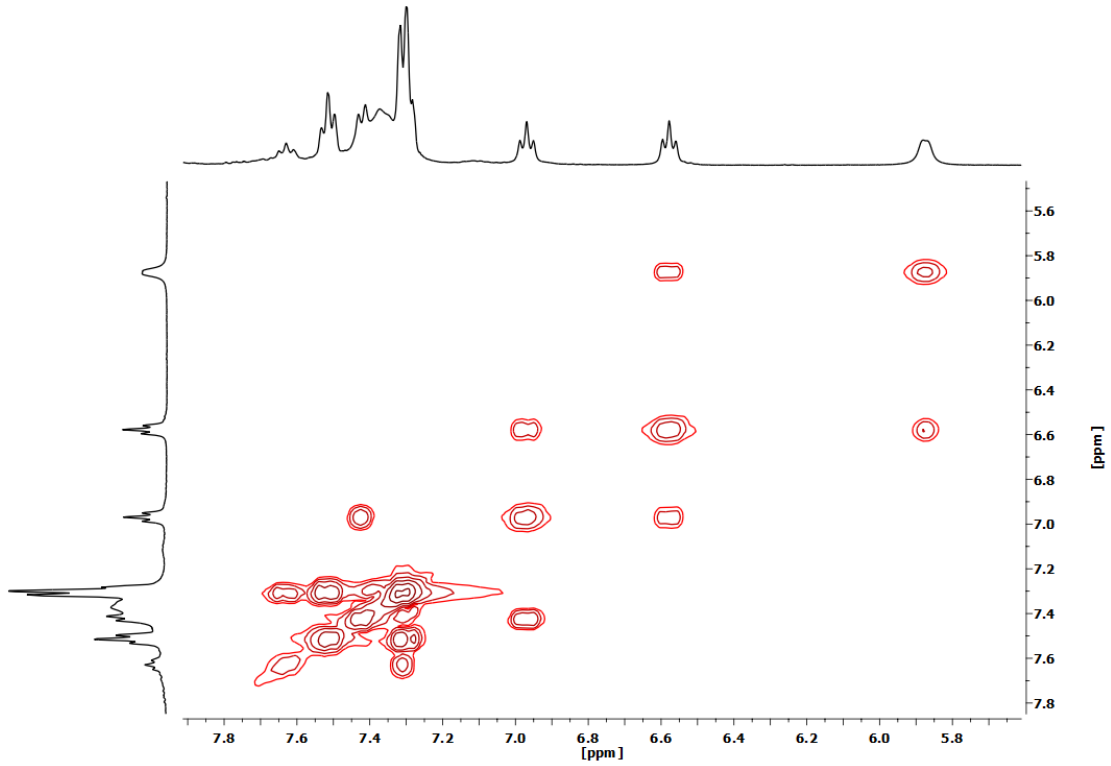

Figure S1.54. ^{1}H-^{1}H COSY NMR spectrum (CD_2Cl_2, RT) of complex [{Pd(CNC)(PPh_3)}$_2$Ag](ClO_4) (**9**).

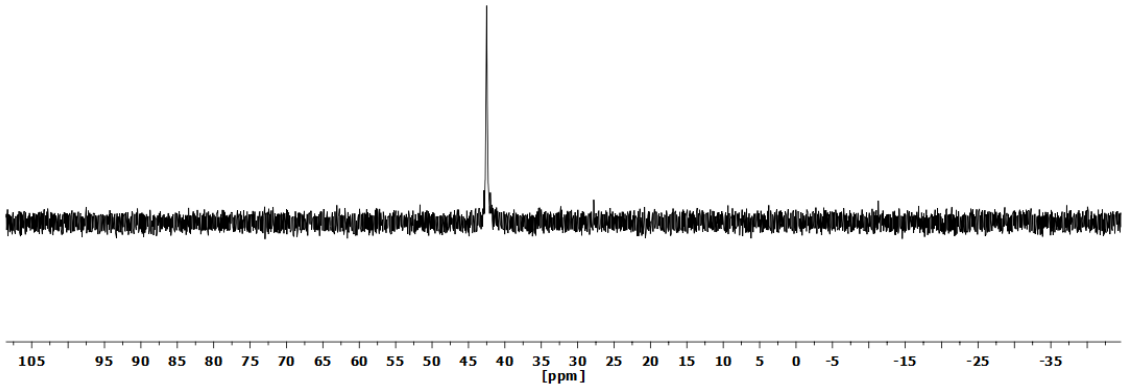

Figure S1.55. $^{31}P\{^{1}H\}$ NMR spectrum (CD_2Cl_2, RT) of complex [{Pd(CNC)(PPh_3)}$_2$Ag](ClO_4) (**9**).

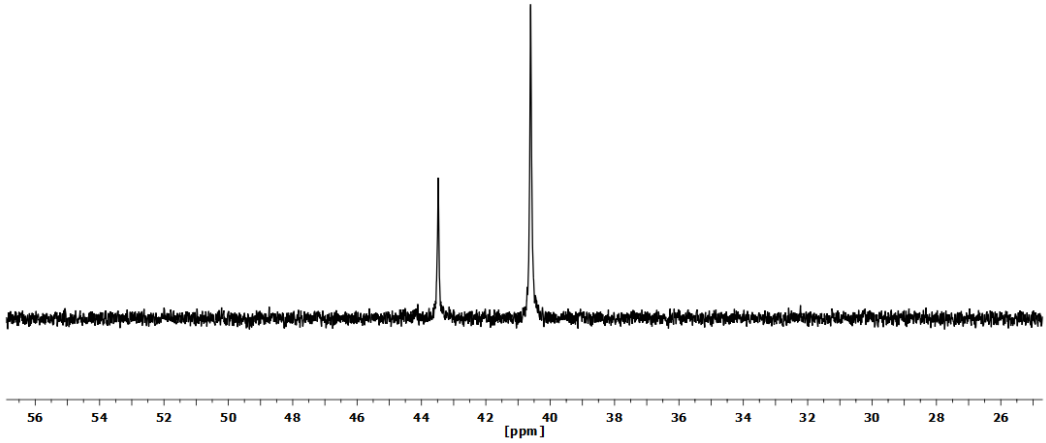

Figure S1.56. $^{31}P\{^{1}H\}$ NMR spectrum (CD_2Cl_2, 193K) of complex $[\{Pd(CNC)(PPh_3)\}_2Ag](ClO_4)$ (**9**) .

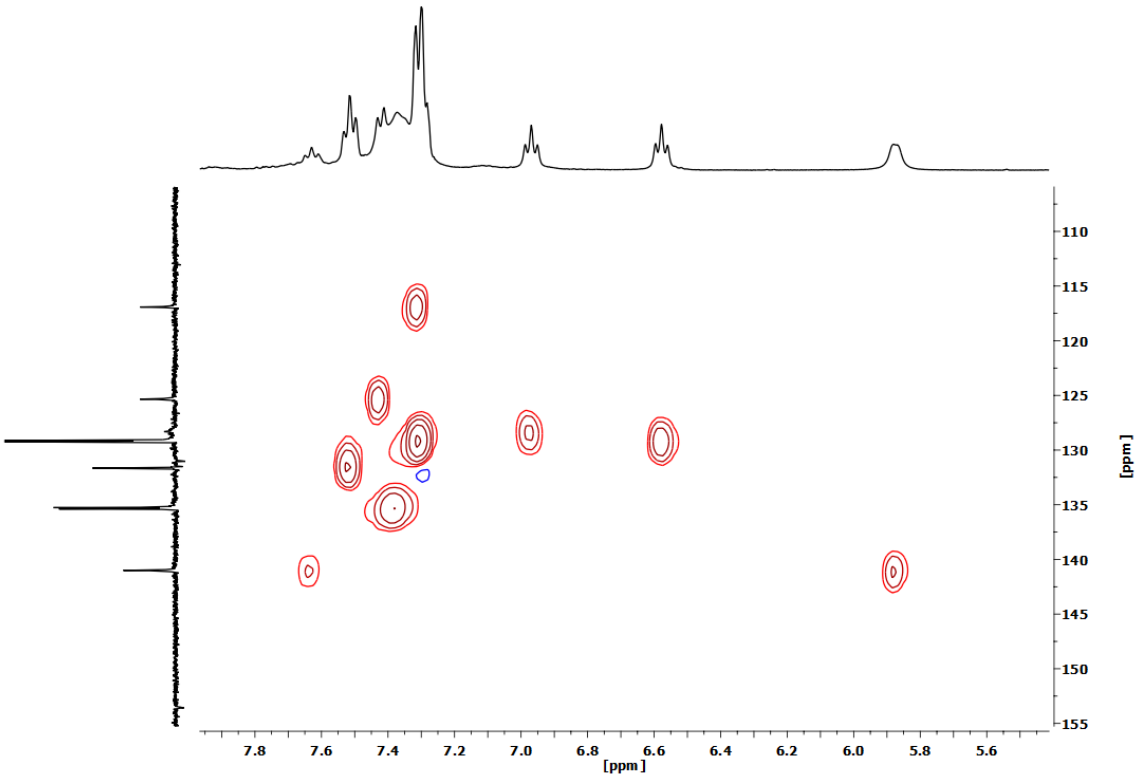

Figure S1.57. ^{1}H-^{13}C HSQC NMR spectrum (RT, CD_2Cl_2) of complex $[\{Pd(CNC)(PPh_3)\}_2Ag](ClO_4)$ (**9**).

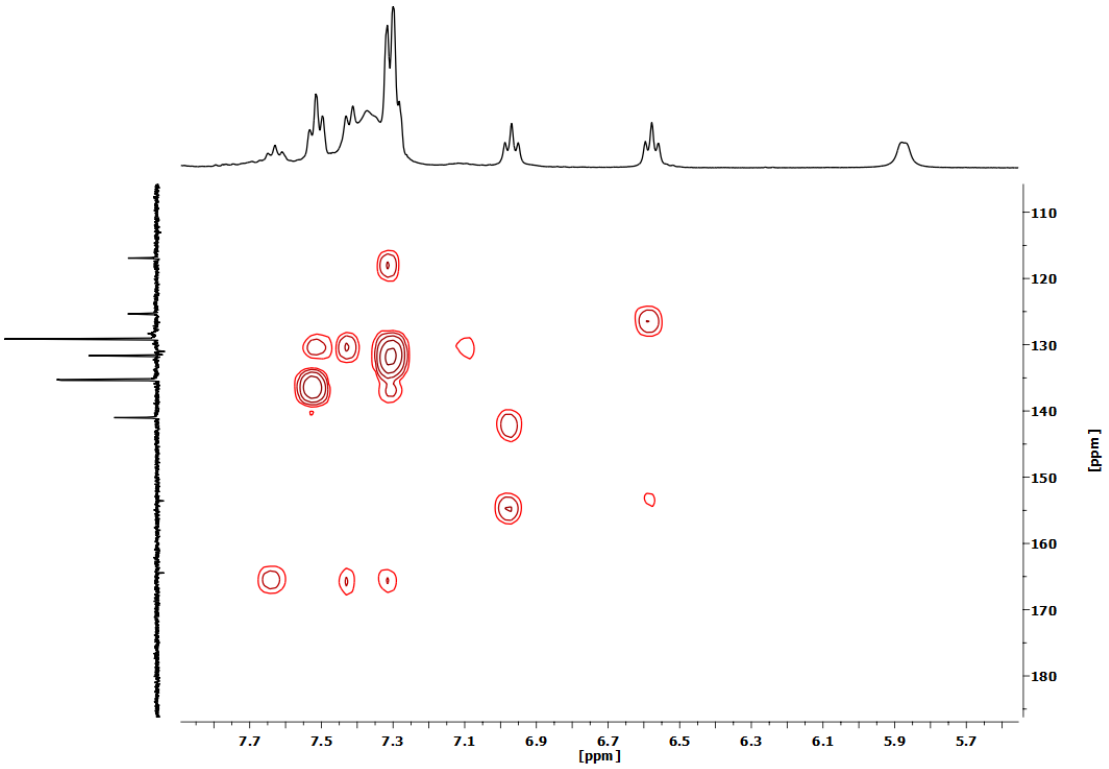

Figure S1.58. ^{1}H-^{13}C HMBC NMR spectrum (CD_2Cl_2, RT) of complex [{Pd(CNC)(PPh_3)}$_2$Ag](ClO_4) (**9**).

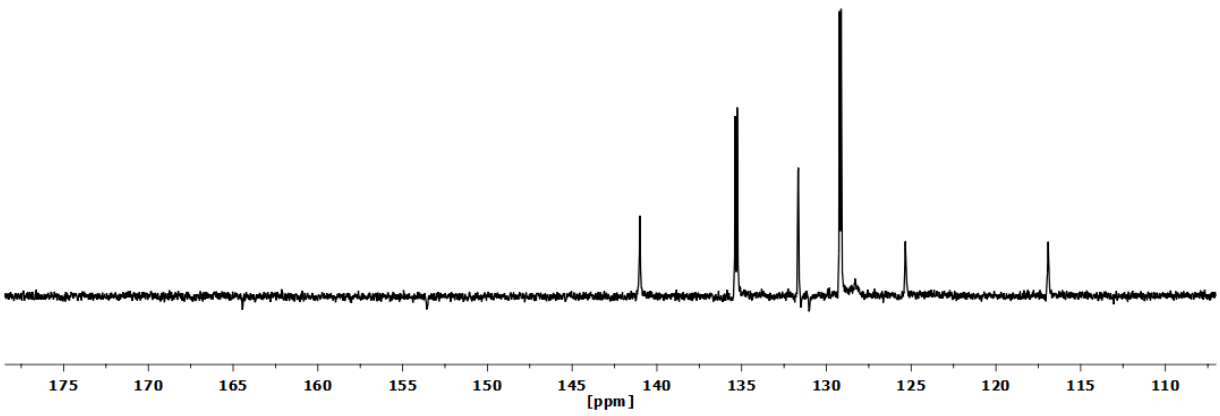

Figure S1.59. APT $^{13}C\{^{1}H\}$ NMR spectrum (CD_2Cl_2, RT) of complex [{Pd(CNC)(PPh_3)}$_2$Ag](ClO_4) (**9**).

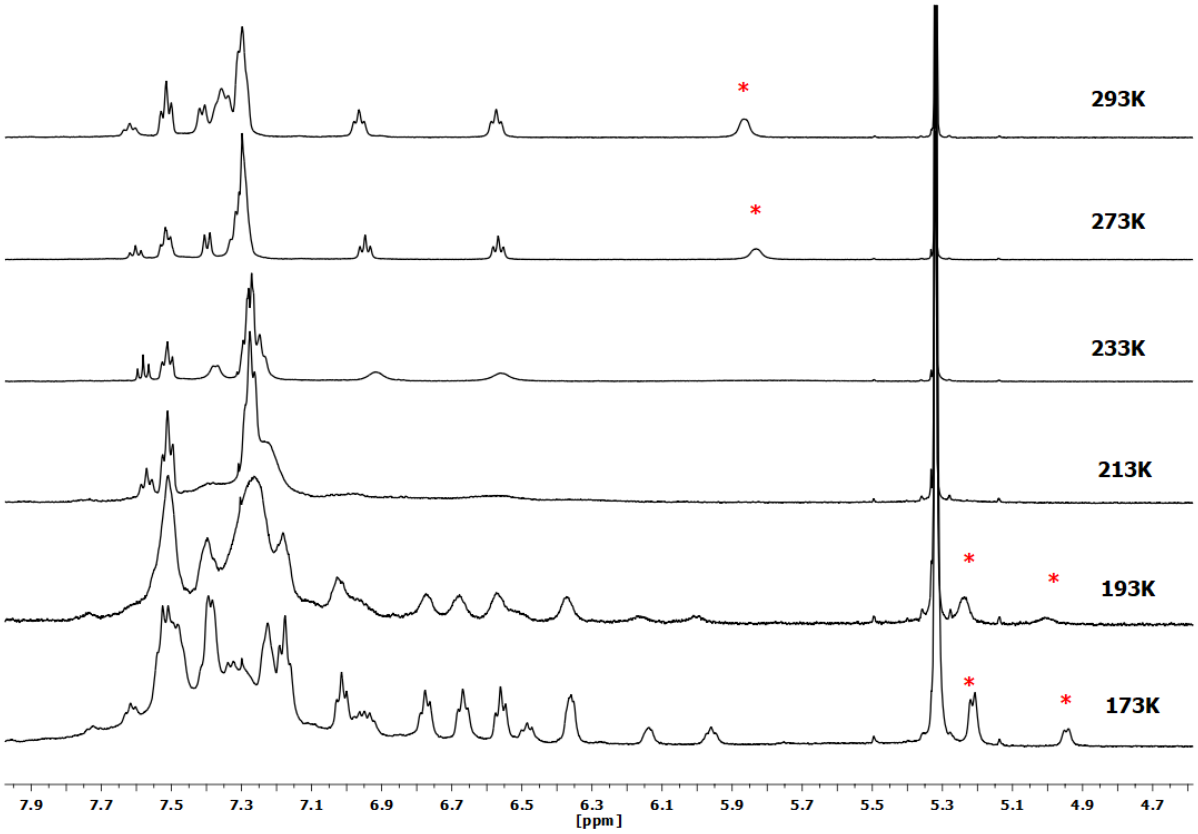

Figure S1.60. ^{1}H VT NMR (CD_2Cl_2) of complex [{Pd(CNC)(PPh_3)}$_2$Ag](ClO_4) (**9**).

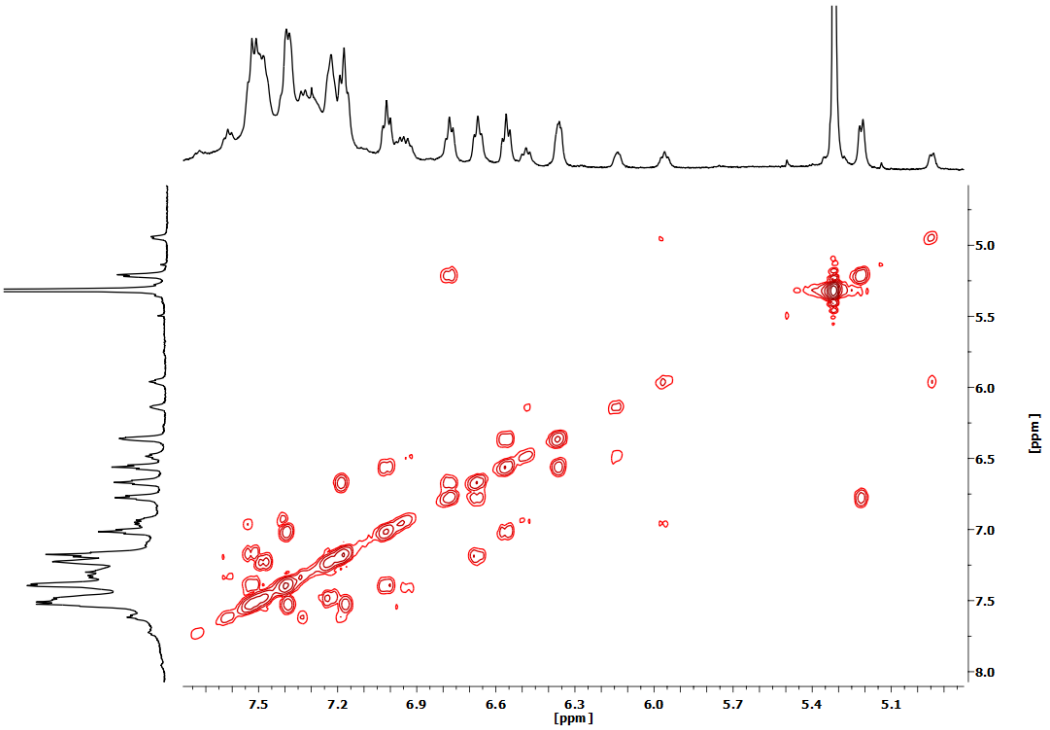

Figure S1.61. ^{1}H-^{1}H COSY NMR (CD_2Cl_2, 173K) of complex [{Pd(CNC)(PPh_3)}$_2$Ag](ClO_4) (**9**).

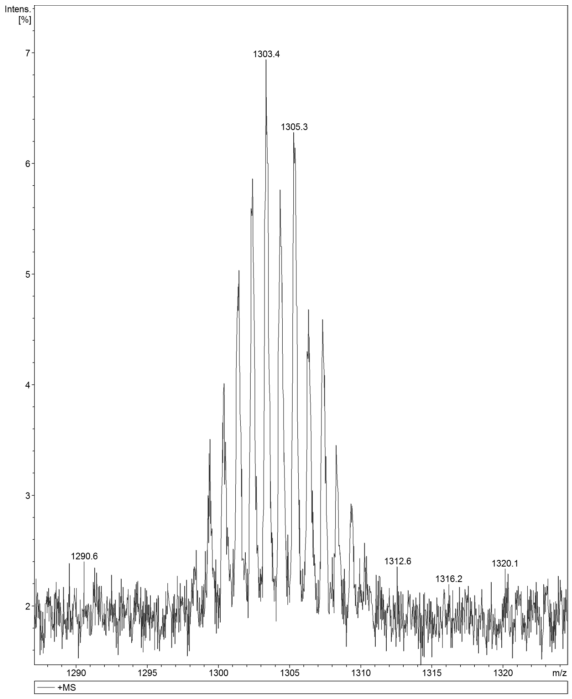

Figure S1.62. MS (MALDI+ DCTB) molecular peak of complex [{Pd(CNC)(PPh_3)}$_2$Ag](ClO_4) (**9**).

2.9. Spectra of mixture 10*.

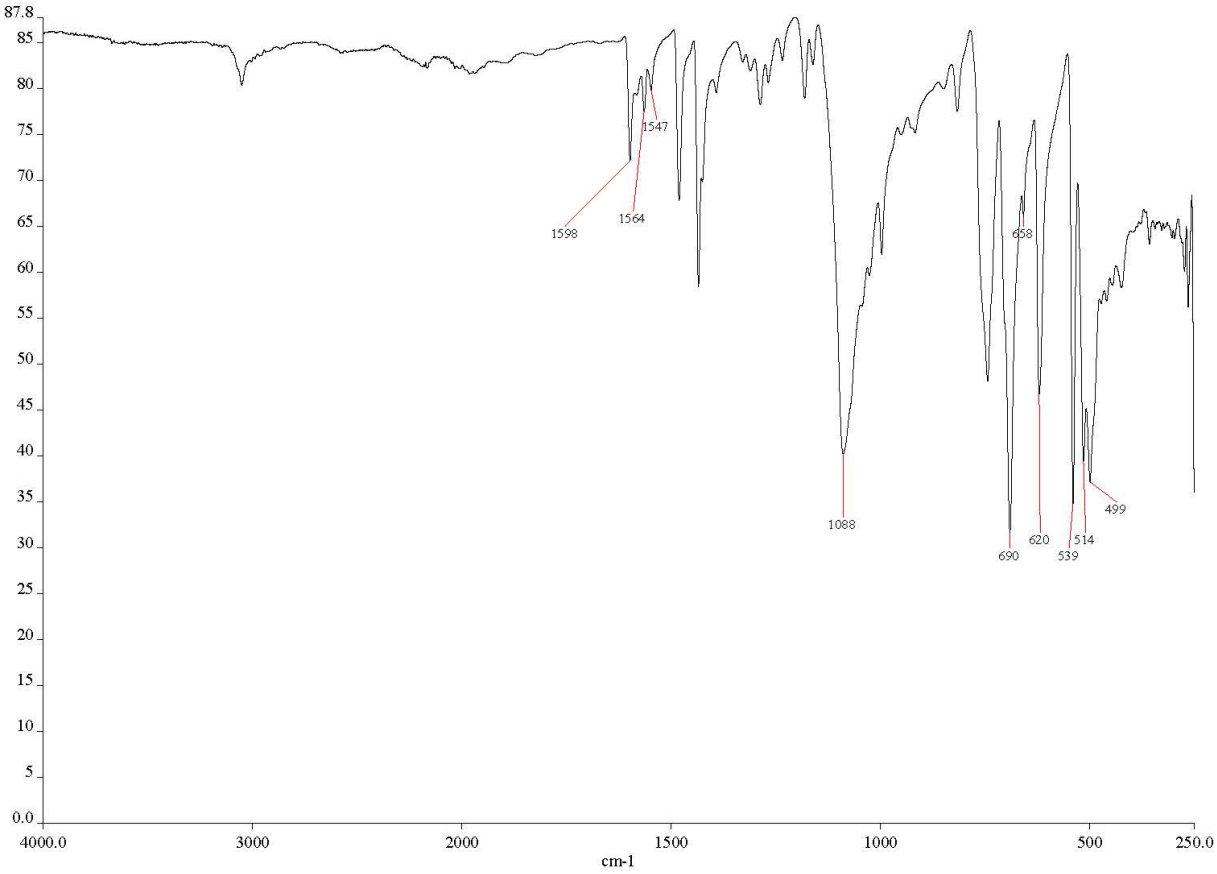

Figure S1.63. IR spectrum of mixture **10***.

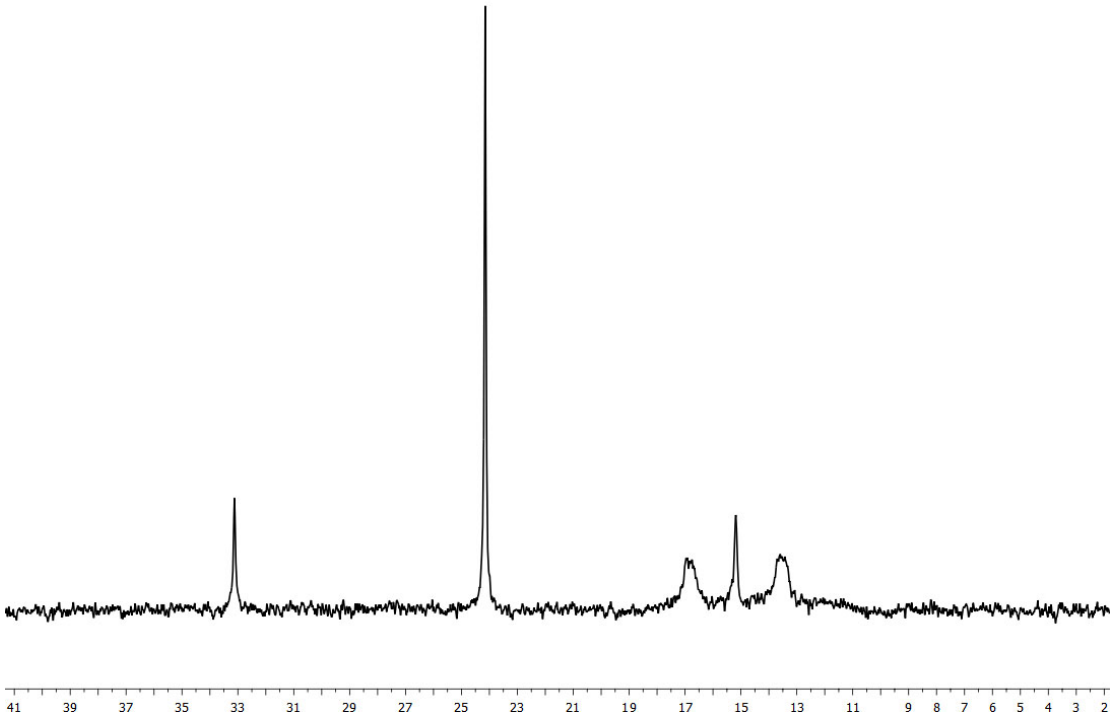

Figure S1.64. $^{31}P\{^{1}H\}$ NMR spectrum (CD_2Cl_2, 293K) of mixture **10***.

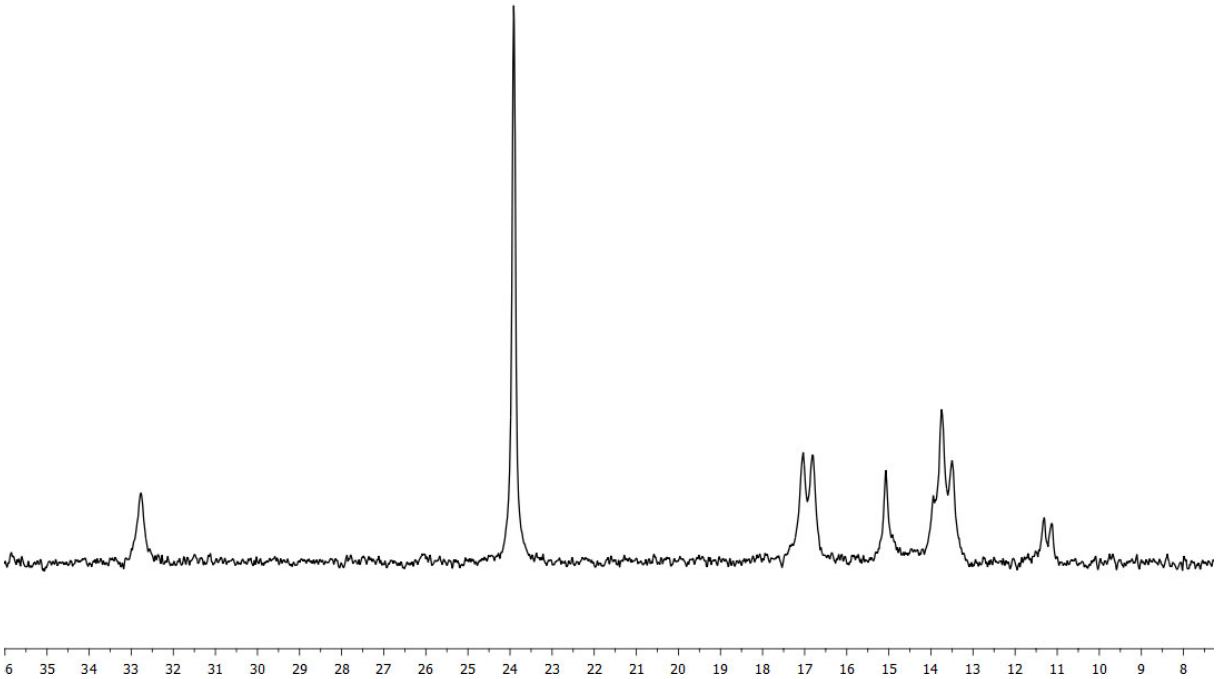

Figure S1.65. $^{31}P\{^{1}H\}$ NMR spectrum (CD_2Cl_2, 243K) of mixture **10***.

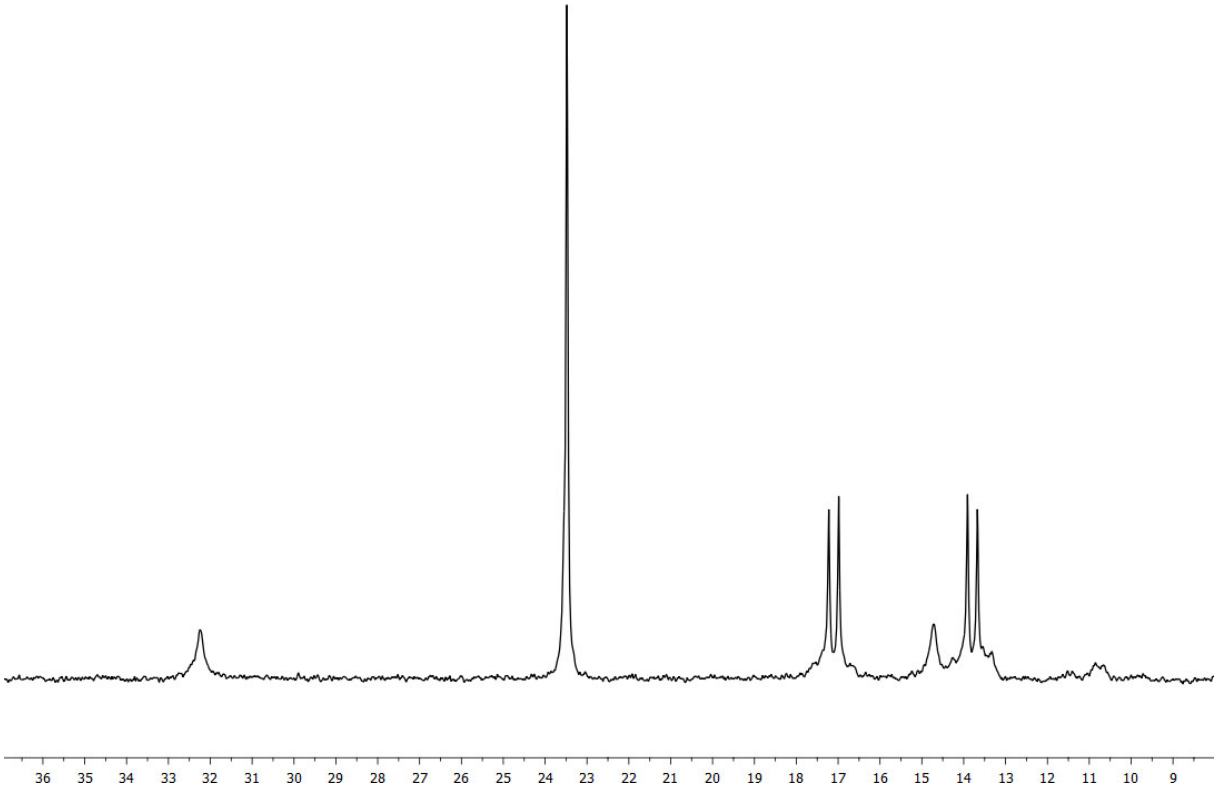

Figure S1.66. $^{31}P\{^{1}H\}$ NMR spectrum (CD_2Cl_2,183K) of mixture **10***.

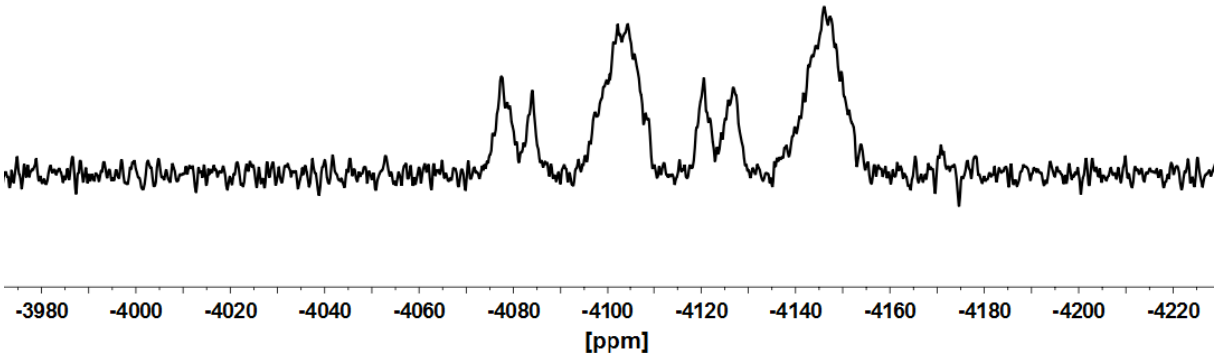

Figure S1.67. $^{195}Pt\{^{1}H\}$ NMR spectrum (CD_2Cl_2, 293K) of mixture **10***.

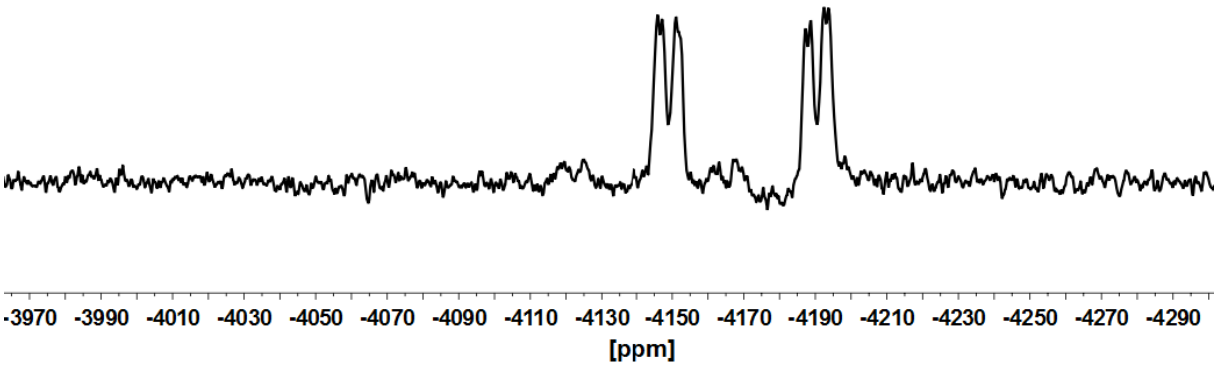

Figure S1.68. $^{195}Pt\{^{1}H\}$ NMR spectrum (CD_2Cl_2,193K) of mixture **10***.

.

2.10. Spectra of mixture 11*.

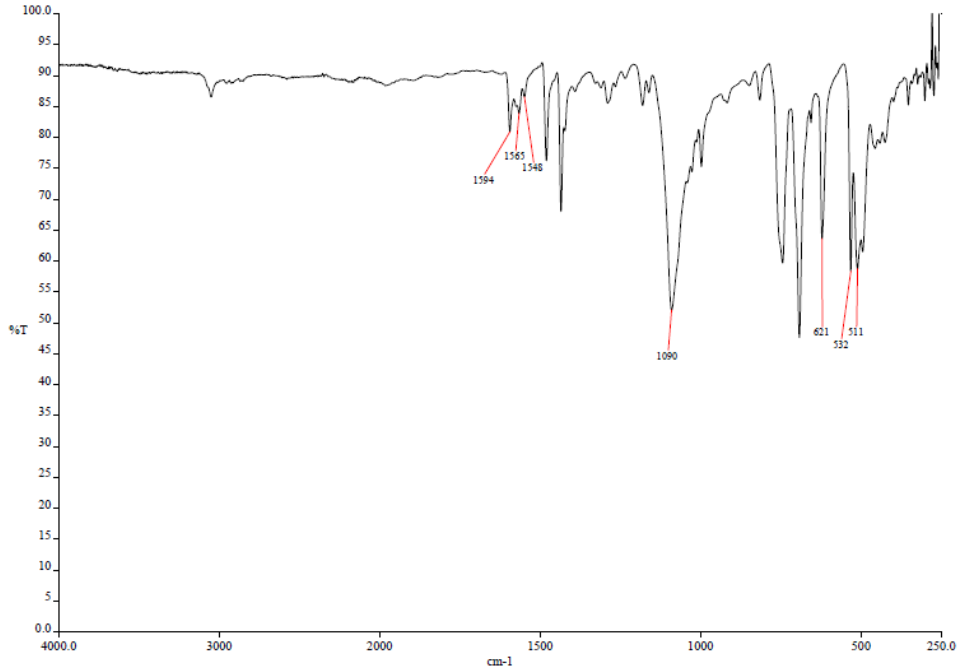

Figure S1.69. IR spectrum of mixture **11***.

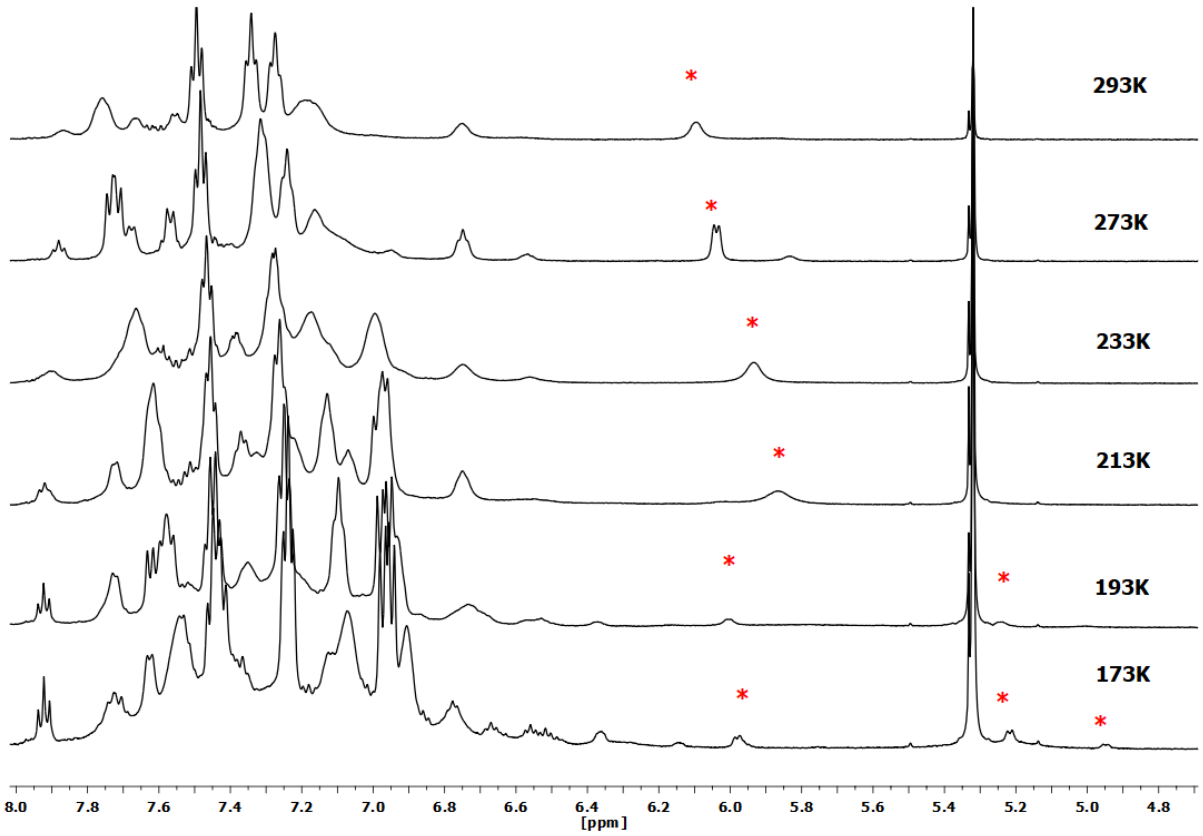

Figure S1.70. ^{1}H VT NMR spectra (CD_2Cl_2) of mixture **11***.

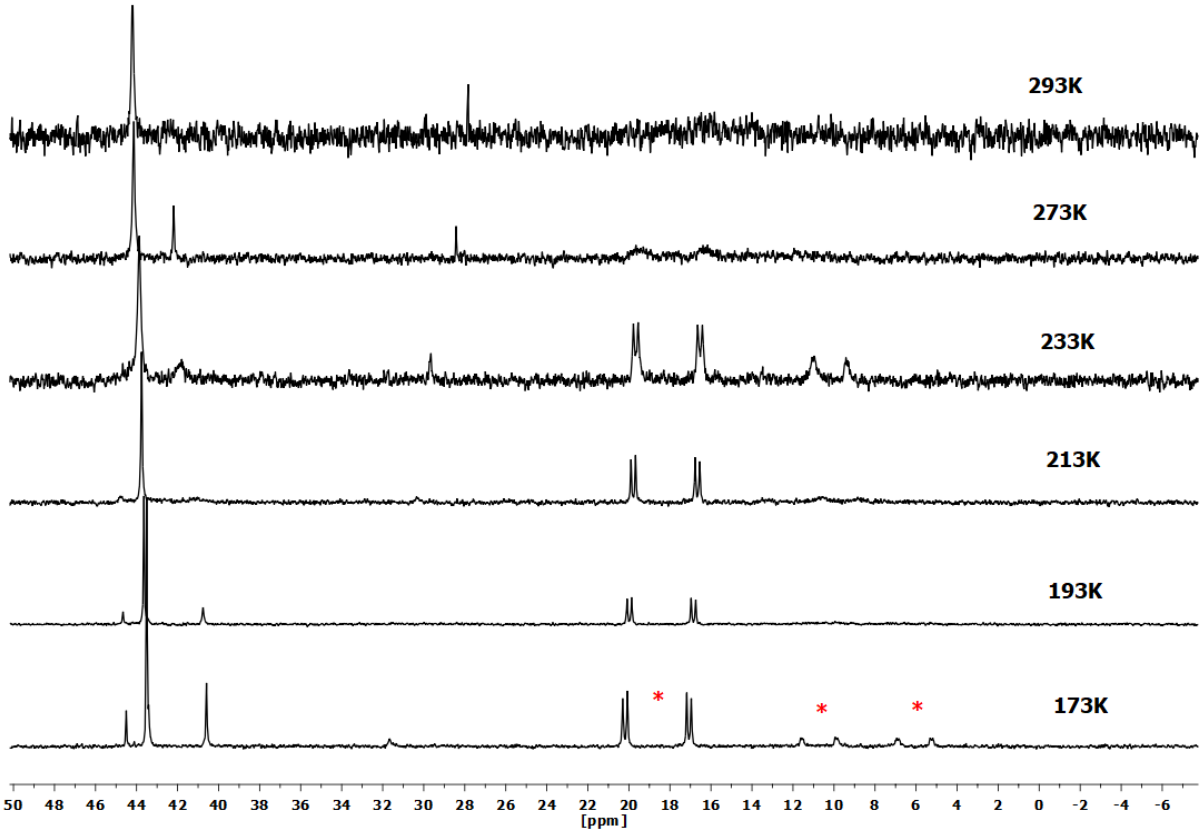

Figure S1.71. $^{31}P\{^{1}H\}$ VT NMR spectra (CD_2Cl_2) of mixture **11***.

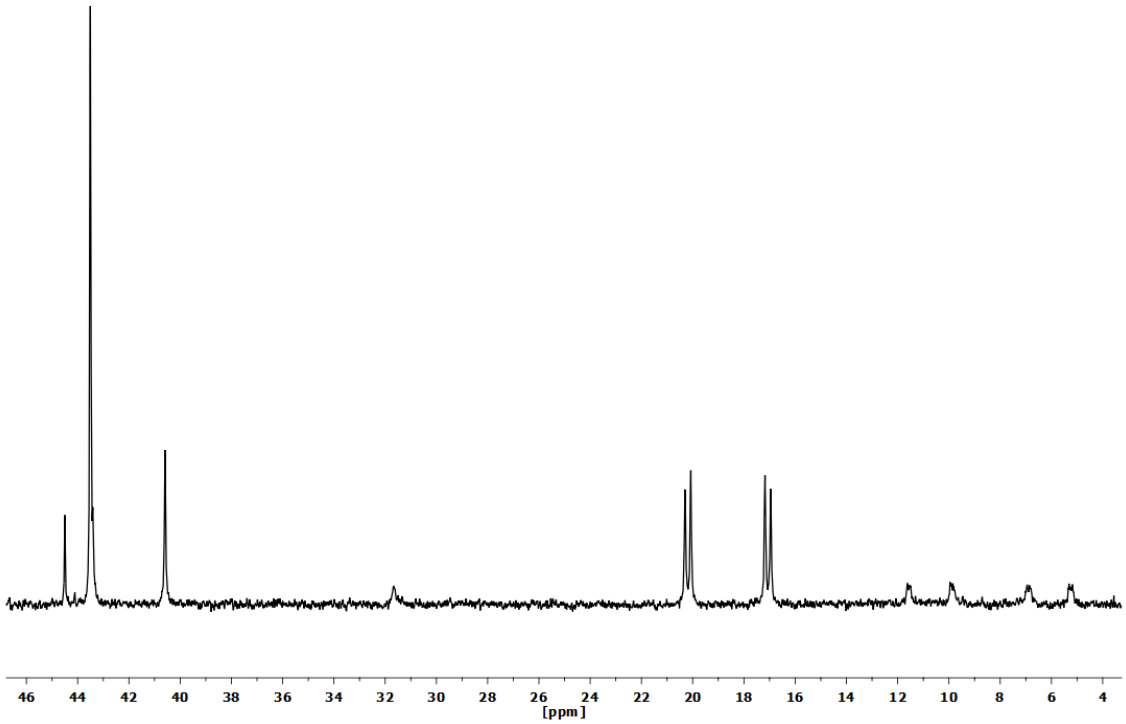

Figure S1.72. $^{31}P\{^{1}H\}$ NMR spectrum (CD_2Cl_2, 173K) of mixture **11***.

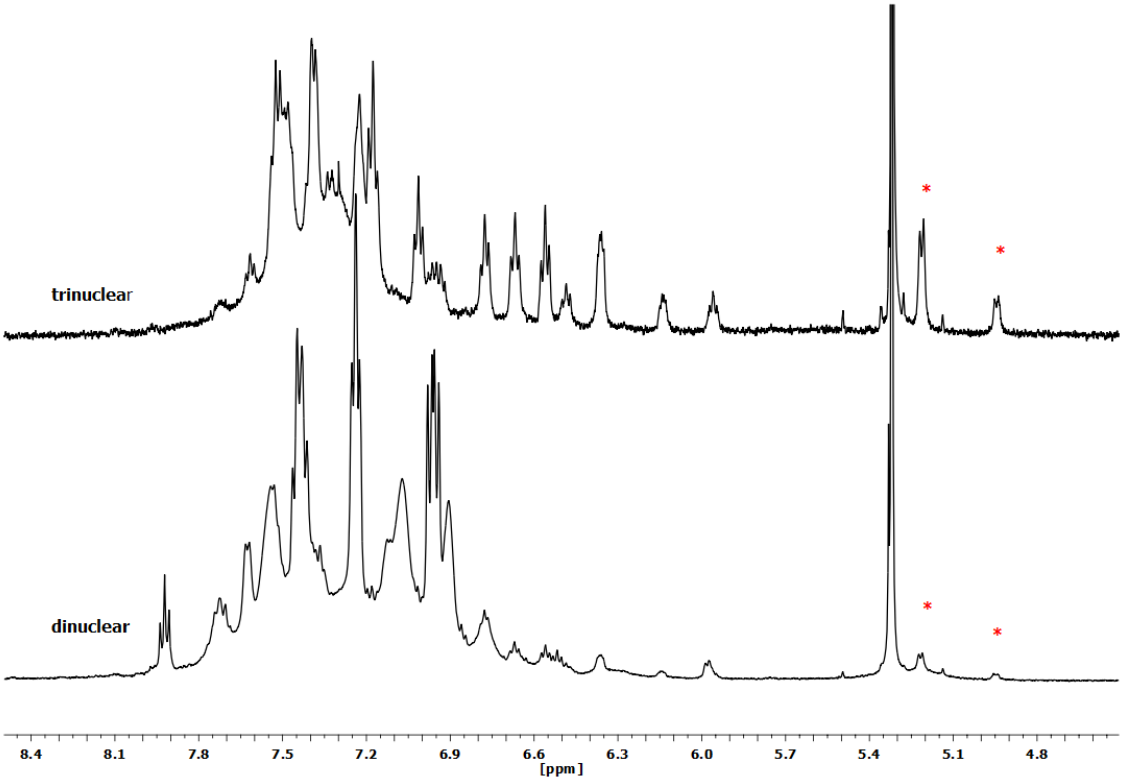

Figure S1.73. ^{1}H NMR spectra (CD_2Cl_2, 173K) comparison of [{Pd(CNC)(PPh_3)}$_2$Ag](ClO_4) (**9**) (above) and mixture **11*** (below).

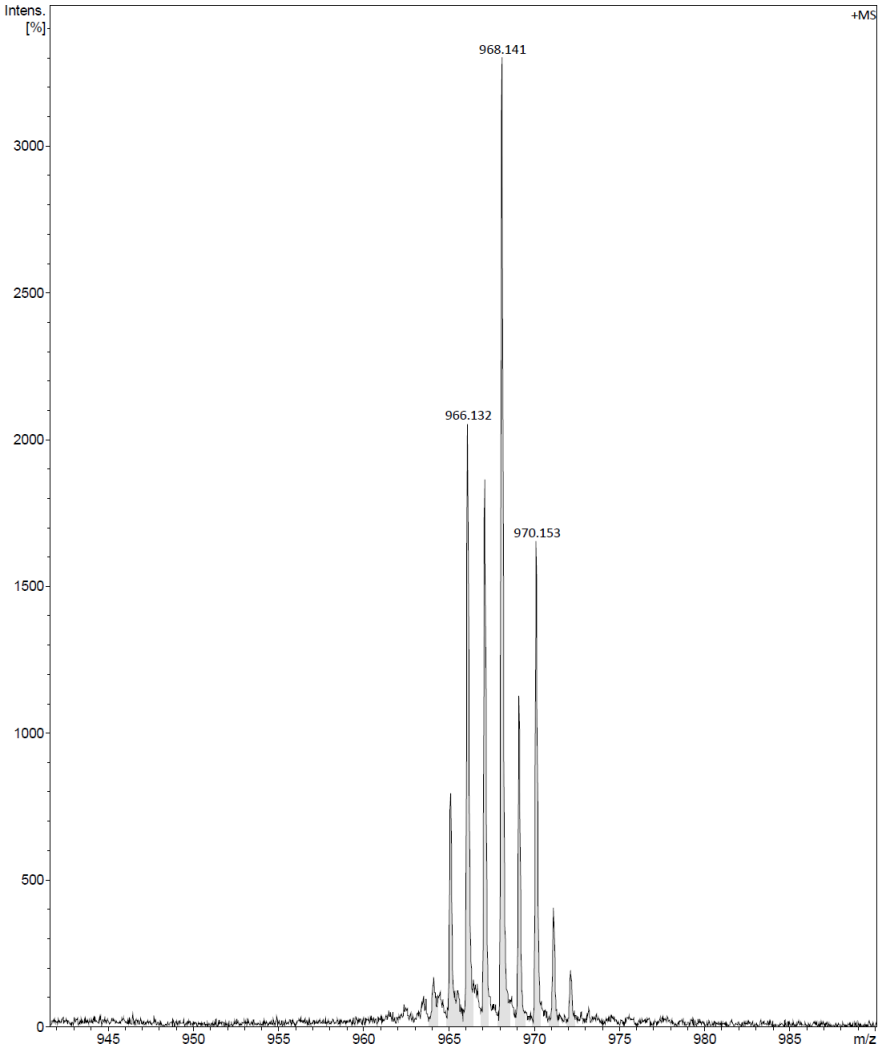

Figure S1.74. MS (MALDI+ DCTB) molecular peak of complex [(CNC)(PPh_3)PdAg(PPh_3)](ClO_4) (**11**).

3. Computational details

Density Functional Theory (DFT) calculations were carried out with the Gaussian 16 suite of programs,[3] using the BP-86 density functional[4] together with Grimme's D3 dispersion correction.[5] The ECP-60-mwb pseudopotential[6] was used for platinum and gold, the ECP-28-mwb pseudopotential was used for palladium and silver,[6] and the 6-31G(d)[7] basis set was used for all other atoms. Geometry optimizations were performed without any symmetry constraint, either in CH_2Cl_2 by using the solvation model based on density (SMD)[8] or in the gas phase. Stationary points were characterized by calculating the Hessian matrix analytically to confirm that all species are minima (no imaginary frequencies) or transition states (one single imaginary frequency) on the potential energy surface. The BP86-D3 optimized structures obtained were subsequently used for the following analyses: Wiberg Bond Indexes (WBI) were calculated by using the NBO analysis option as incorporated in Gaussian 16. Quantum Theory of the Atoms In Molecules (QTAIM) topological analyses of the electron densities were performed with the AIMAll package.[9] Energy Decomposition Analysis (EDA) studies were carried out with the Turbomole 7.1 program package,[10] using the same version of the functional BP86-D3 as implemented in Gaussian 16 and the def2-TZVP basis set.[11] Specifically, the generalized Kohn–Sham (GKS) scheme, i.e., GKS-EDA, was used, as implemented in the Turbomole package.[12] Atomic coordinates (x, y, z) for the optimized structures in the gas phase are included in a separate file (***DFT-chapter1.xyz***).

4. Comparison of relevant geometrical parameters obtained from the X-Ray structure determinations and DFT calculations.

Table S1.3. Comparison of some distances (Å) and angles (º) of for complexes **4, 6, 8** and **10** obtained from the X-Ray structure determinations (white columns) and DFT calculations (blue columns).

	[(CNC)(PPh_3)PtAu(PPh_3)] (ClO_4) (**4**)		[{Pt(CNC)(PPh_3)}$_2$Au](ClO_4) (**6**)		[{Pt(CNC)(PPh_3)}$_2$Ag](ClO_4) (**8**)		[(CNC)(PPh_3)PtAg(PPh_3)] (ClO_4) (**10**)	
M–M'	2.72221(2)	2.780	2.72965(2) 2.74259(2)	2.777 2.777	2.8549(3) 2.9078(3)	2.849 2.849	-	2.798
M–C_A	2.158(3)	2.255	2.212(3) 2.244(3)	2.244 2.243	2.128(3) 2.125(3)	2.165 2.165	-	2.177
M'–C_A	2.225(3)	2.208	2.174(3) 2.157(3)	2.177 2.177	2.277(3) 2.258(3)	2.236 2.237	-	2.246
M–C_B	2.063(3)	2.058	2.051(3) 2.045(3)	2.058 2.058	2.055(3) 2.056(3)	2.074 2.074	-	2.075
M–N	2.036(3)	2.067	2.035(3) 2.034(3)	2.066 2.066	2.020(3) 2.023(3)	2.059 2.059	-	2.064
M–P_M	2.2433(9)	2.275	2.2477(8) 2.2364(8)	2.275 2.275	2.2327(8) 2.2357(8)	2.274 2.274	-	2.275
M'–$P_{M'}$	2.2422(9)	2.294	-	-	-	-	-	2.351
C_A–M'–C_A	-	-	176.75(1)	176.53	173.96(1)	167.22	-	-
N–M–C_A	78.95(1)	78.05	78.64(1) 78.40(1)	77.84 77.85	79.28(1) 79.68(1)	78.63 78.63	-	78.66
N–M–C_B	80.04(1)	80.01	79.95(1)	79.80	80.38(1)	79.75	-	79.93

			80.27(1)	79.81	80.07(1)	79.75		
C_A–M–C_B	156.30(1)	157.44	155.99(1) 157.71(1)	155.23 155.22	158.13(1) 158.62(1)	155.25 155.25	-	157.70
174.66N–M–P_M	173.92(8)	175.68	176.31(8) 175.82(8)	175.31 175.31	175.31(8) 175.70(8)	174.91 174.91	-	174.66
M–M'–(P_M, or M)	152.38(2)	128.17	131.425(6)	123.74	126.834(9)	116.26	-	125.41
C_A–M'–(P_M, or M)	153.25(8)	172.34	121.70(9) 130.45(8)	125.80 125.81	129.80(8) 129.17(8)	122.94 122.97	-	171.32

Table S1.4. Comparison of some distances (Å) and angles (º) of for complexes **5, 7, 9, 11** obtained from the X-Ray structure determinations (white columns) and DFT calculations (blue columns).

	[(CNC)(PPh_3)PdAu(PPh_3)](ClO_4) (**5**)		[{Pd(CNC)(PPh_3)}$_2$Au](ClO_4) (**7**)		[{Pd(CNC)(PPh_3)}$_2$Ag](ClO_4) (**9**)		[(CNC)(PPh_3)PdAg(PPh_3)](ClO_4) (**11**)	
M–M'	2.7422(3)	2.755	2.7366(4) 2.7491(4)	2.746 2.746	2.8597(2) 2.9419(2)	2.772 2.811	-	2.753
M–C_A	2.393(3)	2.438	2.498(5) 2.419(5)	2.509 2.509	2.143(2) 2.164(2)	2.176 2.213	-	2.206
M'–C_A	2.119(3)	2.130	2.098(5) 2.108(5)	2.118 2.118	2.239(2) 2.212(2)	2.250 2.204	-	2.216
M–C_B	2.031(3)	2.036	2.020(5) 2.029(5)	2.028 2.028	2.072(2) 2.071(2)	2.072 2.065	-	2.067
M–N	2.033(2)	2.056	2.033(4) 2.041(4)	2.054 2.054	2.021(2) 2.026(2)	2.044 2.044	-	2.048
M–P_M	2.2646(8)	2.290	2.2686(14) 2.2717(13)	2.287 2.287	2.2578(6) 2.2473(6)	2.292 2.292	-	2.291
M'–$P_{M'}$	2.2736(8)	2.315	-	-	-	-	-	2.355
C_A–M'–C_A	-	-	175.2(2)	176.58	168.32(9)	171.61	-	-
N–M–C_A	77.18(11)	76.83	76.53(17) 77.44(18)	76.56 76.56	79.79(8) 79.45(8)	79.14 78.88	-	78.87
N–M–C_B	80.66(12)	80.59	80.79(19) 80.5(2)	80.69 80.70	80.29(8) 80.70(9)	80.46 79.90	-	80.36
C_A–M–C_B	157.68(12)	157.24	157.3(2)	157.25	159.25(9)	158.87	-	158.57

			157.9(2)	157.25	158.74(9)	155.96		
N–M–P_M	176.01(8)	177.00	173.47(12) 174.62(12)	175.49 175.50	176.15(6) 174.00(6)	177.55 175.21	-	173.58
M–M'–(P_M, or M)	127.87(2)	124.20	128.66(1)	123.92	132.77(1)	120.01	-	126.33
C_A–M'–(P_M, or M)	173.82(8)	176.90	125.83(14) 120.26(13)	121.37 121.37	124.21(6) 129.30(6)	122.42 126.90	-	172.94

Table S1.5. Some geometrical parameters used as descriptors for the structures of the complexes described in this chapter. Distances are given in Å and angles and dihedral angles in degrees. The nomenclature used for the atoms is represented in the scheme below.

	[(CNC)(PPh$_3$)MM'(PPh$_3$)](ClO$_4$)				**[{M(CNC)(PPh$_3$)}$_2$M'](ClO$_4$)**			
	M = Pd, M' = Ag (**11-DFT**) (a)	M = Pt, M' = Ag (**10-DFT**) (a)	M = Pd, M' = Au (**5**) (b)	M = Pt, M' = Au(**4**) (b)	M = Pd, M' = Ag (**9**) (b)	M = Pt, M' = Ag (**8**) (b)	M = Pd, M' = Au (**7**) (b)	M = Pt, M' = Au (**6**) (b)
M–M'	2.753	2.798	2.7422(3)	2.7222(2)	2.8597(2) 2.9419(2)	2.8549(3) 2.9078(3)	2.7366(4) 2.7491(4)	2.7297(2) 2.7426(2)
M–C$_A$	2.206	2.177	2.393(3)	2.158(3)	2.143(2) 2.164(2)	2.128(3) 2.125(3)	2.498(5) 2.419(5)	2.212(3) 2.244(3)
M'–C$_A$	2.216	2.246	2.119(3)	2.225(3)	2.239(2) 2.212(2)	2.277(3) 2.258(3)	2.098(5) 2.108(5)	2.174(3) 2.157(3)
M–C$_B$	2.067	2.075	2.031(3)	2.063(3)	2.072(2) 2.071(2)	2.055(3) 2.056(3)	2.020(5) 2.029(5)	2.051(3) 2.045(3)
C$_A$–M'–C$_A$	-	-	-	-	168.32(9)	173.96(12)	175.2(2)	176.75(12)
C$_C$–C$_A$-M	157.7	163.0	140.7	160.45	160.9 162.4	164.2 165.6	135.5 131.0	153.7 152.0
C$_C$–C$_A$-M'	123.2	115.7	143.1	120.1	111.7 111.2	110.7 106.3	149.3 156.0	127.5 128.9
M–M'–(P or M)	126.3	125.4	127.87(2)	152.38(2)	132.77(1)	126.83(1)	128.66(1)	131.43(1)
M plane–N ring plane	13.2	11.5	12.7(1)	13.2(1)	7.8(1) 8.0(1)	11.5(1) 9.8(1)	8.8(1) 6.1(1)	11.4(1) 12.8(1)
M plane–C$_A$ ring plane	25.1	20.2	38.9 (1)	27.7(1)	18.7(1) 24.1(1)	18.9(1) 15.4(1)	48.1(1) 43.0(1)	28.9(1) 31.9(1)

M plane– C_B ring plane	13.3	11.0	12.9(1)	11.4(1)	11.1(1) 4.1(1)	13.3(1) 11.5(1)	6.4(1) 4.0(1)	12.5(1) 10.4(1)
M plane– M plane	-		-	-	4.3(1)	0.6(1)	8.8(1)	4.0(1)

(a) DFT structure, DFT/BP86-D3 level, gas phase. (b) X-Ray structure. M plane = MC_BNP.

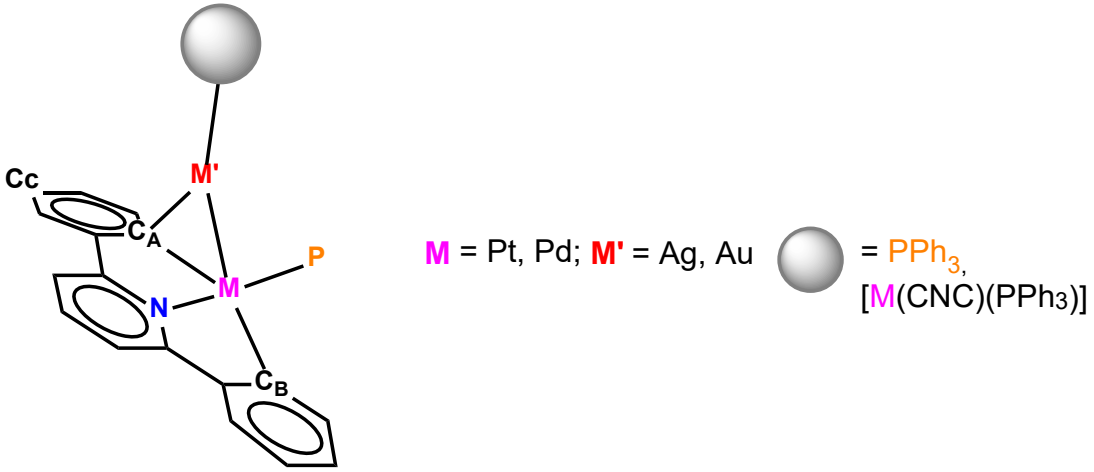

5. QTAIM analyses (DFT/BP86-D3 level, gas phase) of the heteropolynuclear complexes.

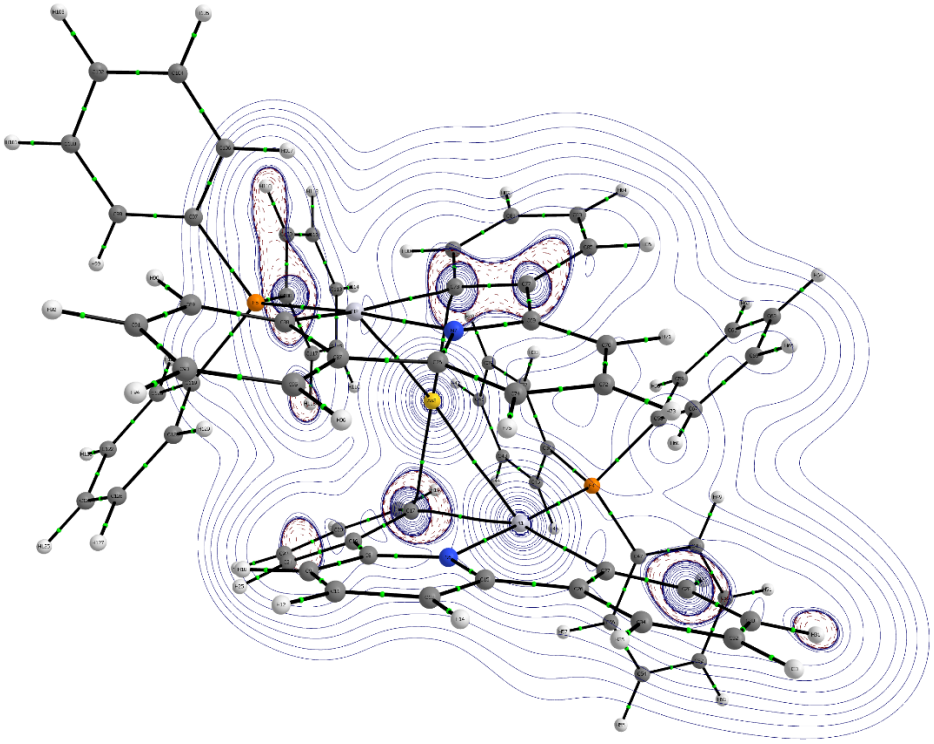

a)

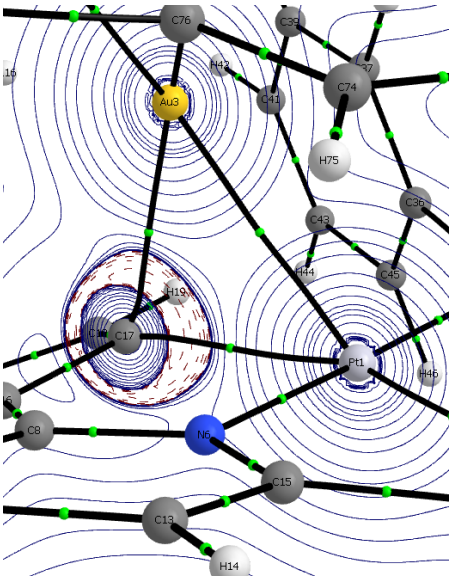

b)

Figure S1.75. Contour line diagrams $\nabla^2\rho(r)$ for the cation of complex **6-DFT** in the Au–C–Pt plane (solid lines connecting nuclei: Bond Paths; green dots: Bond Critical Points) (a). Detail of the complex core (b).

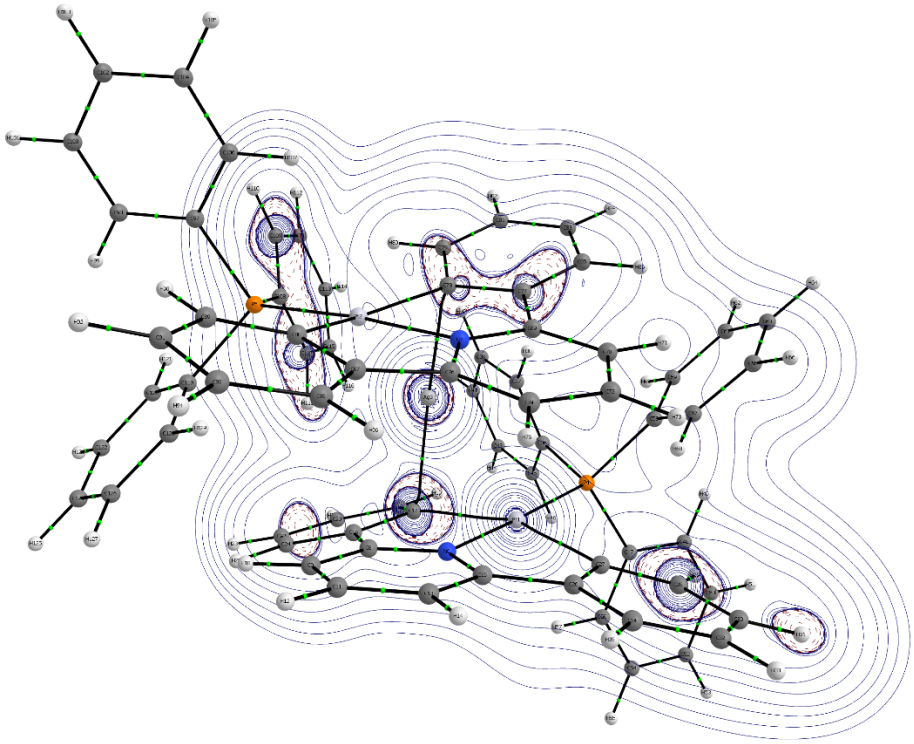

a)

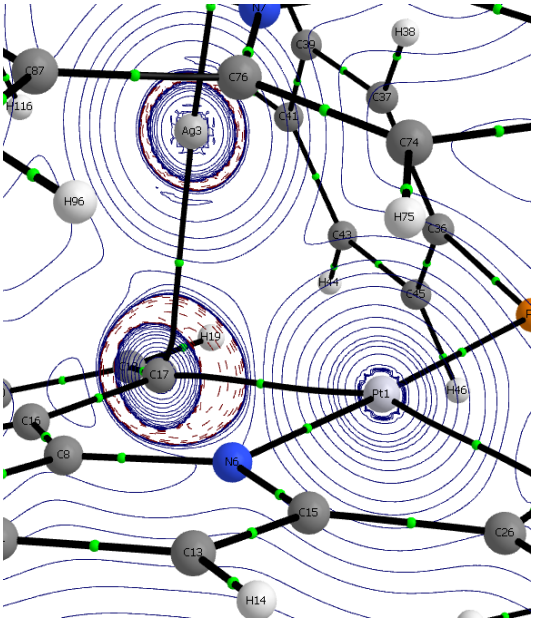

b)

Figure S1.76. Contour line diagrams $\nabla^2\rho(r)$ for the cation of complex **8-DFT** in the Ag–C–Pt plane (solid lines connecting nuclei: Bond Paths; green dots: Bond Critical Points) (a). Detail of the complex core (b).

Table S1.6. Topological characteristics of selected critical points in complexes **4-DFT** and **10-DFT**.

BCP (A-B)	4-DFT - Pt-Au			
	Pt-Au	**Pt-C_A**	**Pt-C_B**	**C_A-Au**
***ρ*(r) (au)**	0.049	0.087	0.133	0.090
$\nabla^2\rho$(r)	0.123	0.136	0.139	0.142
Ellipt	0.545	0.130	0.062	0.104
BL (Å)	2.78	2.26	2.06	2.21
BPL (Å)	2.78	2.26	2.06	2.21
***G*(r) (au)**	0.040	0.063	0.097	0.067
***V*(r) (au)**	-0.048	-0.092	-0.159	-0.098
***H*(r) (au)**	-0.008	-0.029	-0.062	-0.031
***G*(r)/*ρ*(r)**	0.81	0.72	0.73	0.74
BCP (A-B)	**10-DFT - Pt-Ag**			
	Pt-Ag	**Pt-C_A**	**Pt-C_B**	**C_A-Ag**
***ρ*(r) (au)**	-	0.104	0.130	0.071
$\nabla^2\rho$(r)	-	0.154	0.149	0.156
Ellipt	-	0.099	0.056	0.158
BL (Å)	2.80	2.18	2.08	2.25
BPL (Å)	-	2.18	2.07	2.26
***G*(r) (au)**	-	0.078	0.096	0.057
***V*(r) (au)**	-	-0.118	-0.154	-0.076
***H*(r) (au)**	-	-0.040	-0.058	-0.019
***G*(r)/*ρ*(r)**	-	0.75	0.74	0.80

Table S1.7. Topological characteristics of selected critical points in complexes **6-DFT** and **8-DFT**.

BCP (A-B)	6-DFT - Pt-Au-Pt							
	Pt-Au	**Pt-Au**	**Pt-C_A**	**Pt-C_A**	**Pt-C_B**	**Pt-C_B**	**C_A-Au**	**C_A-Au**
***ρ*(r) (au)**	0.050	0.050	0.090	0.090	0.134	0.134	0.095	0.095
$\nabla^2\rho$(r)	0.123	0.123	0.133	0.133	0.142	0.142	0.145	0.145
Ellipt	0.731	0.734	0.118	0.118	0.051	0.051	0.094	0.094
BL (Å)	2.78	2.78	2.24	2.24	2.06	2.06	2.18	2.18
BPL (Å)	2.78	2.78	2.25	2.25	2.06	2.06	2.18	2.18
***G*(r) (au)**	0.040	0.040	0.064	0.064	0.097	0.097	0.071	0.071
***V*(r) (au)**	-0.049	-0.049	-0.095	-0.095	-0.160	-0.160	-0.107	-0.107
***H*(r) (au)**	-0.009	-0.009	-0.031	-0.031	-0.063	-0.063	-0.036	-0.036
***G*(r)/*ρ*(r)**	0.80	0.80	0.71	0.71	0.72	0.72	0.75	0.75
BCP (A-B)	8-DFT - Pt-Ag-Pt							
	Pt-Ag	**Pt-Ag**	**Pt-C_A**	**Pt-C_A**	**Pt-C_B**	**Pt-C_B**	**C_A-Ag**	**C_A-Ag**
***ρ*(r) (au)**	-	-	0.107	0.107	0.130	0.130	0.072	0.072
$\nabla^2\rho$(r)	-	-	0.153	0.153	0.151	0.151	0.158	0.158
Ellipt	-	-	0.089	0.089	0.047	0.047	0.140	0.140
BL (Å)	2.85	2.85	2.17	2.17	2.07	2.07	2.24	2.24
BPL (Å)	-	-	2.17	2.17	2.07	2.07	2.25	2.25
***G*(r) (au)**	-	-	0.080	0.080	0.096	0.096	0.059	0.059
***V*(r) (au)**	-	-	-0.121	-0.121	-0.155	-0.155	-0.078	-0.078
***H*(r) (au)**	-	-	-0.041	-0.041	-0.059	-0.059	-0.019	-0.019
***G*(r)/*ρ*(r)**	-	-	0.75	0.75	0.74	0.74	0.82	0.82

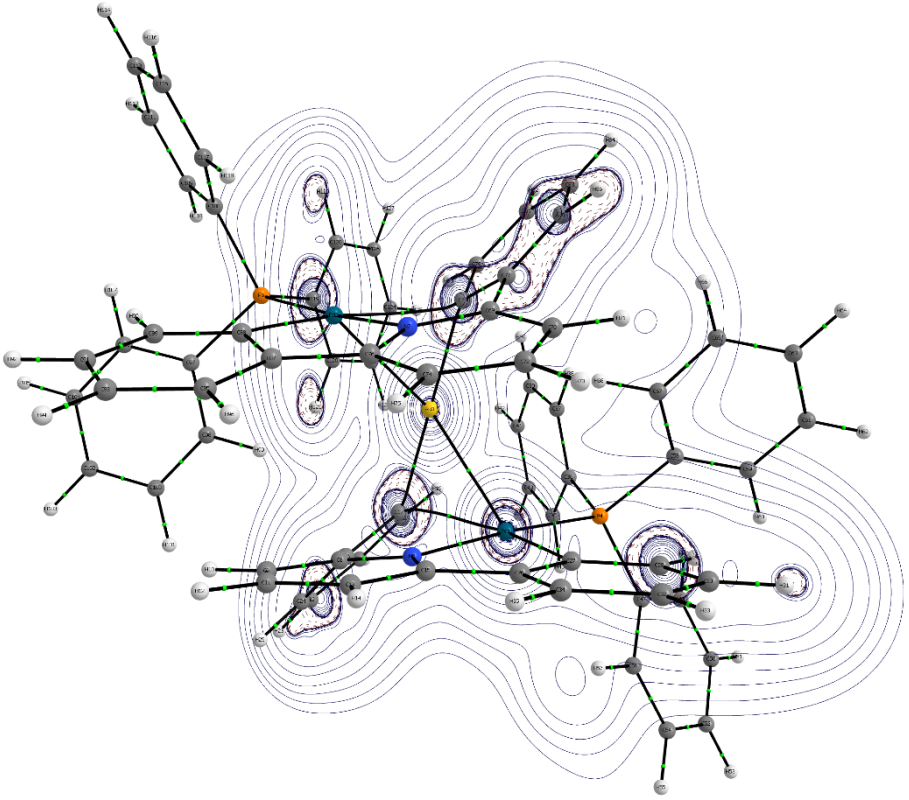

a)

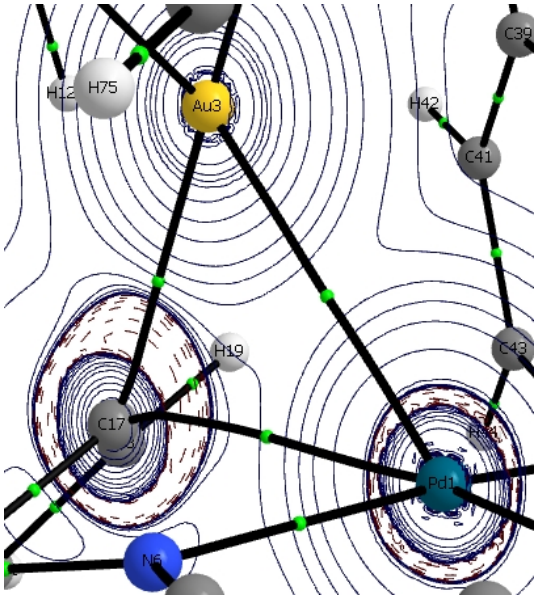

b)

Figure S1.77. Contour line diagrams $\nabla^2\rho(r)$ for the cation of complex **7-DFT** in the Au–C–Pd plane (solid lines connecting nuclei: Bond Paths; green dots: Bond Critical Points) (a). Detail of the complex core (b).

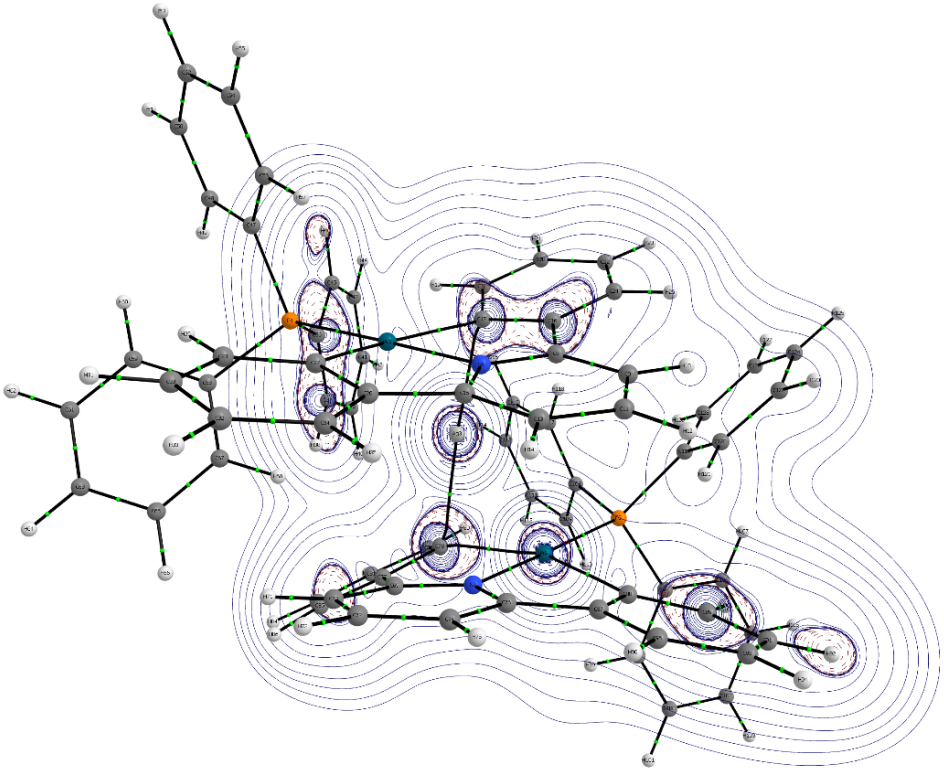

a)

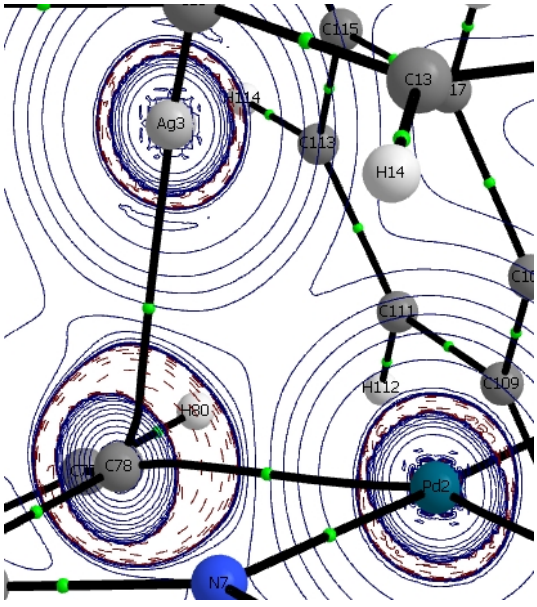

b)

Figure S1.78. Contour line diagrams $\nabla^2\rho(r)$ for the cation of complex **9-DFT** in the Ag–C–Pd plane (solid lines connecting nuclei: Bond Paths; green dots: Bond Critical Points) (a). Detail of the complex core (b).

Table S1.8. Topological characteristics of selected critical points in complexes **5-DFT** and **11-DFT**.

BCP (A-B)	5-DFT - Pd-Au			
	Pd-Au	**Pd-C_A**	**Pd-C_B**	**C_A-Au**
ρ**(r) (au)**	0.045	0.052	0.124	0.110
$\nabla^2\rho$**(r)**	0.113	0.116	0.163	0.154
Ellipt	0.275	0.313	0.063	0.062
BL (Å)	2.76	2.44	2.04	2.13
BPL (Å)	2.76	2.45	2.04	2.13
***G*(r) (au)**	0.036	0.038	0.091	0.082
***V*(r) (au)**	-0.044	-0.047	-0.142	-0.126
***H*(r) (au)**	-0.008	-0.009	-0.050	-0.044
***G*(r)/ρ(r)**	0.80	0.73	0.74	0.75
BCP (A-B)	**11-DFT - Pd-Ag**			
	Pd-Ag	**Pd-C_A**	**Pd-C_B**	**C_A-Ag**
ρ**(r) (au)**	-	0.086	0.117	0.077
$\nabla^2\rho$**(r)**	-	0.172	0.178	0.164
Ellipt	-	0.097	0.050	0.125
BL (Å)	2.75	2.21	2.07	2.21
BPL (Å)	-	2.21	2.07	2.23
***G*(r) (au)**	-	0.068	0.090	0.062
***V*(r) (au)**	-	-0.093	-0.135	-0.083
***H*(r) (au)**	-	-0.025	-0.045	-0.021
***G*(r)/ρ(r)**	-	0.79	0.76	0.81

Table S1.9. Topological characteristics of selected critical points in complexes **7-DFT** and **9-DFT**.

BCP (A-B)	7-DFT - Pd-Au-Pd							
	Pd-Au	**Pd-Au**	**Pd-C_A**	**Pd-C_A**	**Pd-C_B**	**Pd-C_B**	**C_A-Au**	**C_A-Au**
***ρ*(r) (au)**	0.046	0.046	0.046	0.046	0.126	0.126	0.113	0.113
$\nabla^2\rho$(r)	0.114	0.114	0.104	0.104	0.161	0.161	0.166	0.166
Ellipt	0.161	0.161	0.554	0.554	0.067	0.067	0.055	0.055
BL (Å)	2.75	2.75	2.51	2.51	2.00	2.00	2.12	2.12
BPL (Å)	2.75	2.75	2.53	2.53	2.03	2.03	2.12	2.12
***G*(r) (au)**	0.037	0.037	0.033	0.033	0.092	0.092	0.088	0.088
***V*(r) (au)**	-0.045	-0.045	-0.039	-0.039	-0.144	-0.144	-0.134	-0.134
***H*(r) (au)**	-0.008	-0.008	-0.006	-0.006	-0.052	-0.052	-0.046	-0.046
***G*(r)/*ρ*(r)**	0.80	0.80	0.71	0.71	0.73	0.73	0.78	0.78
BCP (A-B)	9-DFT - Pd-Ag-Pd							
	Pd-Ag	**Pd-Ag**	**Pd-C_A**	**Pd-C_A**	**Pd-C_B**	**Pd-C_B**	**C_A-Ag**	**C_A-Ag**
***ρ*(r) (au)**	-	-	0.085	0.092	0.118	0.116	0.079	0.071
$\nabla^2\rho$(r)		-	0.085	0.180	0.177	0.182	0.169	0.157
Ellipt	-	-	0.089	0.081	0.044	0.051	0.107	0.134
BL (Å)	2.77	2.81	2.18	2.21	2.07	2.06	2.25	2.20
BPL (Å)	-	-	2.22	2.18	2.07	2.07	2.21	2.26
***G*(r) (au)**	-	-	0.066	0.073	0.090	0.090	0.064	0.057
***V*(r) (au)**	-	-	-0.090	-0.101	-0.135	-0.134	-0.086	-0.075
***H*(r) (au)**	-	-	-0.024	-0.028	-0.045	-0.044	-0.022	-0.018
***G*(r)/*ρ*(r)**	-	-	0.78	0.80	0.76	0.77	0.82	0.81

6. References

(1) CrysAlis Pro 1.171.39.44a, Rigaku Oxford Diffraction **2018**.

(2) Sheldrick, G. M. *Acta Crystallogr.* **2015**, *A71*, 3-8.

(3) Frisch, M. J.; Trucks, G.W.; Schlegel, H. B.; Scuseria, G. E.; Robb, M. A.; Cheeseman, J. R.; Scalmani, G.; Barone, V.; Petersson, G. A.; Nakatsuji, H.; Li, X.; Caricato, M.; Marenich, A. V.; Bloino, J.; Janesko, B. G.; Gomperts, R.; Mennucci, B.; Hratchian, H. P.; Ortiz, J. V.; Izmaylov, A. F.; Sonnenberg, J. L.; Williams-Young, D.; Ding, F.; Lipparini, F.; Egidi, F.; Goings, J.; Peng, B.; Petrone, A.; Henderson, T.; Ranasinghe, D.; Zakrzewski, V. G.; Gao, J.; Rega, N.; Zheng, G.; Liang, W.; Hada, M.; Ehara, M.; Toyota, K.; Fukuda, R.; Hasegawa, J.; Ishida, M.; Nakajima, T.; Honda, Y.; Kitao, O.; Nakai, H.; Vreven, T.; Throssell, K.; Montgomery Jr., J. A.; Peralta, J. E.; Ogliaro, F.; Bearpark, M. J.; Heyd, J. J.; Brothers, E. N.; Kudin, K. N.; Staroverov, V. N.; Keith, T. A.; Kobayashi, R.; Normand, J.; Raghavachari, K.; Rendell, A. P.; Burant, J. C.; Iyengar, S. S.; Tomasi, J.; Cossi, M.; Millam, J. M.; Klene, M.; Adamo, C.; Cammi, R.; Ochterski, J. W.; Martin, R. L.; Morokuma, K.; Farkas, O.; Foresman, J. B.; Fox, D. J. *Gaussian 16 Rev. C.01*, Wallingford, CT, **2016**.

(4) a) Becke, D. *Phys. Rev. A* **1988**, *38*, 3098-3100. b) Perdew, J. P. *Phys. Rev. B* **1986**, *33*, 8822-8824.

(5) Grimme, S.; Antony, J.; Ehrlich, S.; Krieg, H. *J. Chem. Phys.* **2010**, *132*, 154104.

(6) Andrae, D.; Häußermann, U.; Dolg, M.; Stoll, H.; Preuß, H. *Theor. Chim. Acta* **1990**, *77*, 123−141.

(7) a) Ditchfield, R.; Hehre, W. J.; Pople, J. A. *J. Chem. Phys.* **1971**, *54,* 724-728. b) Hariharan, P. C.; Pople, J. A. *Theor. Chim. Acta* **1973**, *28*, 213-222.

(8) Marenich, A. V.; Cramer, C. J.; Truhlar, D. G. *J. Phys. Chem. B* **2009**, *113*, 6378-6396.

(9) Keith, T. A. 13.05.06 ed., AIMAII 2010. TK Gristmill Software, Overland Park KS, USA, **2010**.

(10) TURBOMOLE, Ver. 7.1 TURBOMOLE GmbH: Karlsruhe, Germany, **2016**.

(11) Weigend, F.; Ahlrichs, R. *Phys. Chem. Chem. Phys.* **2005**, 7, 3297−3305.

(12) a) Tang, Z.; Jiang, Z.; Chen, H.; Su, P.; Wu, W. *J. Chem. Phys.* **2019**, *151(24)*, *244106.* b) Su, P; Jiang, Z.; Chen, Z.; Wu, W. *J. Phys. Chem. A* **2014**, *118(13)*, 2531-2542.

Supporting Information

for

Chapter 2. Reactivity of platinum(II) and palladium(II) cyclometallated substrates toward sources of H^+.

1. Crystal data and structural refinement

Crystal data and other details of the structure analyses are presented in Tables S2.1, S2.2, S2.3 and S2.4. Suitable crystals for X-Ray diffraction studies were obtained by slow diffusion of *n*-hexane into concentrated solutions of the complexes in 3 mL of CH_2Cl_2. Crystals were mounted at the end of a quartz fibre. The radiation used in all cases was graphite monochromated Mo-K_α (λ = 71.073 pm). X-Ray intensity data were collected on an Oxford Diffraction Xcalibur diffractometer. The diffraction frames were integrated and corrected from absorption by using the CrysAlis RED program.[1] The structures were solved by Patterson and Fourier methods and refined by full-matrix least squares on F^2 with SHELXL.[2] All atoms were assigned anisotropic displacement parameters and refined without positional constraints. The positions of the H atoms were constrained to idealised geometries and assigned isotropic displacement parameters equal to 1.2 or 1.5 times the U_{iso} values of their respective parent atoms. Full-matrix least-squares refinement of the models against F^2 converged to final residual indices given in Tables S2.1, S2.2, S2.3 and S2.4.

Table S2.1. Crystal data and structure refinement for complexes [Pt(CNC-H)Cl(PPh_3)] (**13**), [Pt(CNC-H)Cl(dmso)] (**14**), [Pt(CNC-H)(MeCN)(PPh_3)](ClO_4) (**15**) and [Pd(CNC-H)(MeCN)(PPh_3)](ClO_4) (**16**).

	13	**14**	**15**	**16**
Formula	$C_{35}H_{27}ClNPPt$	$C_{19}H_{18}ClNOPtS$	$C_{37}H_{30}ClN_2O_4PPt$	$C_{37}H_{30}ClN_2O_4PPd$
M_t	723.08	538.94	828.14	739.45
Crystal system	monoclinic	monoclinic	triclinic	triclinic
Space group	*P2₁/c*	*P2₁/c*	*P-1*	*P-1*
a/Å	9.31510(1)	15.1106(2)	9.6378(3)	9.6825(8)
b/Å	32.4661(4)	7.33207(1)	10.3379(2)	10.3491(9)
c/Å	10.0041(2)	32.5266(4)	15.9509(3)	15.9544(1)
a/º	90	90	95.5802(2)	95.7980(1)
β/º	109.621(2)	95.6212(1)	98.606(2)	98.6970(1)
γ/º	90	90	93.6794(2)	93.5820(1)
V/Å^3	2849.81(8)	3586.35(9)	1558.92(6)	1567.3(2)

Z	4	8	2	2
D_c/g cm^{-3}	1.685	1.996	1.764	1.567
T/K	100(2)	293(2)	100(2)	296(2)
μ/mm^{-1}	5.099	8.096	4.683	0.773
F(000)	1416	2064	816	752
2θ range/^{o}	5.8-61.2	5.7-56.7	5.6-58.9	2.6-60.2
Collected reflections	70790	65955	27380	18125
Unique reflections	8312	8319	7591	8379
R_{int}	0.0348	0.0383	0.0591	0.0113
R_1, wR_2[a] ($I > 2\sigma(I)$)	0.0245, 0.0582	0.0241, 0.0485	0.0343, 0.0765	0.0198, 0.0512
R_1, wR_2[a] (all data)	0.0282, 0.0594	0.0280, 0.0496	0.0420, 0.0820	0.0210, 0.0520
GOF (F^2)[b]	1.098	1.118	1.036	1.005

[a] $R_1 = \sum(|F_o| - |F_c|) / \sum |F_o|$. $wR_2 = [\sum w (F_o^2 - F_c^2)^2 / \sum w(F_o^2)^2]^{1/2}$. [b] Goodness-of-fit = $[\sum w (F_o^2 - F_c^2)^2 / (n_{obs} - n_{param})]^{1/2}$.

Table S2.2. Crystal data and structure refinement for complexes [Pt(CNC-H)(H_2O)(PPh_3)](ClO_4) (**17**), [Pd(CNC-H)(H_2O)(PPh_3)](ClO_4) (**18**), [Pt(CNC-H)(tht)(PPh_3)](ClO_4)·CH_2Cl_2 (**19**·CH_2Cl_2) and [Pt(CNC-H)(μ-S-2Py)]$_2$·2CH_2Cl_2 (**21**·2CH_2Cl_2).

	17	**18**	**19**·CH_2Cl_2	**21**·2CH_2Cl_2
Formula	$C_{35}H_{29}ClNO_5PPt$	$C_{35}H_{29}ClNO_5PPd$	$C_{39}H_{35}ClNO_4PPtS$· CH_2Cl_2	$C_{44}H_{32}N_4Pt_2S_2$ ·2CH_2Cl_2
M_t	805.10	716.41	960.17	1240.89
Crystal system	triclinic	triclinic	monoclinic	orthorhombic
Space group	*P-1*	*P-1*	$P2_1/c$	$P2_12_12_1$
a/Å	9.47247(2)	9.4934(7)	9.27131(1)	10.35727(14)
b/Å	10.2602(2)	10.2710(8)	19.6874(2)	18.1281(3)
c/Å	15.8821(3)	15.8699(1)	20.5535(2)	22.4772(5)
a/º	94.1019(2)	94.1000(1)	90	90
β/º	98.3549(2)	98.4230(1)	94.4415(1)	90
γ/º	95.8330(2)	95.2610(1)	90	90

V/Å^3	1513.42(6)	1518.6(2)	3740.32(7)	4220.27(1)
Z	2	2	4	4
D_c/g cm^{-3}	1.767	1.567	1.705	1.953
T/K	100(2)	100(2)	100(2)	100(2)
μ/mm^{-1}	4.822	0.797	4.108	7.014
F(000)	792	728	1904	2384
2θ range/^{o}	5.6-58.8	2.6-60.2	5.4-61.2	5.8-61.2
Collected reflections	33455	17579	48344	32134
Unique reflections	7508	8128	10501	11436
R_{int}	0.0378	0.0103	0.0508	0.0338
R_1, wR_2[a] ($I > 2\sigma(I)$)	0.0208, 0.0433	0.0208, 0.0526	0.0304, 0.0683	0.0260, 0.0456
R_1, wR_2[a] (all data)	0.0234, 0.0442	0.0218, 0.0532	0.0389, 0.0732	0.0306, 0.0469
GOF (F^2)[b]	1.051	1.046	1.045	1.012

[a] $R_1 = \sum(|F_o| - |F_c|) / \sum |F_o|$. $wR_2 = [\sum w (F_o^2 - F_c^2)^2 / \sum w(F_o^2)^2]^{1/2}$. [b] Goodness-of-fit = $[\sum w (F_o^2 - F_c^2)^2 / (n_{obs} - n_{param})]^{1/2}$.

Table S2.3. Crystal data and structure refinement for complexes [Pt(CNC-H)(8-hq)]·0.5*n*-C_6H_{14} (**22**·0.5*n*-C_6H_{14}), [Pt(CNC-H){PPh_2(C_6H_4-*o*-O)}]·CH_2Cl_2 (**23**·CH_2Cl_2), [Pd(CNC-H){PPh_2(C_6H_4-*o*-O)}] (**24**·CH_2Cl_2), *trans*-(N,O)[Pt(CNC-H)(NC_5H_4-*o*-COO)] (**25A**·0.25CH_2Cl_2) and *trans*-(N,N)[Pt(CNC-H)(NC_5H_4-*o*-COO)]·1.5CH_2Cl_2 (**25B**·1.5CH_2Cl_2).

	22·0.5*n*-C_6H_{14}	**23**·CH_2Cl_2	**24**·CH_2Cl_2	**25A**·0.25CH_2Cl_2	**25B**·1.5CH_2Cl_2
Formula	$C_{26}H_{18}N_2OPt$	$C_{35}H_{26}NOPPt$	$C_{35}H_{26}NOPPd$	$C_{23}H_{16}N_2O_2Pt$	$C_{23}H_{16}N_2O_2Pt$
	0.5*n*-C_6H_{14}	·CH_2Cl_2	·CH_2Cl_2	·0.25CH_2Cl_2	·1.5CH_2Cl_2
M_t	612.60	787.55	698.86	568.70	1131.98(17)
Crystal system	monoclinic	monoclinic	monoclinic	triclinic	triclinic
Space group	*C2/c*	*P2₁/c*	*P2₁/c*	*P-1*	*P-1*
a/Å	33.0602(8)	8.4494(2)	8.44669(2)	10.97298(2)	9.8352(9)
b/Å	11.7636(2)	22.3359(5)	22.4058(4)	14.3885(2)	10.7295(9)
c/Å	12.5106(3)	16.3739(4)	16.3735(3)	24.9907(5)	12.7362(1)
a/º	90	90	90	74.1536(17)	68.6480(1)
β/º	105.879(2)	104.788(3)	104.4639(2)	85.2977(16)	71.3790(10)

γ/°	90	90	90	82.1657(14)	67.6590(10)
V/Å^3	4679.80(2)	2987.80(1)	3000.55(9)	3756.13(1)	1131.98(2)
Z	8	4	4	8	2
D_c/g cm^{-3}	1.739	1.751	1.547	2.011	1.980
T/K	100(2)	100(2)	293(2)	293(2)	100(2)
μ/mm^{-1}	6.021	4.960	0.881	7.565	6.578
F(000)	2392	1544	1416	2180	650
2θ range/°	8.4-57.6	6.0-61.2	6.0-56.8	5.4-56.6	3.4-60.2
Collected reflections	30123	22421	29156	71308	13049
Unique reflections	5656	8040	6565	16400	6042
R_{int}	0.0335	0.0264	0.0234	0.0462	0.0150
R_1, wR_2[a] ($I > 2\sigma(I)$)	0.0275, 0.0688	0.0236, 0.0522	0.0231, 0.0539	0.0352, 0.0811	0.0135, 0.0325
R_1, wR_2[a] (all data)	0.0347, 0.0726	0.0286, 0.0542	0.0269, 0.0557	0.0481, 0.0874	0.0143, 0.0328
GOF (F^2)[b]	1.040	1.029	1.033	1.056	1.046

[a] $R_1 = \sum(|F_o| - |F_c|) / \sum |F_o|$. $wR_2 = [\sum w (F_o^2 - F_c^2)^2 / \sum w(F_o^2)^2]^{1/2}$. [b] Goodness-of-fit = $[\sum w (F_o^2 - F_c^2)^2 / (n_{obs} - n_{param})]^{1/2}$.

Table S2.4. Crystal data and structure refinement for complexes [Pt(CNC-H){$PPh_2(C_6H_4$-*o*-COO)}]·CH_2Cl_2 (**26**·CH_2Cl_2) and [Pd(CNC-H){$PPh_2(C_6H_4$-*o*-COO)}]·CH_2Cl_2 (**27**·CH_2Cl_2).

	26·CH_2Cl_2	**27**·CH_2Cl_2
Formula	$C_{36}H_{26}NO_2PPt$	$C_{36}H_{26}NO_2PPd$
	·CH_2Cl_2	·CH_2Cl_2
M_t	815.56	726.87
Crystal system	monoclinic	monoclinic
Space group	*P2₁/n*	*P2₁/n*
a/Å	9.32842(2)	9.36969(2)
b/Å	16.0093(3)	15.9432(3)
c/Å	20.9697(4)	20.9922(4)
a/º	90	90
β/º	90.3715(2)	90.5995(2)
γ/º	90	90

V/Å^3	3131.58(9)	3135.70(9)
Z	4	4
D_c/g cm^{-3}	1.730	1.540
T/K	100(2)	293(2)
μ/mm^{-1}	4.738	0.849
F(000)	1600	1472
2θ range/^{o}	5.4-56.8	5.4-56.6
Collected reflections	30952	30607
Unique reflections	6772	6929
R_{int}	0.0405	0.0302
R_1, wR_2[a] ($I > 2\sigma(I)$)	0.0268, 0.0535	0.0271, 0.0600
R_1, wR_2[a] (all data)	0.0356, 0.0574	0.0330, 0.0629
GOF (F^2)[b]	1.028	1.057

[a] $R_1 = \sum(|F_o| - |F_c|) / \sum |F_o|$. $wR_2 = [\sum w (F_o^2 - F_c^2)^2 / \sum w(F_o^2)^2]^{1/2}$. [b] Goodness-of-fit = $[\sum w (F_o^2 - F_c^2)^2 / (n_{obs} - n_{param})]^{1/2}$.

2. IR, NMR and MS spectra of complexes

2.1. Spectra of complex [Pt(CNC-H)Cl(PPh$_3$)] (13).

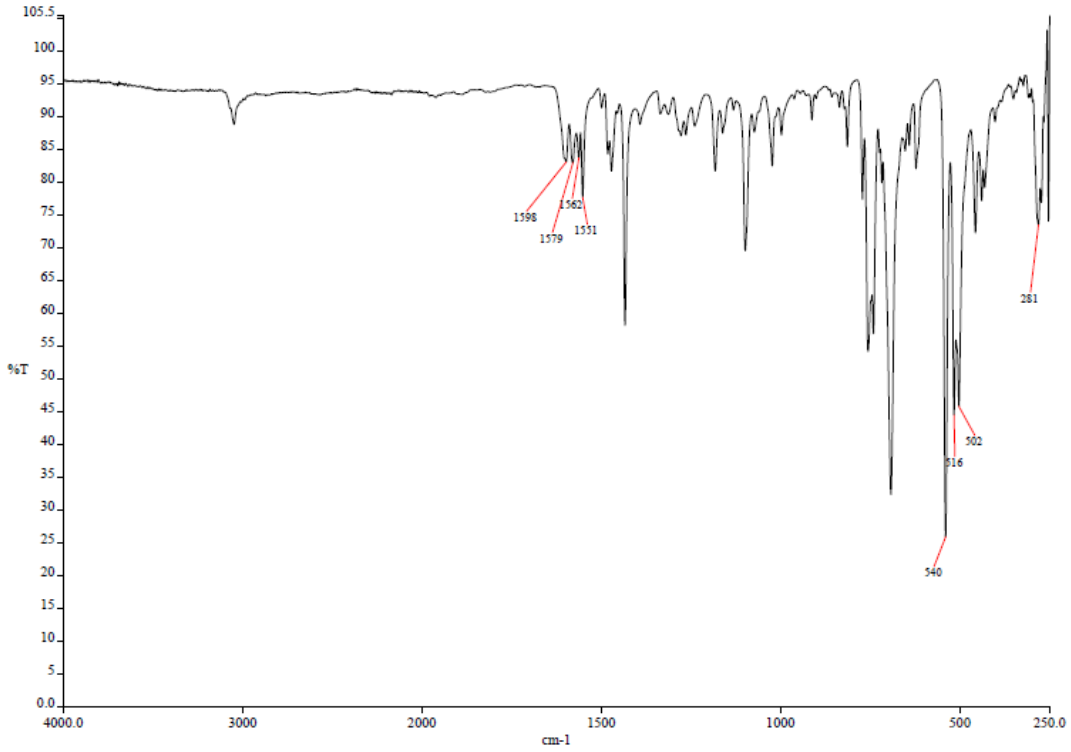

Figure S2.1. IR spectrum of complex [Pt(CNC-H)Cl(PPh$_3$)] (**13**).

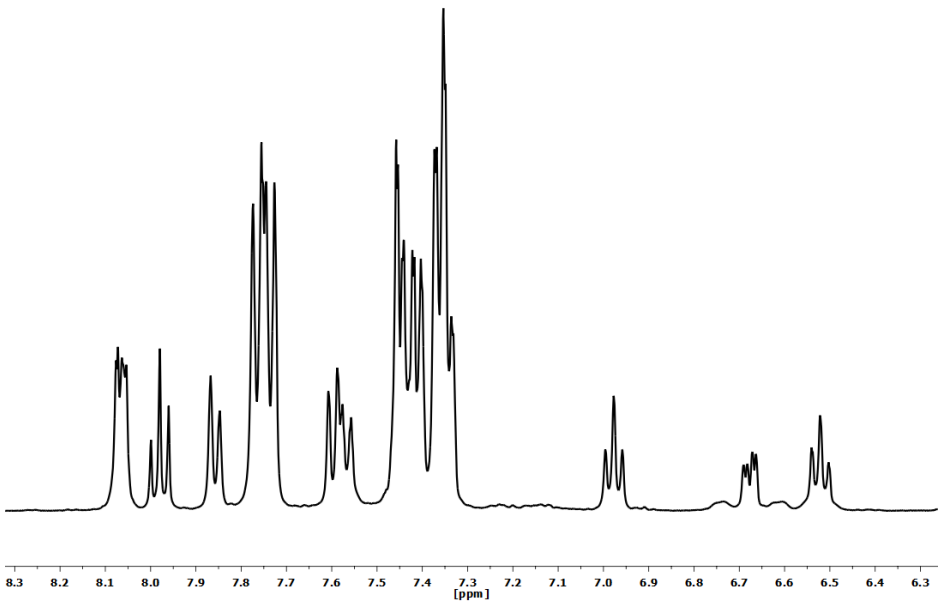

Figure S2.2. ^{1}H NMR spectrum (CD_2Cl_2, RT) of complex [Pt(CNC-H)Cl(PPh$_3$)] (**13**).

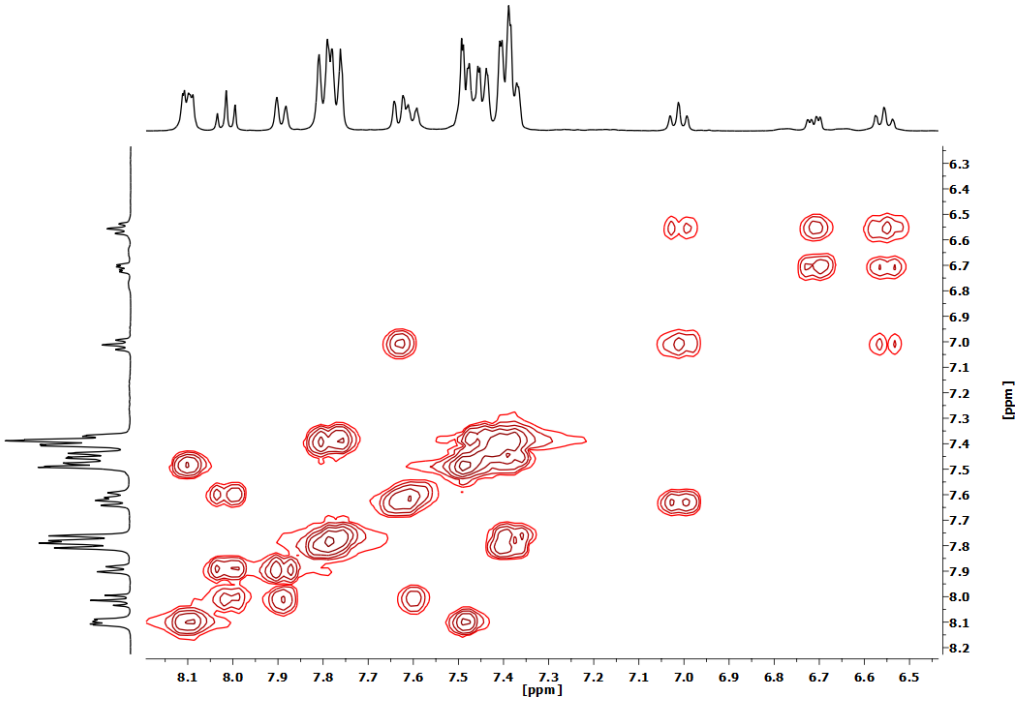

Figure S2.3. ^{1}H-^{1}H COSY NMR spectrum (CD_2Cl_2, RT) of complex [Pt(CNC-H)Cl(PPh_3)] (**13**).

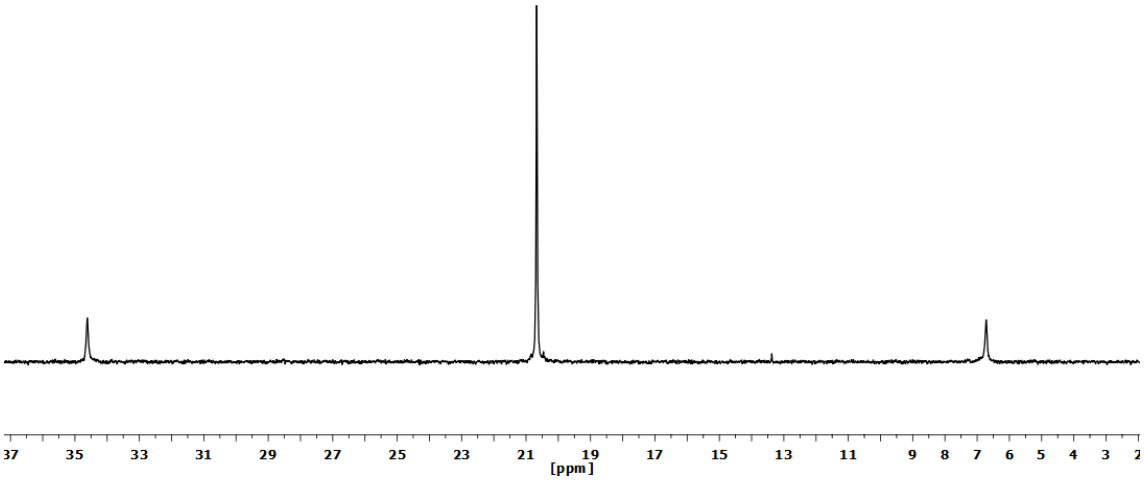

Figure S2.4. ^{31}P{^{1}H} NMR spectrum (CD_2Cl_2, RT) of complex [Pt(CNC-H)Cl(PPh_3)] (**13**).

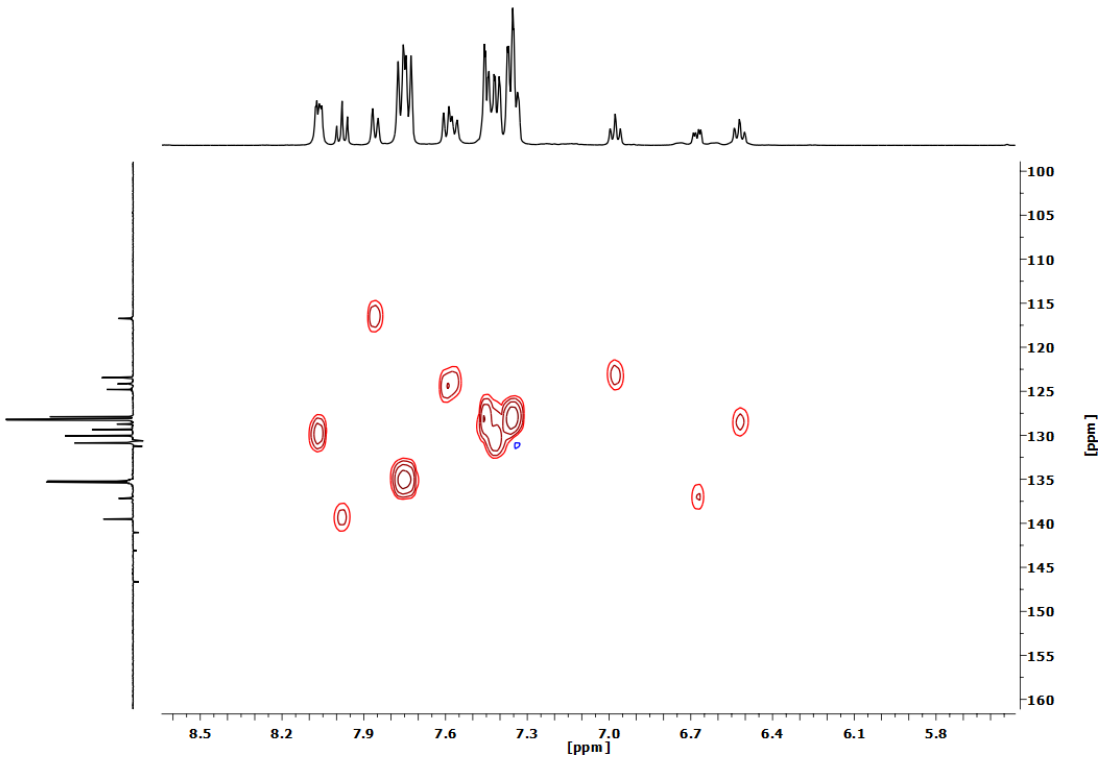

Figure S2.5. ^{1}H-^{13}C HSQC NMR spectrum (CD_2Cl_2, RT) of complex [Pt(CNC-H)Cl(PPh_3)] (**13**).

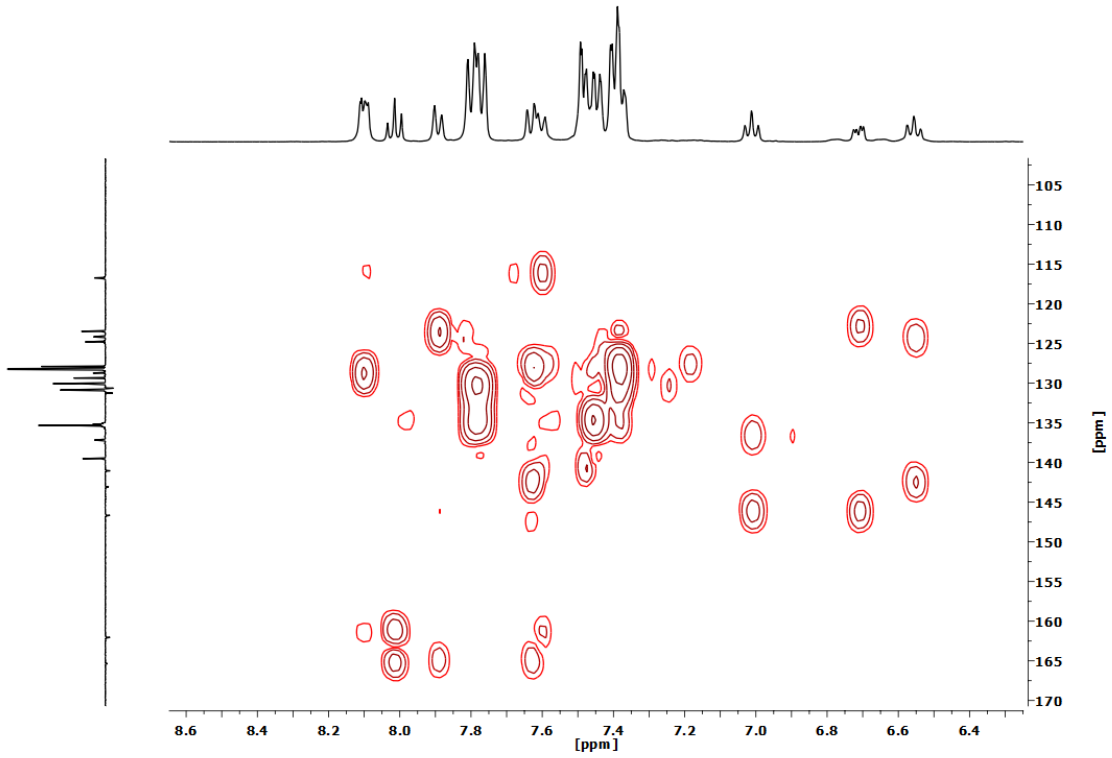

Figure S2.6. ^{1}H-^{13}C HMBC NMR spectrum (CD_2Cl_2, RT) of complex [Pt(CNC-H)Cl(PPh_3)] (**13**).

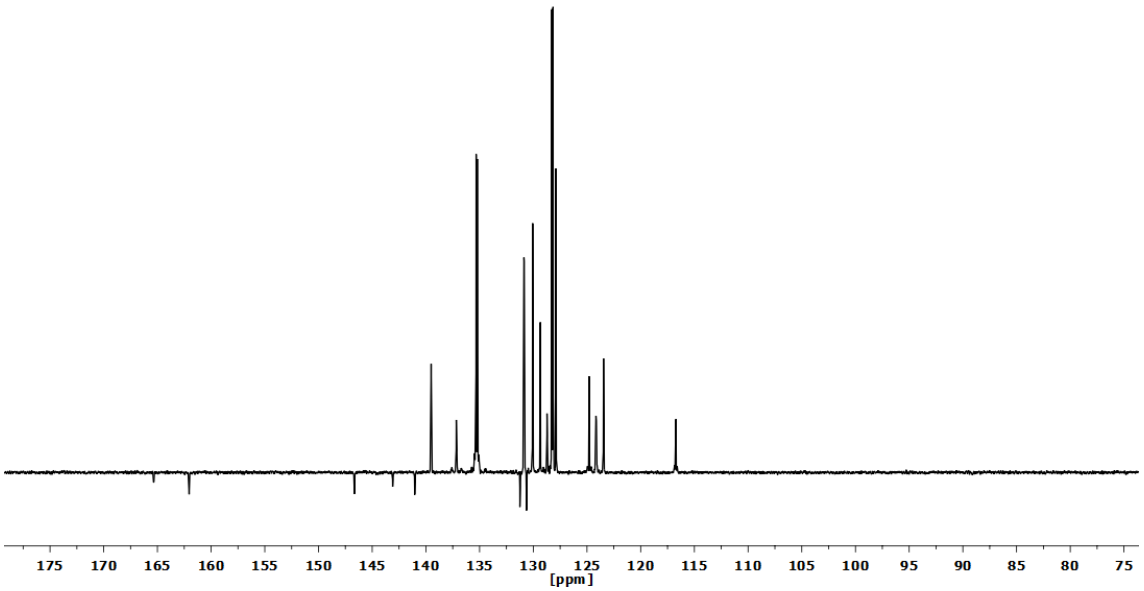

Figure S2.7. APT $^{13}C\{^{1}H\}$ NMR spectrum (CD_2Cl_2, RT) of complex [Pt(CNC-H)(Cl)(PPh_3)] (**13**).

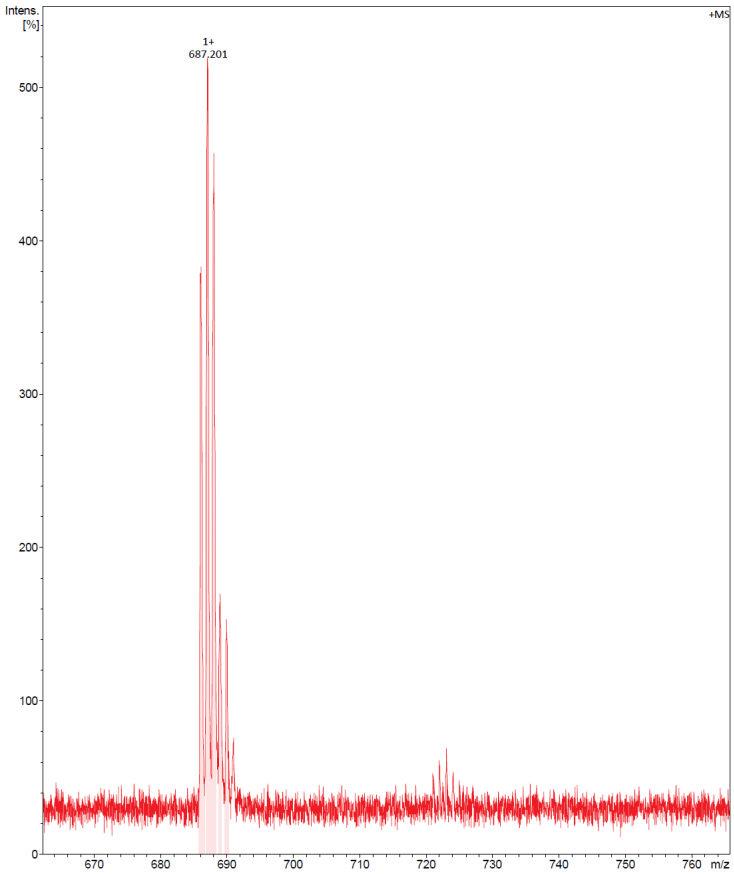

Figure S2.8. MS (MALDI+ DCTB) selected peaks of complex [Pt(CNC-H)Cl(PPh_3)] (**13**).

2.2. Spectra of complex [Pt(CNC-H)Cl(dmso)] (14).

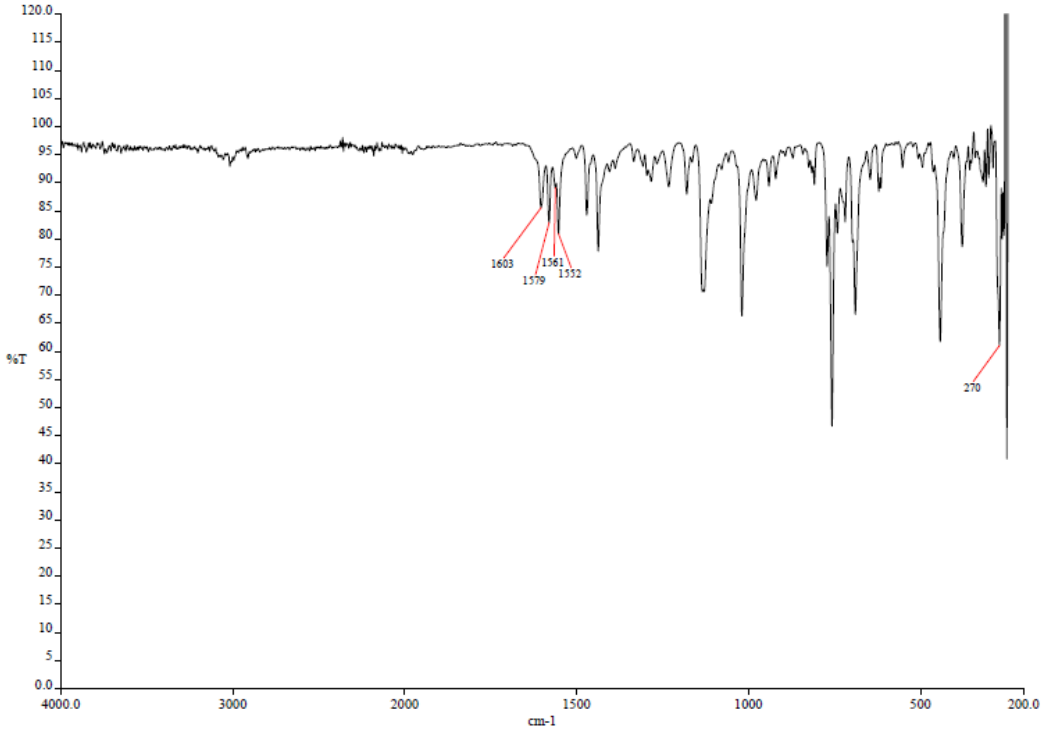

Figure S2.9. IR spectrum of complex [Pt(CNC-H)Cl(dmso)] (**14**).

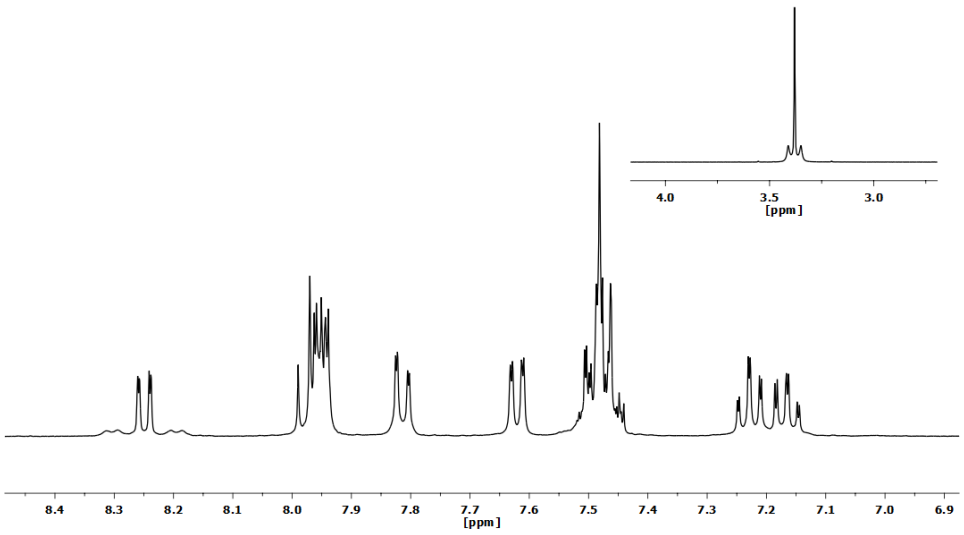

Figure S2.10. ^{1}H NMR (CD_2Cl_2, RT) of complex [Pt(CNC-H)Cl(dmso)] (**14**).

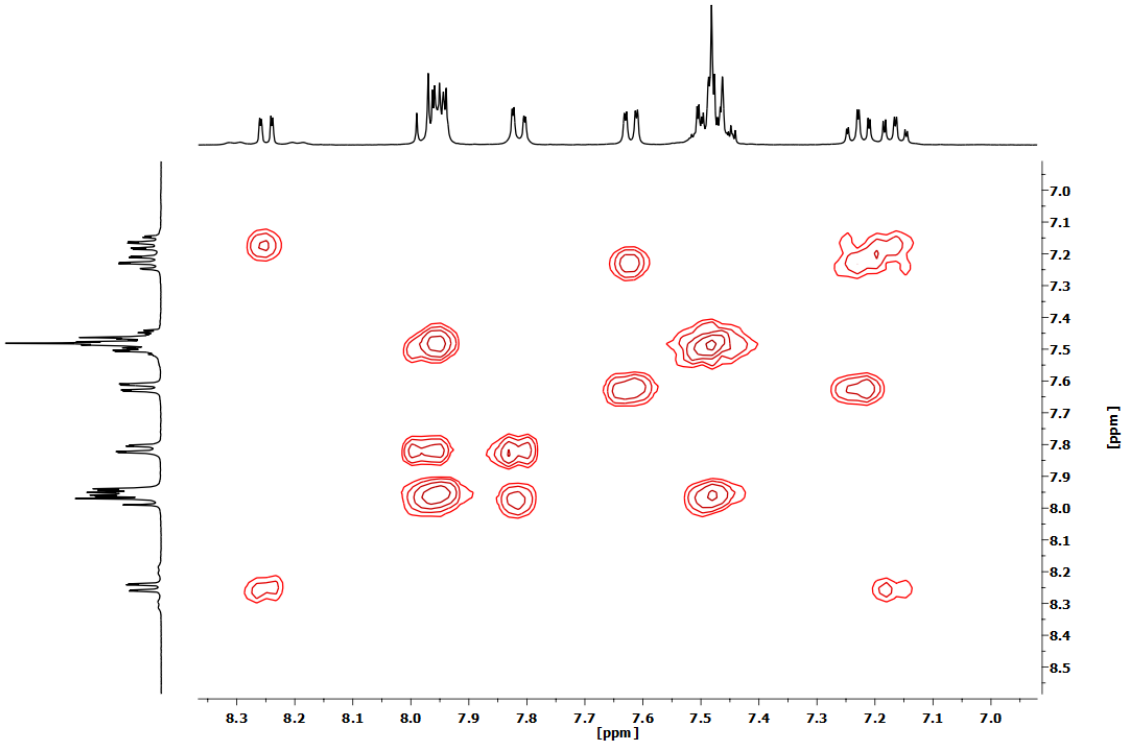

Figure S2.11. ^{1}H-^{1}H COSY NMR spectrum (CD_2Cl_2, RT) of complex [Pt(CNC-H)Cl(dmso)] (**14**).

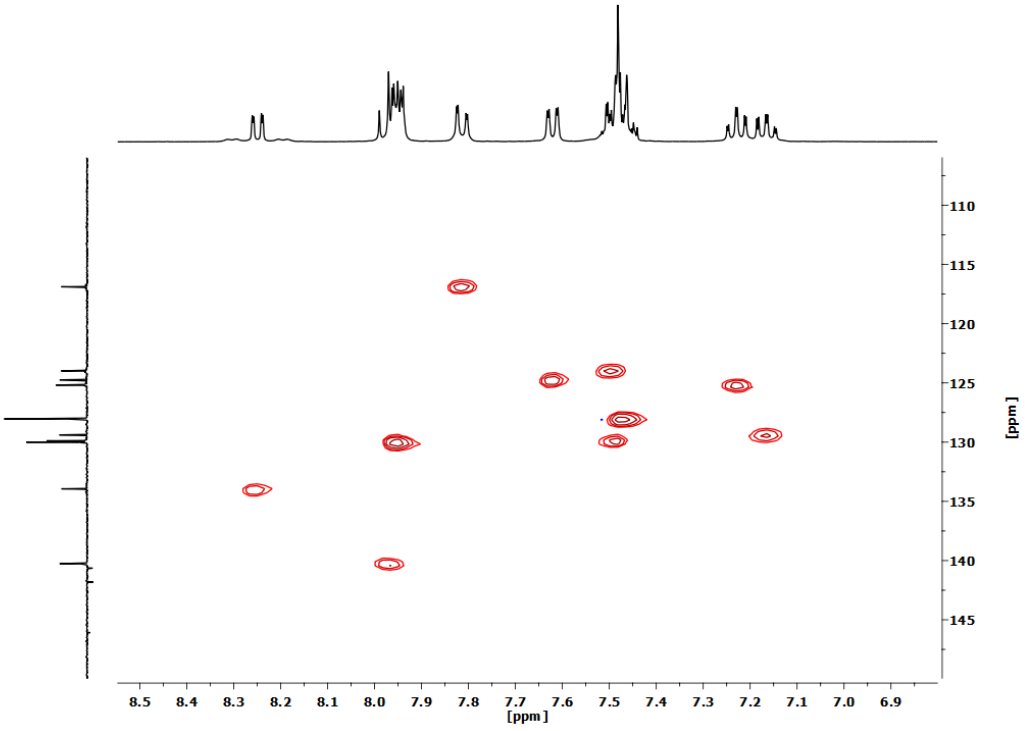

Figure S2.12. ^{1}H-^{13}C HSQC NMR spectrum (CD_2Cl_2, RT) of complex [Pt(CNC-H)Cl(dmso)] (**14**).

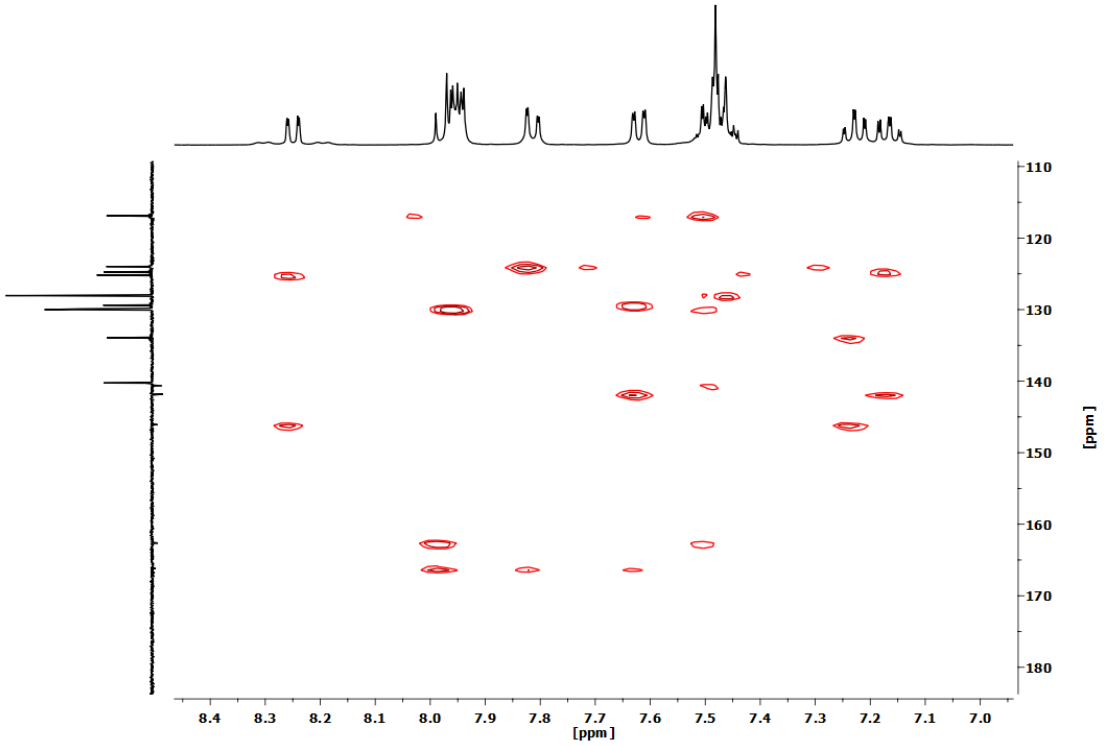

Figure S2.13. ^{1}H-^{13}C HMBC NMR spectrum (CD_2Cl_2, RT) of complex [Pt(CNC-H)Cl(dmso)] (**14**).

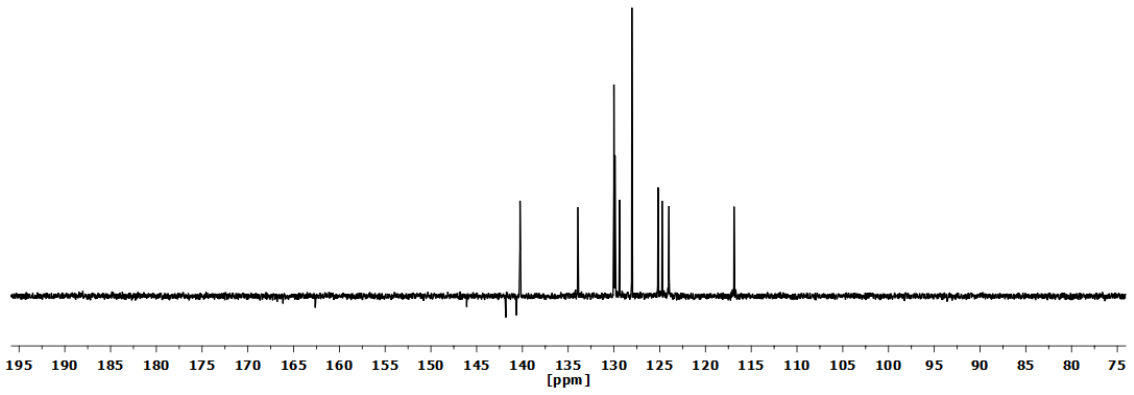

Figure S2.14. APT $^{13}C\{^{1}H\}$ NMR spectrum (CD_2Cl_2, RT) of complex [Pt(CNC-H)Cl(dmso)] (**14**).

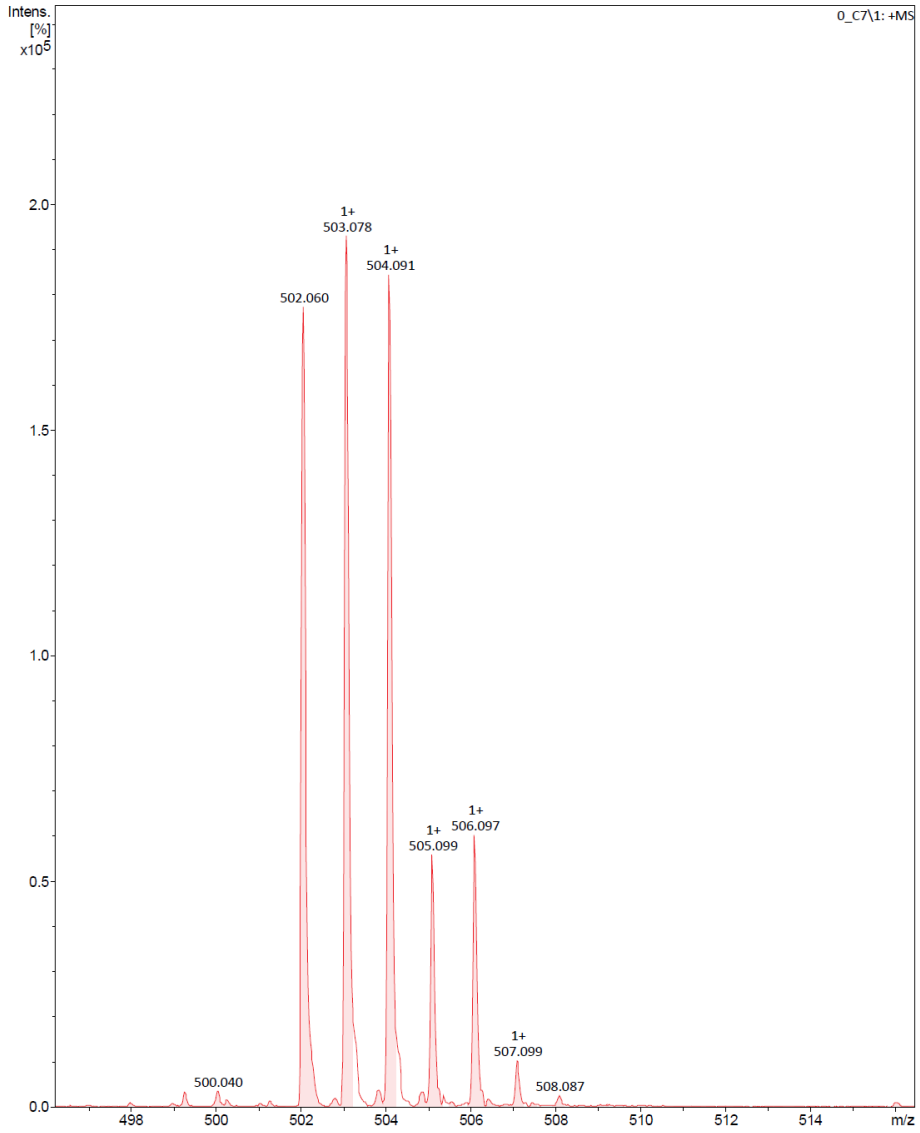

Figure S2.15. MS (MALDI+ DCTB) selected peak of complex [Pt(CNC-H)(Cl)(dmso)] (**14**).

2.3. Spectra of complex [Pt(CNC-H)(MeCN)(PPh$_3$)](ClO$_4$) (15).

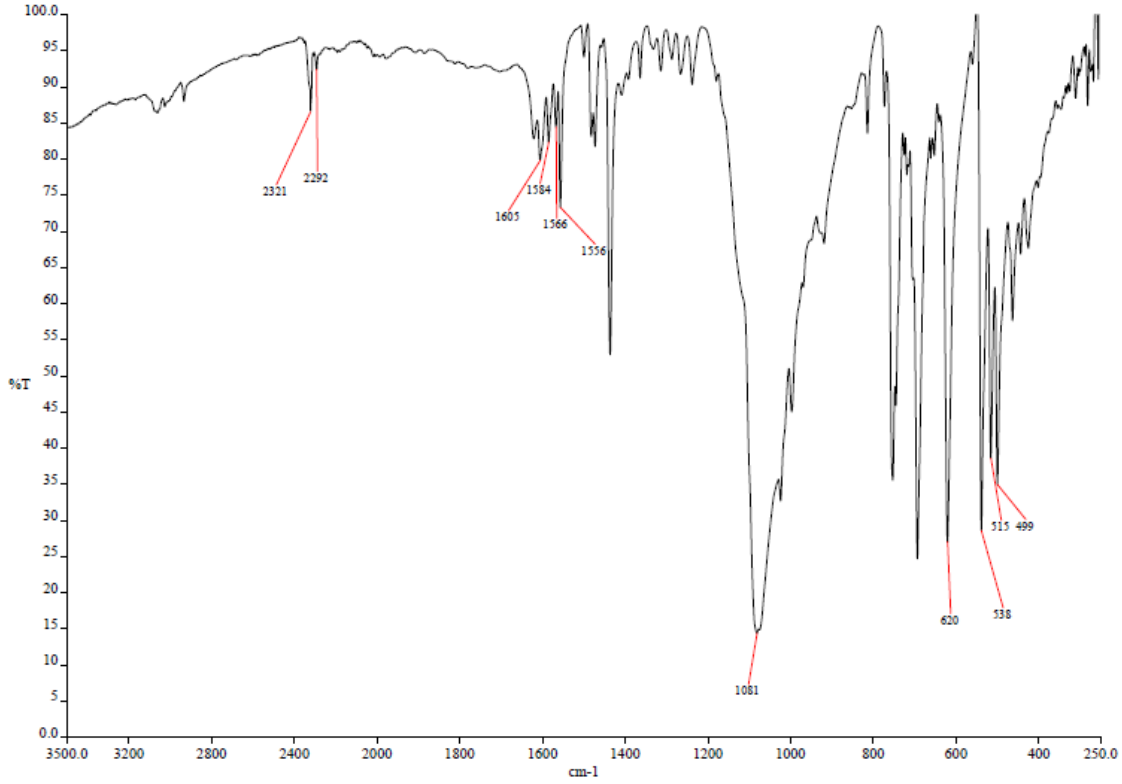

Figure S2.16. IR spectrum of complex [Pt(CNC-H)(MeCN)(PPh$_3$)](ClO$_4$) (**15**).

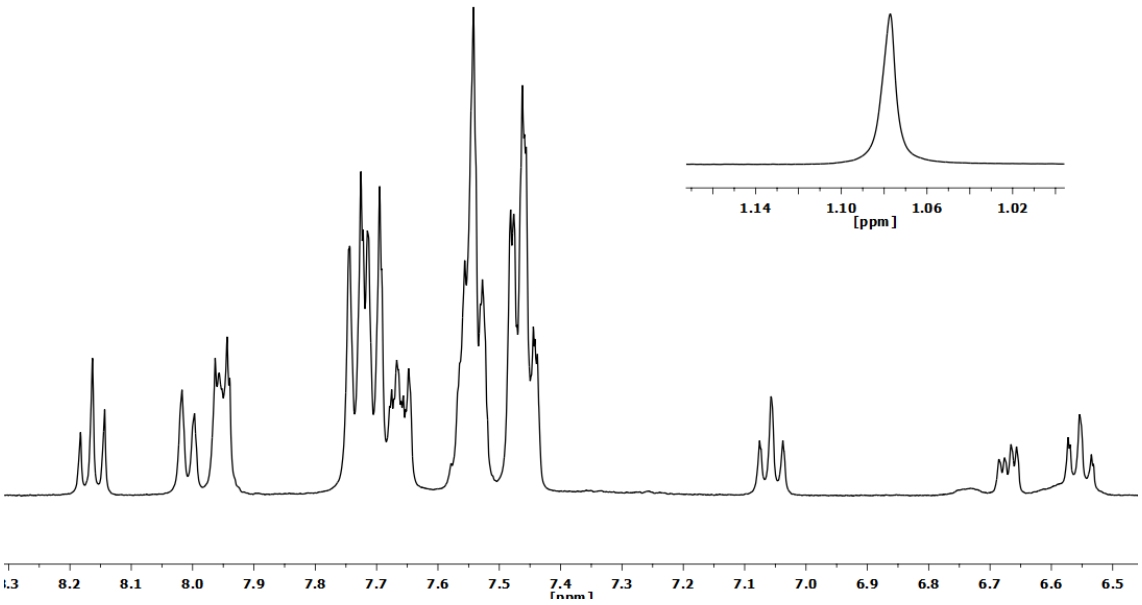

Figure S2.17. ^{1}H NMR spectrum (CD_2Cl_2, RT) of complex [Pt(CNC-H)(MeCN)(PPh$_3$)](ClO$_4$) (**15**).

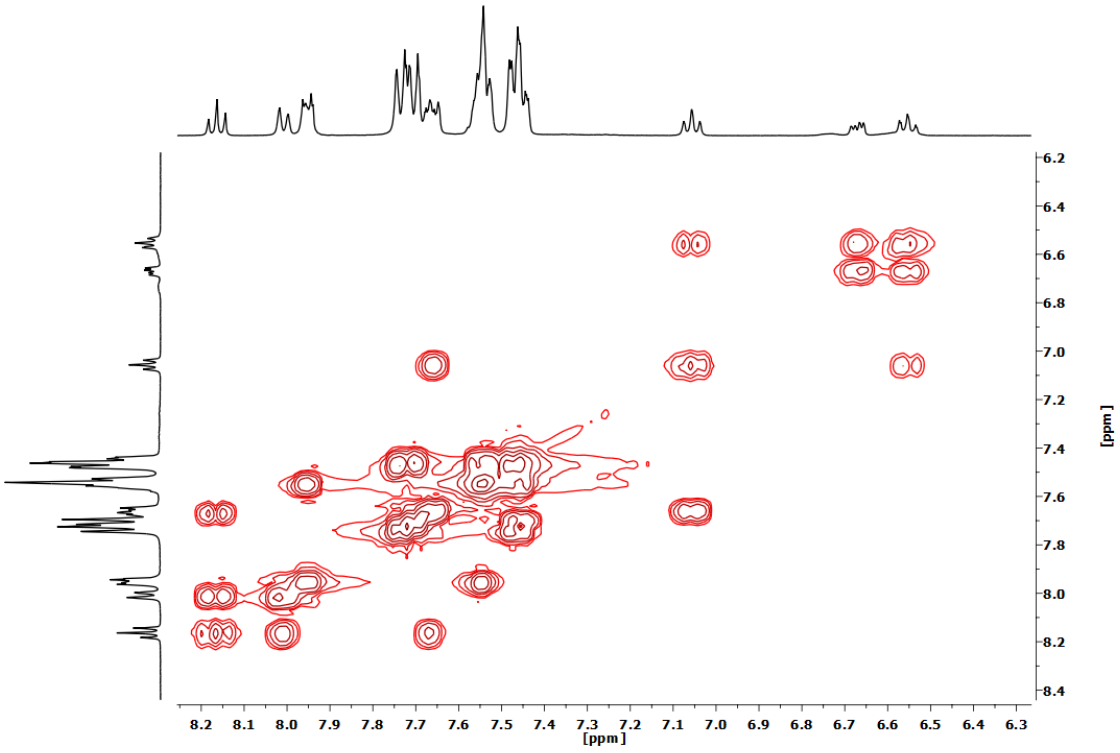

Figure S2.18. ^{1}H-^{1}H COSY NMR spectrum (CD_2Cl_2, RT) of complex [Pt(CNC-H)(MeCN)(PPh_3)](ClO_4) (**15**).

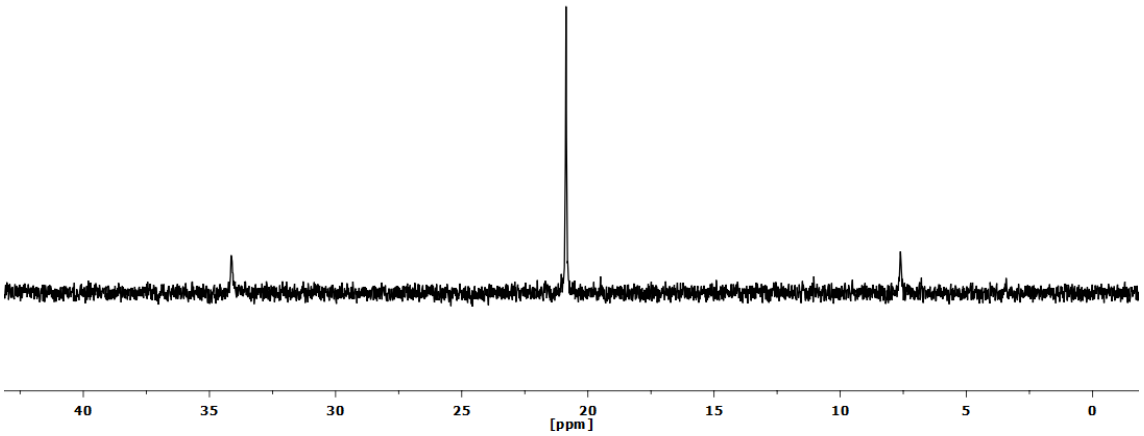

Figure S2.19. ^{31}P{^{1}H} NMR spectrum (CD_2Cl_2, RT) of complex [Pt(CNC-H)(MeCN)(PPh_3)](ClO_4) (**15**).

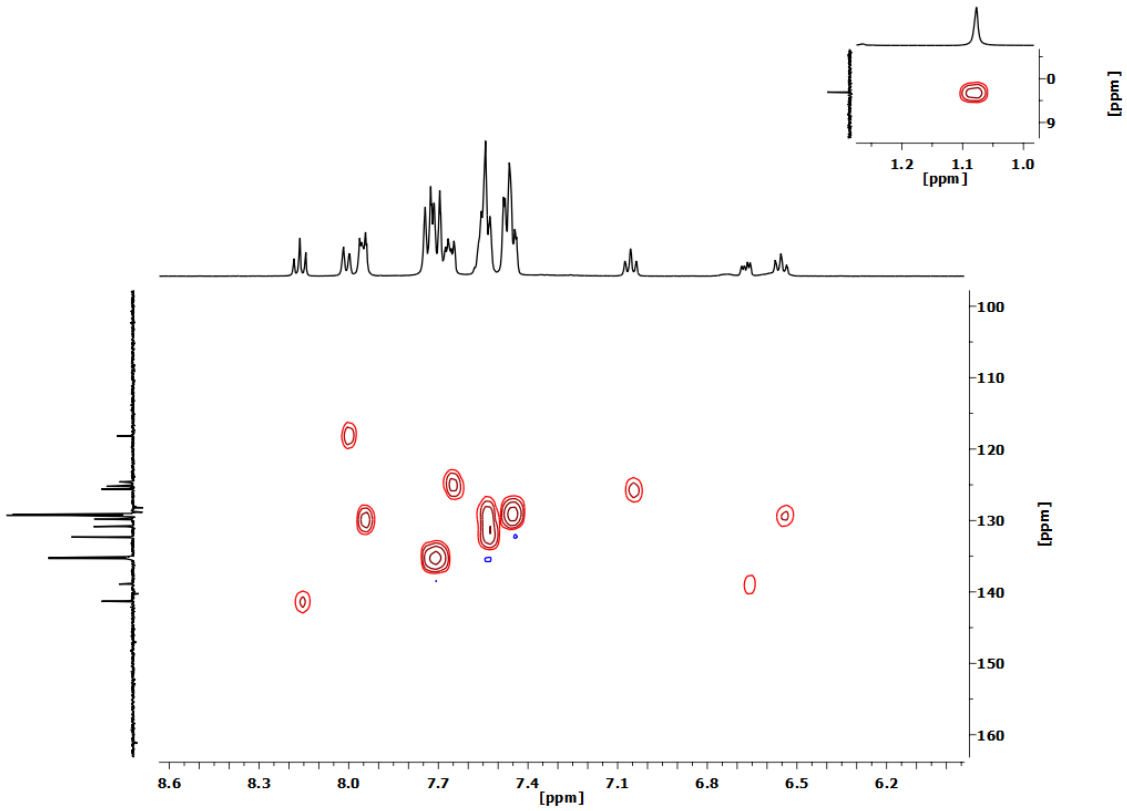

Figure S2.20. ^{1}H-^{13}C HSQC NMR spectrum (CD_2Cl_2, RT) of complex [Pt(CNC-H)(MeCN)(PPh_3)](ClO_4) (**15**).

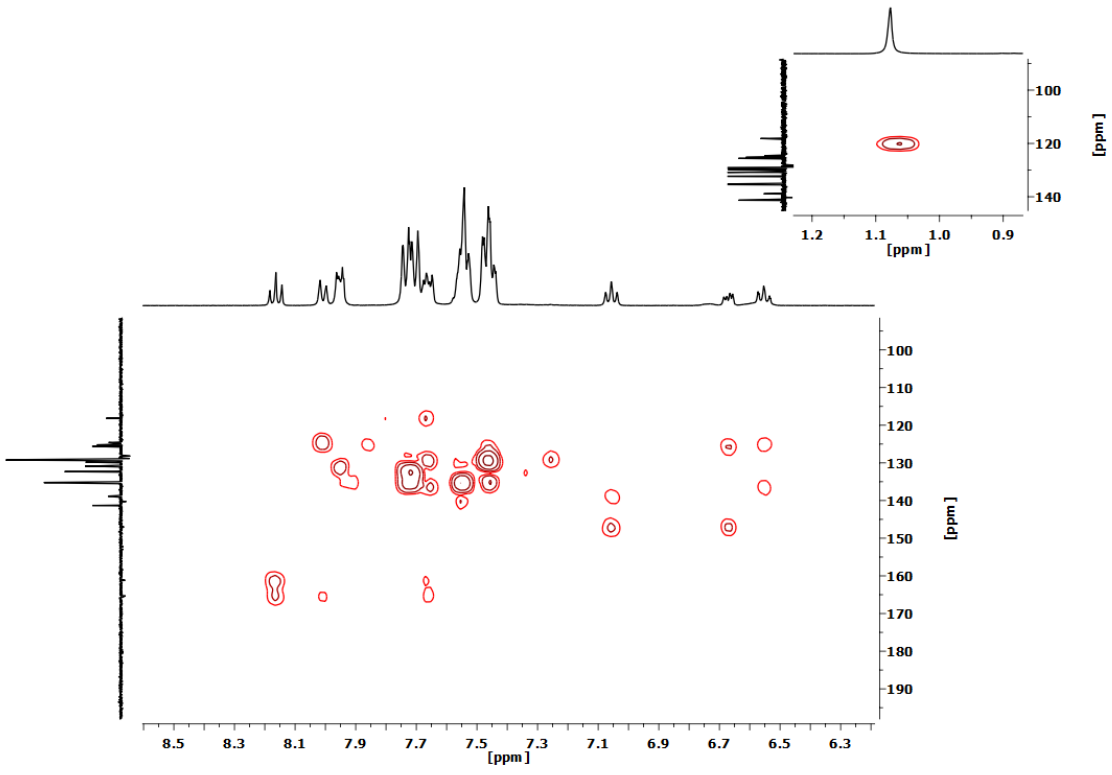

Figure S2.21. ^{1}H-^{13}C HMBC NMR spectrum (CD_2Cl_2, RT) of complex [Pt(CNC-H)(MeCN)(PPh_3)](ClO_4) (**15**).

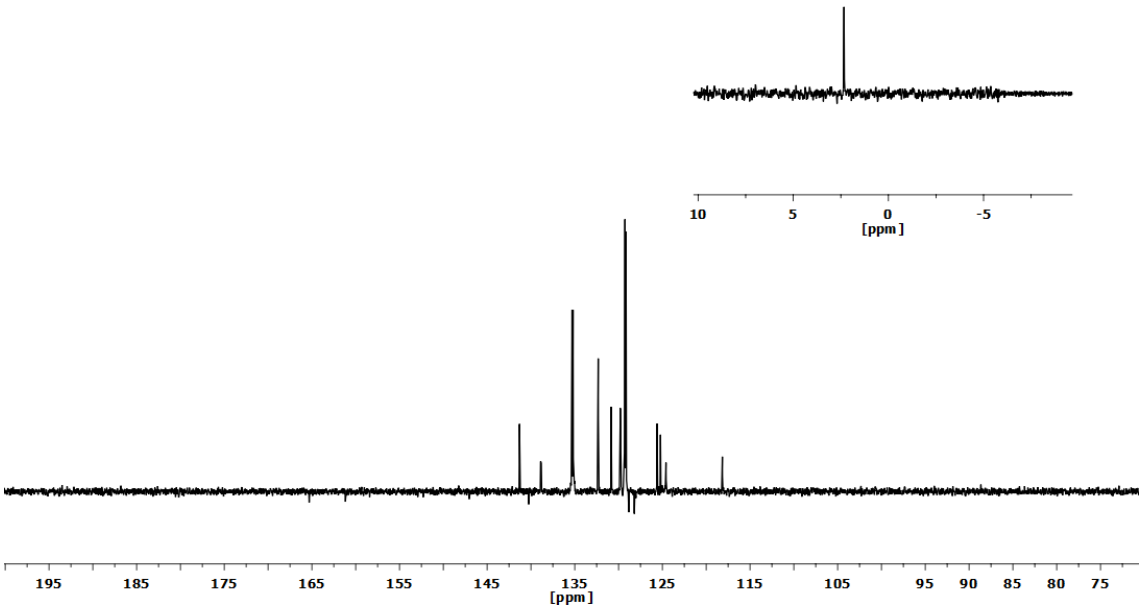

Figure S2.22. APT $^{13}C\{^{1}H\}$ NMR spectrum (CD_2Cl_2, RT) of complex [Pt(CNC-H)(MeCN)(PPh_3)](ClO_4) (**15**).

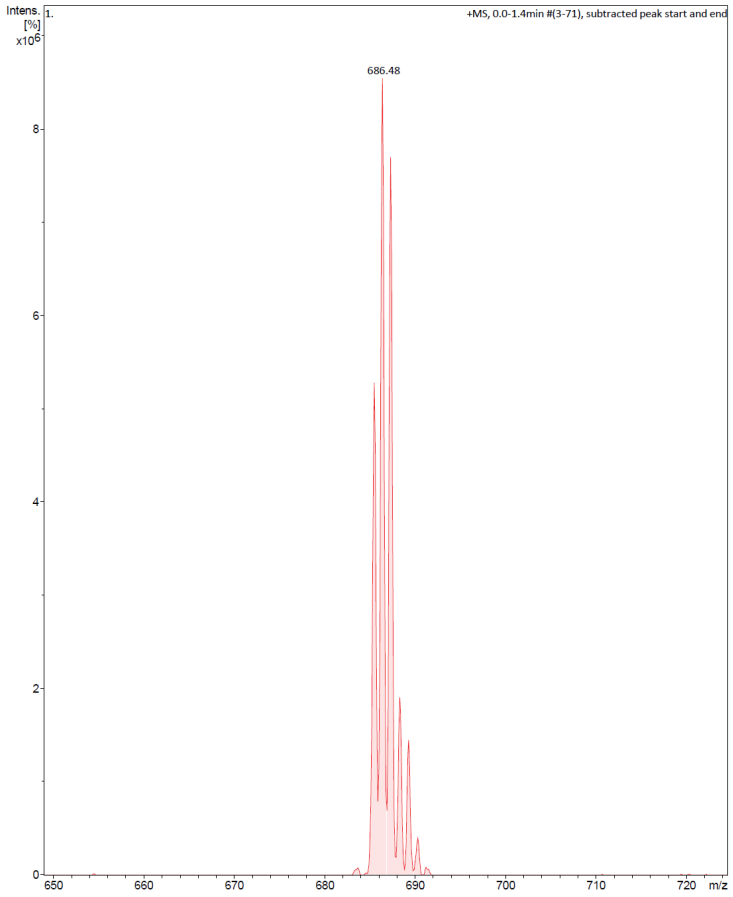

Figure S2.23. MS (ESI+) selected peak of complex [Pt(CNC-H)(MeCN)(PPh_3)](ClO_4) (**15**).

2.4. Spectra of complex [Pd(CNC-H)(MeCN)(PPh$_3$)](ClO$_4$) (16).

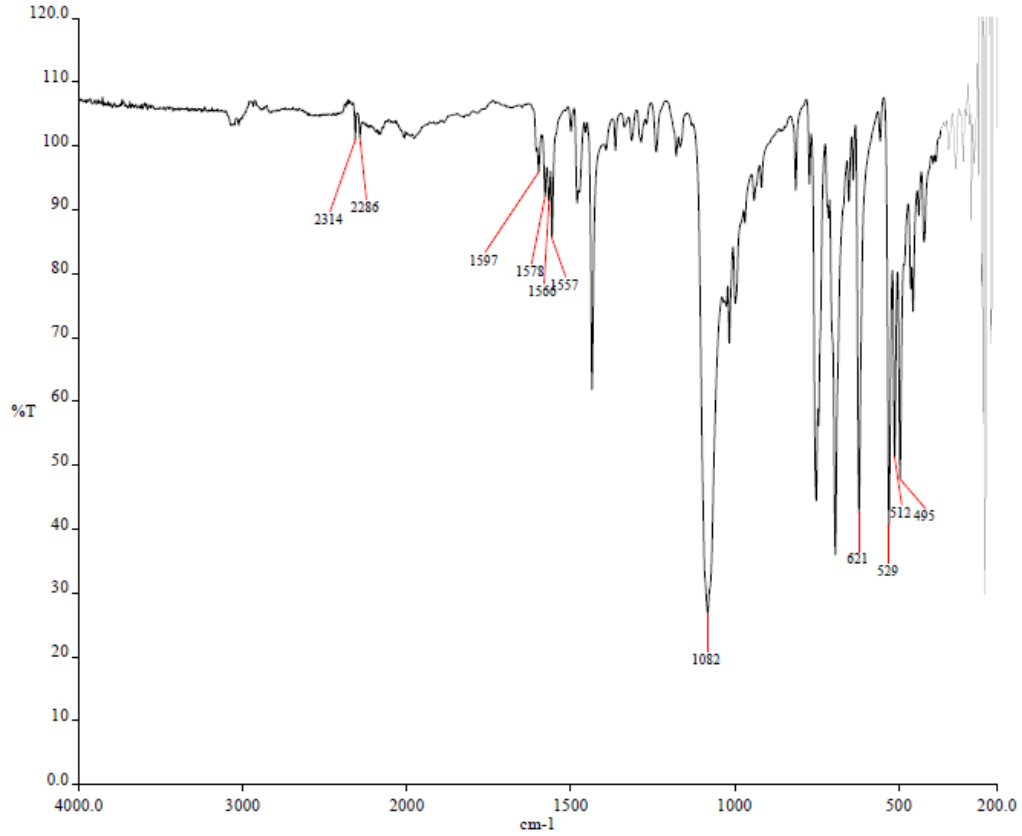

Figure S2.24. IR spectrum of complex [Pd(CNC-H)(MeCN)(PPh$_3$)](ClO$_4$) (**16**).

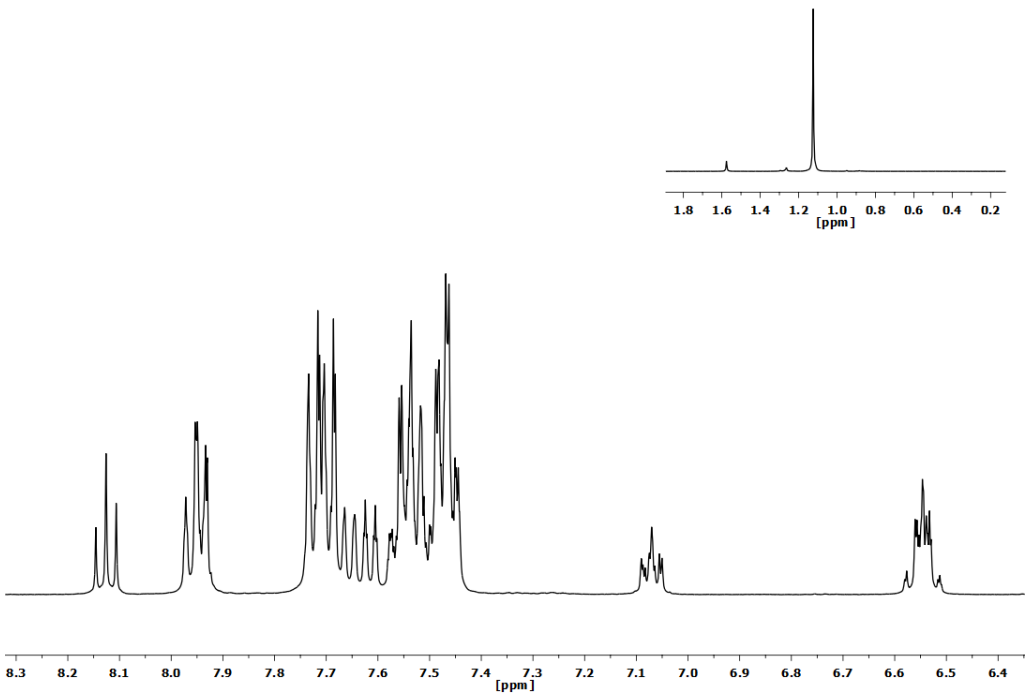

Figure S2.25. ^{1}H NMR spectrum (CD_2Cl_2, RT) of complex [Pd(CNC-H)(MeCN)(PPh$_3$)](ClO$_4$) (**16**).

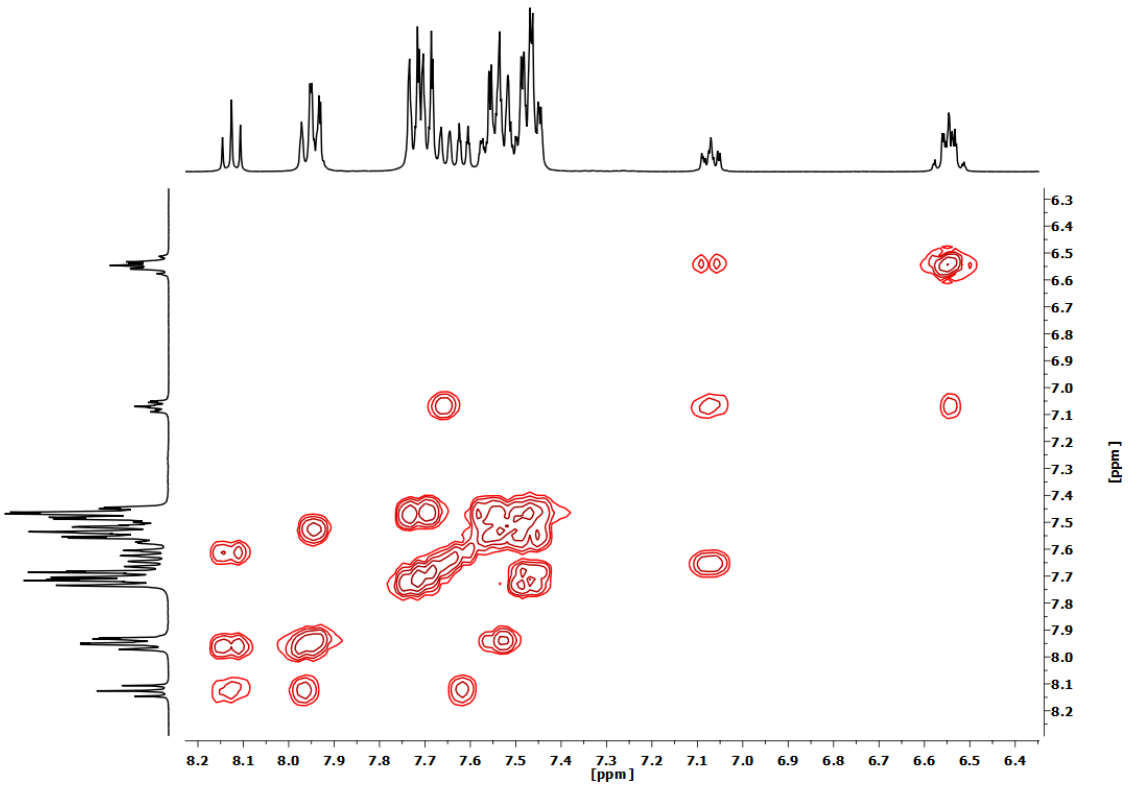

Figure S2.26. ^{1}H-^{1}H COSY NMR spectrum (CD_2Cl_2, RT) of complex [Pd(CNC-H)(MeCN)(PPh_3)](ClO_4) (**16**).

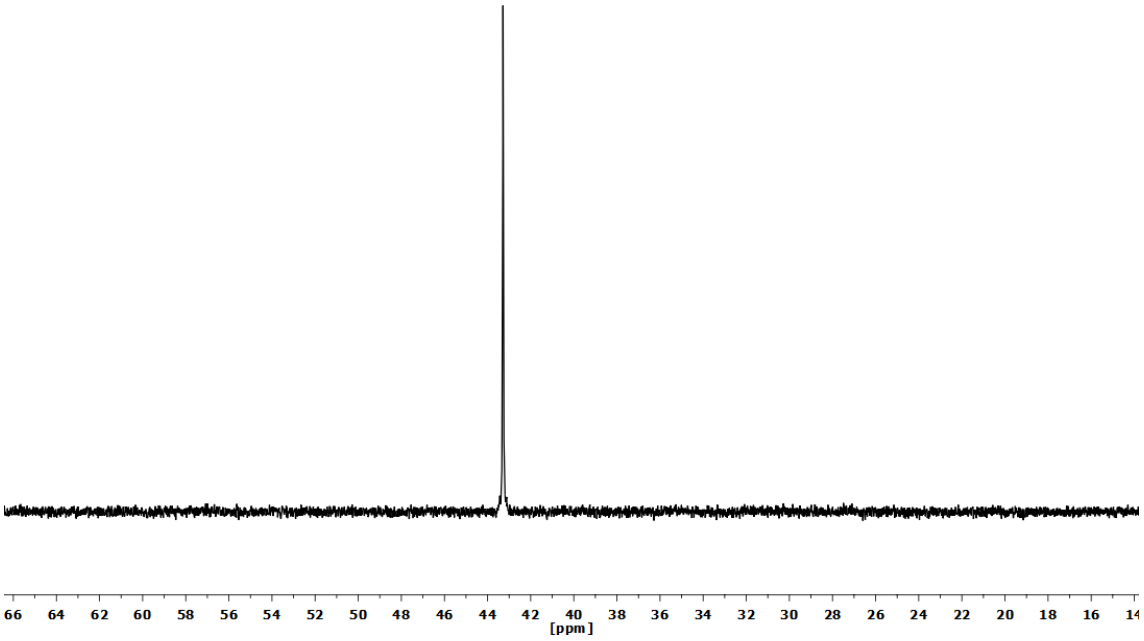

Figure S2.27. $^{31}P\{^{1}H\}$ NMR spectrum (CD_2Cl_2, RT) of complex [Pd(CNC-H)(MeCN)(PPh_3)](ClO_4) (**16**).

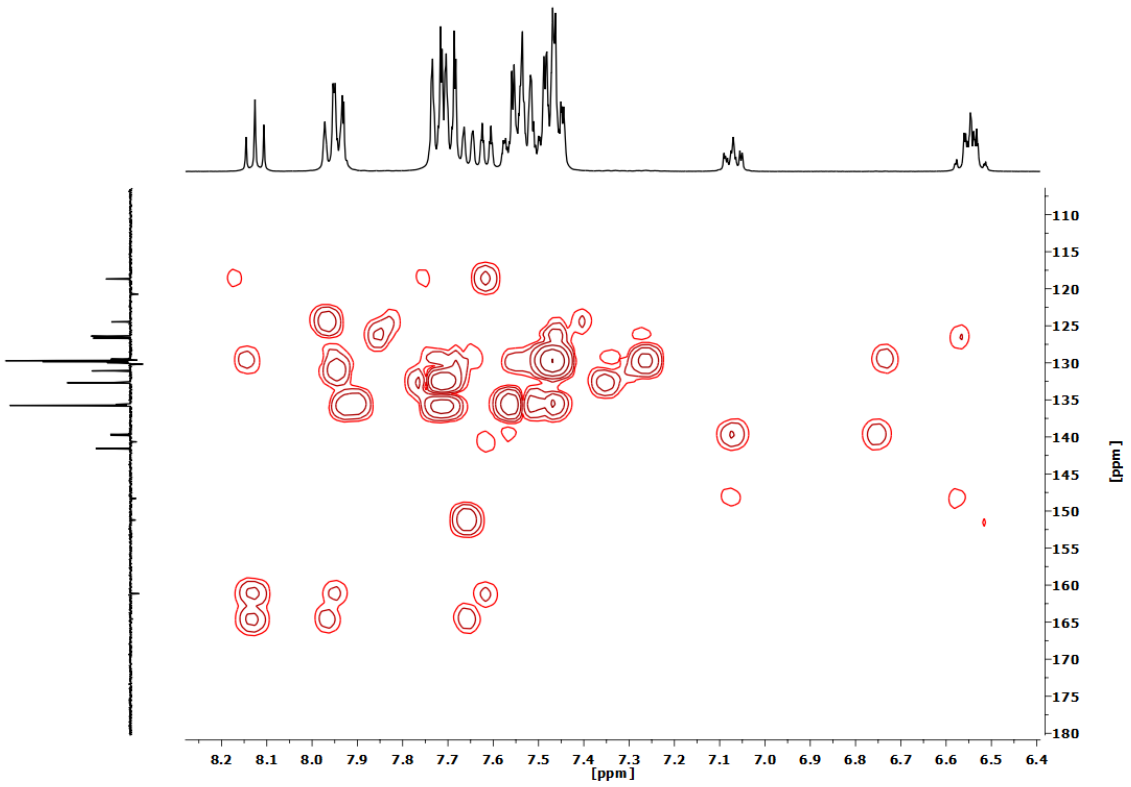

Figure S2.28. ^{1}H-^{13}C HSQC NMR spectrum (CD_2Cl_2, RT) of complex [Pd(CNC-H)(MeCN)(PPh_3)](ClO_4) (**16**).

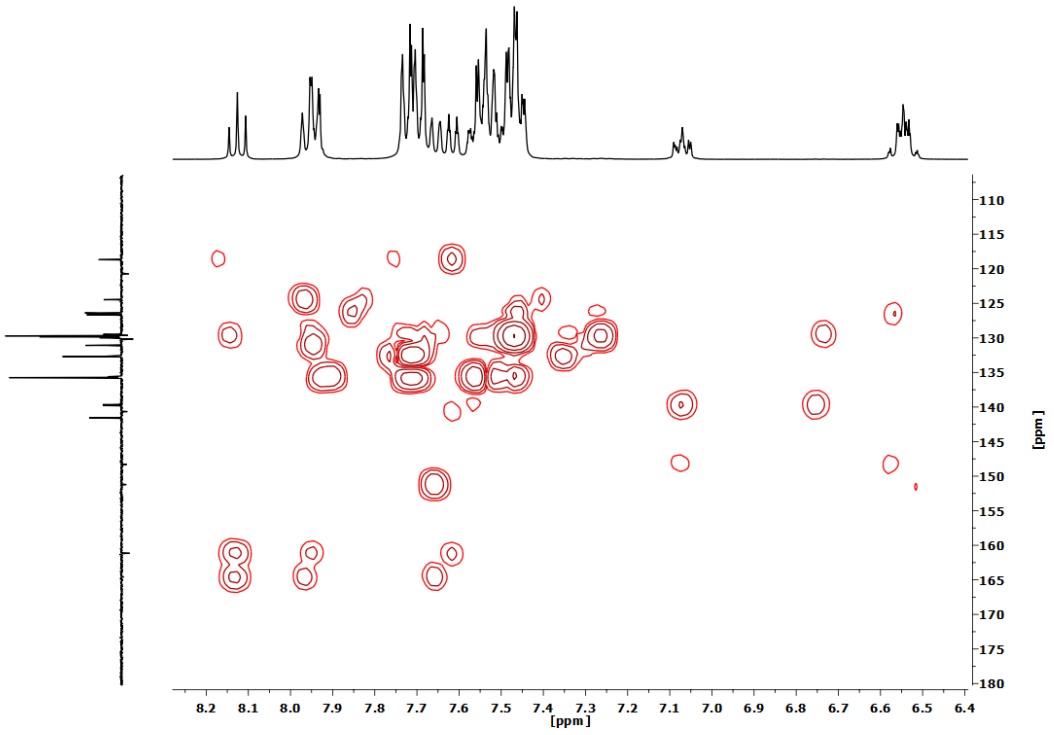

Figure S2.29. ^{1}H-^{13}C HMBC NMR spectrum (CD_2Cl_2, RT) of complex [Pd(CNC-H)(MeCN)(PPh_3)](ClO_4) (**16**).

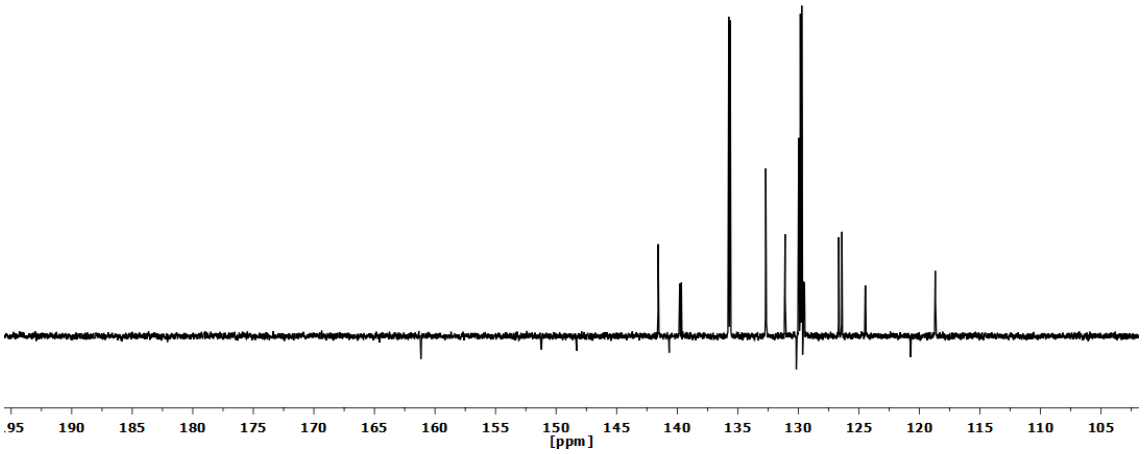

Figure S2.30. APT $^{13}C\{^{1}H\}$ NMR spectrum (CD_2Cl_2, RT) of complex [Pd(CNC-H)(MeCN)(PPh_3)](ClO_4) (**16**).

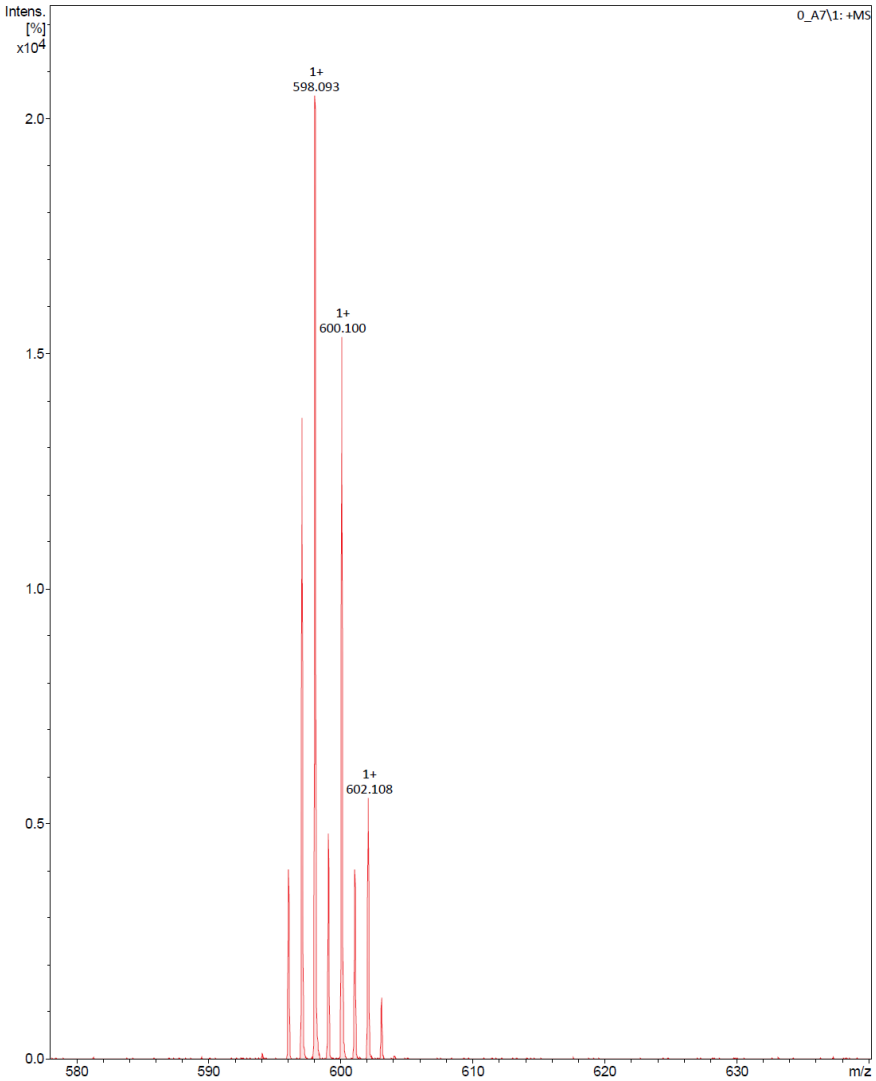

Figure S2.31. MS (MALDI+ DCTB) selected peak of complex [Pd(CNC-H)(MeCN)(PPh_3)](ClO_4) (**16**).

2.5. Spectra of complex [Pt(CNC-H)(H_2O)(PPh_3)](ClO_4) (17).

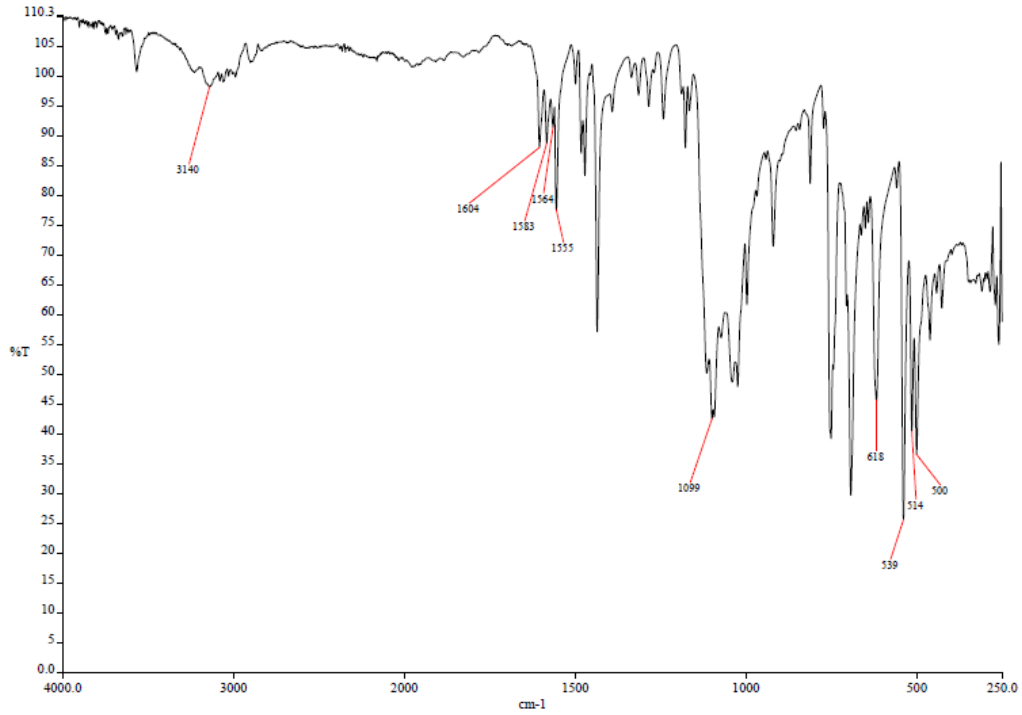

Figure S2.32. IR spectrum of complex [Pt(CNC-H)(H_2O)(PPh_3)](ClO_4) (**17**).

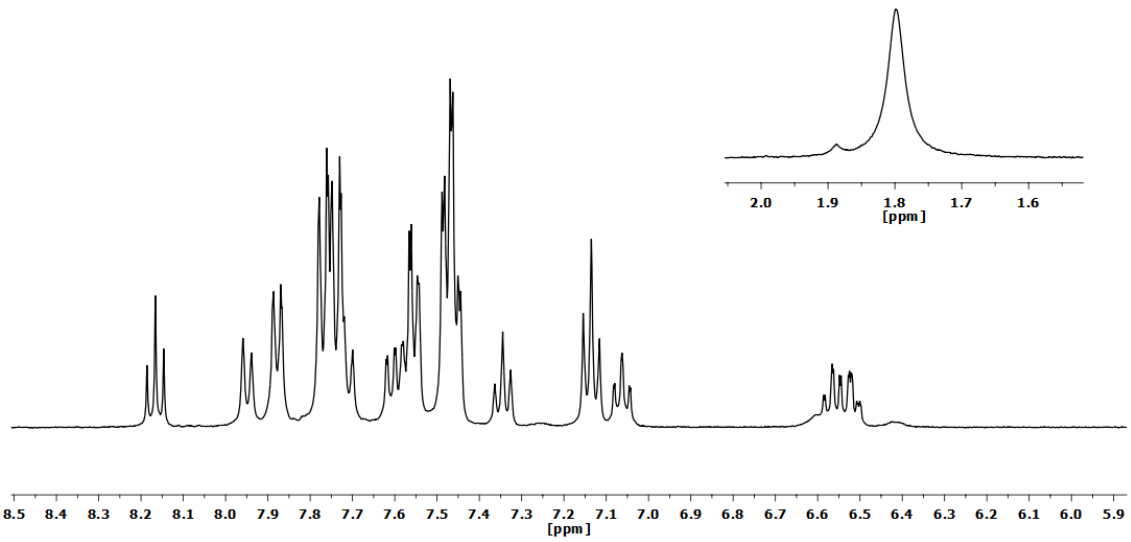

Figure S2.33. ^1H NMR spectrum (CD_2Cl_2, RT) of complex [Pt(CNC-H)(H_2O)(PPh_3)](ClO_4) (**17**).

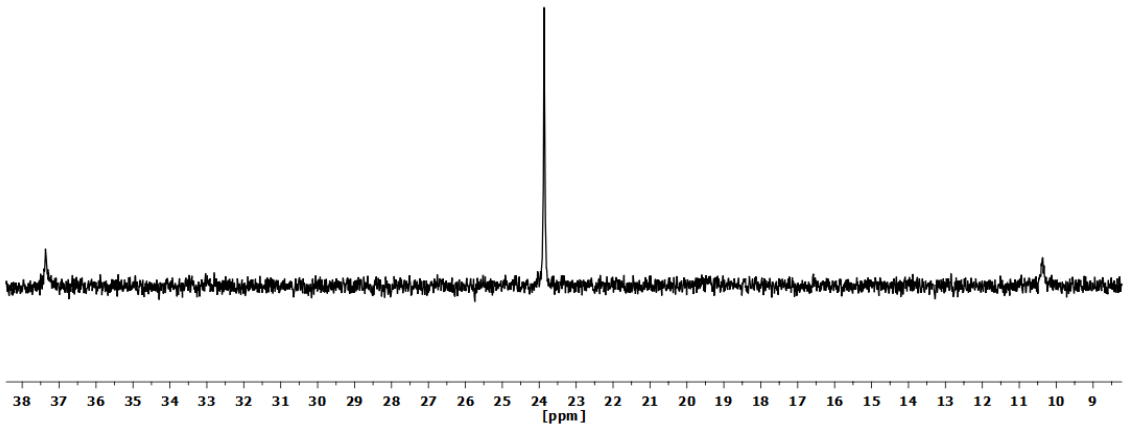

Figure S2.34. $^{31}P\{^{1}H\}$ NMR spectrum (CD_2Cl_2, RT) of complex [Pt(CNC-H)(H_2O)(PPh_3)](ClO_4) (**17**).

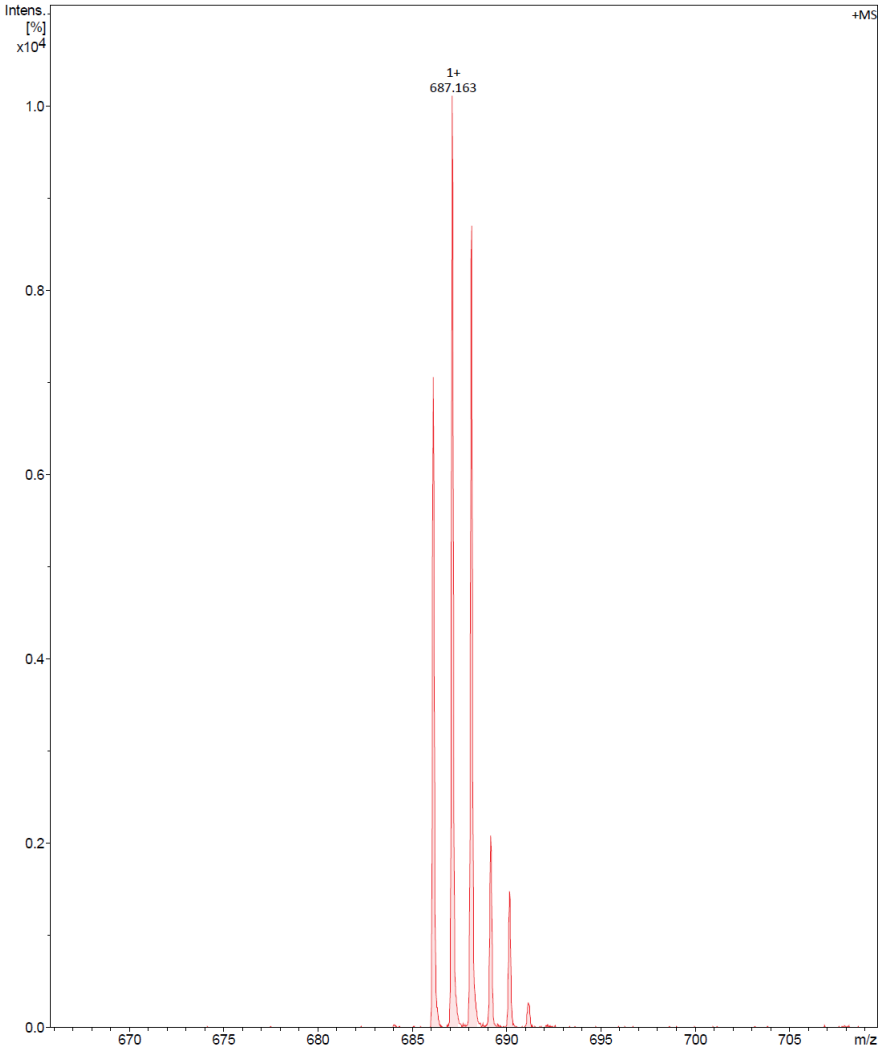

Figure S2.35. MS (MALDI+ DCTB) selected peak of complex [Pt(CNC-H)(H_2O)(PPh_3)](ClO_4) (**17**).

2.6. Spectra of complex [Pd(CNC-H)(H_2O)(PPh_3)](ClO_4) (18).

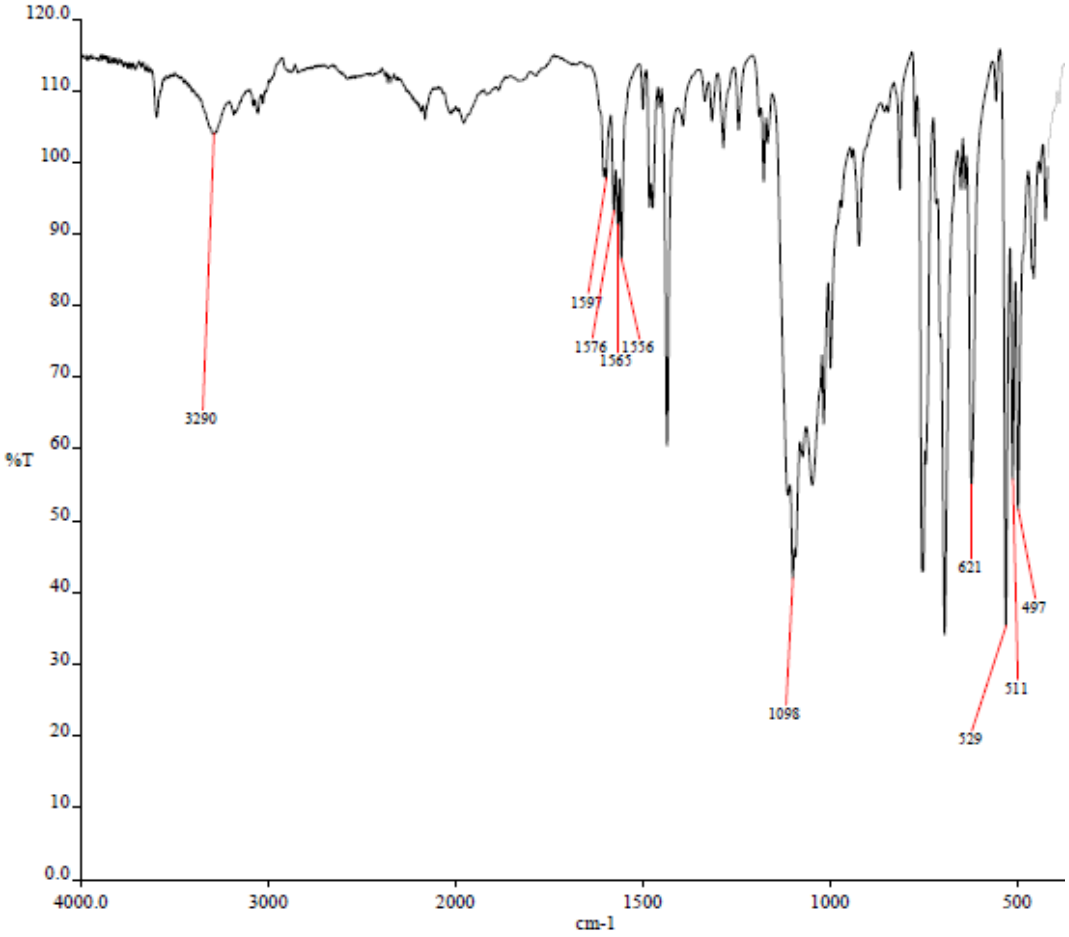

Figure S2.36. IR spectrum of complex [Pd(CNC-H)(H_2O)(PPh_3)](ClO_4) (**18**).

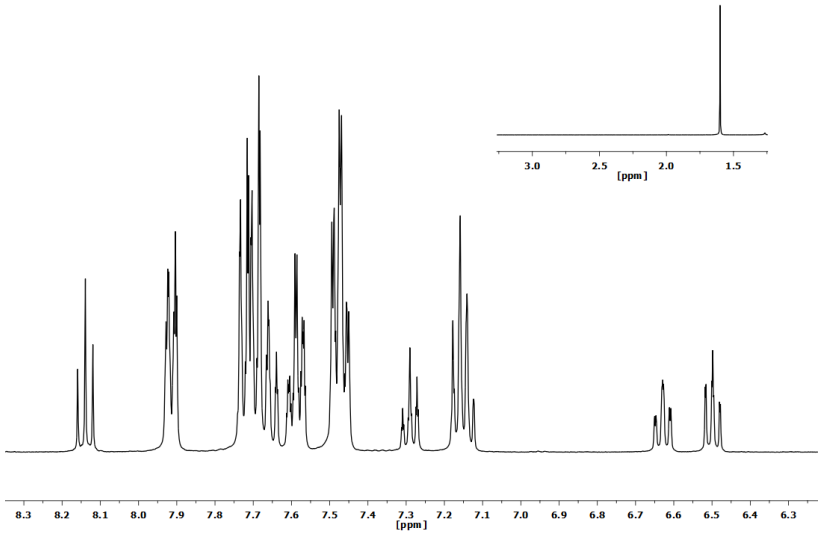

Figure S2.37. ^1H NMR spectrum (CD_2Cl_2, RT) of complex [Pd(CNC-H)(H_2O)(PPh_3)](ClO_4) (**18**).

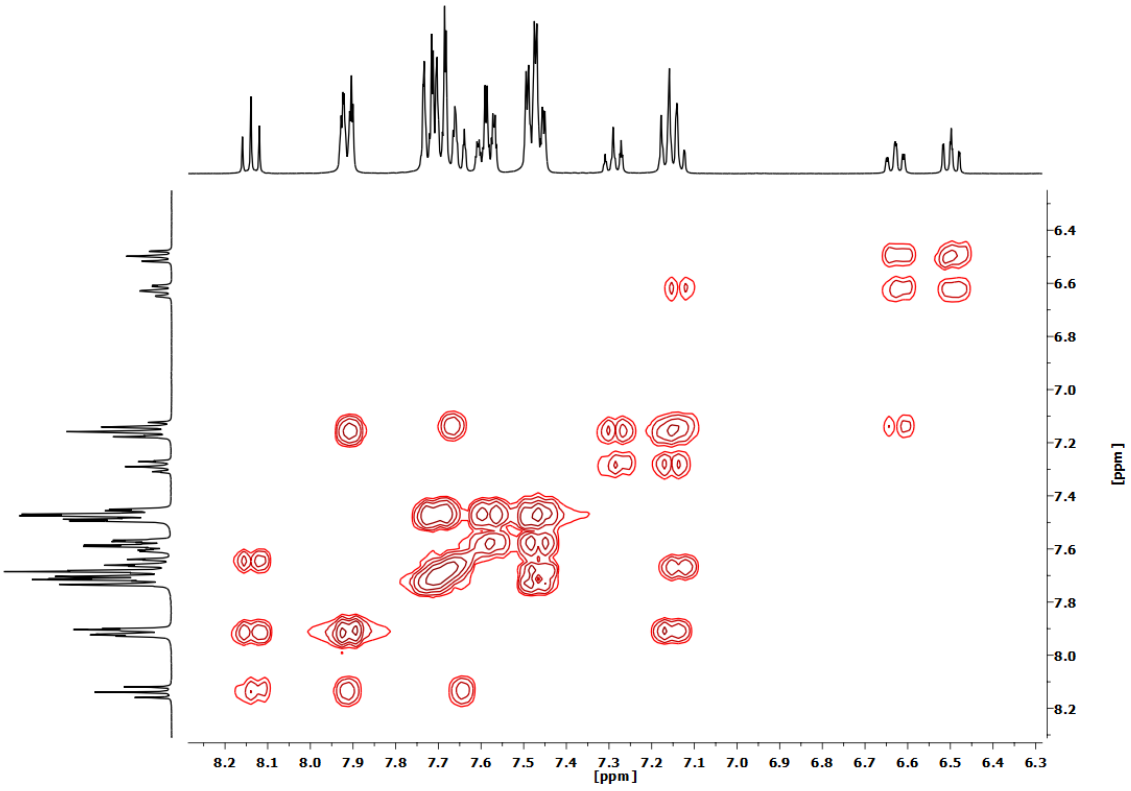

Figure S2.38. ^{1}H-^{1}H COSY NMR spectrum (CD_2Cl_2, RT) of complex [Pd(CNC-H)(H_2O)(PPh_3)](ClO_4) (**18**).

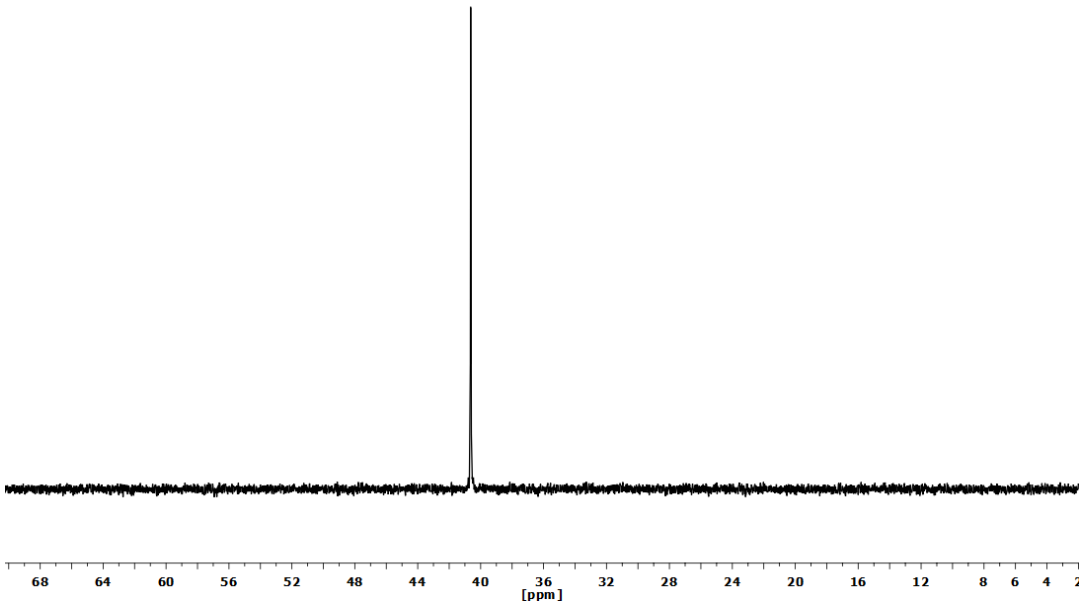

Figure S2.39. $^{31}P\{^{1}H\}$ NMR spectrum (CD_2Cl_2, RT) of complex [Pd(CNC-H)(H_2O)(PPh_3)](ClO_4) (**18**).

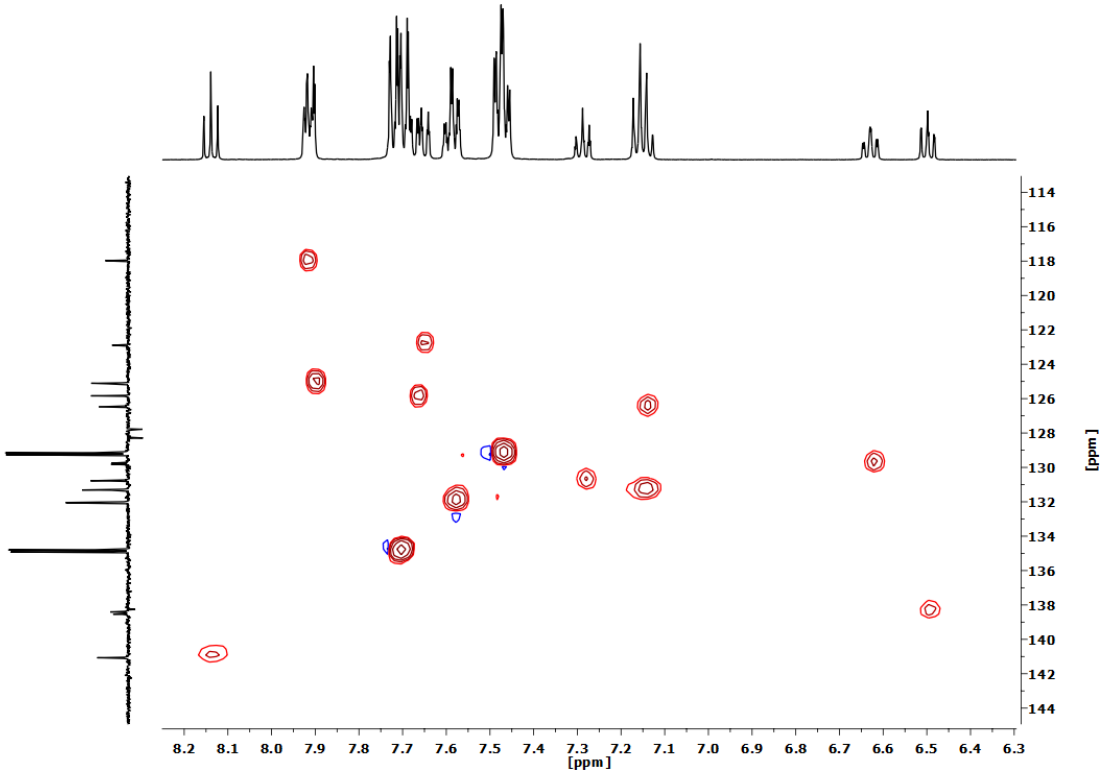

Figure S2.40. ^{1}H-^{13}C HSQC NMR spectrum (CD_2Cl_2, RT) of complex [Pd(CNC-H)(H_2O)(PPh_3)](ClO_4) (**18**).

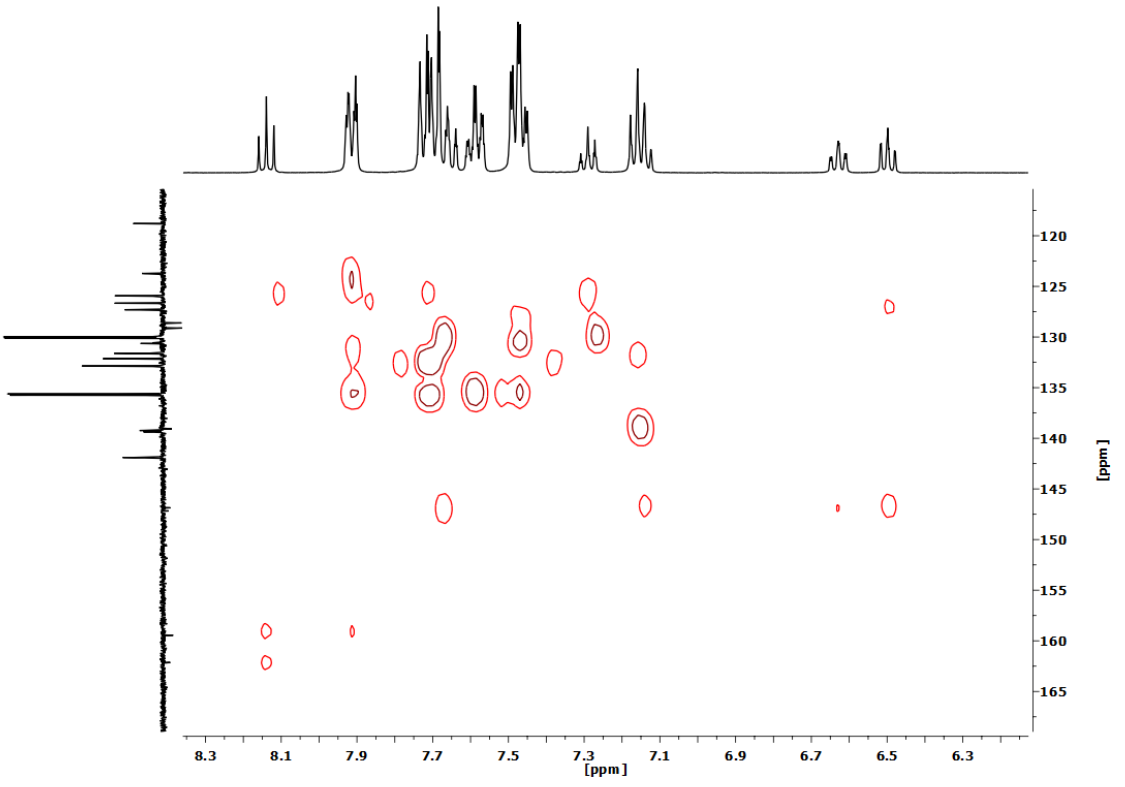

Figure S2.41. ^{1}H-^{13}C HMBC NMR spectrum (CD_2Cl_2, RT) of complex [Pd(CNC-H)(H_2O)(PPh_3)](ClO_4) (**18**).

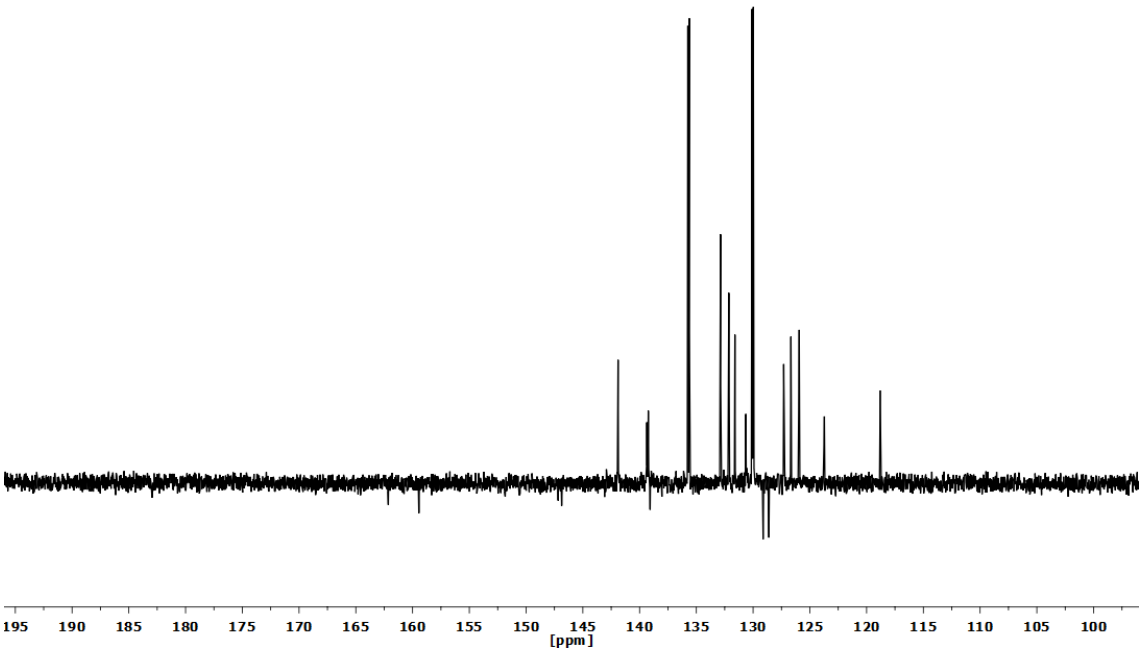

Figure S2.42. APT $^{13}C\{^{1}H\}$ NMR spectrum (CD_2Cl_2, RT) of complex [Pd(CNC-H)(H_2O)(PPh_3)](ClO_4) (**18**).

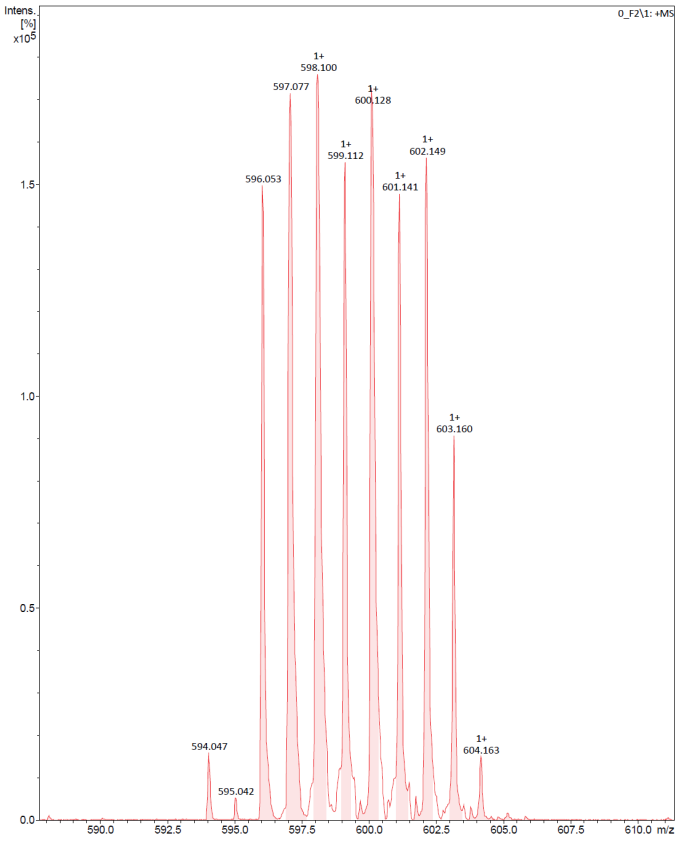

Figure S2.43. MS (MALDI+ DCTB) selected peak of complex [Pd(CNC-H)(H_2O)(PPh_3)](ClO_4) (**18**).

2.7. Spectra of complex [Pt(CNC-H)(tht)(PPh$_3$)](ClO$_4$) (19).

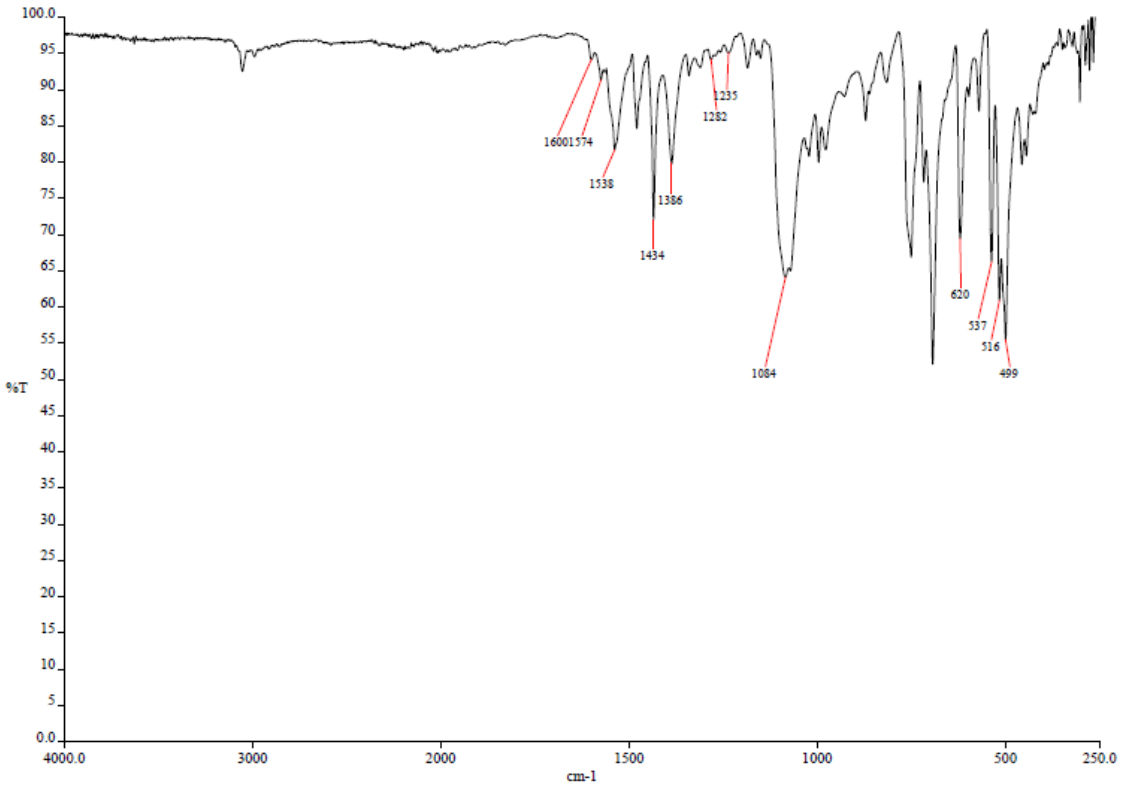

Figure S2.44. IR spectrum of complex [Pt(CNC-H)(tht)(PPh$_3$)](ClO$_4$) (**19**).

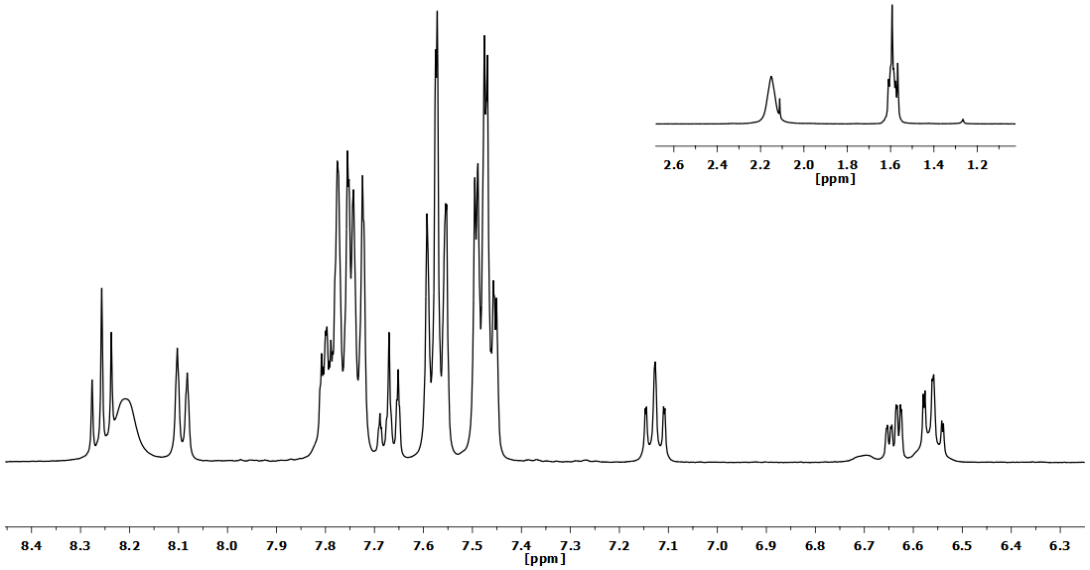

Figure S2.45. ^{1}H NMR spectrum (CD_2Cl_2, RT) of complex [Pt(CNC-H)(tht)(PPh$_3$)](ClO$_4$) (**19**).

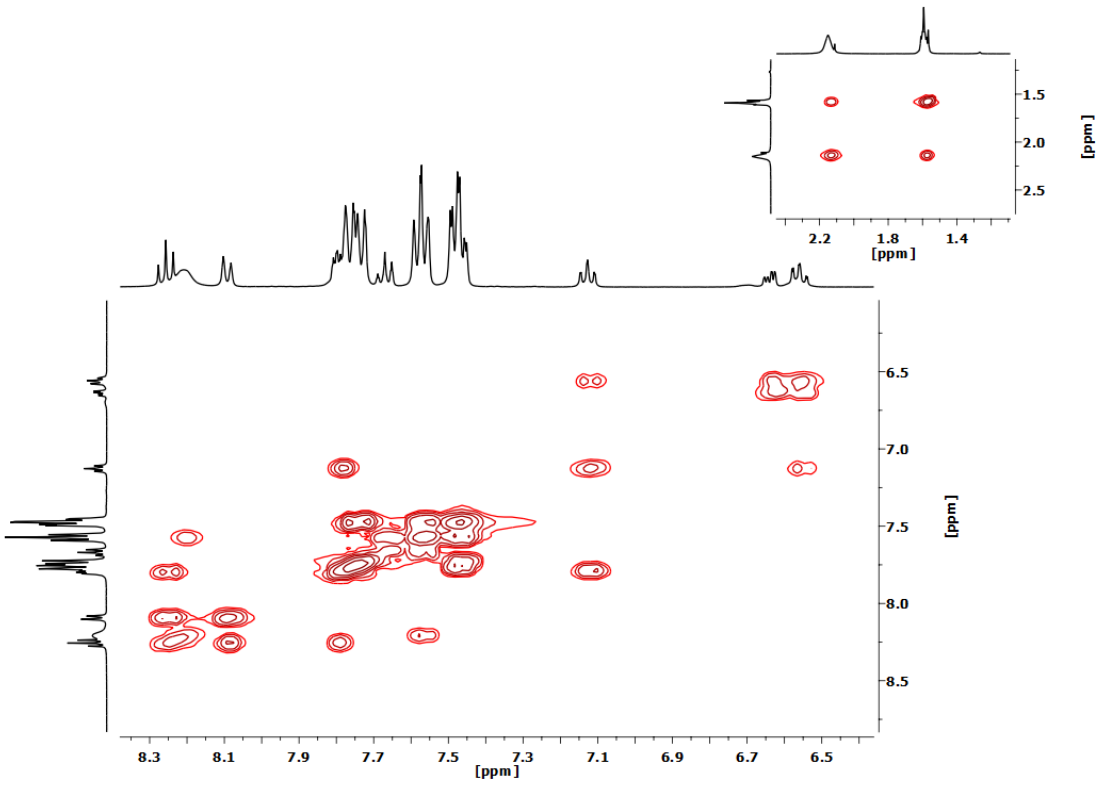

Figure S2.46. ^{1}H-^{1}H COSY NMR spectrum (CD_2Cl_2, RT) of complex [Pt(CNC-H)(tht)(PPh_3)](ClO_4) (**19**).

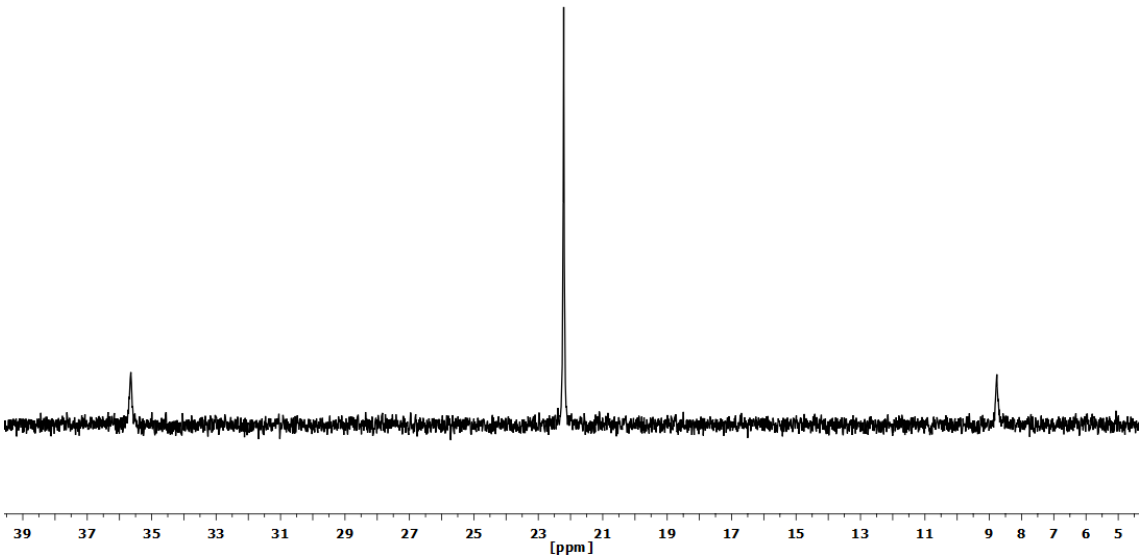

Figure S2.47. $^{31}P\{^{1}H\}$ NMR spectrum (CD_2Cl_2, RT) of complex [Pt(CNC-H)(tht)(PPh_3)](ClO_4) (**19**).

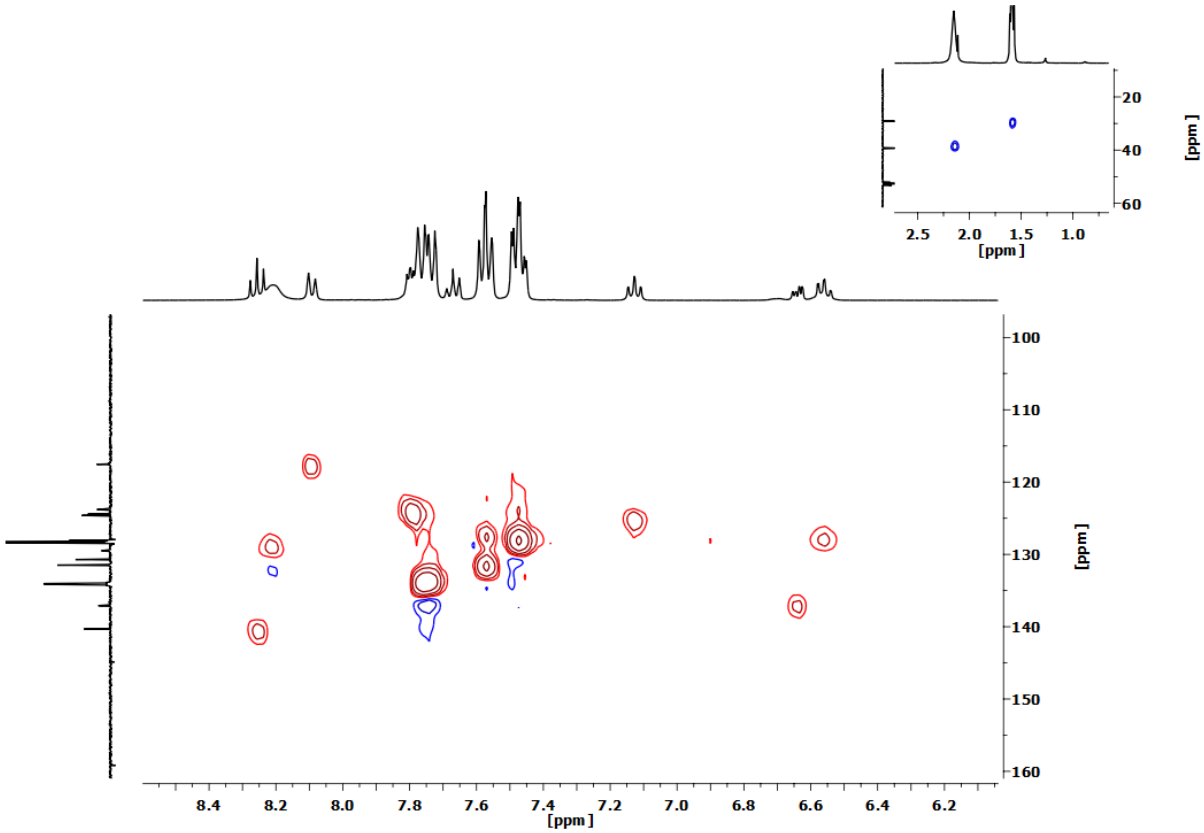

Figure S2.48. ^{1}H-^{13}C HSQC NMR spectrum (CD_2Cl_2, RT) of complex [Pt(CNC-H)(tht)(PPh_3)](ClO_4) (**19**).

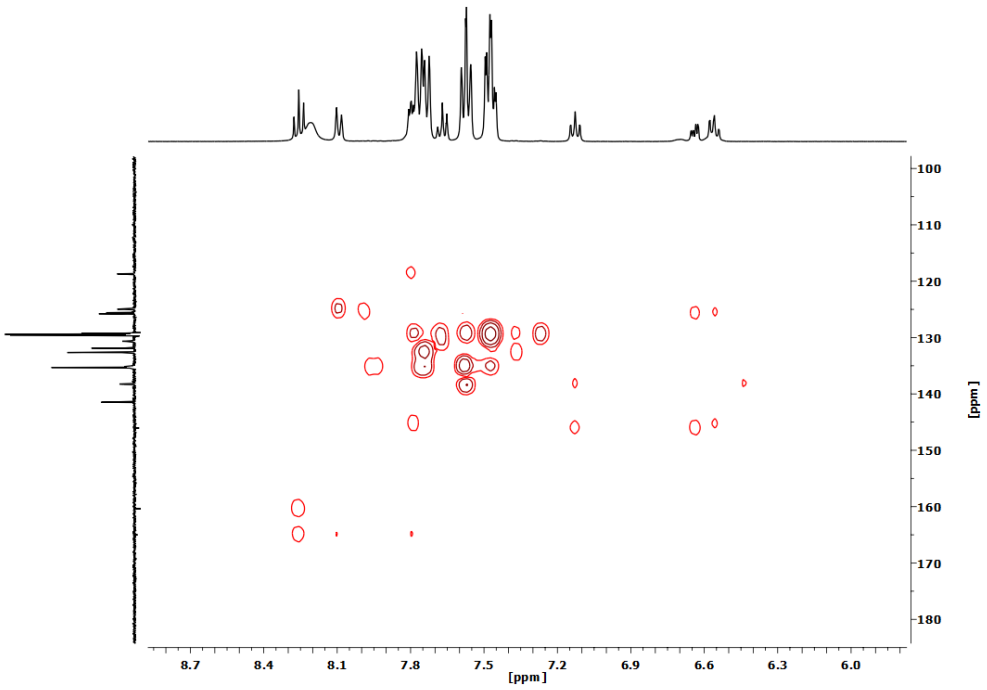

Figure S2.49. ^{1}H-^{13}C HMBC NMR spectrum (CD_2Cl_2, RT) of complex [Pt(CNC-H)(tht)(PPh_3)](ClO_4) (**19**).

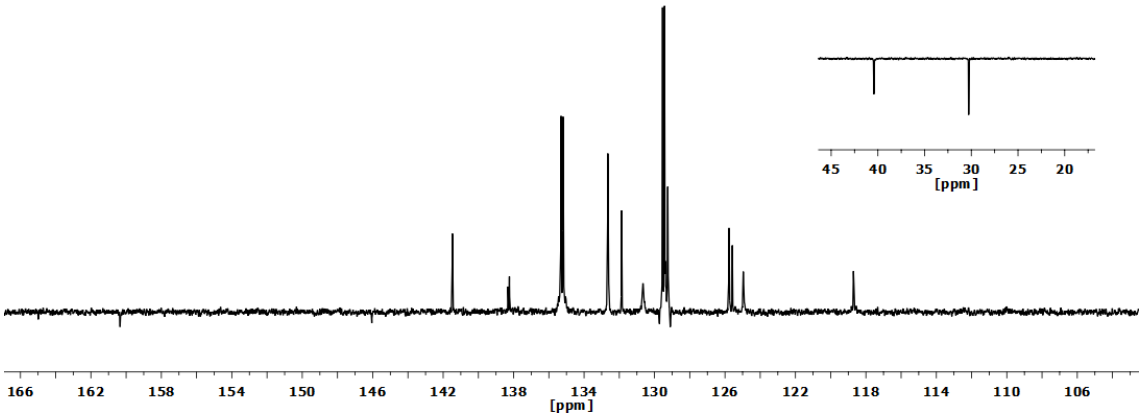

Figure S2.50. APT $^{13}C\{^{1}H\}$ NMR spectrum (CD_2Cl_2, RT) of complex [Pt(CNC-H)(tht)(PPh_3)](ClO_4) (**19**).

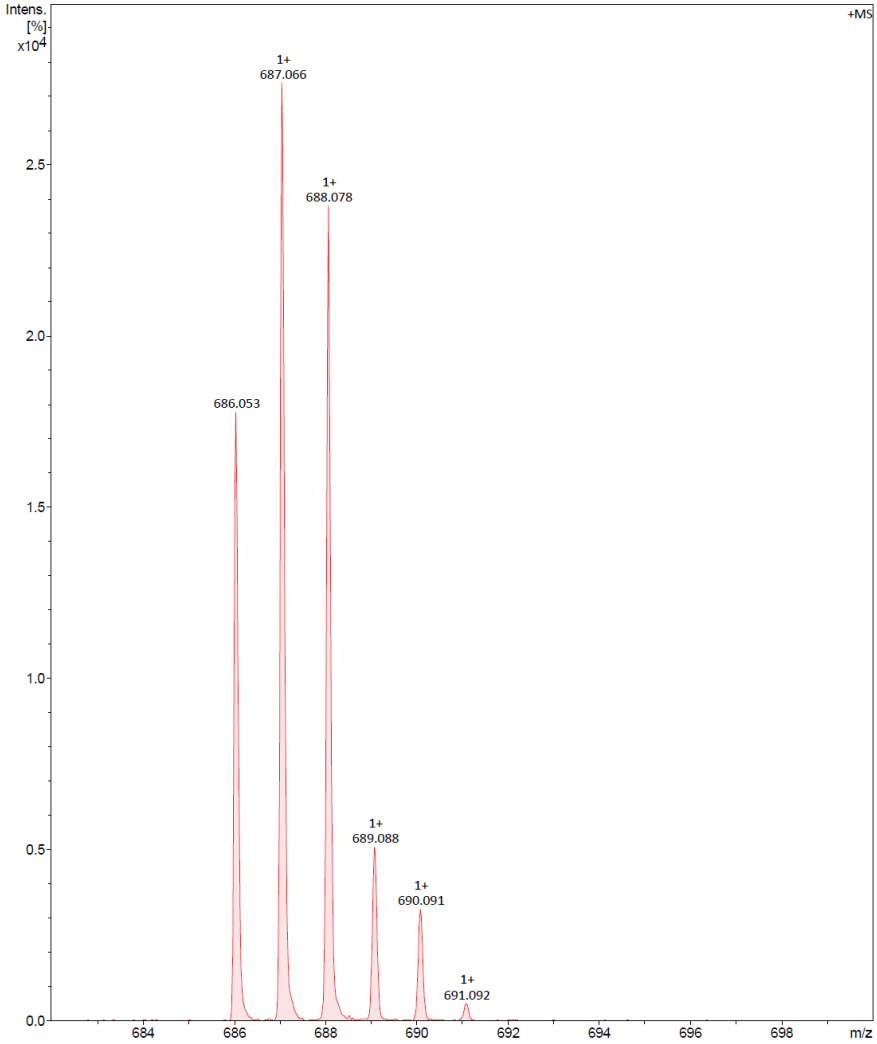

Figure S2.51. MS (MALDI+ DCTB) selected peak of complex [Pt(CNC-H)(tht)(PPh_3)](ClO_4) (**19**).

2.8. Spectra of complex [Pd(CNC-H)(tht)(PPh_3)](TfO) (20).

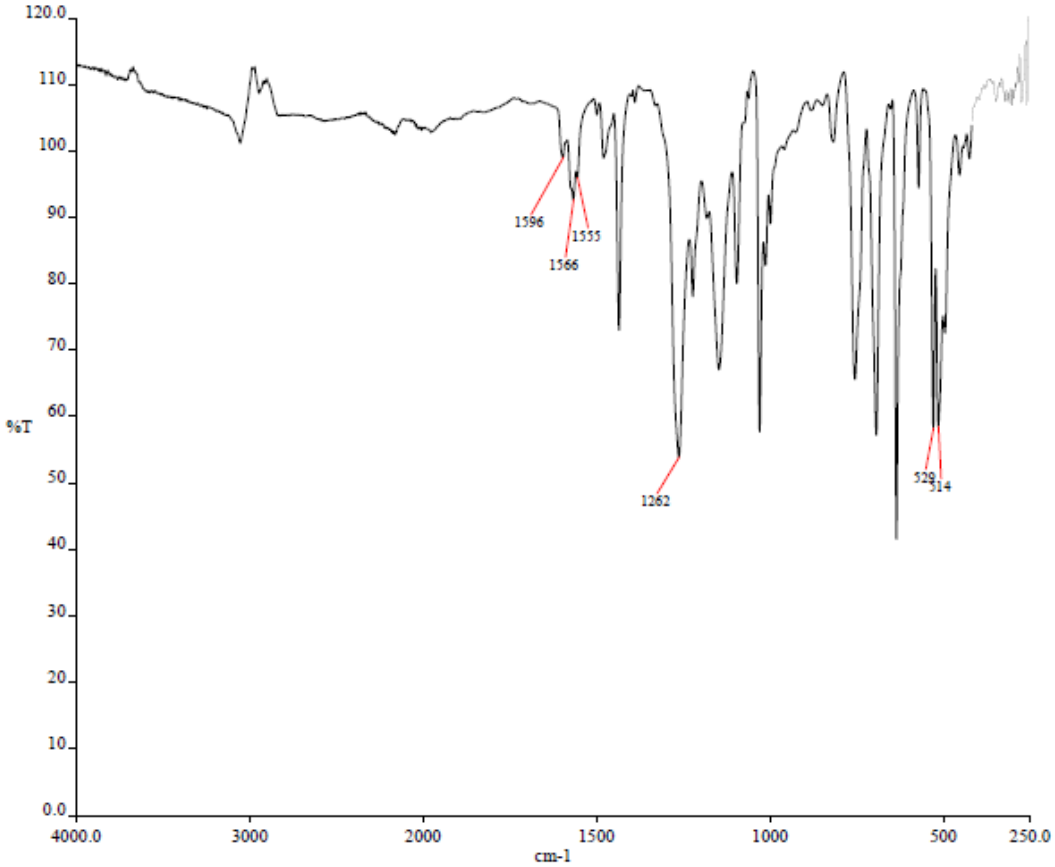

Figure S2.52. IR spectrum of complex [Pd(CNC-H)(tht)(PPh_3)](TfO) (**20**).

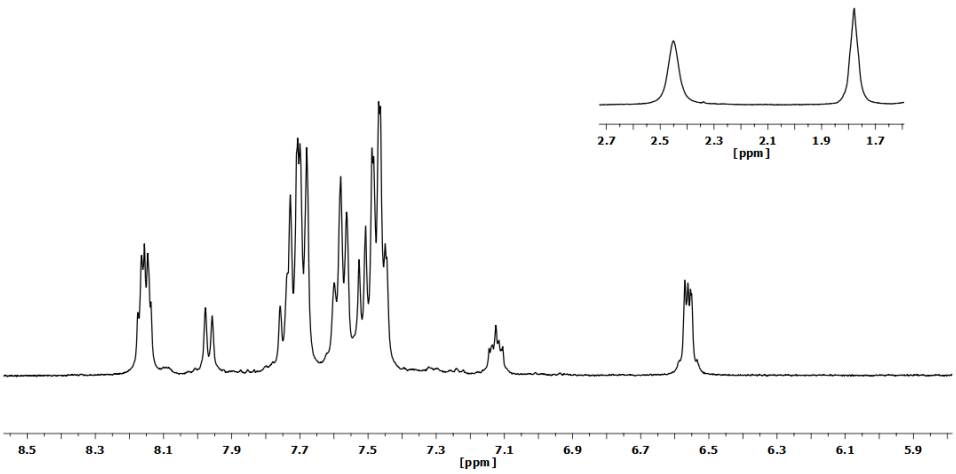

Figure S2.53. ^1H NMR spectrum (CD_2Cl_2, RT) of complex [Pd(CNC-H)(tht)(PPh_3)](TfO) (**20**).

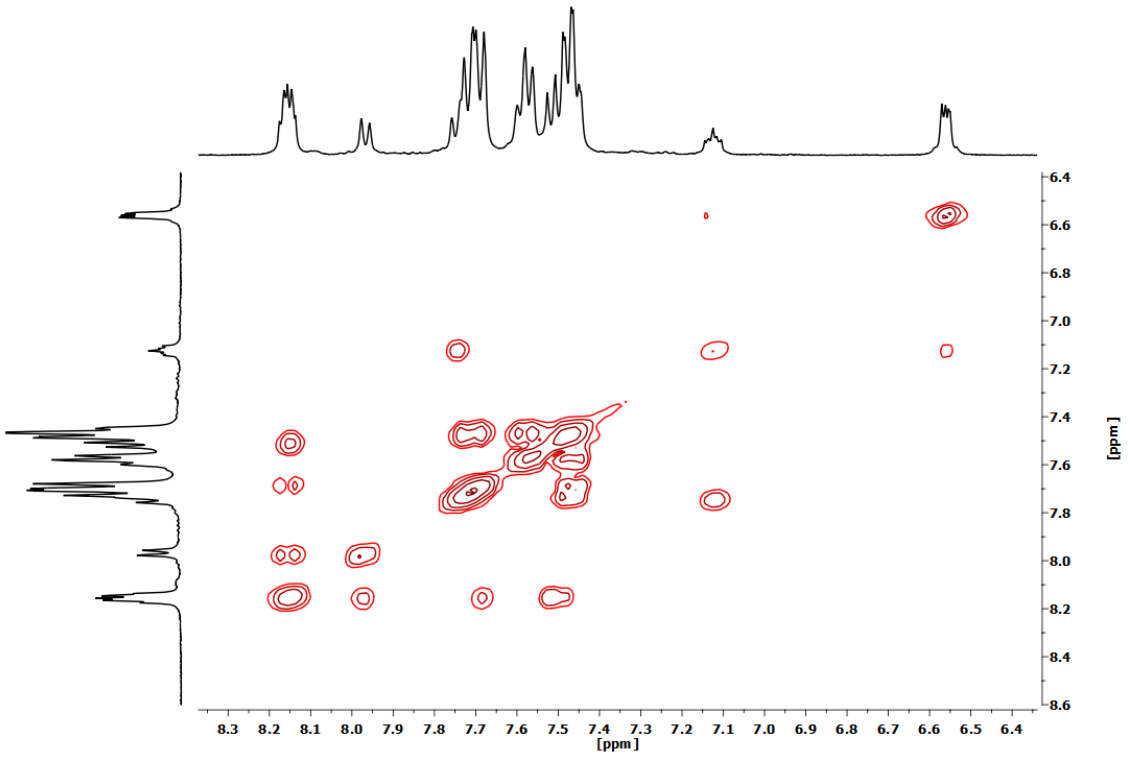

Figure S2.54. ^{1}H-^{1}H COSY NMR spectrum (CD_2Cl_2, RT) of complex [Pd(CNC-H)(tht)(PPh_3)](TfO) (**20**).

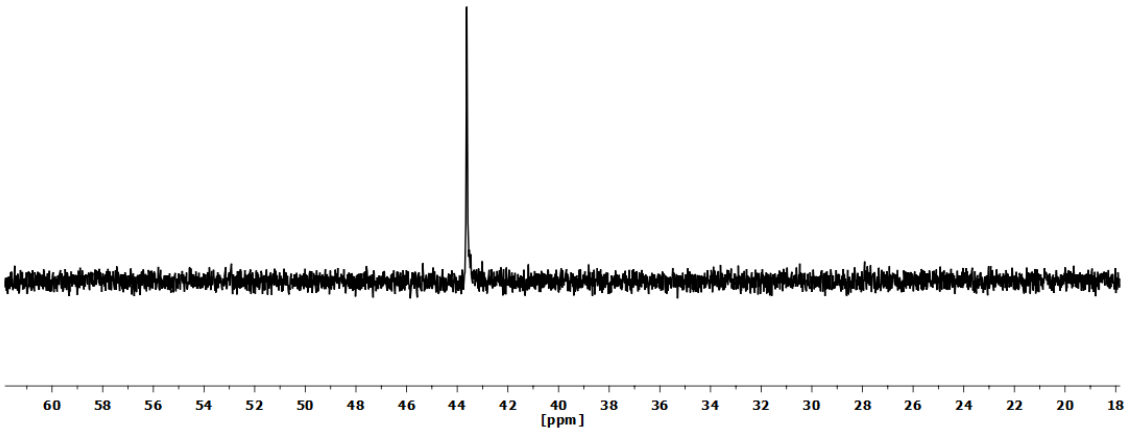

Figure S2.55. ^{31}P{^{1}H} NMR spectrum (CD_2Cl_2, RT) of complex [Pd(CNC-H)(tht)(PPh_3)](TfO) (**20**).

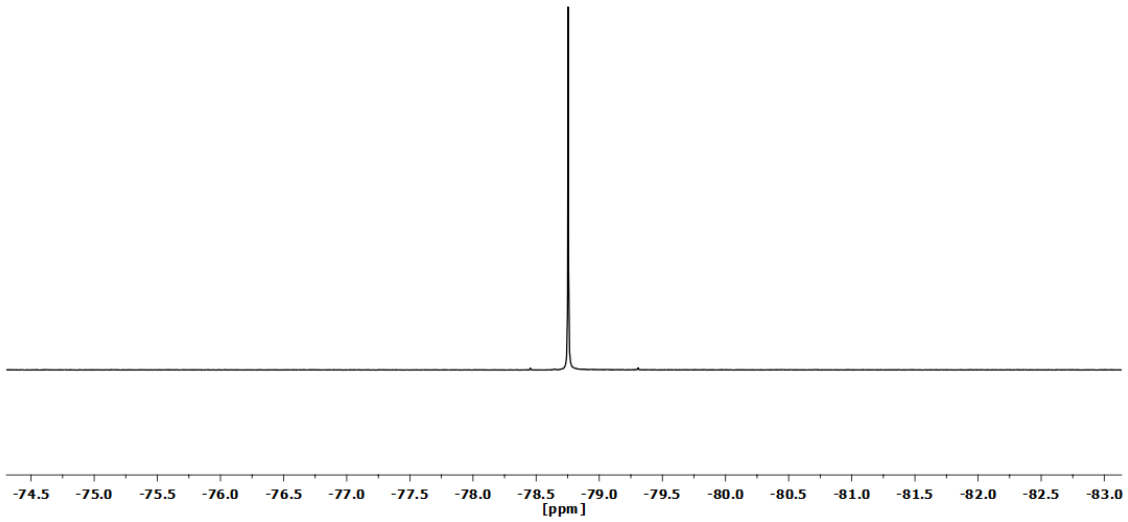

Figure S2.56. $^{19}F\{^{1}H\}$ NMR spectrum (CD_2Cl_2, RT) of complex [Pd(CNC-H)(tht)(PPh_3)](TfO) (**20**).

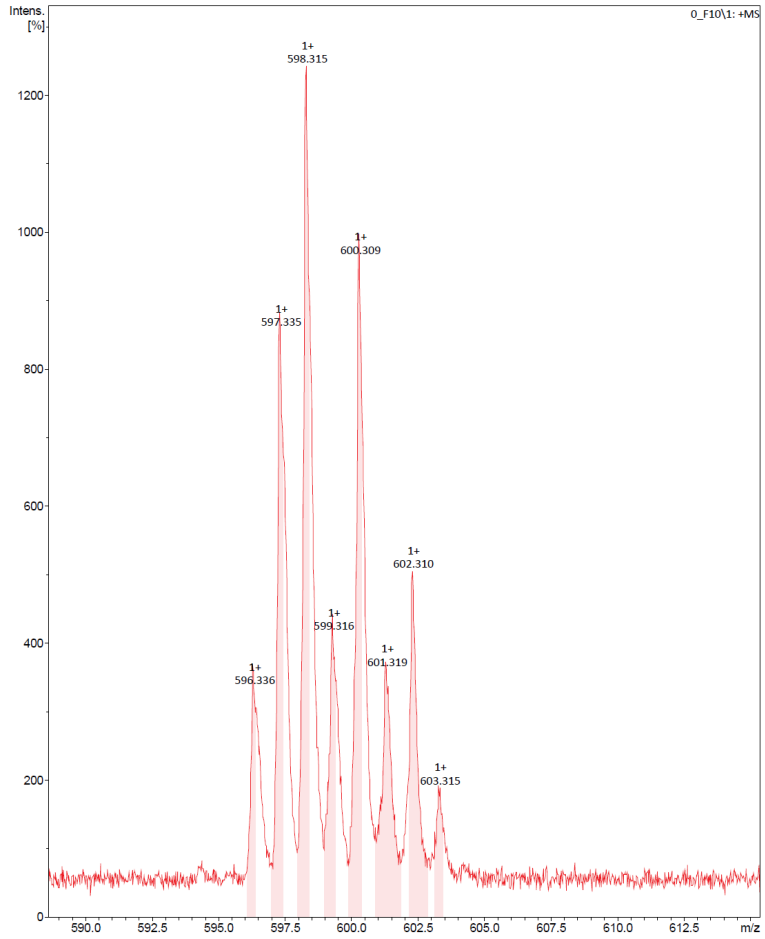

Figure S2.57. MS (MALDI+ DCTB) selected peak of complex [Pd(CNC-H)(tht)(PPh_3)](TfO) (**20**).

2.9. Spectra of complex [Pt(CNC-H)(μ-S-2Py)]$_2$ (21).

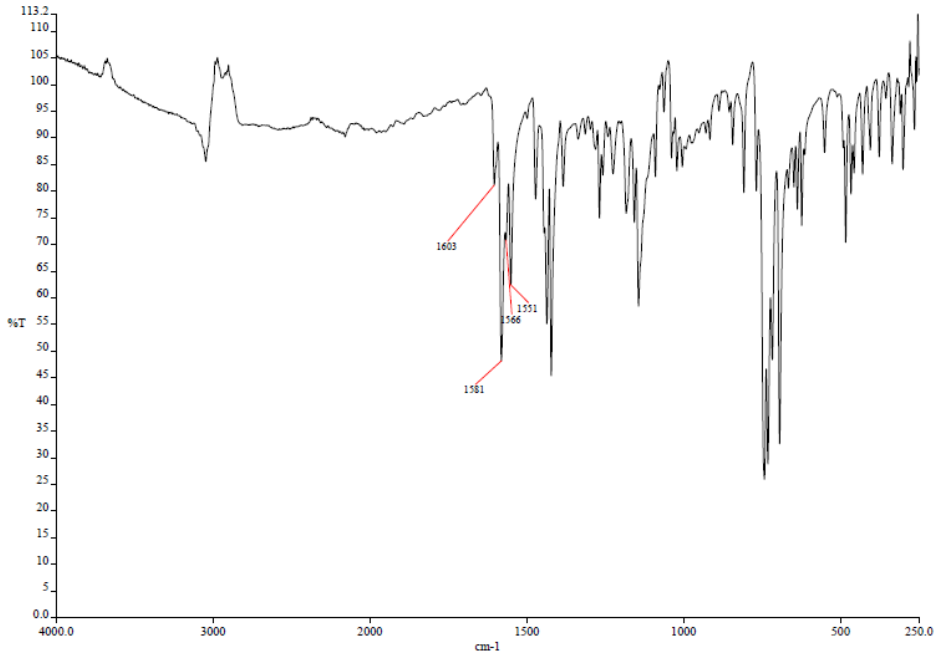

Figure S2.58. IR spectrum of complex [Pt(CNC-H)(μ-S-2Py)]$_2$ (**21**).

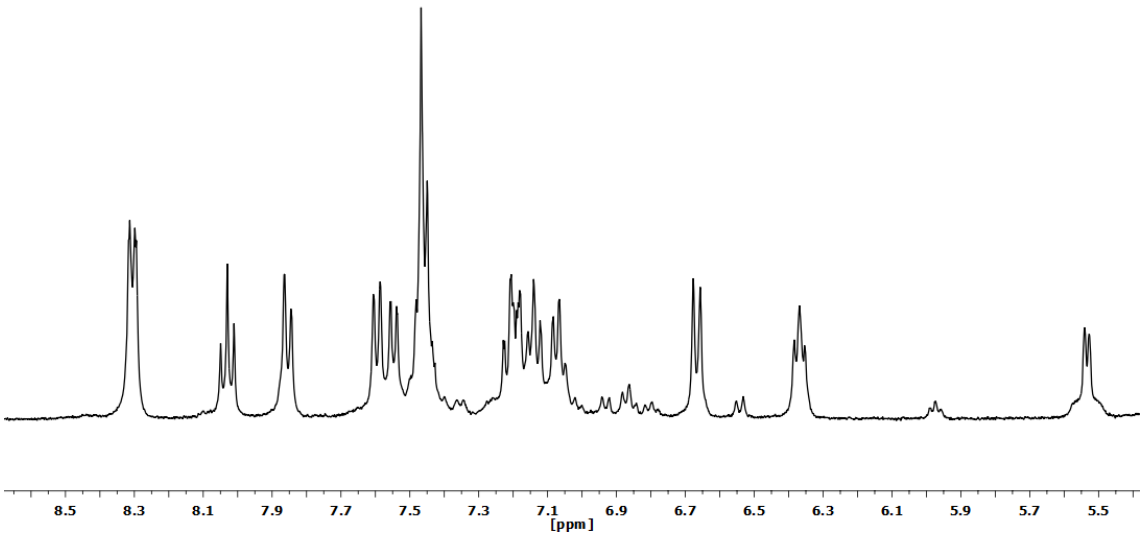

Figure S2.59. ^{1}H NMR (CD_2Cl_2, RT) spectrum of complex [Pt(CNC-H)(μ-S-2Py)]$_2$ (**21**).

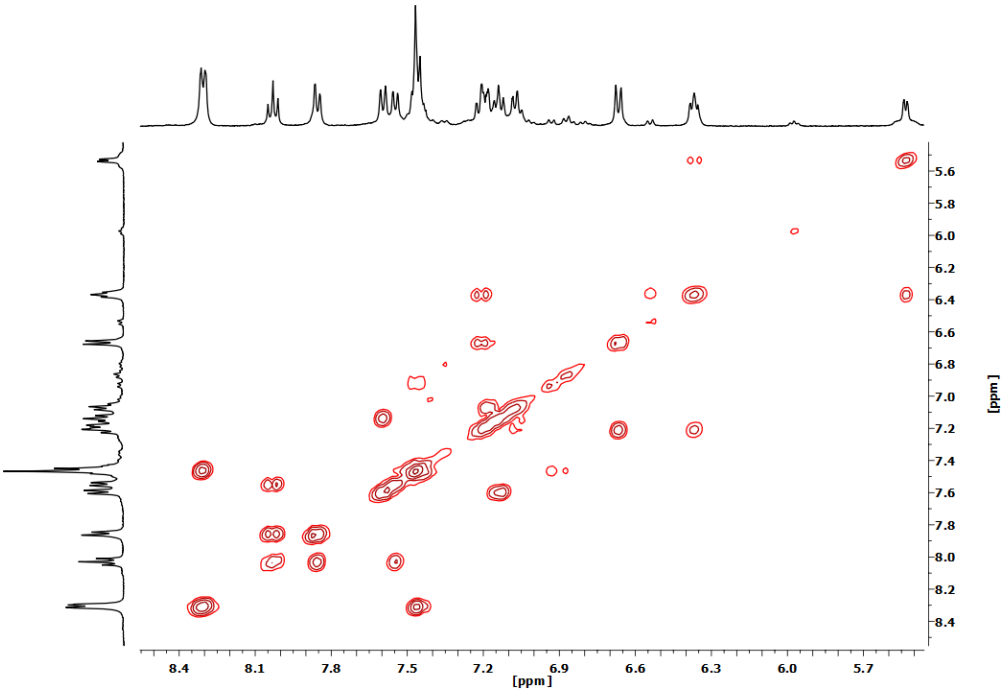

Figure S2.60. ^{1}H-^{1}H COSY NMR (CD_2Cl_2, RT) spectrum of complex [Pt(CNC-H)(μ-S-2Py)]$_2$ (**21**).

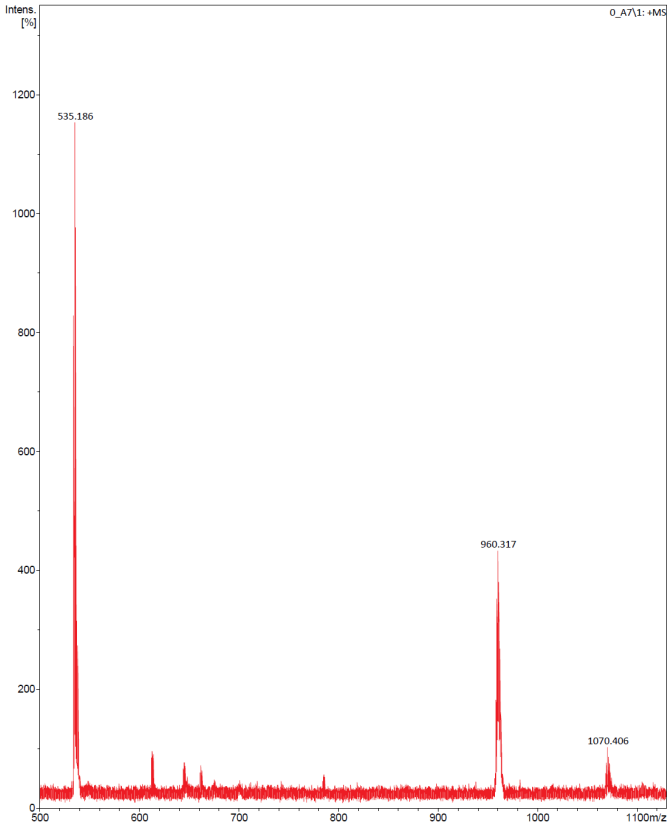

Figure S2.61. MS (MALDI+ DCTB) selected peaks of complex [Pt(CNC-H)(μ-S-2Py)]$_2$ (**21**).

2.10. Spectra of complex [Pt(CNC-H)(8-hq)] (22).

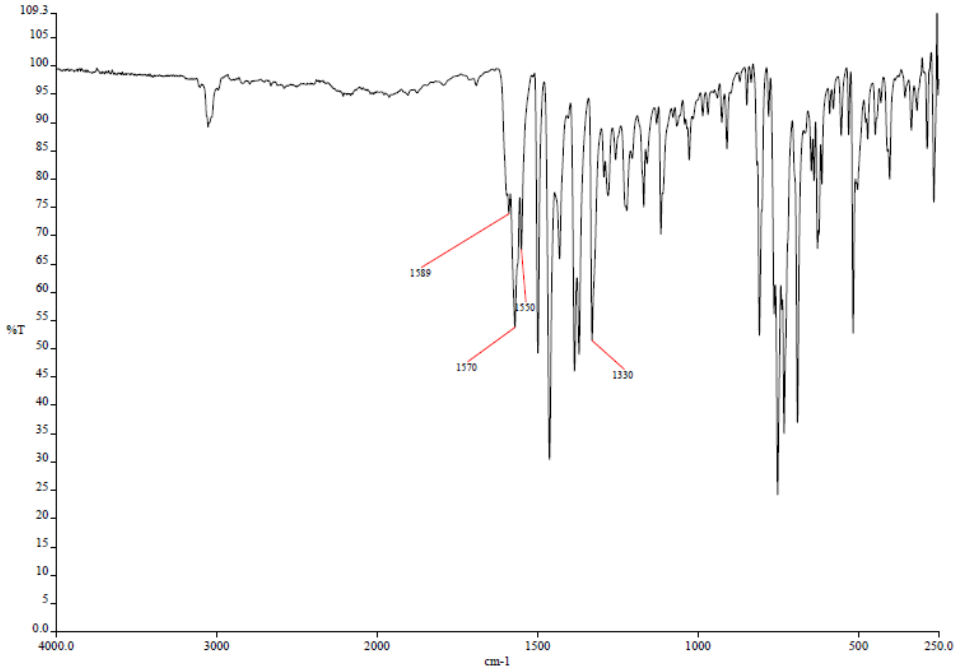

Figure S2.62. IR spectrum of complex [Pt(CNC-H)(8-hq)] (**22**).

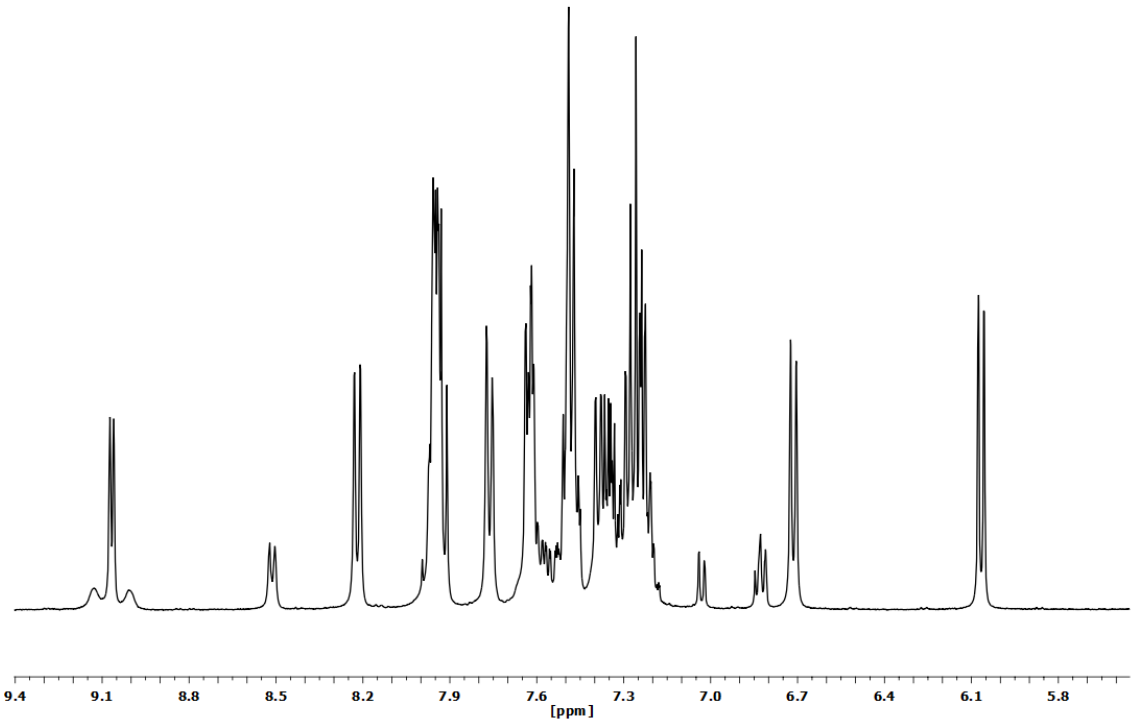

Figure S2.63. ^{1}H NMR spectrum (CD_2Cl_2, RT) of complex [Pt(CNC-H)(8-hq)] (**22**).

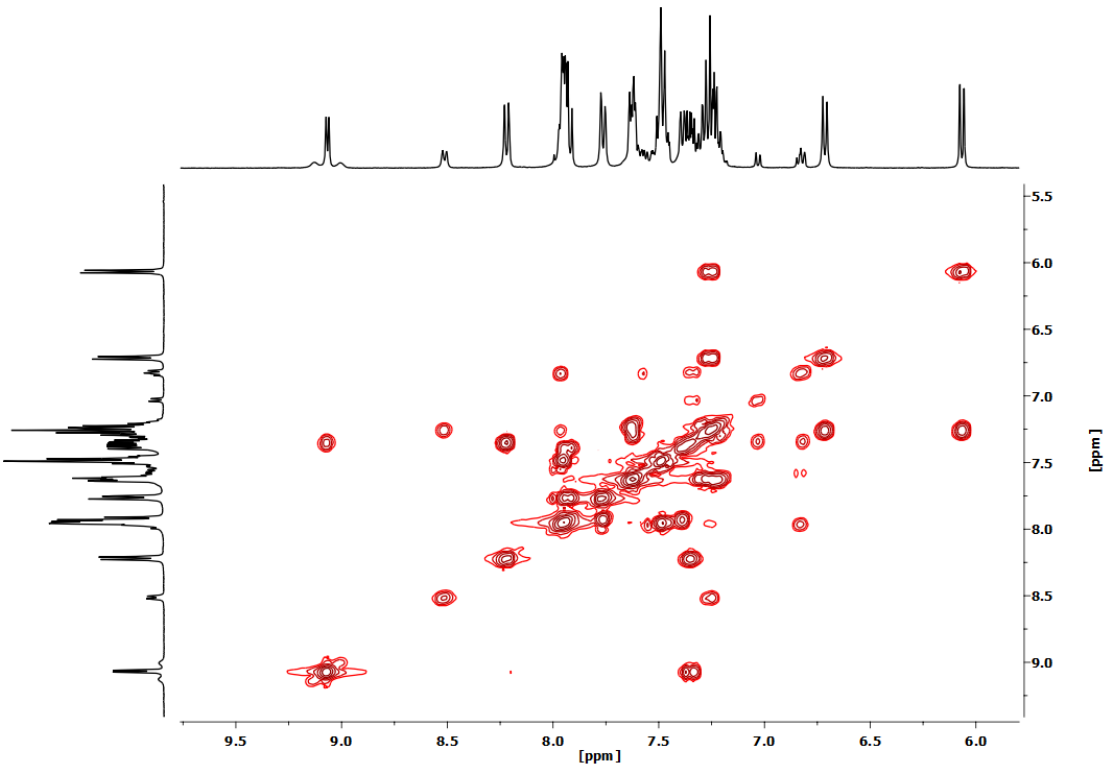

Figure S2.64. ^{1}H-^{1}H COSY NMR spectrum (CD_2Cl_2, RT) of complex [Pt(CNC-H)(8-hq)] (**22**).

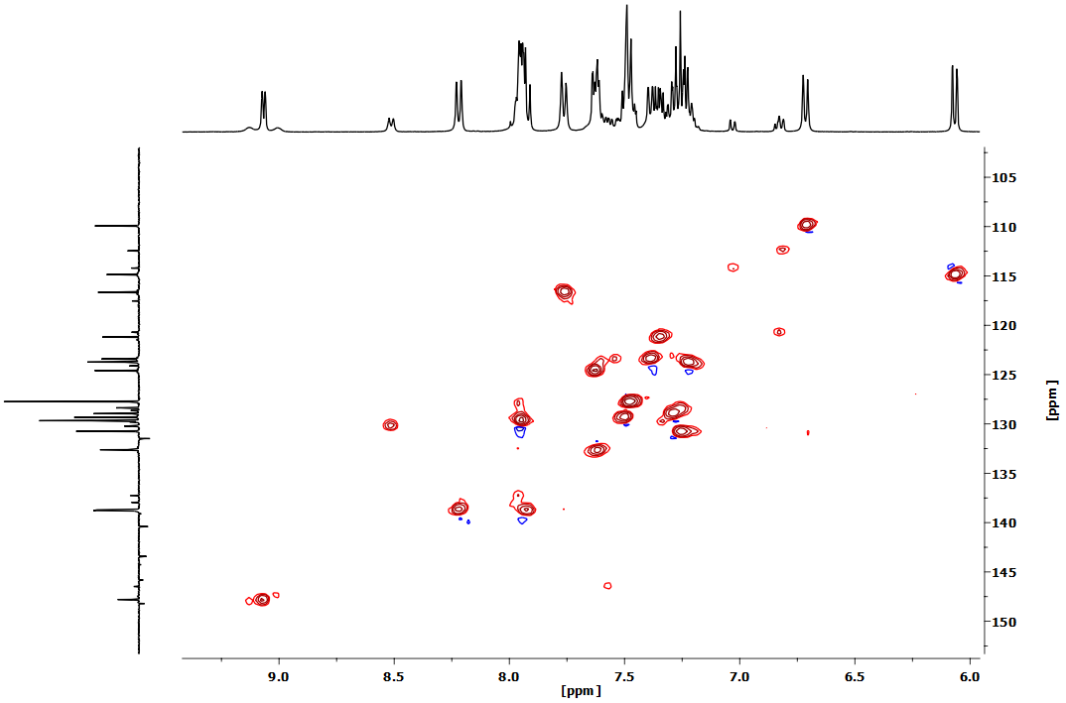

Figure S2.65. ^{1}H-^{13}C HSQC NMR spectrum (CD_2Cl_2, RT) of complex [Pt(CNC-H)(8-hq)] (**22**).

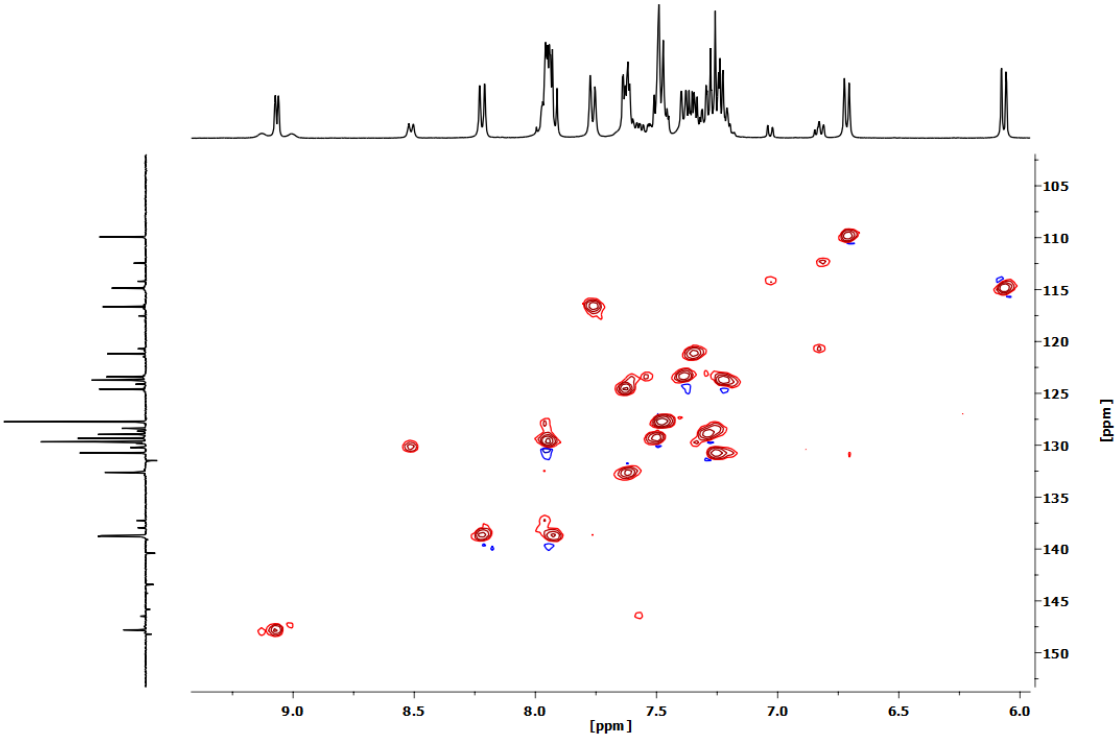

Figure S2.66. ^{1}H-^{13}C HMBC NMR spectrum (CD_2Cl_2, RT) of complex [Pt(CNC-H)(8-hq)] (**22**).

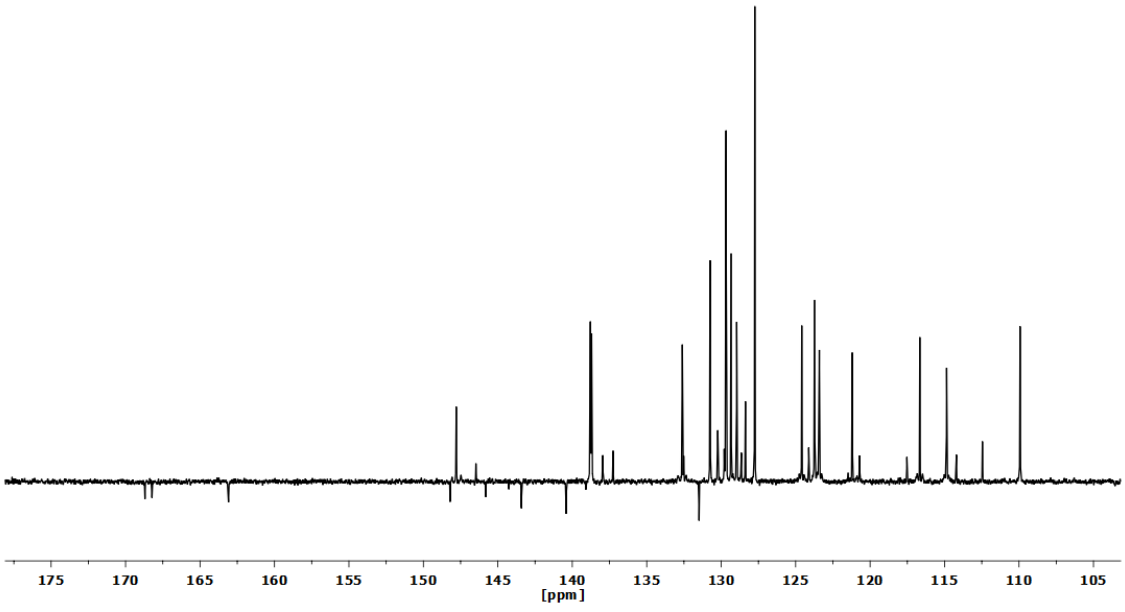

Figure S2.67. APT $^{13}C\{^{1}H\}$ NMR spectrum (CD_2Cl_2, RT) of complex [Pt(CNC-H)(8-hq)] (**22**).

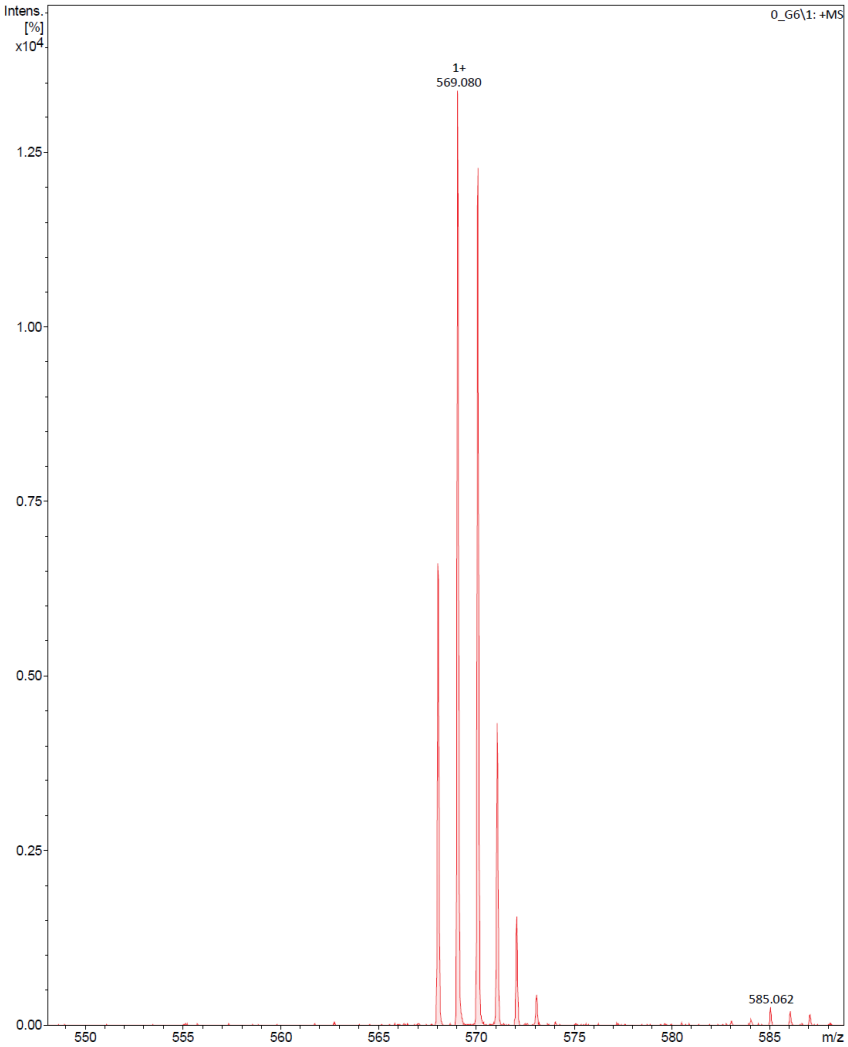

Figure S2.68. MS (MALDI+ DCTB) selected peak of complex [Pt(CNC-H)(8-hq)] (**22**).

2.11. Spectra of complex [Pt(CNC-H){PPh$_2$(C$_6$H$_4$-*o*-O)}] (23).

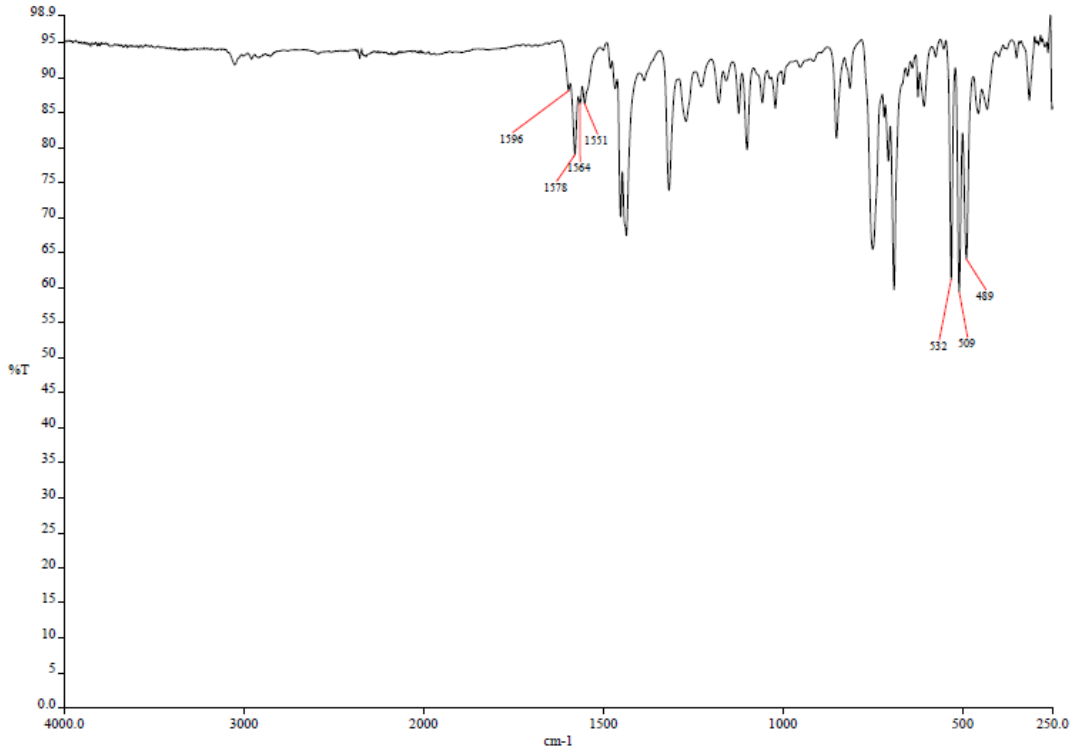

Figure S2.69. IR spectrum of complex [Pt(CNC-H){PPh$_2$(C$_6$H$_4$-*o*-O)}] (**23**).

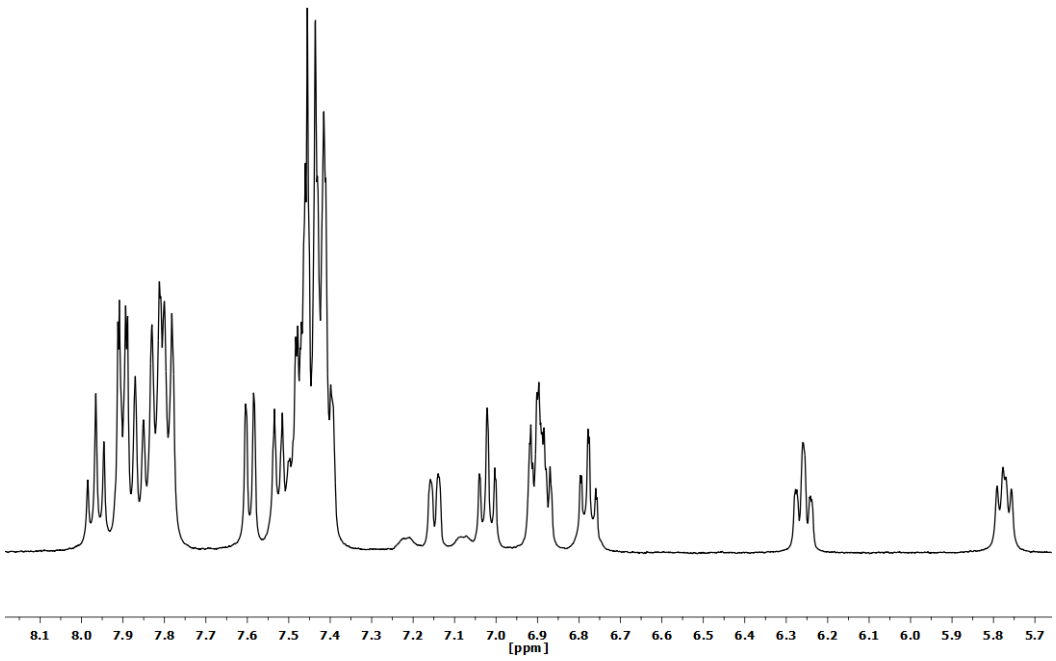

Figure S2.70. ^{1}H NMR spectrum (CD_2Cl_2, RT) of complex [Pt(CNC-H){PPh$_2$(C$_6$H$_4$-*o*-O)}] (**23**).

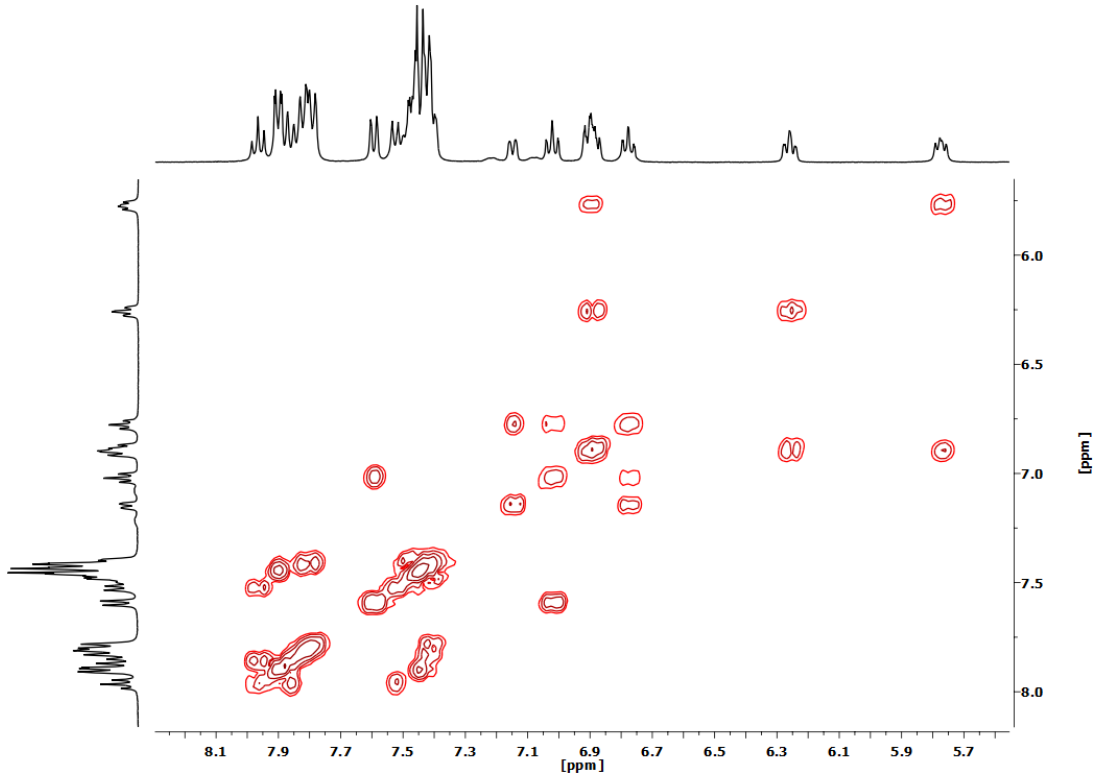

Figure S2.71. ^{1}H-^{1}H COSY NMR spectrum (CD_2Cl_2, RT) of complex [Pt(CNC-H){$PPh_2(C_6H_4$-*o*-O)}] (**23**).

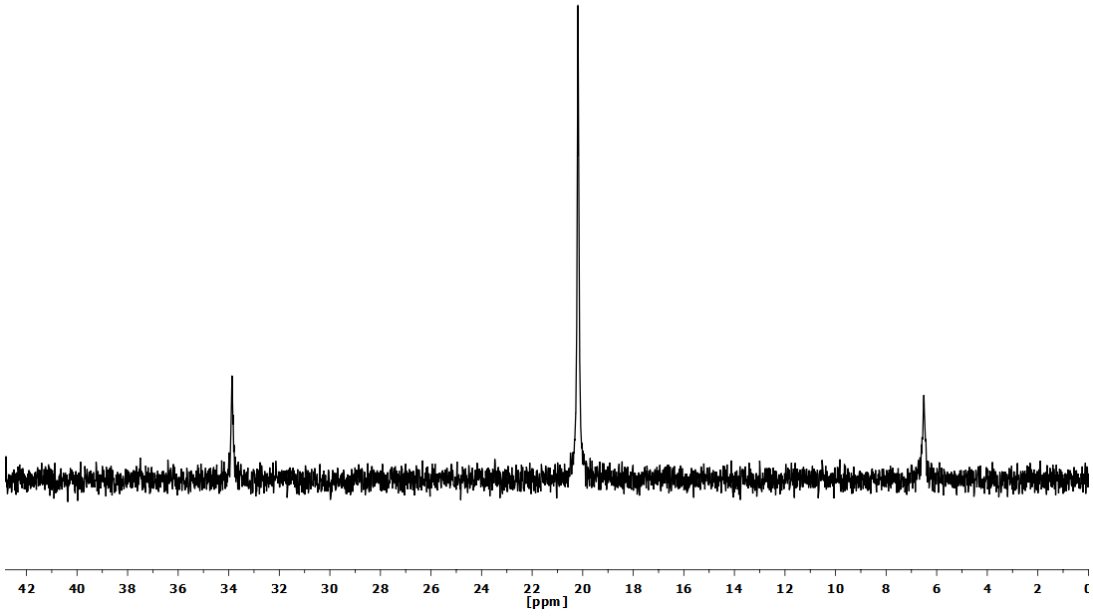

Figure S2.72. ^{31}P{^{1}H} NMR spectrum (CD_2Cl_2, RT) of complex [Pt(CNC-H){$PPh_2(C_6H_4$-*o*-O)}] (**23**).

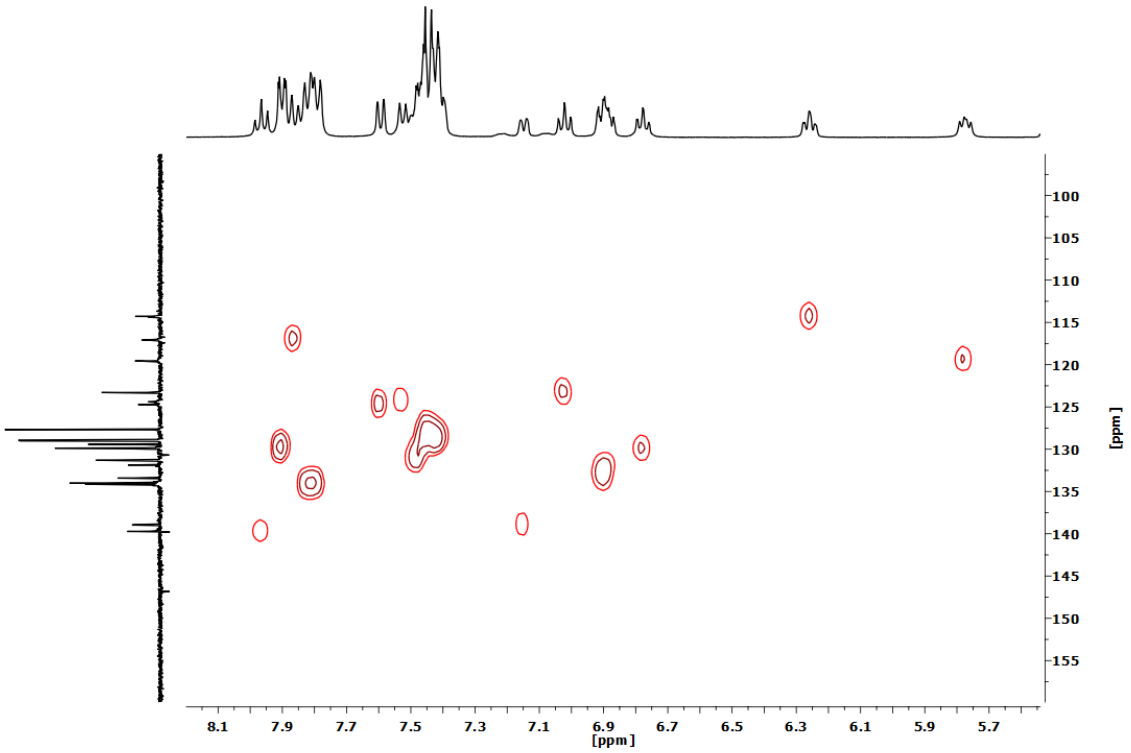

Figure S2.73. ^{1}H-^{13}C HSQC NMR spectrum (CD_2Cl_2, RT) of complex [Pt(CNC-H){$PPh_2(C_6H_4$-*o*-O)}] (**23**).

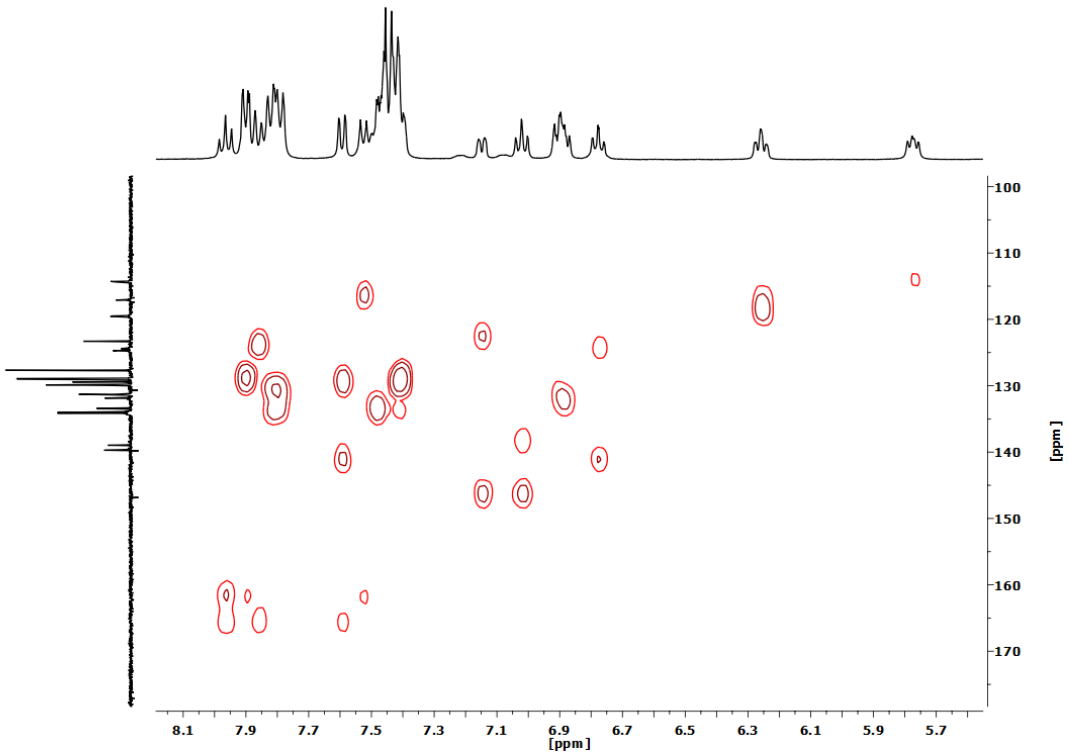

Figure S2.74. ^{1}H-^{13}C HMBC NMR spectrum (CD_2Cl_2, RT) of complex [Pt(CNC-H){$PPh_2(C_6H_4$-*o*-O)}] (**23**).

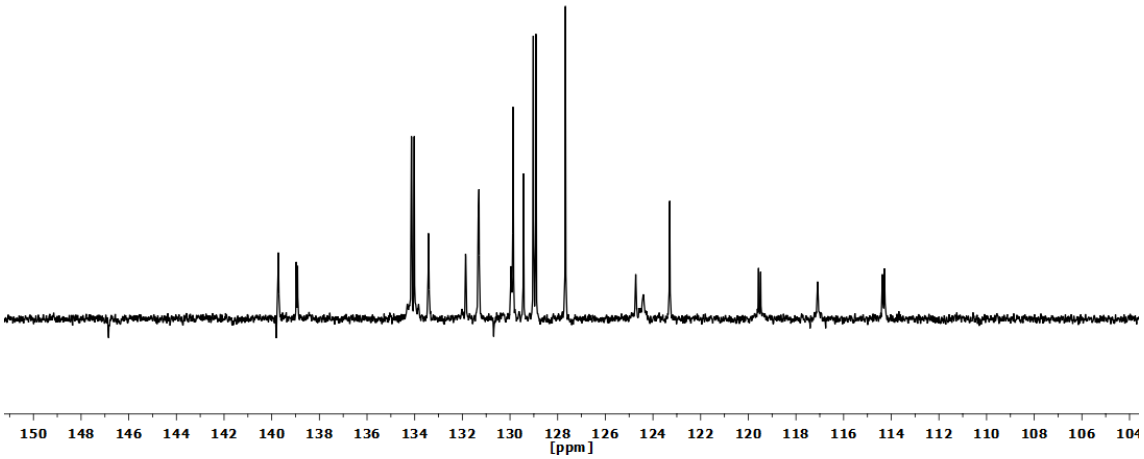

Figure S2.75. APT $^{13}C\{^{1}H\}$ NMR spectrum (CD_2Cl_2, RT) of complex [Pt(CNC-H){$PPh_2(C_6H_4$-*o*-O)}] (**23**).

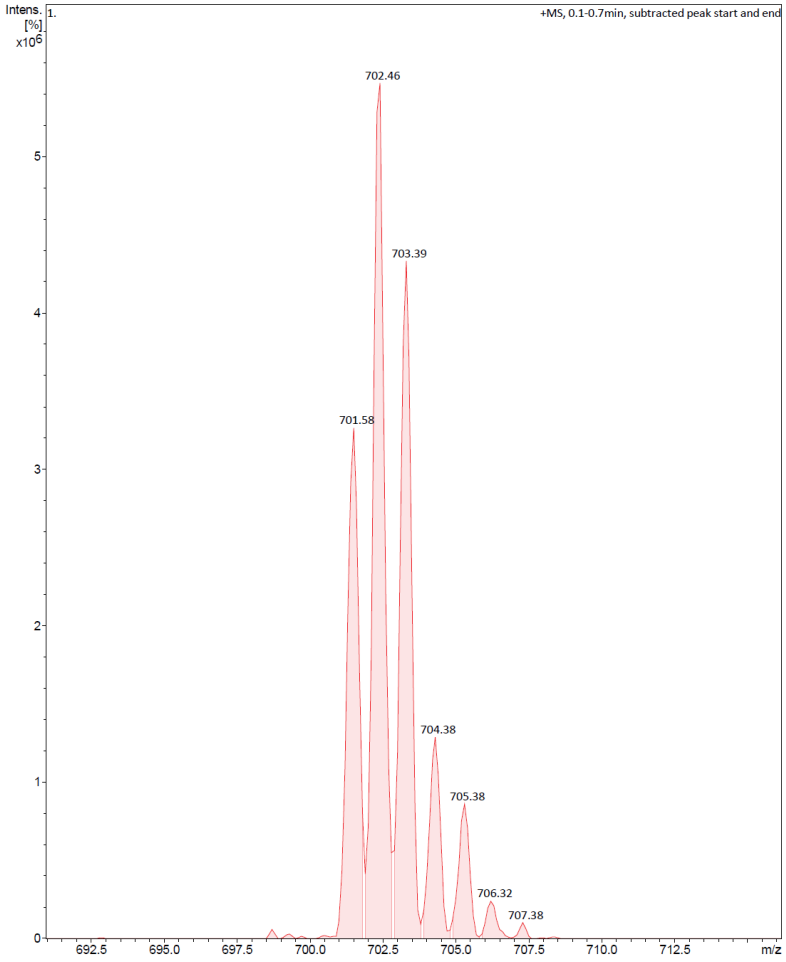

Figure S2.76. MS (ESI+) selected peak of complex [Pt(CNC-H){$PPh_2(C_6H_4$-*o*-O)}] (**23**).

2.12. Spectra of complex [Pd(CNC-H) {$PPh_2(C_6H_4$-*o*-O)}] (24).

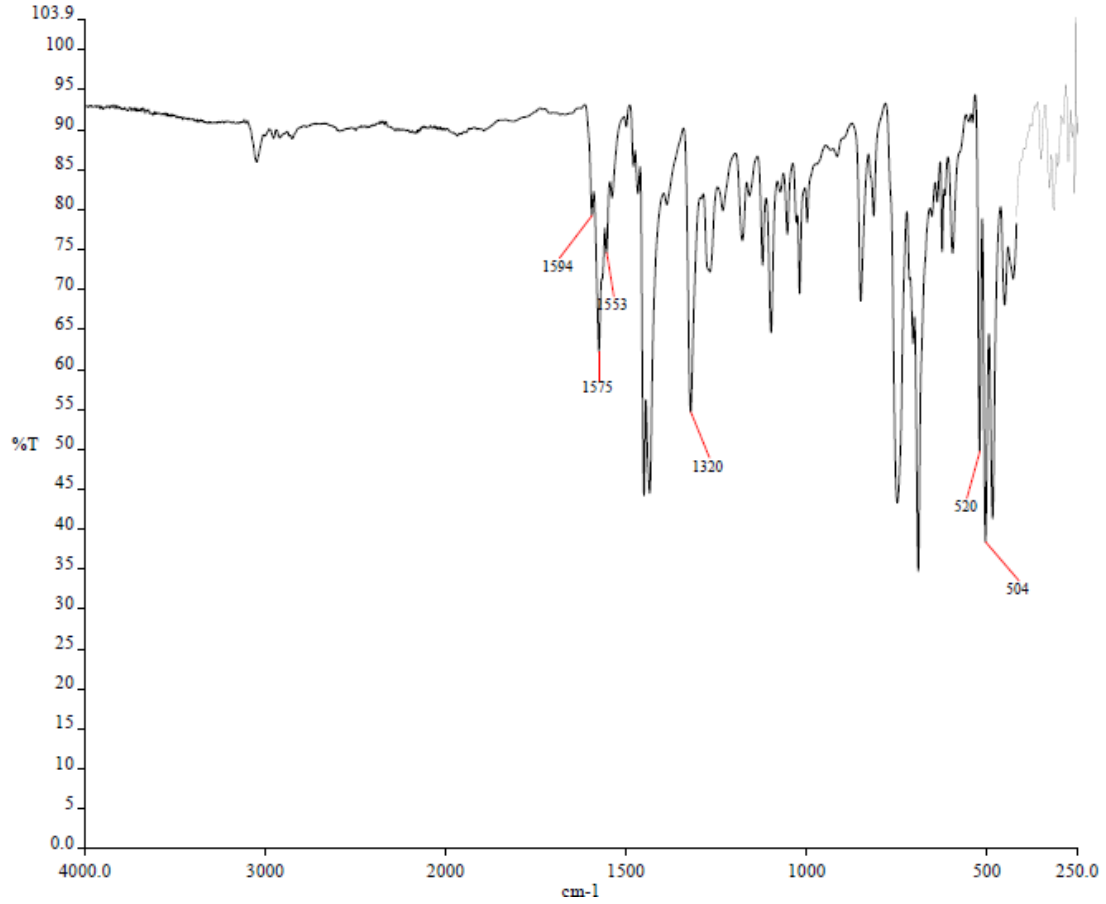

Figure S2.77. IR spectrum of complex [Pd(CNC-H){$PPh_2(C_6H_4$-*o*-O)}] (**24**).

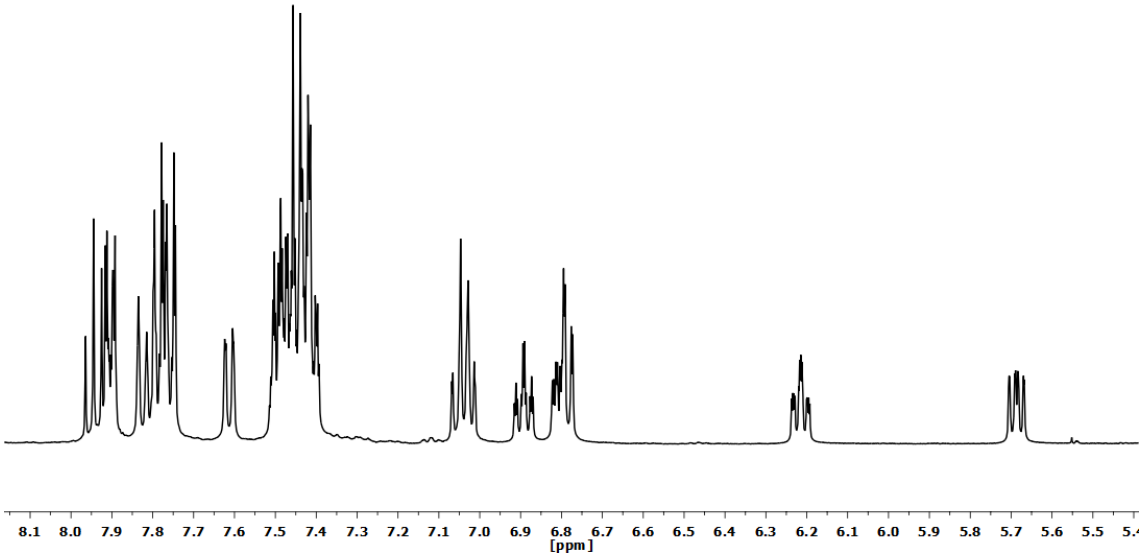

Figure S2.78. ^{1}H NMR spectrum (CD_2Cl_2, RT) of complex [Pd(CNC-H){$PPh_2(C_6H_4$-*o*-O)}] (**24**).

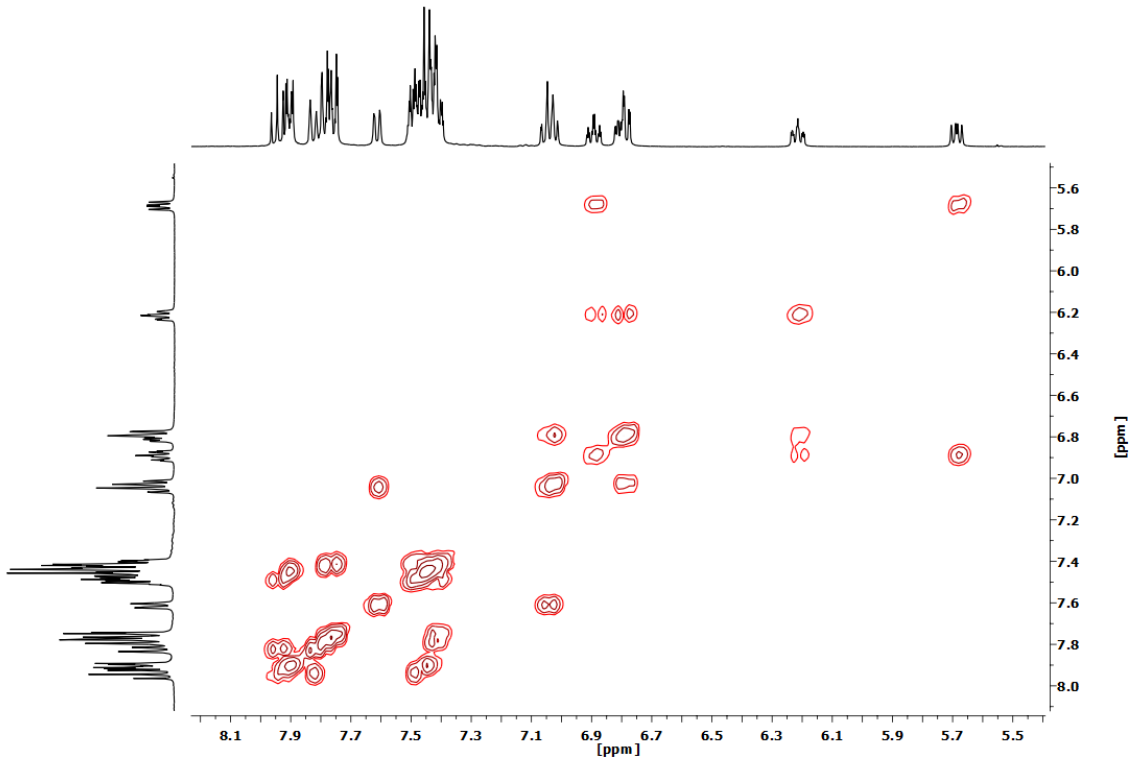

Figure S2.79. ^{1}H-^{1}H COSY NMR spectrum (CD_2Cl_2, RT) of complex [Pd(CNC-H){$PPh_2(C_6H_4$-*o*-O)}] (**24**).

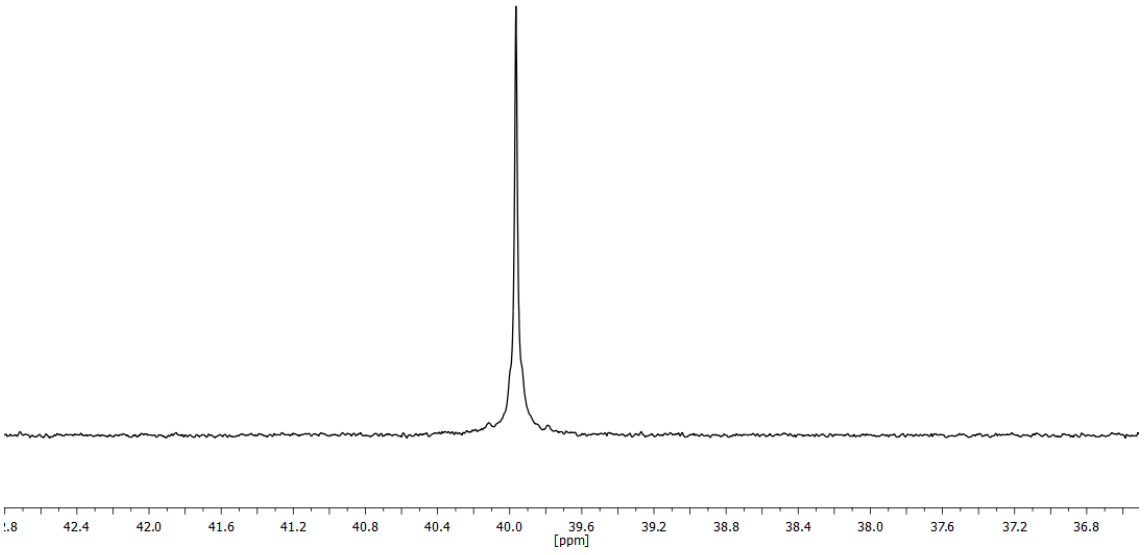

Figure S2.80. $^{31}P\{^{1}H\}$ NMR spectrum (CD_2Cl_2, RT) of complex [Pd(CNC-H){$PPh_2(C_6H_4$-*o*-O)}] (**24**).

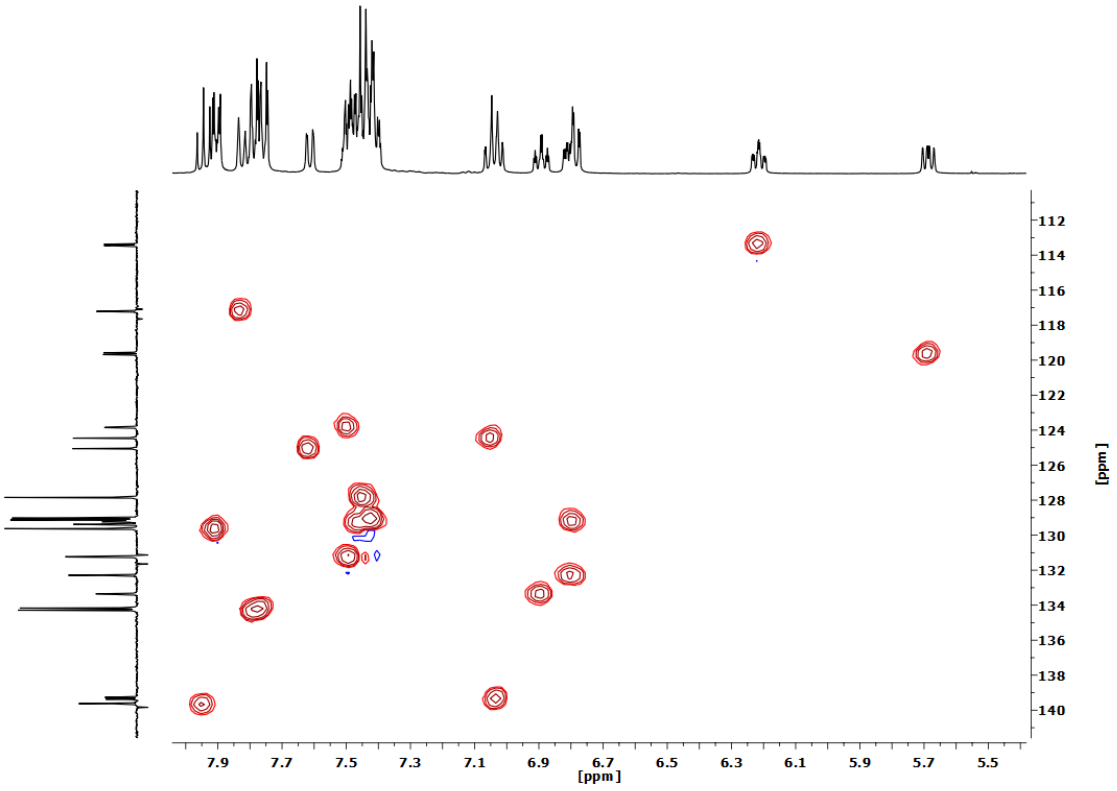

Figure S2.81. ^{1}H-^{13}C HSQC NMR spectrum (CD_2Cl_2, RT) of complex [Pd(CNC-H){$PPh_2(C_6H_4$-*o*-O)}] (**24**).

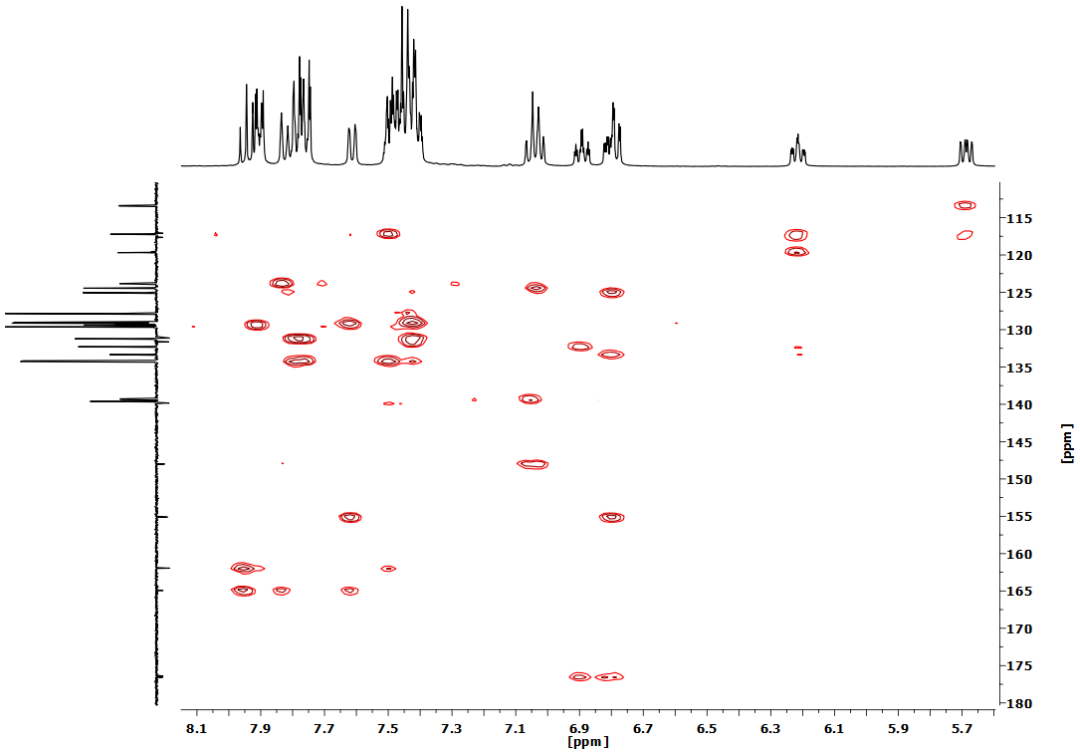

Figure S2.82. ^{1}H-^{13}C HMBC NMR spectrum (CD_2Cl_2, RT) of complex [Pd(CNC-H){$PPh_2(C_6H_4$-*o*-O)}] (**24**).

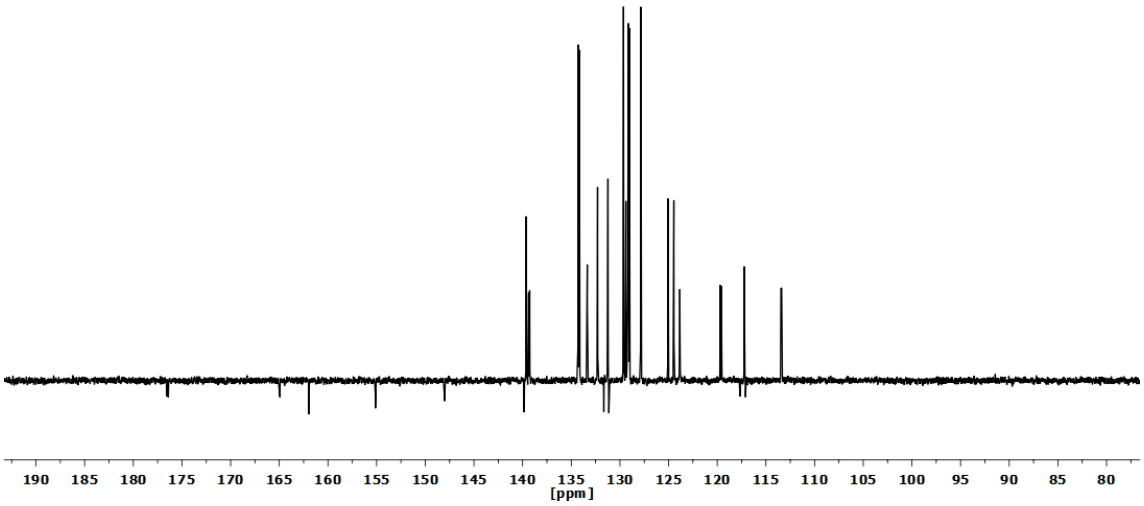

Figure S2.83. APT $^{13}C\{^{1}H\}$ NMR spectrum (CD_2Cl_2, RT) of complex [Pd(CNC-H){$PPh_2(C_6H_4$-*o*-O)}] (**24**).

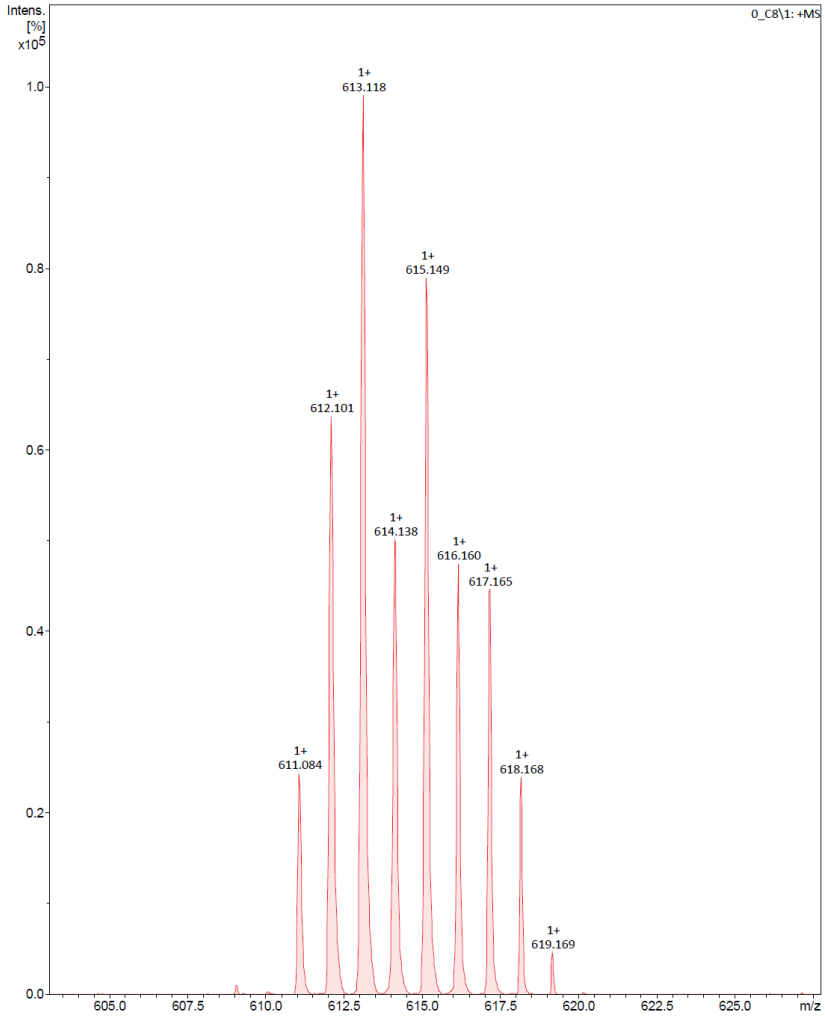

Figure S2.84. MS (MALDI+ DCTB) molecular peak of complex [Pd(CNC-H){$PPh_2(C_6H_4$-*o*-O)}] (**24**).

2.13. Spectra of complex [Pt(CNC-H)(NC$_5$H$_4$-*o*-COO)] (25).

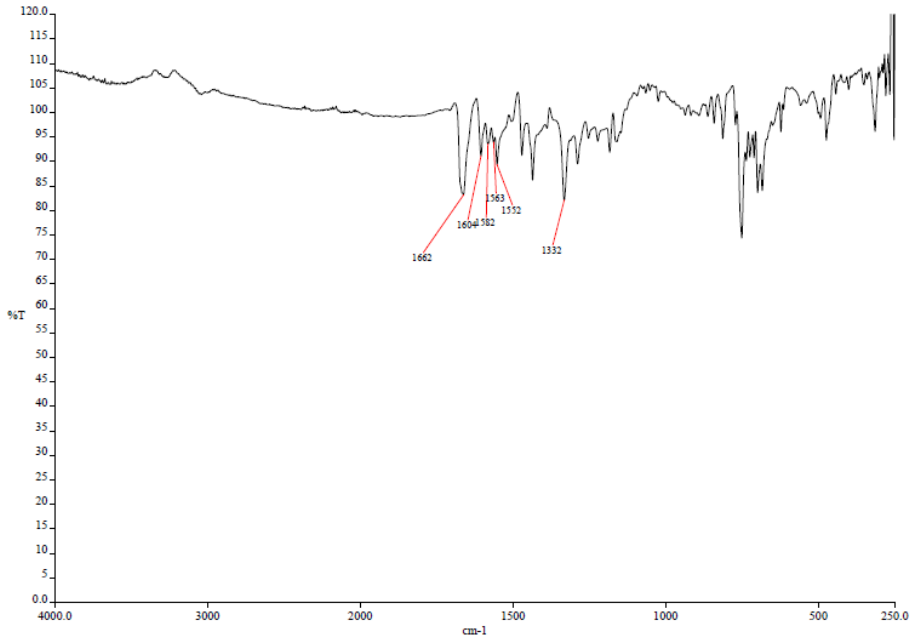

Figure S2.85. IR spectrum of complex [Pt(CNC-H)(NC$_5$H$_4$-*o*-COO)] (**25**).

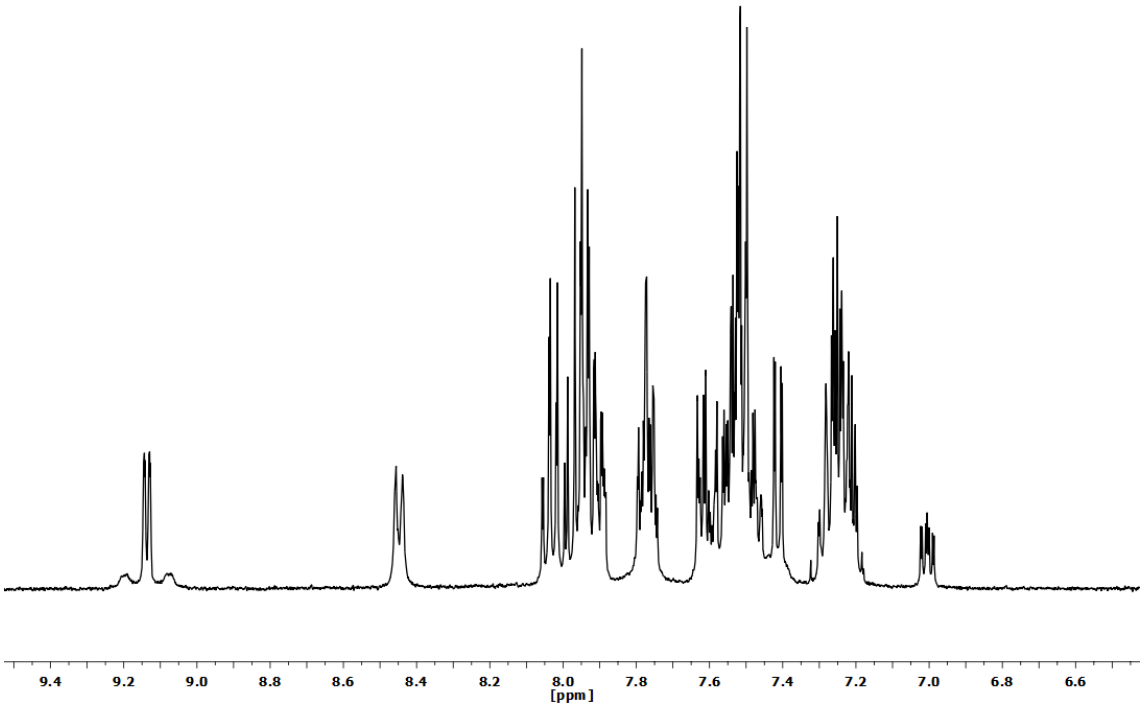

Figure S2.86. ^{1}H NMR spectrum (CD_2Cl_2, RT) of complex [Pt(CNC-H)(NC$_5$H$_4$-*o*-COO)] (**25**).

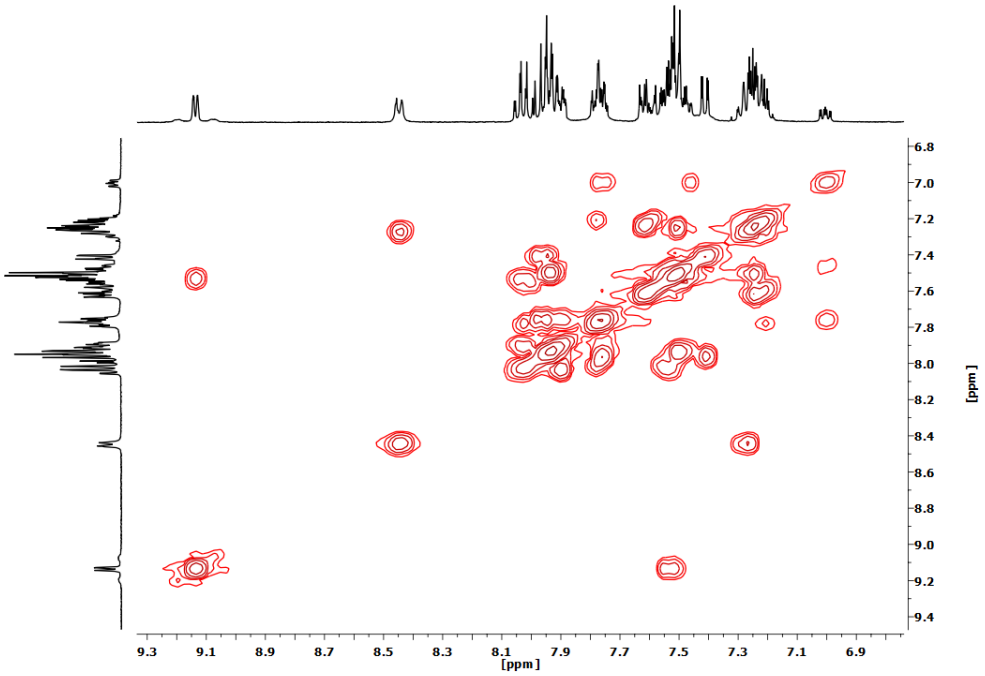

Figure S2.87. ^{1}H-^{1}H COSY NMR spectrum (CD_2Cl_2, RT) of complex [Pt(CNC-H)(NC_5H_4-*o*-COO)] (**25**).

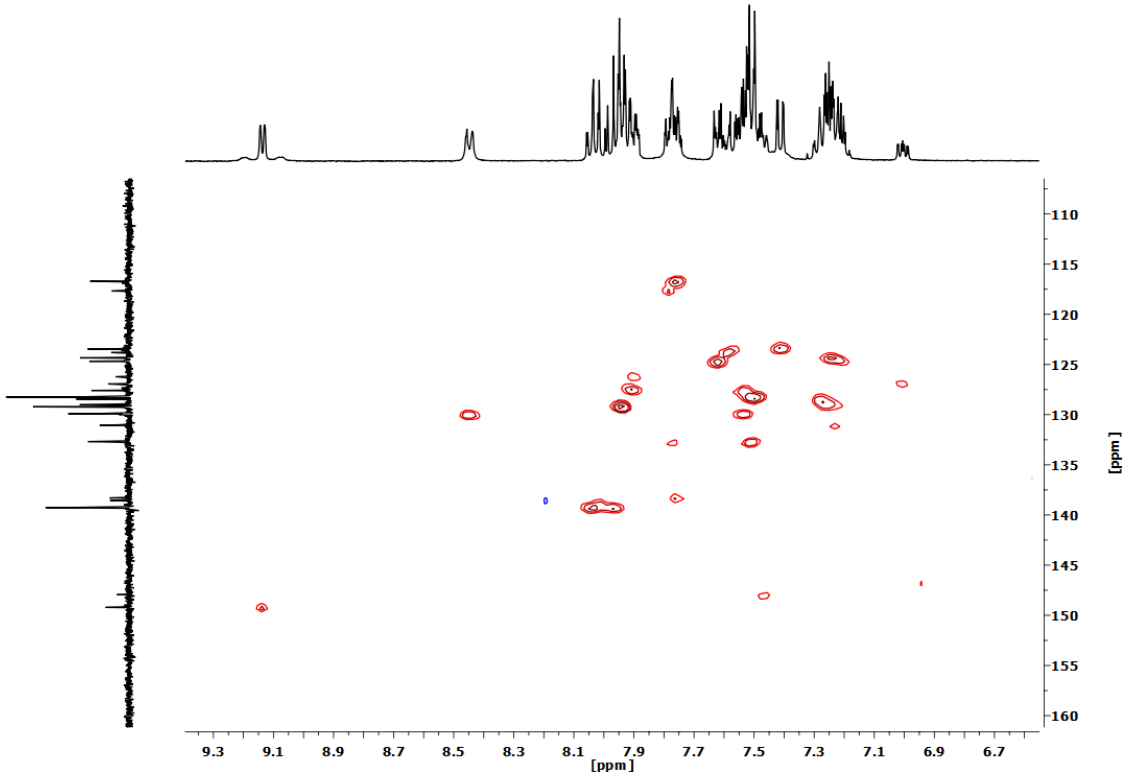

Figure S2.88. ^{1}H-^{13}C HSQC NMR spectrum (CD_2Cl_2, RT) of complex [Pt(CNC-H)(NC_5H_4-*o*-COO)] (**25**).

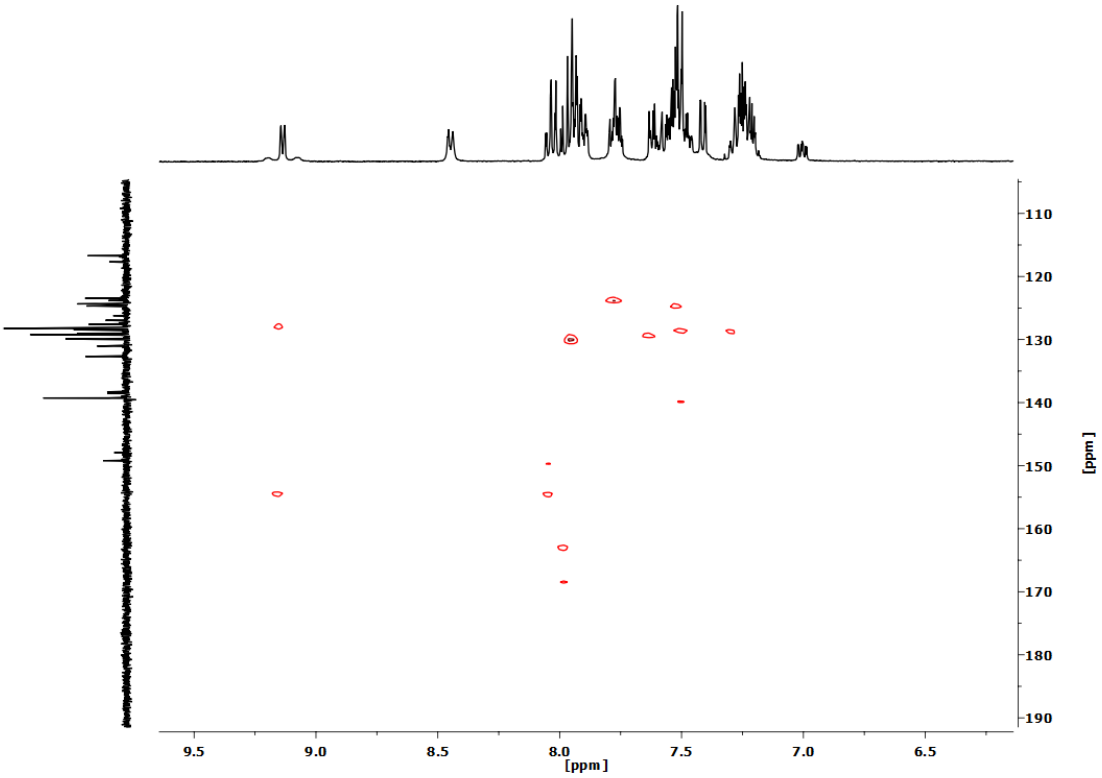

Figure S2.89. ^{1}H-^{13}C HMBC NMR spectrum (CD_2Cl_2, RT) of complex [Pt(CNC-H)(NC_5H_4-*o*-COO)] (**25**).

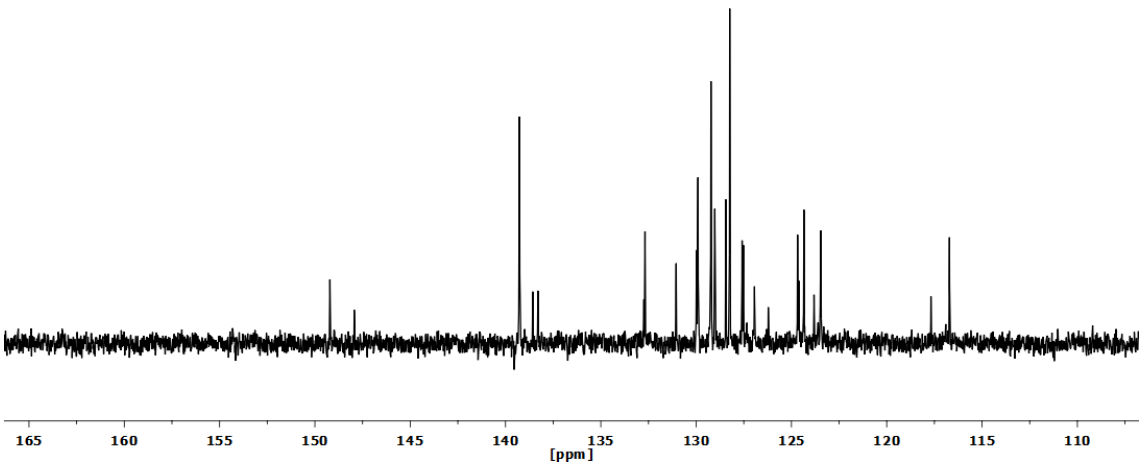

Figure S2.90. APT $^{13}C\{^{1}H\}$ NMR spectrum (CD_2Cl_2, RT) of complex [Pt(CNC-H)(NC_5H_4-*o*-COO)] (**25**).

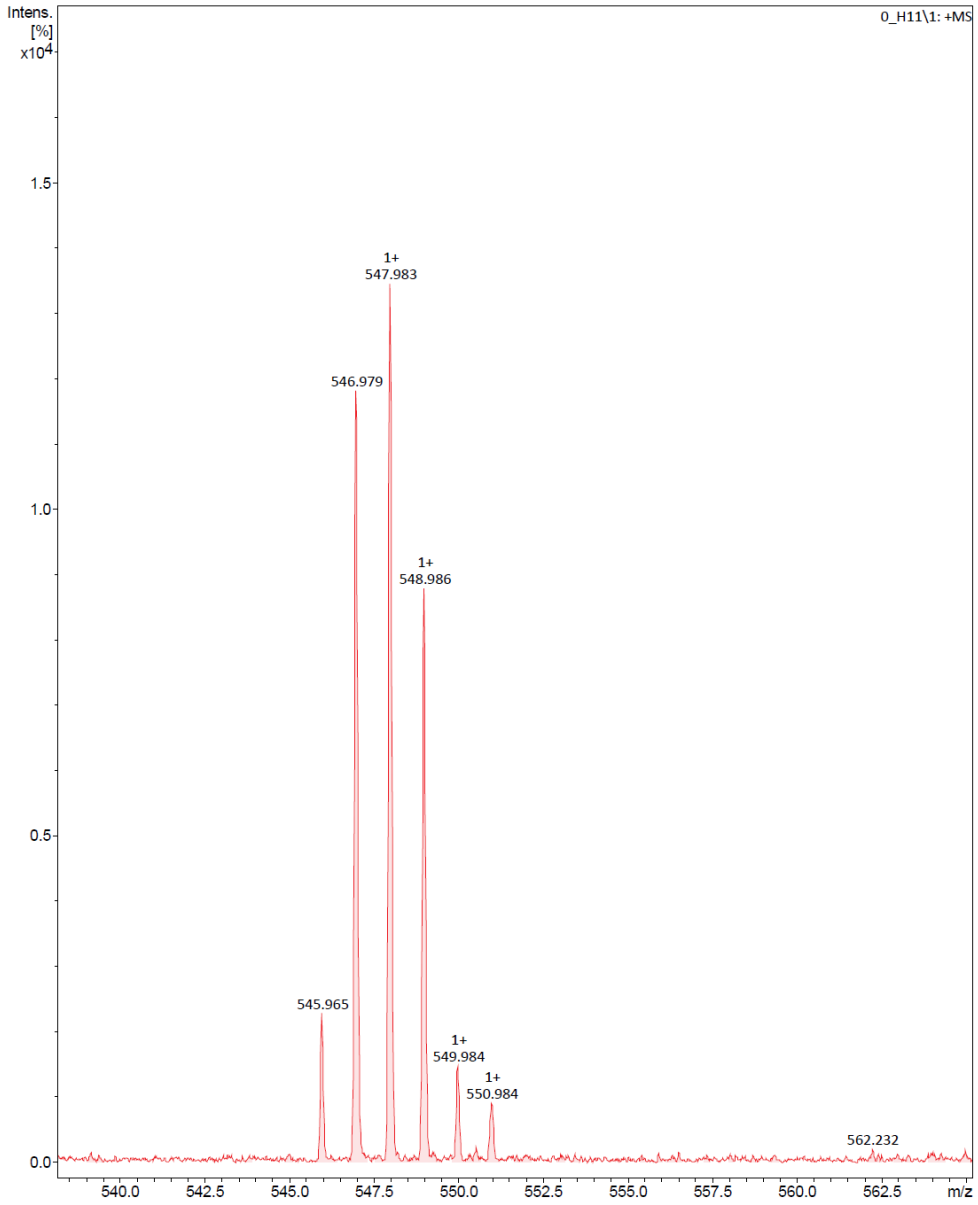

Figure S2.91. MS (MALDI+ DCTB) selected peak of complex [Pt(CNC-H)(NC_5H_4-*o*-COO)] (**25**).

2.14. Spectra of complex [Pt(CNC-H){PPh$_2$(C$_6$H$_4$-*o*-COO)}] (26).

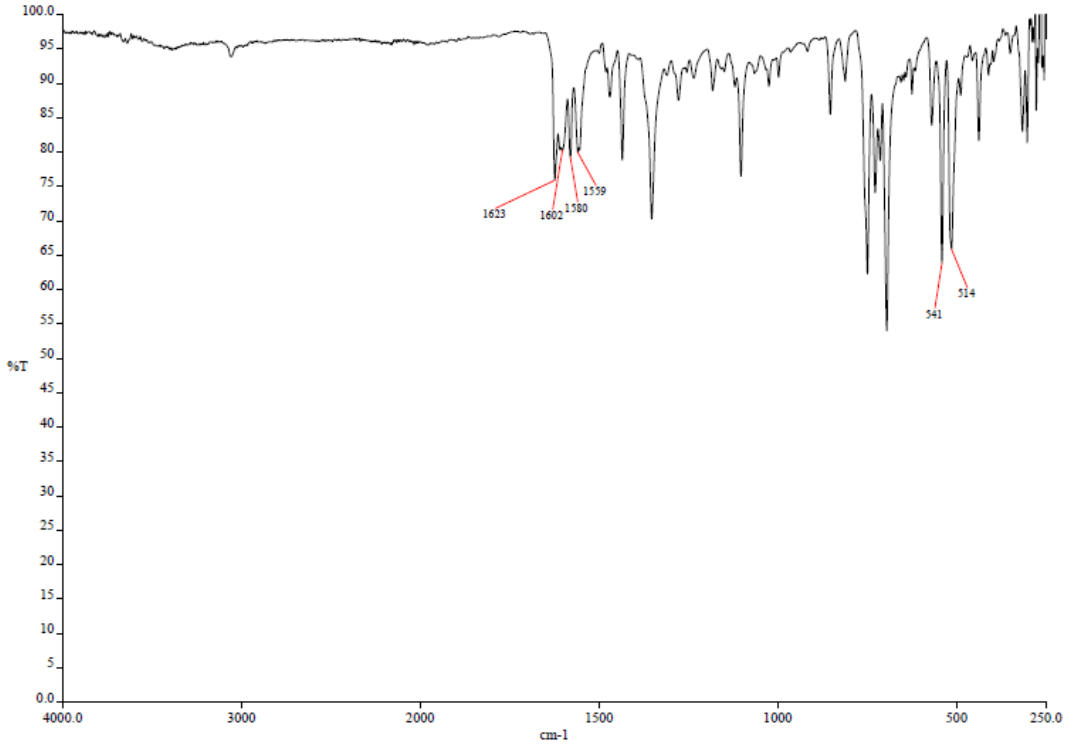

Figure S2.92. IR spectrum of complex [Pt(CNC-H){PPh$_2$(C$_6$H$_4$-*o*-COO)}] (**26**).

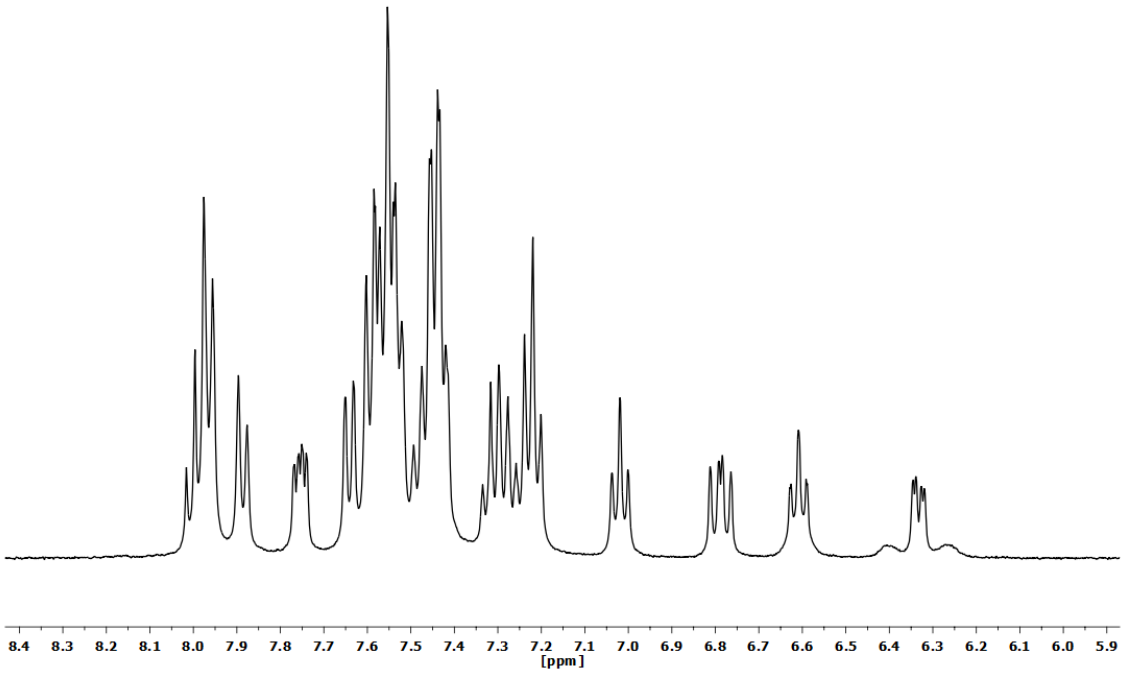

Figure S2.93. ^{1}H NMR spectrum (CD_2Cl_2, RT) of complex [Pt(CNC-H){PPh$_2$(C$_6$H$_4$-*o*-COO)}] (**26**).

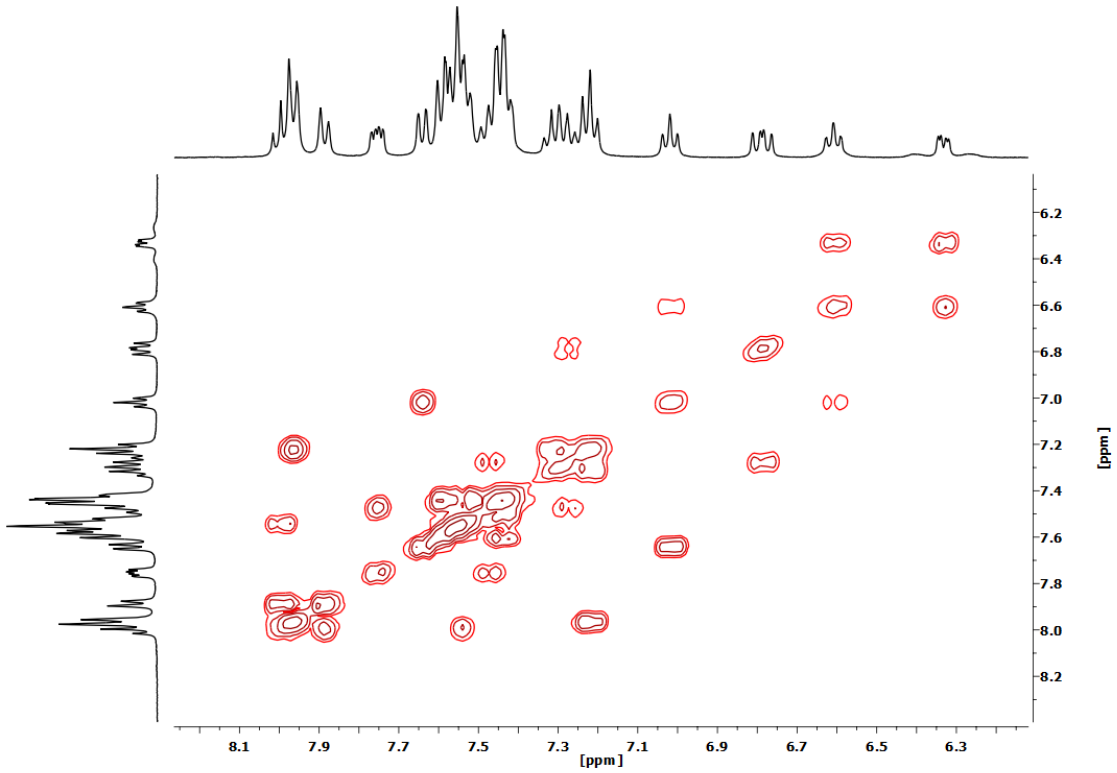

Figure S2.94. ^{1}H-^{1}H COSY NMR spectrum (CD_2Cl_2, RT) of complex [Pt(CNC-H){$PPh_2(C_6H_4$-*o*-COO)}] (**26**).

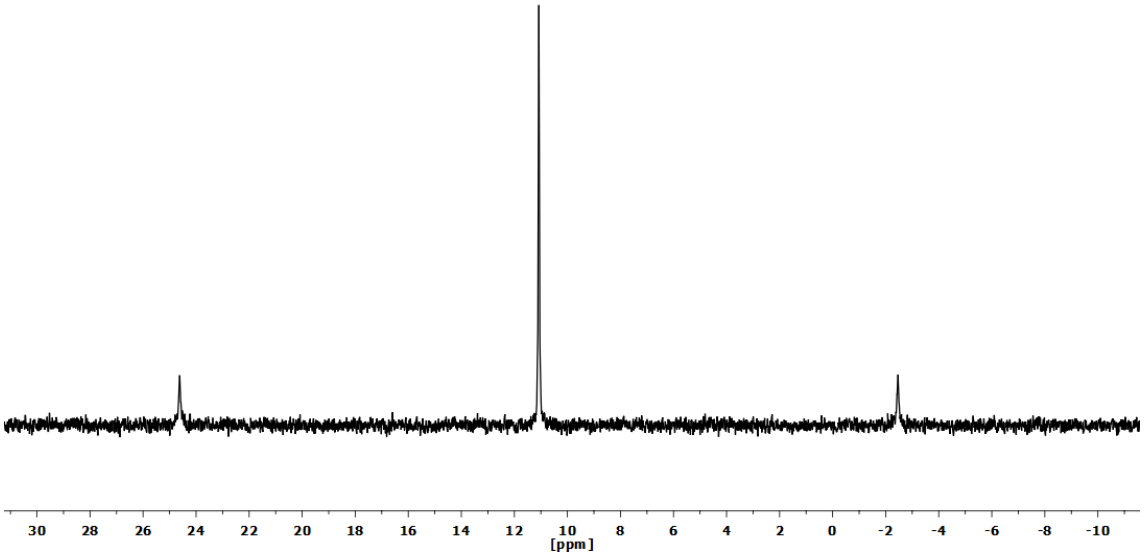

Figure S2.95. ^{31}P{^{1}H} NMR spectrum (CD_2Cl_2, RT) of complex [Pt(CNC-H){$PPh_2(C_6H_4$-*o*-COO)}] (**26**).

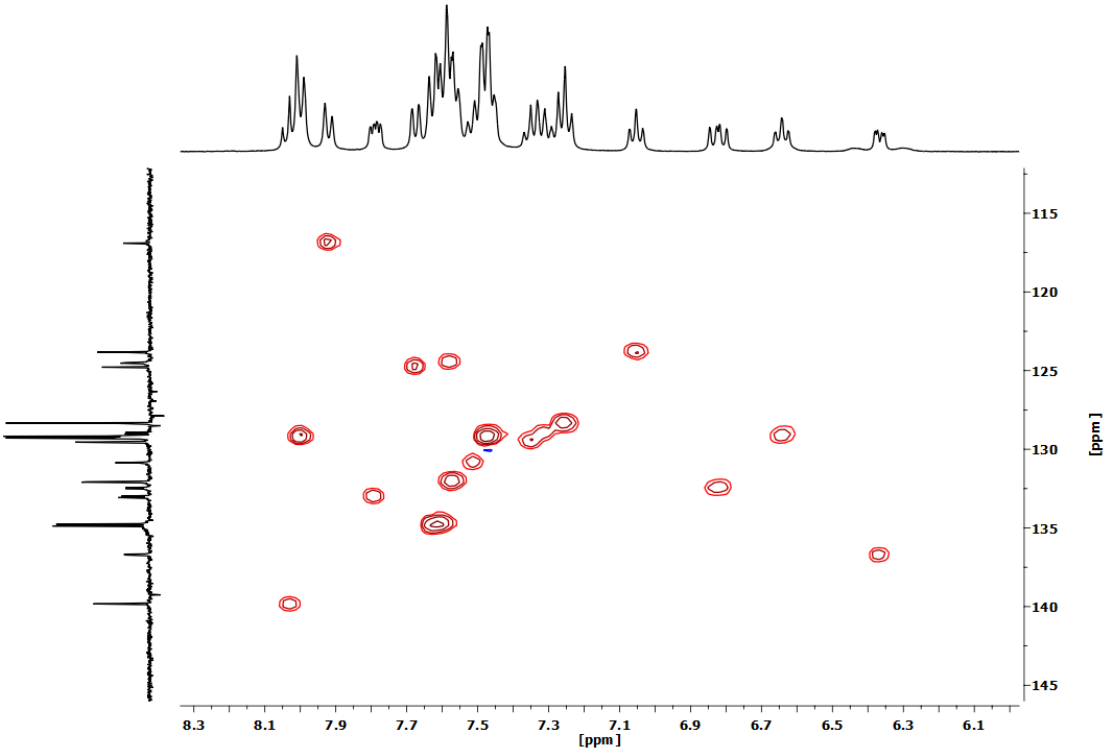

Figure S2.96. ^{1}H-^{13}C HSQC NMR spectrum (CD_2Cl_2, RT) of complex [Pt(CNC-H){$PPh_2(C_6H_4$-*o*-COO)}] (**26**).

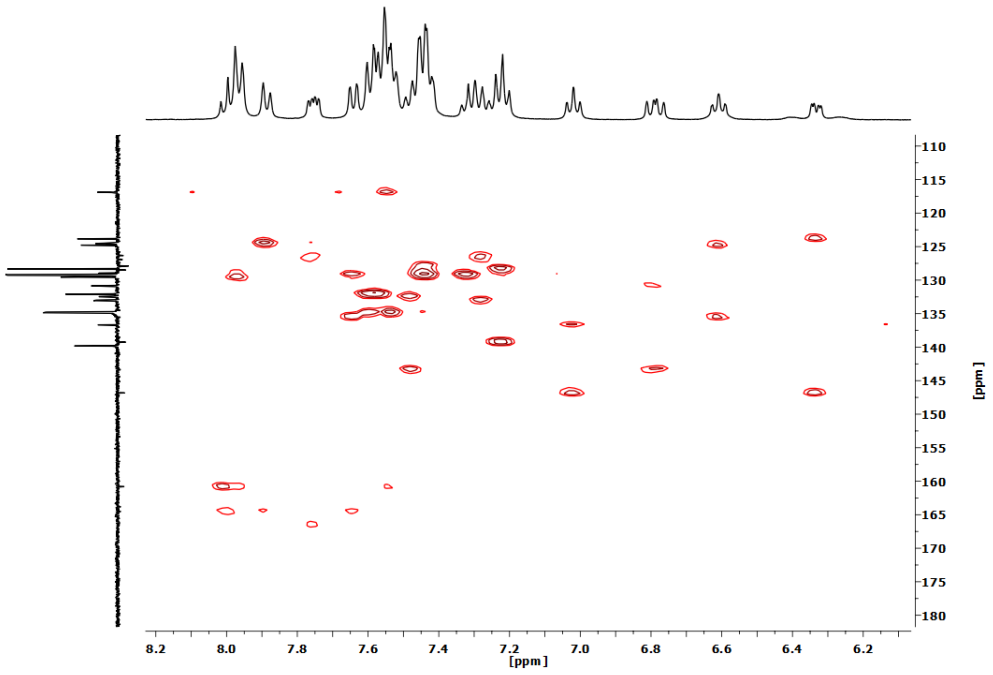

Figure S2.97. ^{1}H-^{13}C HMBC NMR spectrum (CD_2Cl_2, RT) of complex [Pt(CNC-H){$PPh_2(C_6H_4$-*o*-COO)] (**26**).

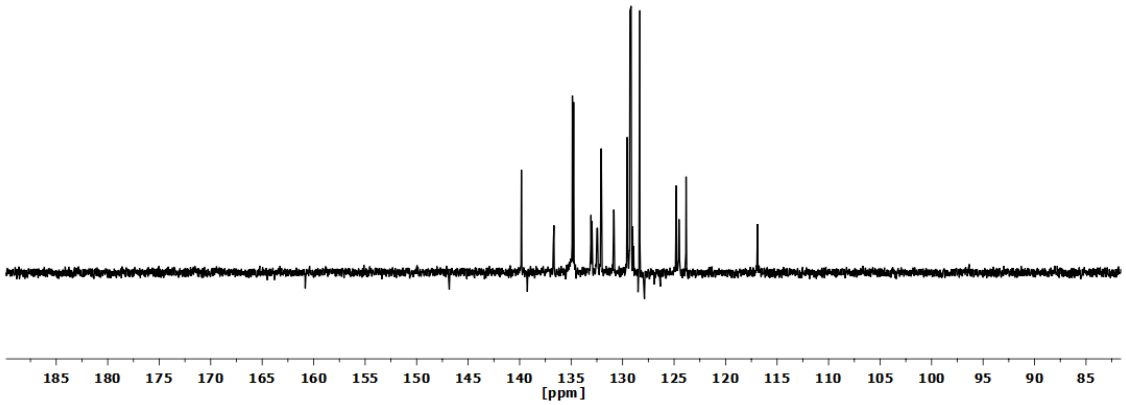

Figure S2.98. APT $^{13}C\{^{1}H\}$ NMR spectrum (CD_2Cl_2, RT) of complex [Pt(CNC-H){$PPh_2(C_6H_4$-*o*-COO)}] (**26**).

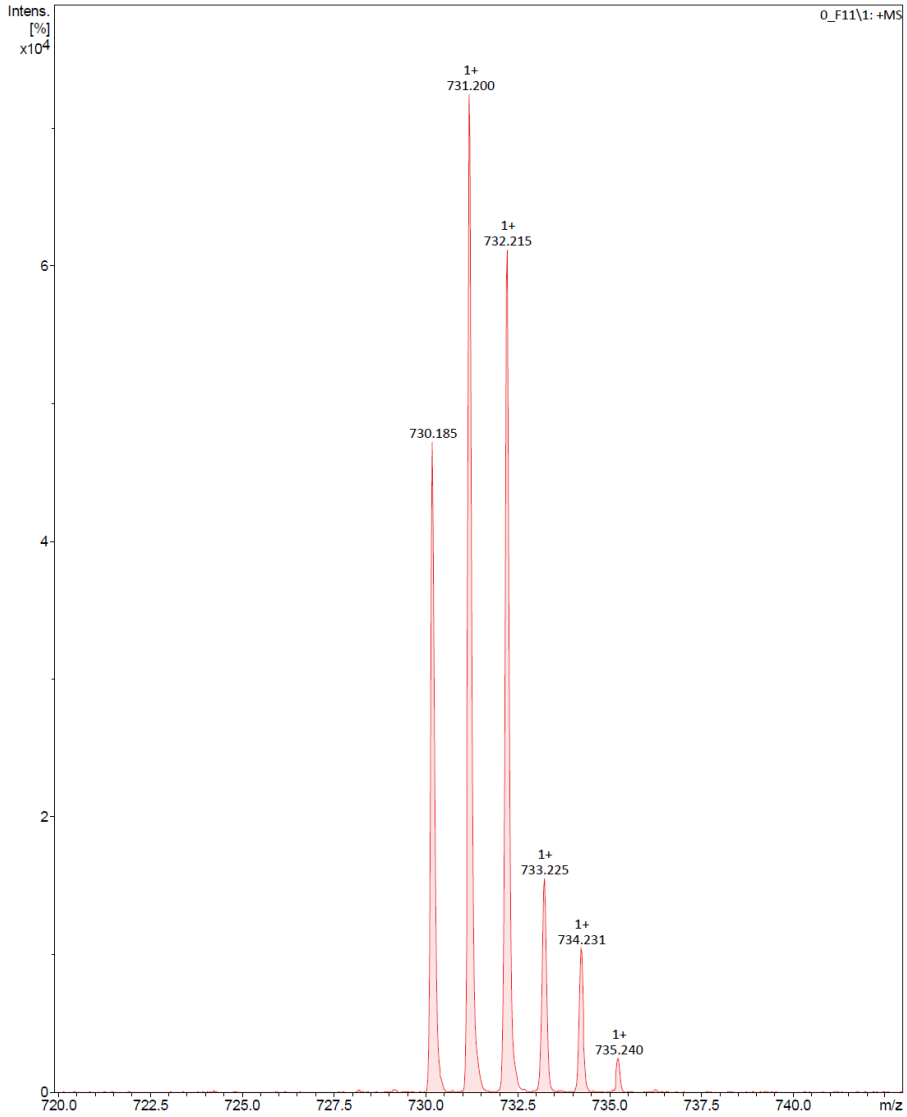

Figure S2.99. MS (MALDI+ DCTB) selected peak of complex [Pt(CNC-H){$PPh_2(C_6H_4$-*o*-COO)}] (**26**).

2.15. Spectra of complex [Pd(CNC-H){PPh$_2$(C$_6$H$_4$-*o*-COO)}] (27).

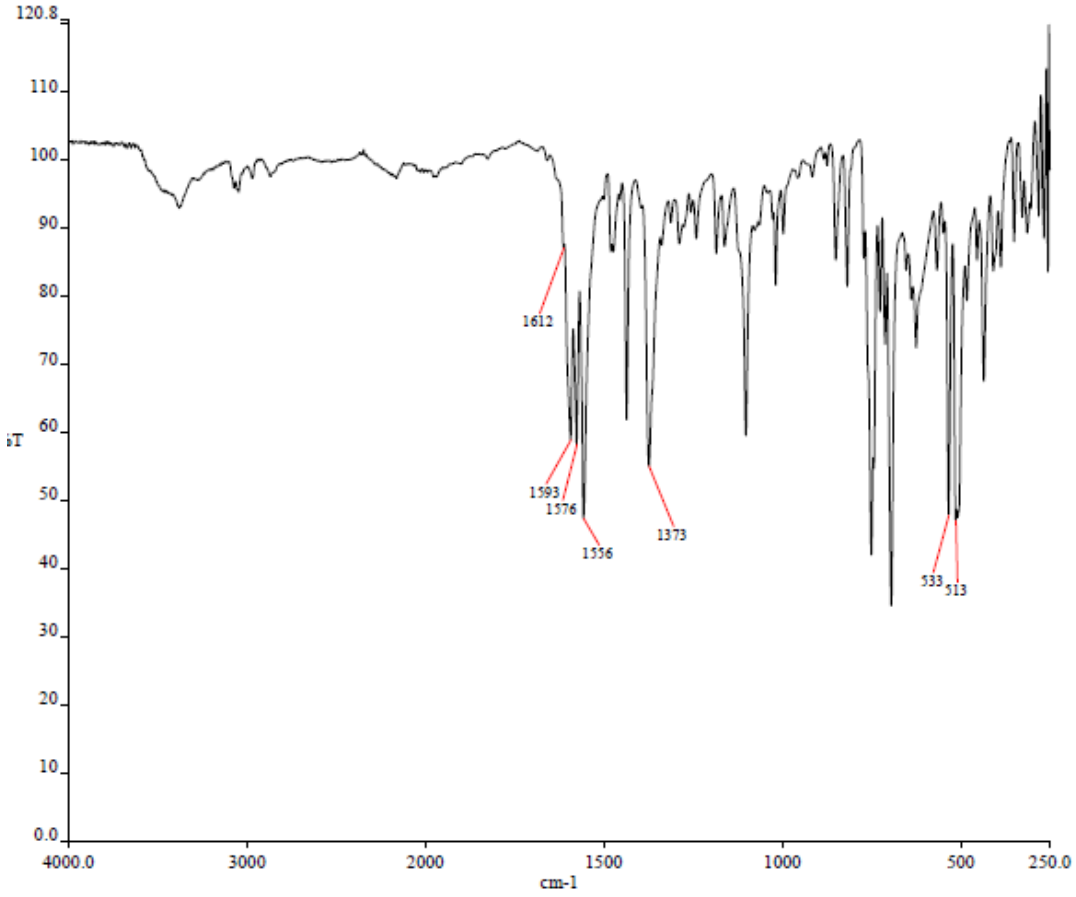

Figure S2.100. IR spectrum of complex [Pd(CNC-H){PPh$_2$(C$_6$H$_4$-*o*-COO)}] (**27**).

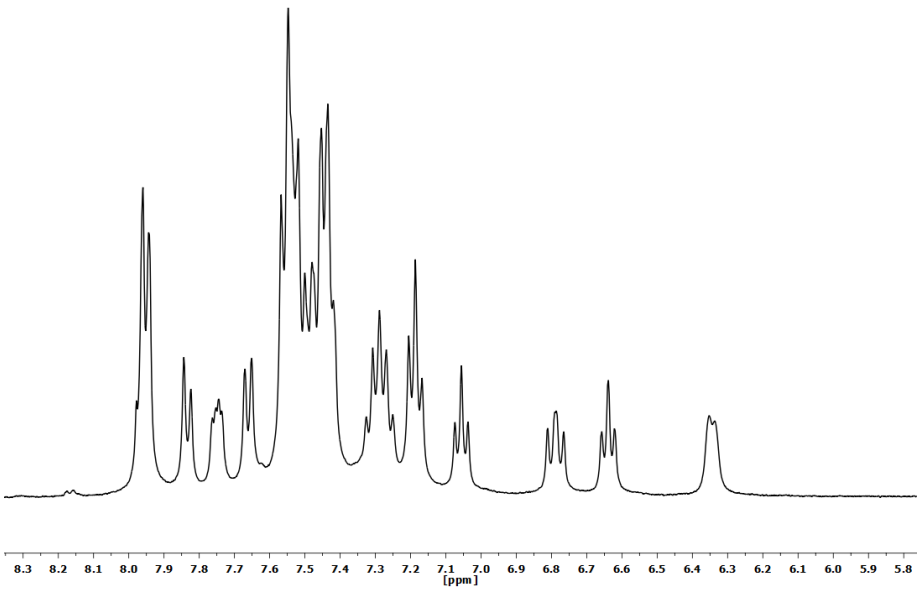

Figure S2.101. ^{1}H NMR spectrum (CD_2Cl_2, RT) of complex [Pd(CNC-H){PPh$_2$(C$_6$H$_4$-*o*-COO)}] (**27**).

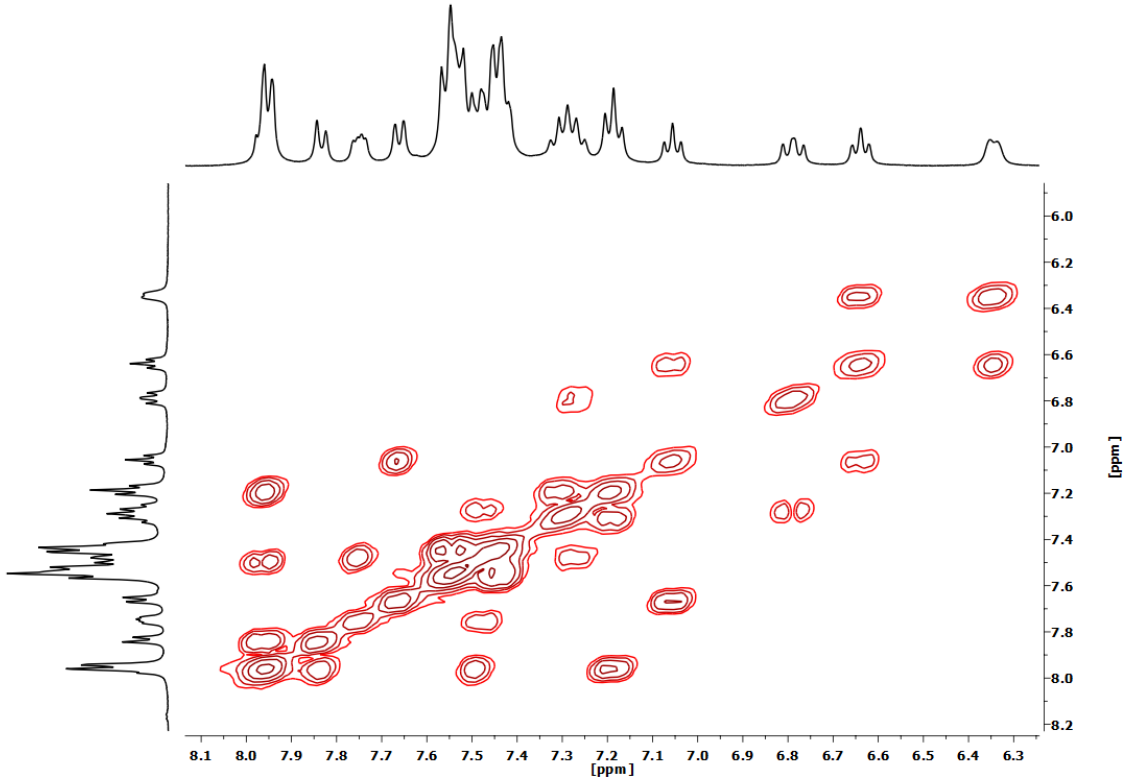

Figure S2.102. ^{1}H-^{1}H COSY NMR spectrum (CD_2Cl_2, RT) of complex [Pd(CNC-H){$PPh_2(C_6H_4$-*o*-COO)}] (**27**).

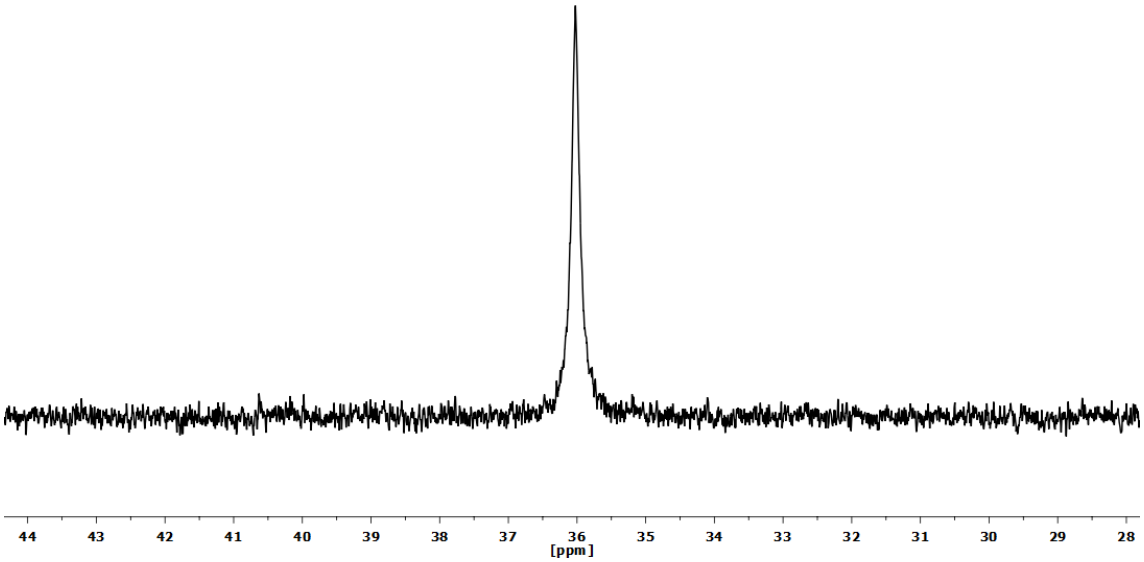

Figure S2.103. ^{31}P{^{1}H} NMR spectrum (CD_2Cl_2, RT) of complex [Pd(CNC-H){$PPh_2(C_6H_4$-*o*-COO)}] (**27**).

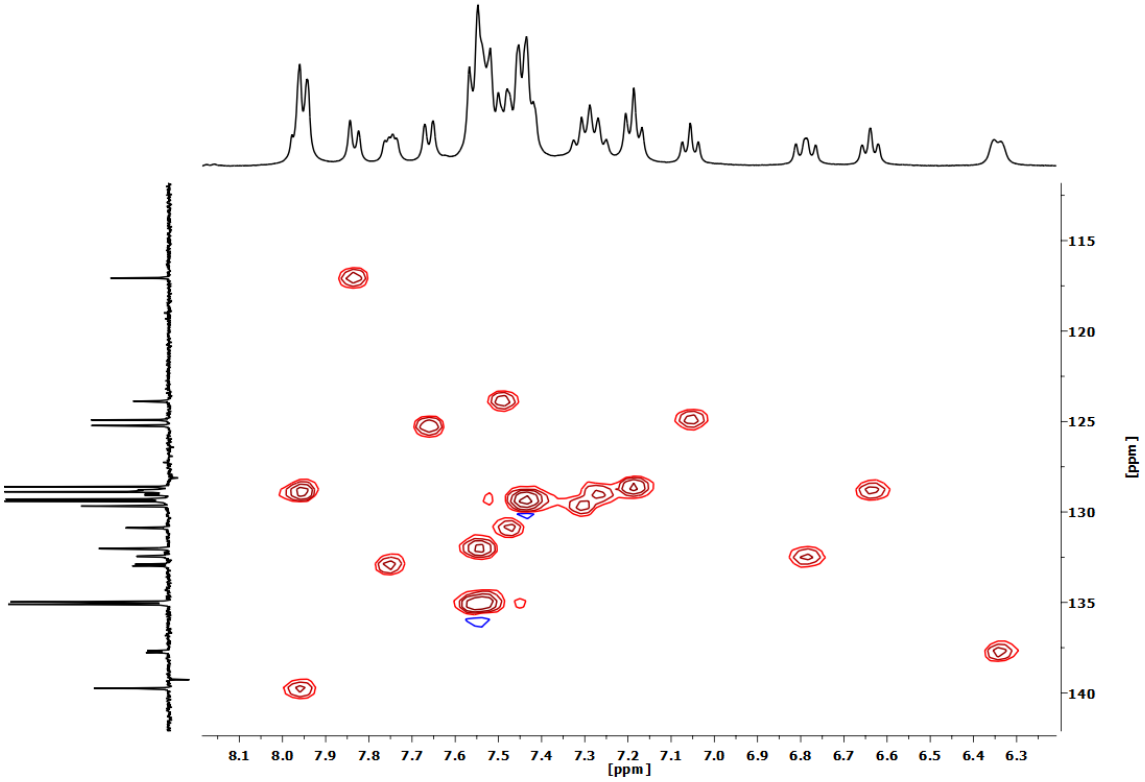

Figure S2.104. ^{1}H-^{13}C HSQC NMR spectrum (CD_2Cl_2, RT) of complex [Pd(CNC-H){$PPh_2(C_6H_4$-*o*-COO)}] (**27**).

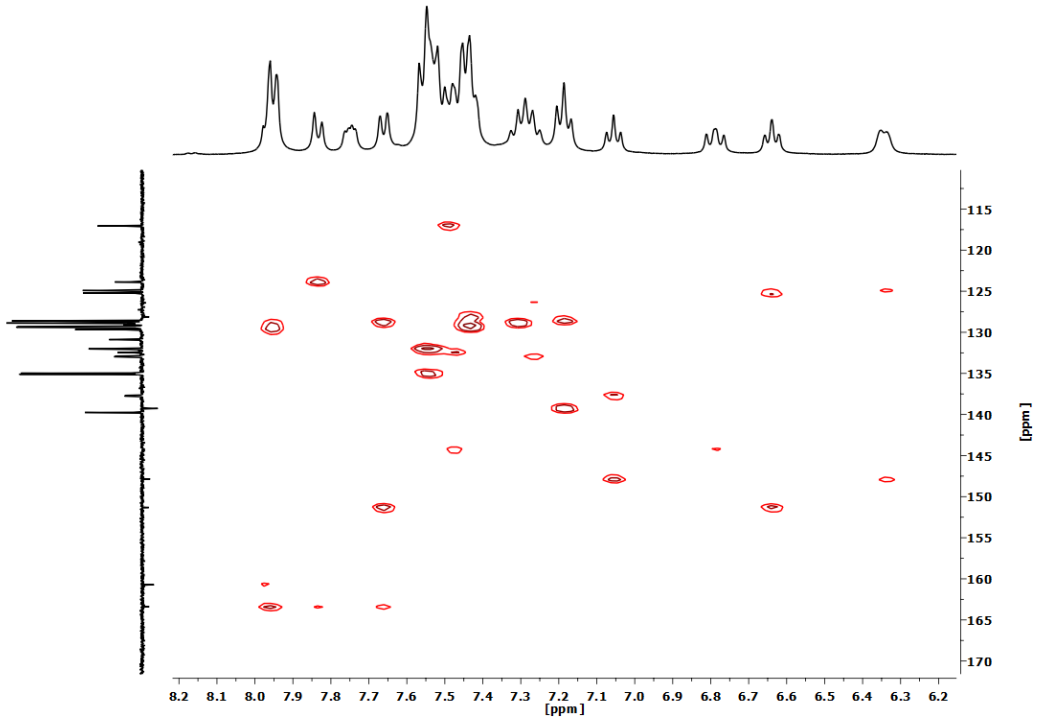

Figure S2.105. ^{1}H-^{13}C HMBC NMR spectrum (CD_2Cl_2, RT) of complex [Pd(CNC-H){$PPh_2(C_6H_4$-*o*-COO)}] (**27**).

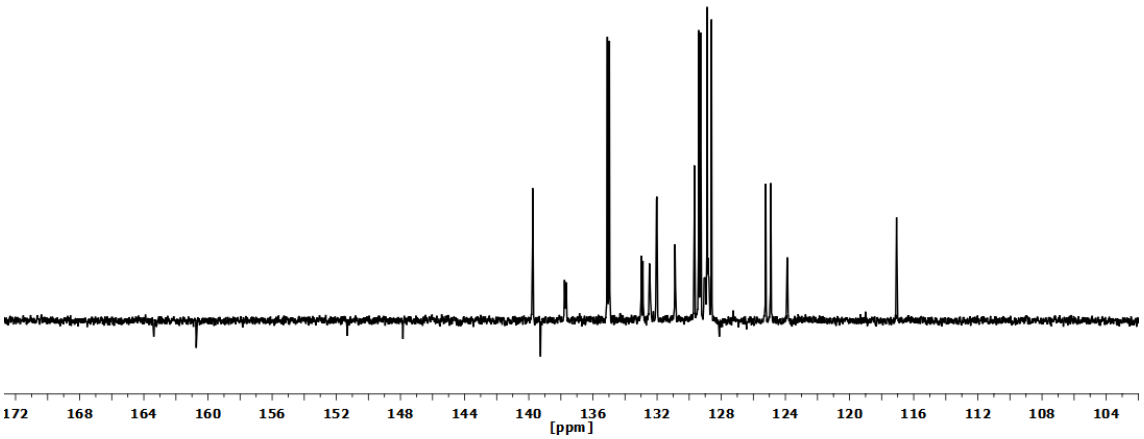

Figure S2.106. APT $^{13}C\{^{1}H\}$ NMR spectrum (CD_2Cl_2, RT) of complex [Pd(CNC-H){$PPh_2(C_6H_4$-*o*-COO)}] (**27**).

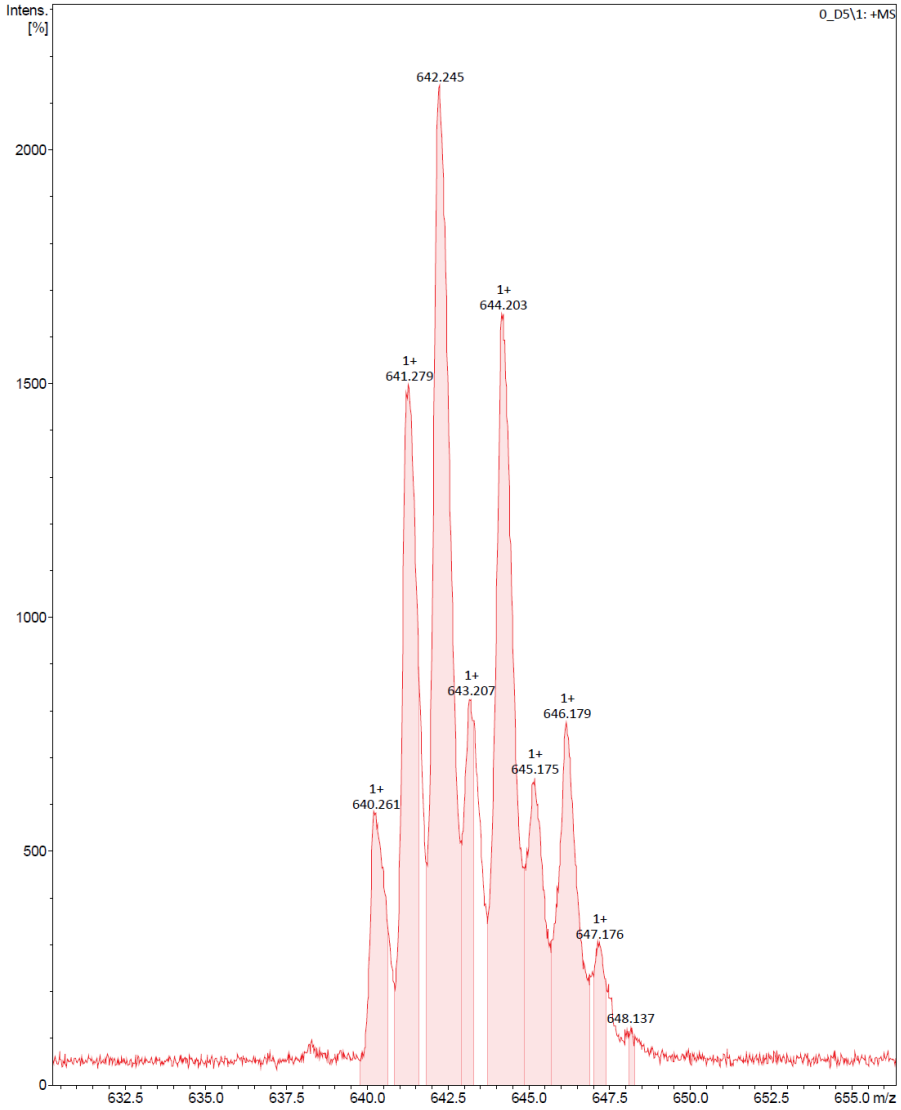

Figure S2.107. MS (MALDI+ DCTB) molecular peak of complex [Pd(CNC-H){$PPh_2(C_6H_4$-*o*-COO)}] (**27**).

3. Computational details

Density Functional Theory (DFT) calculations were carried out with the Gaussian 16 suite of programs,[3] using the BP-86 density functional[4] together with Grimme's D3 dispersion correction.[5] The ECP-60-mwb pseudopotential[6] was used for platinum, the ECP-28-mwb pseudopotential was used for palladium,[6] and the 6-31G(d)[7] basis set was used for all other atoms. Geometry optimizations were performed without any symmetry constraint, either in CH_2Cl_2, acetone or CH_3CN by using the solvation model based on density (SMD)[8]. Stationary points were characterized by calculating the Hessian matrix analytically to confirm that all species are minima (no imaginary frequencies, with exception of INT2 for the reaction with 2-pyridinecarboxilic acid, which showed one very low-intensity imaginary frequency) or transition states (one single imaginary frequency) on the potential energy surface. Atomic coordinates (x, y, z) for the optimized structures are included in a separate file (***DFT-chapter2.xyz***).

4. References

(1) CrysAlis Pro 1.171.39.44a, Rigaku Oxford Diffraction **2018**.

(2) Sheldrick, G. M. *Acta Crystallogr.* **2015**, *A71*, 3-8.

(3) Frisch, M. J.; Trucks, G.W.; Schlegel, H. B.; Scuseria, G. E.; Robb, M. A.; Cheeseman, J. R.; Scalmani, G.; Barone, V.; Petersson, G. A.; Nakatsuji, H.; Li, X.; Caricato, M.; Marenich, A. V.; Bloino, J.; Janesko, B. G.; Gomperts, R.; Mennucci, B.; Hratchian, H. P.; Ortiz, J. V.; Izmaylov, A. F.; Sonnenberg, J. L.; Williams-Young, D.; Ding, F.; Lipparini, F.; Egidi, F.; Goings, J.; Peng, B.; Petrone, A.; Henderson, T.; Ranasinghe, D.; Zakrzewski, V. G.; Gao, J.; Rega, N.; Zheng, G.; Liang, W.; Hada, M.; Ehara, M.; Toyota, K.; Fukuda, R.; Hasegawa, J.; Ishida, M.; Nakajima, T.; Honda, Y.; Kitao, O.; Nakai, H.; Vreven, T.; Throssell, K.; Montgomery Jr., J. A.; Peralta, J. E.; Ogliaro, F.; Bearpark, M. J.; Heyd, J. J.; Brothers, E. N.; Kudin, K. N.; Staroverov, V. N.; Keith, T. A.; Kobayashi, R.; Normand, J.; Raghavachari, K.; Rendell, A. P.; Burant, J. C.; Iyengar, S. S.; Tomasi, J.; Cossi, M.; Millam, J. M.; Klene, M.; Adamo, C.; Cammi, R.; Ochterski, J. W.; Martin, R. L.; Morokuma, K.; Farkas, O.; Foresman, J. B.; Fox, D. J. *Gaussian 16 Rev. C.01*, Wallingford, CT, **2016**.

(4) a) Becke, D. *Phys. Rev. A* **1988**, *38*, 3098-3100. b) Perdew, J. P. *Phys. Rev. B* **1986**, *33*, 8822-8824.

(5) Grimme, S.; Antony, J.; Ehrlich, S.; Krieg, H. *J. Chem. Phys.* **2010**, *132*, 154104.

(6) Andrae, D.; Häußermann, U.; Dolg, M.; Stoll, H.; Preuß, H. *Theor. Chim. Acta* **1990**, *77*, 123−141.

(7) a) Ditchfield, R.; Hehre, W. J.; Pople, J. A. *J. Chem. Phys.* **1971**, *54,* 724-728. b) Hariharan, P. C.; Pople, J. A. *Theor. Chim. Acta* **1973**, *28*, 213-222.

(8) Marenich, A. V.; Cramer, C. J.; Truhlar, D. G. *J. Phys. Chem. B* **2009**, *113*, 6378-6396.

Supporting Information

for

Chapter 3. Reactivity of platinum (II) and palladium (II) cyclometallated substrates towards sources of Me^+.

1. Crystal data and structural refinement

Crystal data and other details of the structure analyses are presented in Tables S3.1 and S3.2. Suitable crystals for X-Ray diffraction studies were obtained by slow diffusion of *n*-hexane into concentrated solutions of the complexes in 3 mL of CH_2Cl_2 or acetone. Crystals were mounted at the end of a quartz fibre. The radiation used in all cases was graphite monochromated Mo-K_α (λ = 71.073 pm). X-Ray intensity data were collected on an Oxford Diffraction Xcalibur diffractometer. The diffraction frames were integrated and corrected from absorption by using the CrysAlis RED program.[1] The structures were solved by Patterson and Fourier methods and refined by full-matrix least squares on F^2 with SHELXL.[2] All atoms were assigned anisotropic displacement parameters and refined without positional constraints. The positions of the H atoms were constrained to idealised geometries and assigned isotropic displacement parameters equal to 1.2 or 1.5 times the U_{iso} values of their respective parent atoms. Full-matrix least-squares refinement of the models against F^2 converged to final residual indices given in Tables S3.1 and S3.2.

Table S3.1. Crystal data and structure refinement for complexes [PtIMe(CNC)(PPh_3)] (**28**), [Pt(CN-*o*-tol)I(PPh_3)]·CH_2Cl_2 (**29**·CH_2Cl_2), [Pt(CN-*o*-tol)(MeCN)(PPh_3)](ClO_4) (**30**) and [Pd(CN-*o*-tol)I(PPh_3)] (**31**·CH_2Cl_2).

	28	**29**·CH_2Cl_2	**30**	**31**·CH_2Cl_2
Formula	$C_{36}H_{29}INPPt$	$C_{36}H_{29}INPPt$ ·CH_2Cl_2	$C_{38}H_{32}ClN_2O_4PPt$	$C_{35}H_{29}INPPd$ ·CH_2Cl_2
M_t	828.56	913.49	842.16	824.80
Crystal system	monoclinic	monoclinic	triclinic	monoclinic
Space group	*P2₁/c*	*P2₁/c*	*P-1*	*P2₁/c*
a/Å	8.9792(2)	17.9149(2)	10.04095(1)	17.8942(3)
b/Å	14.8014(3)	11.76174(2)	10.37391(1)	11.7904(2)
c/Å	21.6854(4)	15.7395(2)	15.61981(2)	15.7499(3)
a/º	90	90	91.7421(8)	90
β/º	91.6012(2)	95.1962(12)	96.8298(9)	95.3038(17)
γ/º	90	90	92.5803(9)	90

V/Å^3	2880.97(1)	3302.85(8)	1612.79(3)	3308.66(10)
Z	4	4	2	4
D_c/g cm^{-3}	1.910	1.837	1.734	1.656
T/K	100(2)	100(2)	293(2)	293(2)
μ/mm^{-1}	6.025	5.421	4.528	1.731
F(000)	1592	1760	832	1632
2θ range/^{o}	5.4-56.6	5.4-56.4	5.6-56.8	5.8-50.0
Collected reflections	28098	25929	62383	29533
Unique reflections	6231	7136	7438	5812
R_{int}	0.0460	0.0351	0.0349	0.0607
R_1, wR_2[a] ($I > 2\sigma(I)$)	0.0311, 0.0695	0.0274, 0.0622	0.0217, 0.0488	0.0450, 0.1156
R_1, wR_2[a] (all data)	0.0390, 0.0736	0.0356, 0.0740	0.0244, 0.0500	0.0508, 0.1202
GOF (F^2)[b]	1.029	1.114	1.036	1.066

[a] $R_1 = \sum(|F_o| - |F_c|) / \sum |F_o|$. $wR_2 = [\sum w (F_o^2 - F_c^2)^2 / \sum w(F_o^2)^2]^{1/2}$. [b] Goodness-of-fit = $[\sum w (F_o^2 - F_c^2)^2 / (n_{obs} - n_{param})]^{1/2}$.

Table S3.2. Crystal data and structure refinement for complexes and [Pt(CNC-Me)(PPh_3)] (**32**), [Pt(CN-2,6-xyl)I(PPh_3)]·0.75Me_2CO (**33**·0.75Me_2CO) and [Pt(CN-*o*-tol)Cl(PPh_3)] (**35**).

	32	**33**·0.75Me_2CO	**35**
Formula	$C_{36}H_{28}NPPt$	$C_{37}H_{31}INPPt$ ·0.75Me_2CO	$C_{36}H_{29}ClNPPt$
M_t	700.65	886.14	737.11
Crystal system	monoclinic	monoclinic	monoclinic
Space group	*P2₁/c*	*C2/c*	*P2₁*
a/Å	15.53448(2)	32.1325(5)	10.0613(3)
b/Å	17.7690(2)	8.54546(1)	8.2138(4)
c/Å	9.75836(1)	27.7966(5)	17.0990(7)
a/º	90	90	90
β/º	91.9145(9)	112.078(2)	90.175(4)
γ/º	90	90	90

V/Å^3	2692.12(5)	7072.9(2)	1413.08(1)
Z	4	8	2
D_c/g cm^{-3}	1.729	1.664	1.732
T/K	100(2)	100(2)	100(2)
μ/mm^{-1}	5.299	4.915	5.143
F(000)	1376	3440	724
2θ range/^{o}	5.4-56.6	5.3-56.8	5.5-56.6
Collected reflections	50852	28346	16248
Unique reflections	6194	7624	5933
R_{int}	0.0405	0.0276	0.0740
R_1, wR_2[a] ($I > 2\sigma(I)$)	0.0233, 0.0506	0.0302, 0.0766	0.0373, 0.0661
R_1, wR_2[a] (all data)	0.0281, 0.0520	0.0343, 0.0790	0.0505, 0.0689
GOF (F^2)[b]	1.006	1.020	1.008

[a] $R_1 = \sum(|F_o| - |F_c|) / \sum |F_o|$. $wR_2 = [\sum w (F_o^2 - F_c^2)^2 / \sum w(F_o^2)^2]^{1/2}$. [b] Goodness-of-fit = $[\sum w (F_o^2 - F_c^2)^2 / (n_{obs} - n_{param})]^{1/2}$.

2. IR, NMR and MS spectra of complexes

2.1. Spectra of complex [PtIMe(CNC)(PPh_3)] (28).

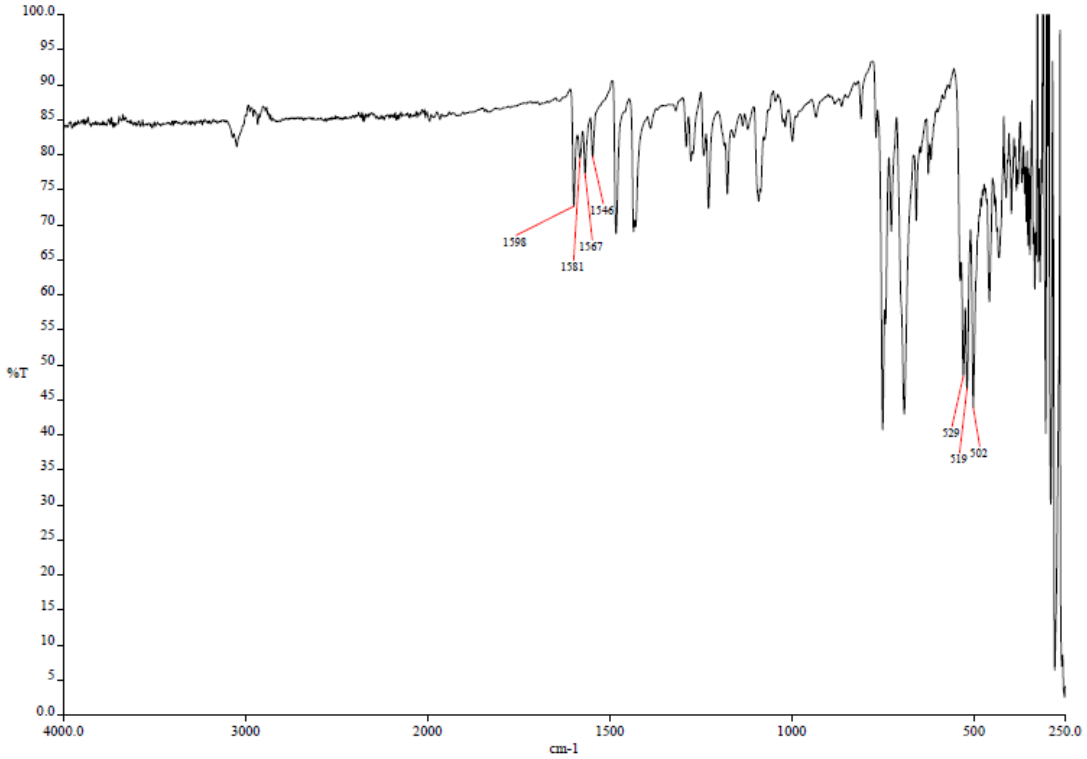

Figure S3.1. IR spectrum of complex [PtIMe(CNC)(PPh_3)] (**28**).

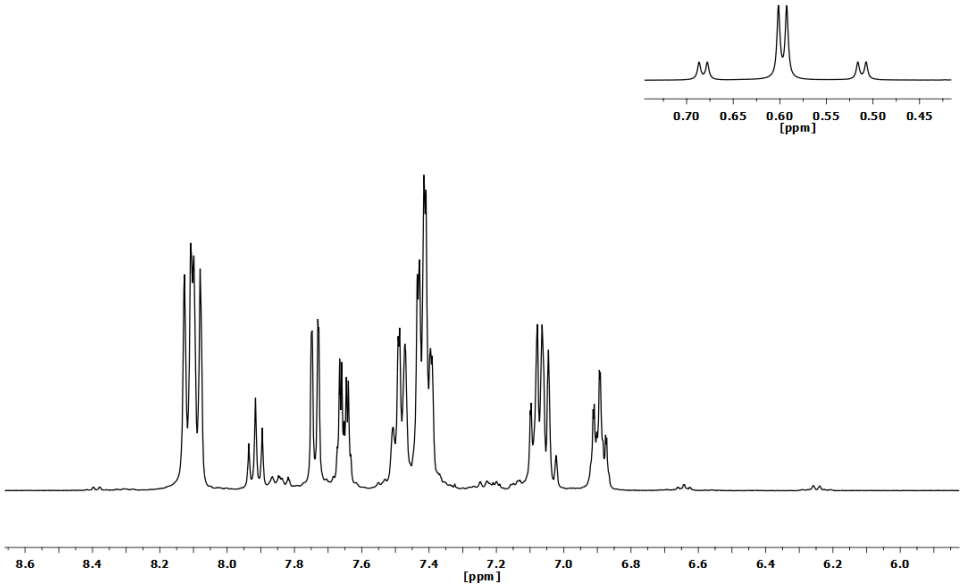

Figure S3.2. ^{1}H NMR spectrum (CD_2Cl_2, RT) of complex [PtIMe(CNC)(PPh_3)] (**28**).

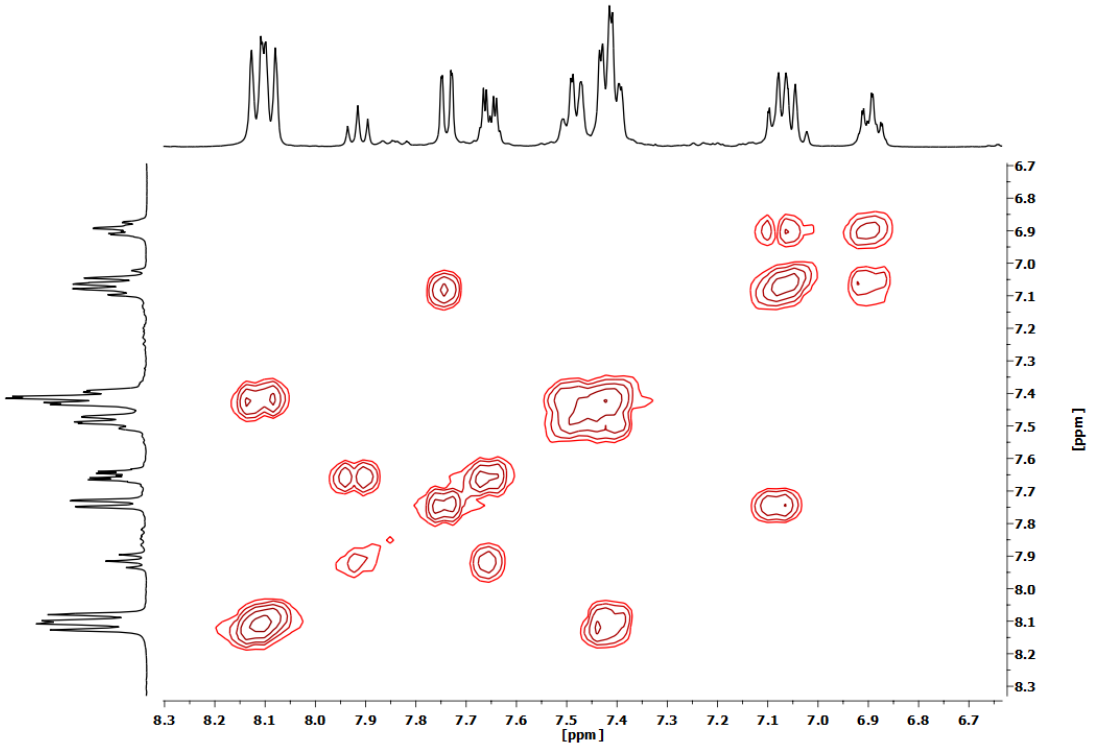

Figure S3.3. ^{1}H-^{1}H COSY NMR spectrum (CD_2Cl_2, RT) of complex [PtIMe(CNC)(PPh_3)] (**28**).

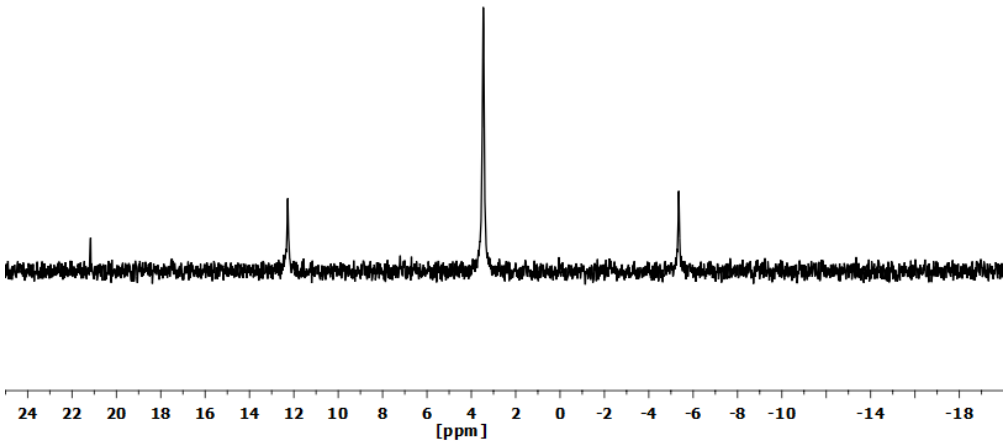

Figure S3.4. $^{31}P\{^{1}H\}$ NMR spectrum (CD_2Cl_2, RT) of complex [PtIMe(CNC)(PPh_3)] (**28**).

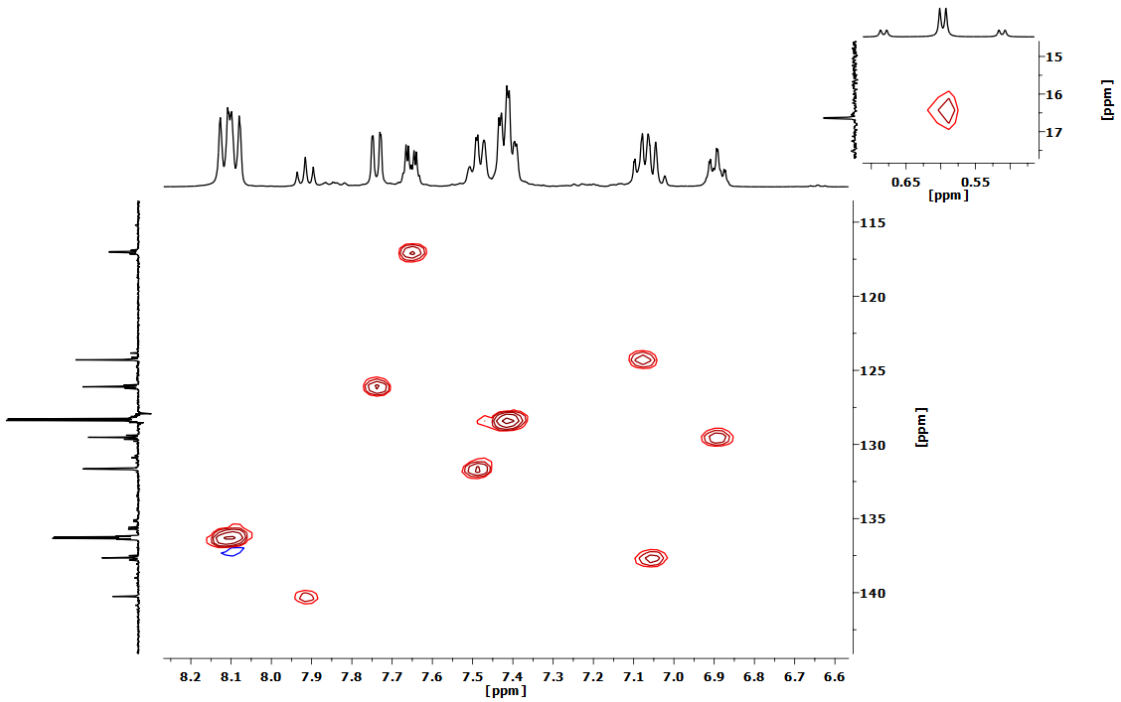

Figure S3.5. ^{1}H-^{13}C HSQC NMR spectrum (CD_2Cl_2, RT) of complex [PtIMe(CNC)(PPh_3)] (**28**).

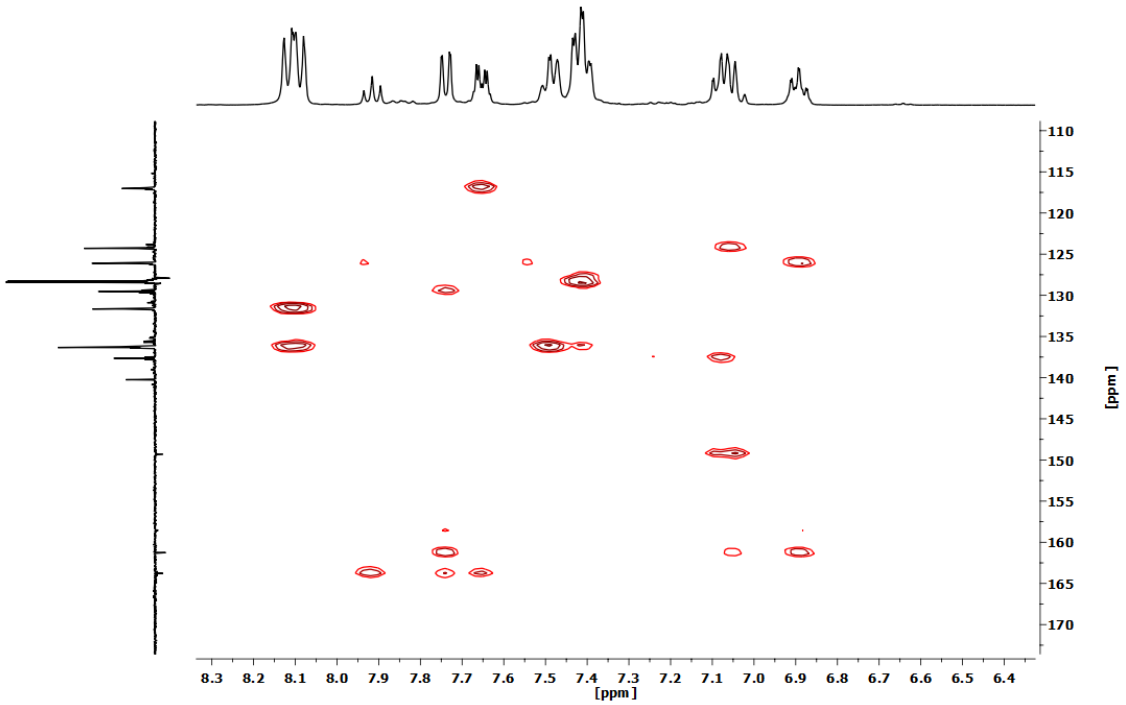

Figure S3.6. ^{1}H-^{13}C HMBC NMR spectrum (CD_2Cl_2, RT) of complex [PtIMe(CNC)(PPh_3)] (**28**).

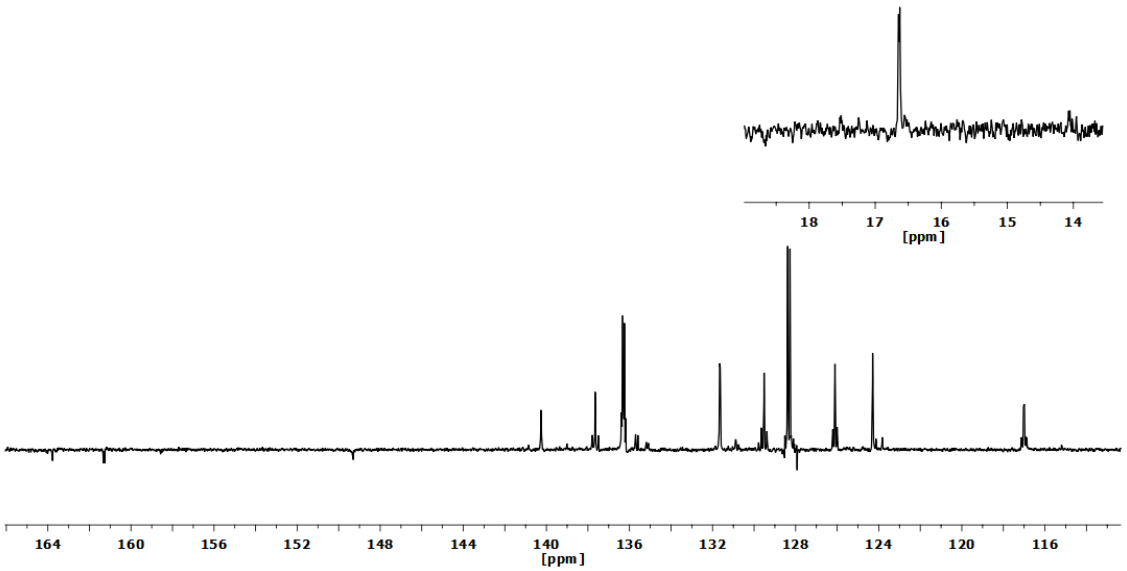

Figure S3.7. APT $^{13}C\{^{1}H\}$ NMR spectrum (CD_2Cl_2, RT) of complex [PtIMe(CNC)(PPh_3)] (**28**).

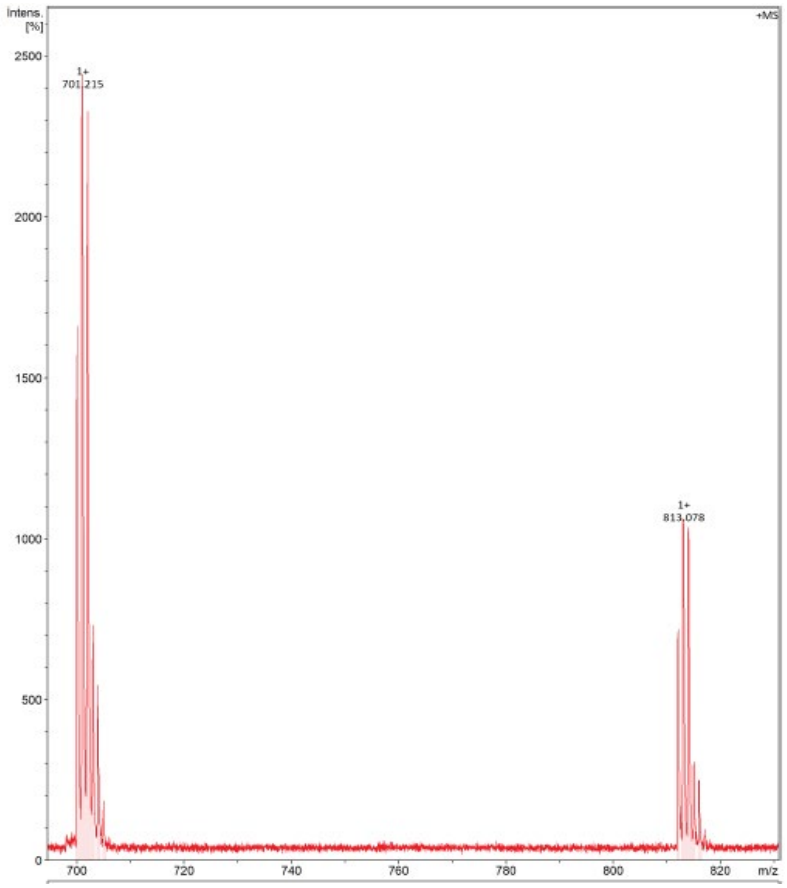

Figure S3.8. MS (MALDI+ DCTB) spectrum of complex [PtIMe(CNC)(PPh_3)] (**28**).

2.2. Spectra of complex [Pt(CN-*o*-tol)I(PPh$_3$)] (29).

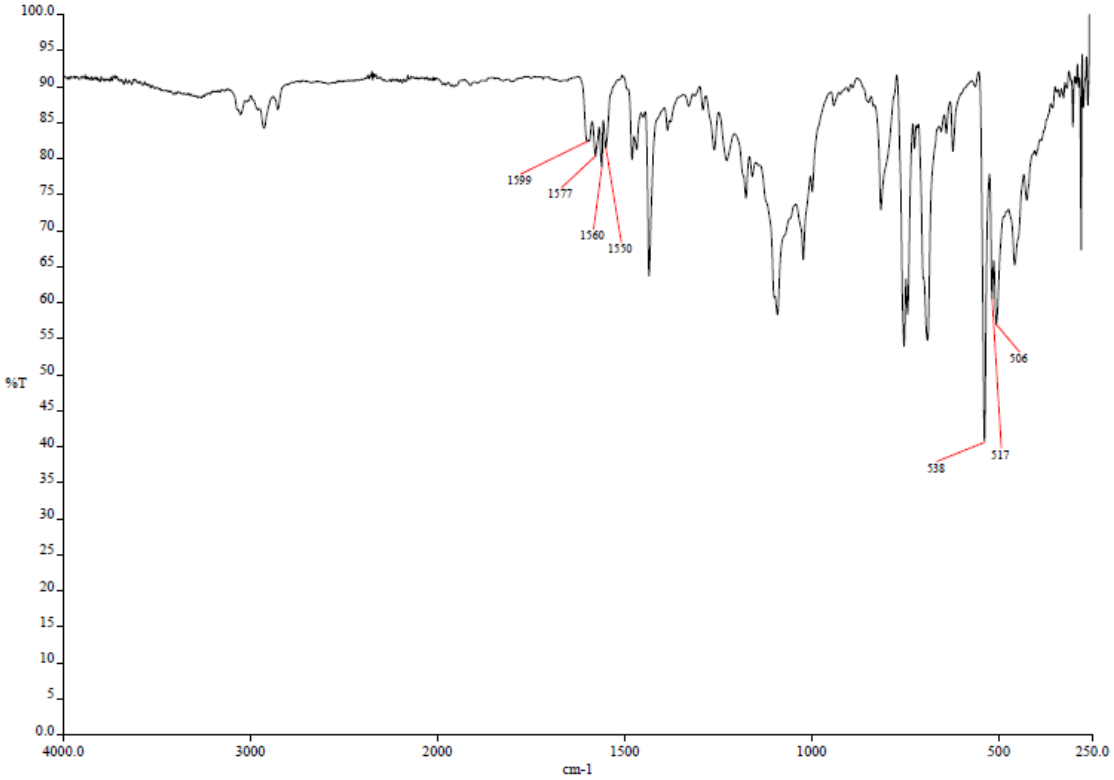

Figure S3.9. IR spectrum of complex [Pt(CN-*o*-tol)I(PPh$_3$)] (**29**).

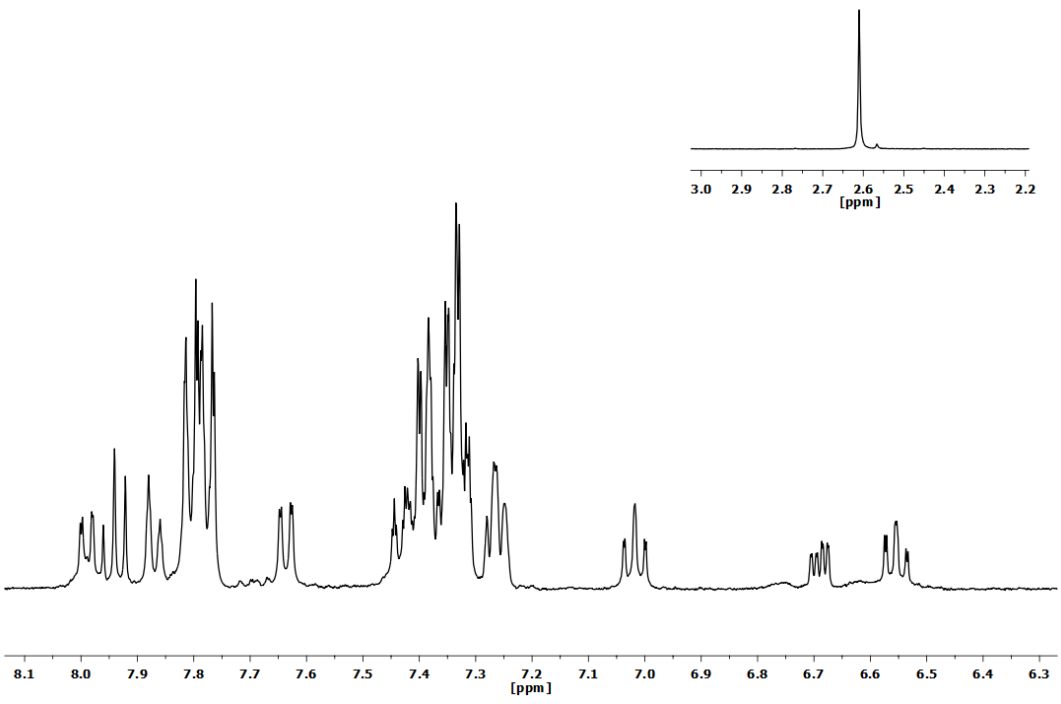

Figure S3.10. ^{1}H NMR spectrum (CD_2Cl_2, RT) of complex [Pt(CN-*o*-tol)I(PPh$_3$)] (**29**).

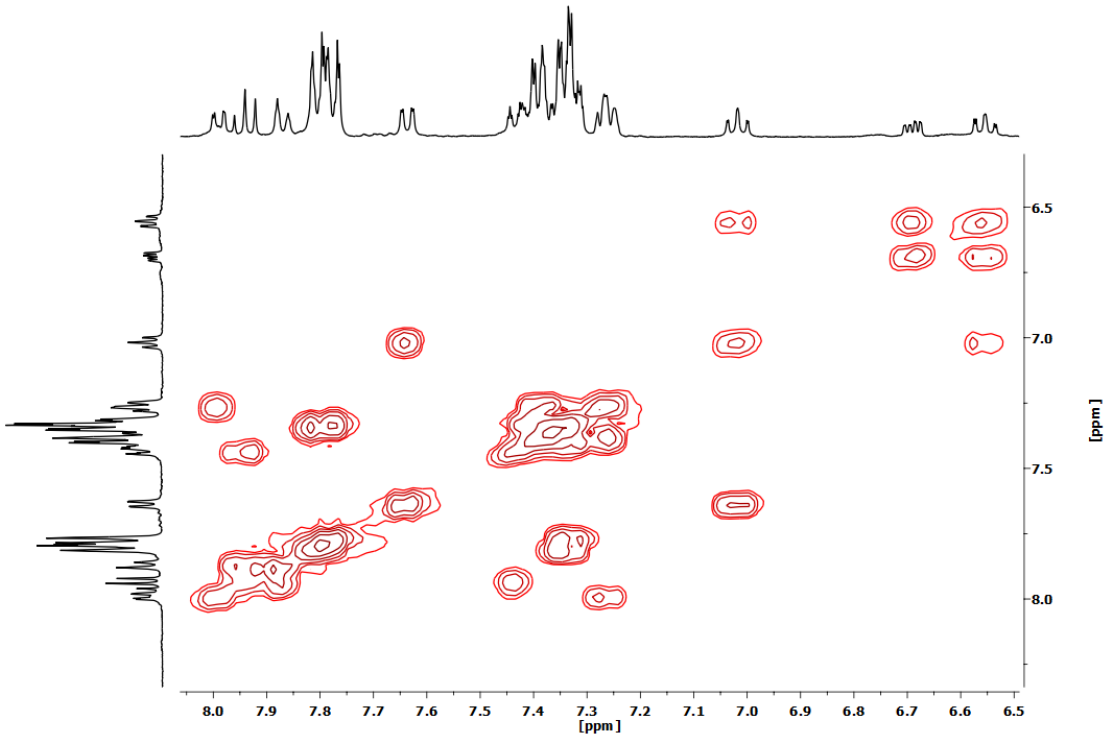

Figure S3.11. ^{1}H-^{1}H COSY NMR spectrum (CD_2Cl_2, RT) of complex [Pt(CN-*o*-tol)I(PPh_3)] (**29**).

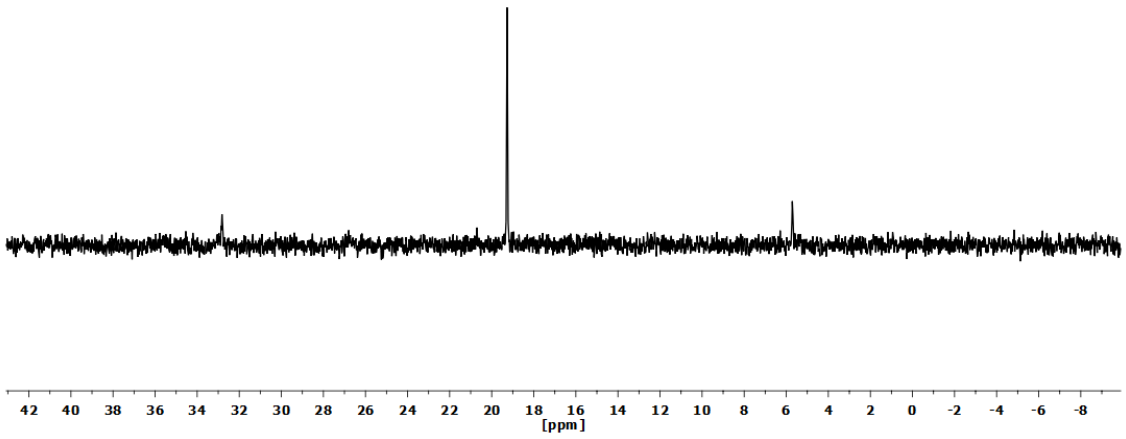

Figure S3.12. $^{31}P\{^{1}H\}$ NMR spectrum (CD_2Cl_2, RT) of complex [Pt(CN-*o*-tol)I(PPh_3)] (**29**).

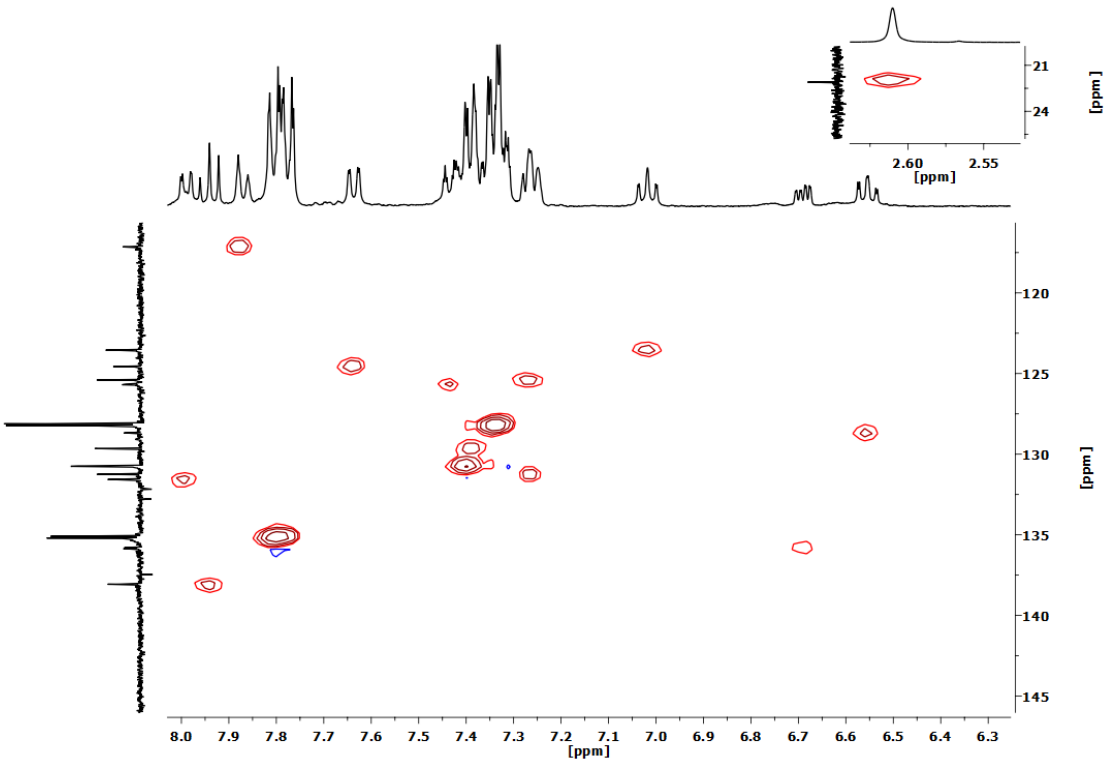

Figure S3.13. ^{1}H-^{13}C HSQC NMR spectrum (CD_2Cl_2, RT) of complex [Pt(CN-*o*-tol)I(PPh_3)] (**29**).

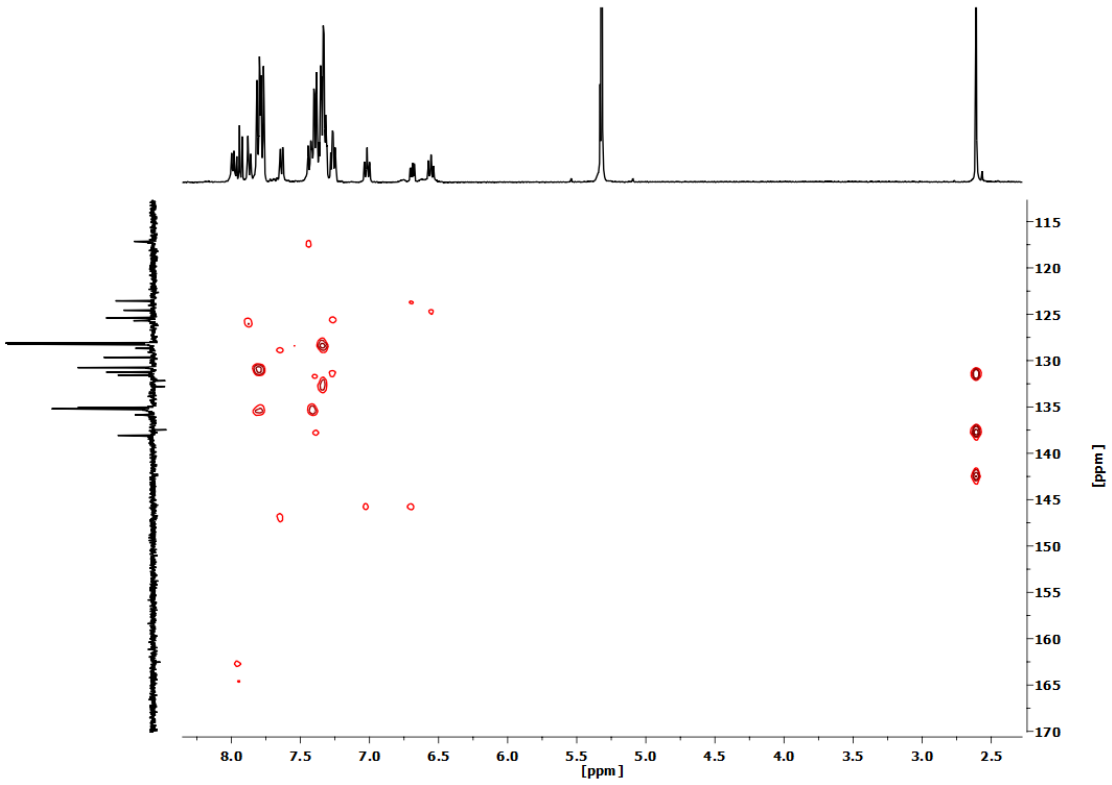

Figure S3.14. ^{1}H-^{13}C HMBC NMR spectrum (CD_2Cl_2, RT) of complex [Pt(CN-*o*-tol)I(PPh_3)] (**29**).

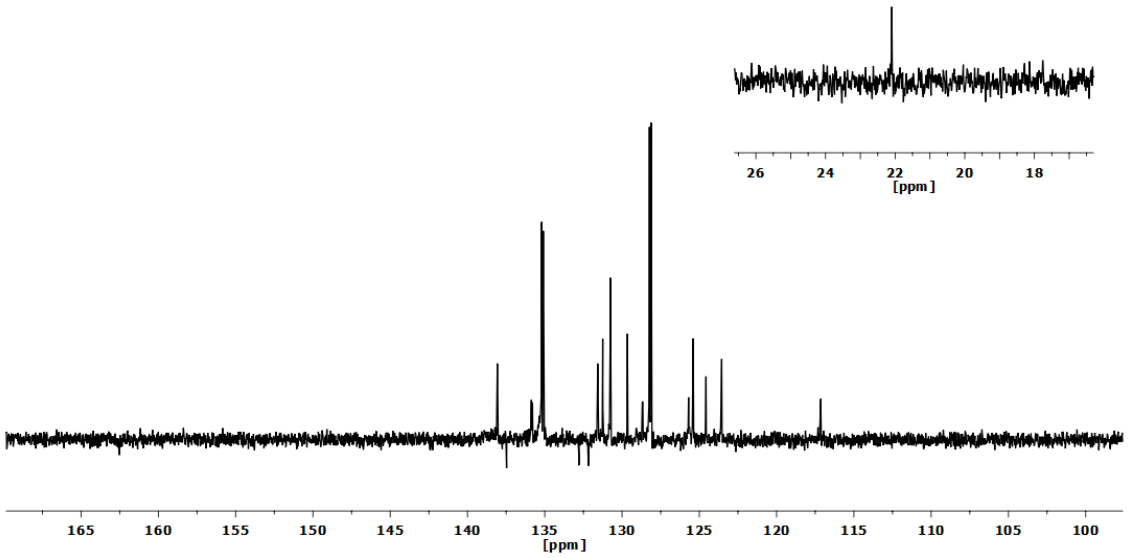

Figure S3.15. APT $^{13}C\{^{1}H\}$ NMR spectrum (CD_2Cl_2, RT) of complex [Pt(CN-*o*-tol)I(PPh_3)] (**29**).

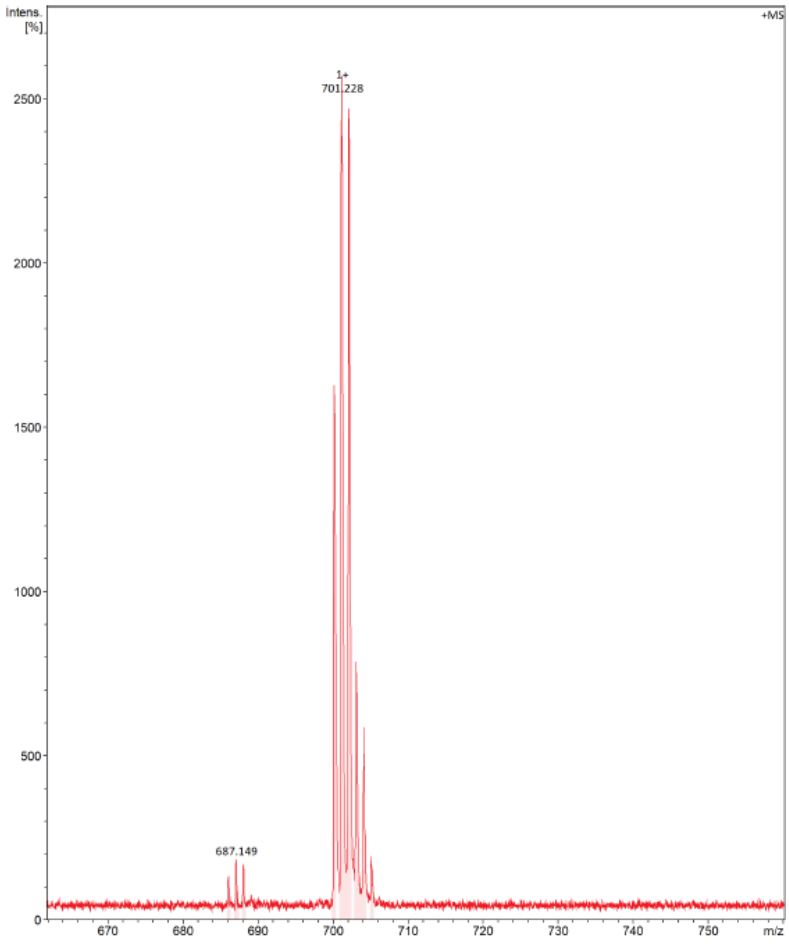

Figure S3.16. MS (MALDI+ DCTB) spectrum of complex [Pt(CN-*o*-tol)I(PPh_3)] (**29**).

2.3. Spectra of complex [Pt(CN-*o*-tol)(MeCN)(PPh_3)](ClO_4) (30).

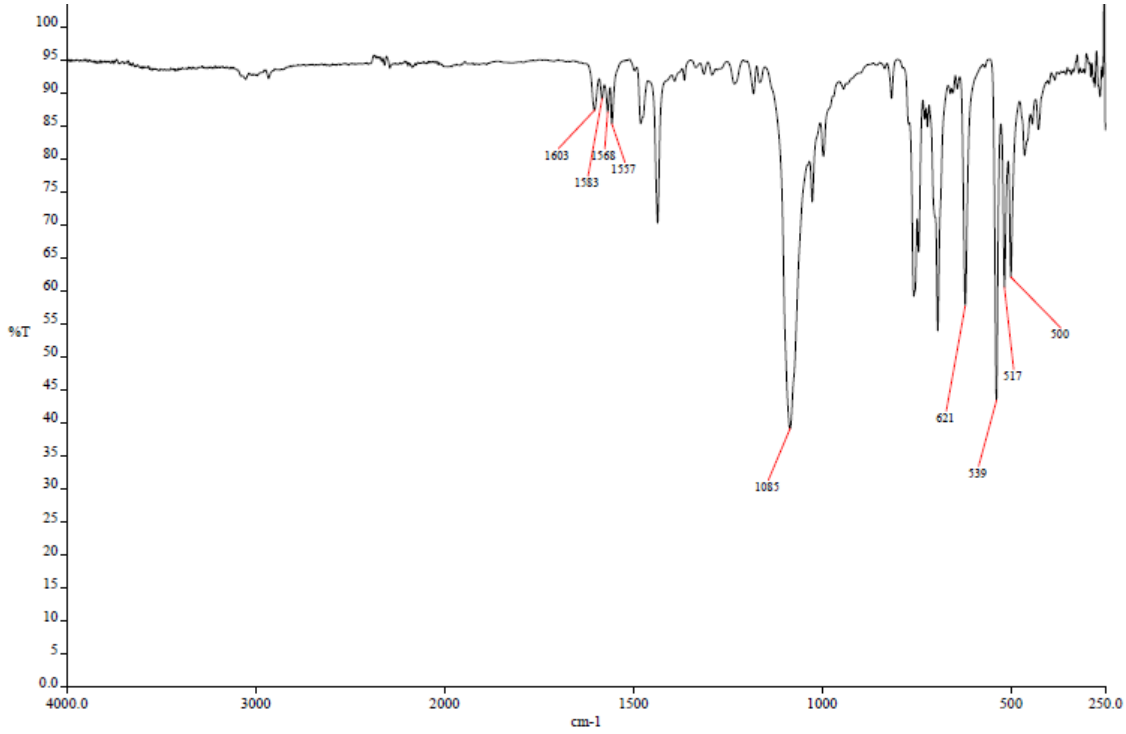

Figure S3.17. IR spectrum of complex [Pt(CN-*o*-tol)(MeCN)(PPh_3)](ClO_4) (**30**).

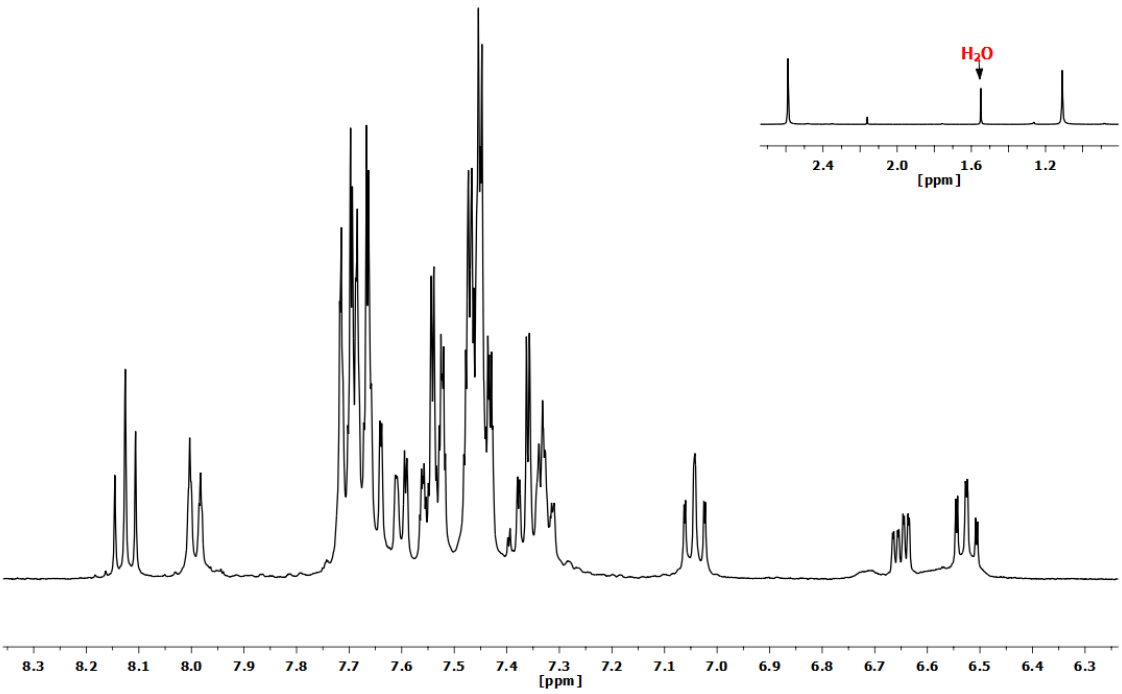

Figure S3.18. ^1H NMR spectrum (CD_2Cl_2, RT) of complex [Pt(CN-*o*-tol)(MeCN)(PPh_3)](ClO_4) (**30**).

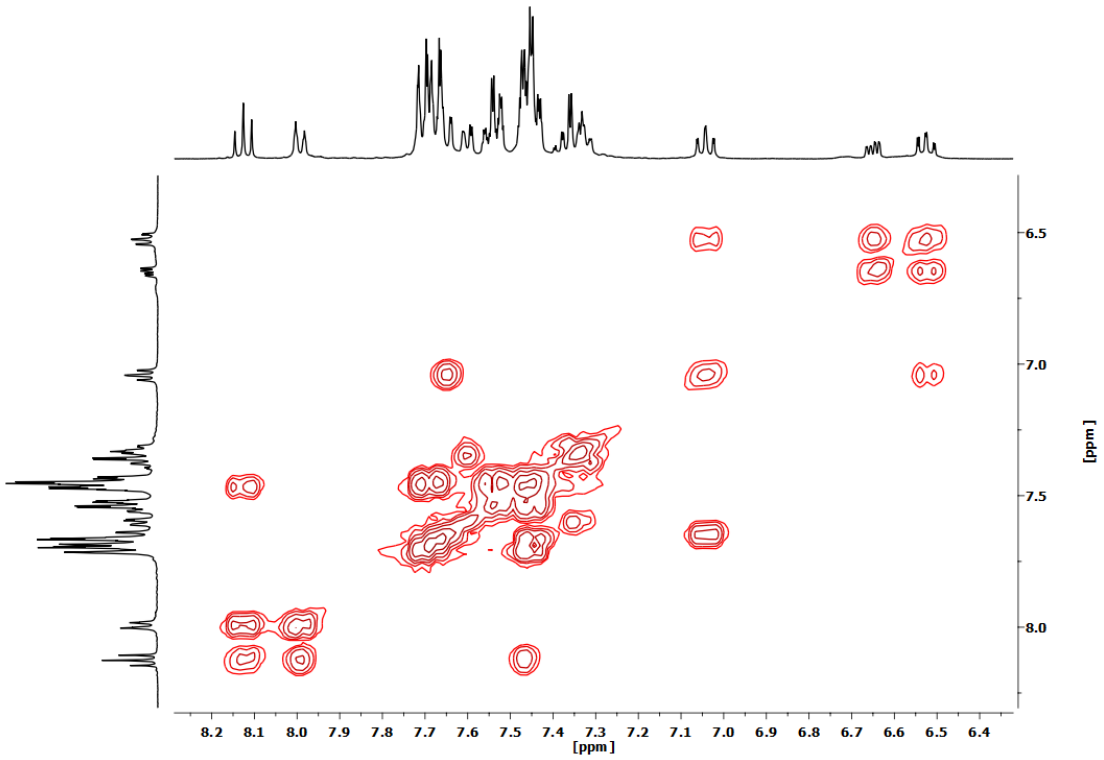

Figure S3.19. ^{1}H-^{1}H COSY NMR spectrum (CD_2Cl_2, RT) of complex [Pt(CN-*o*-tol)(MeCN)(PPh_3)](ClO_4) (**30**).

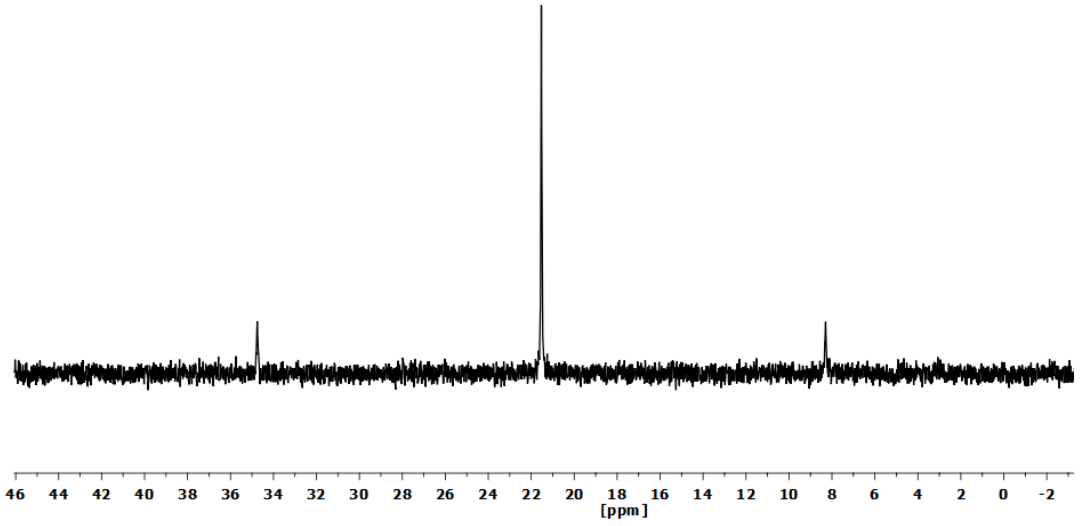

Figure S3.20. ^{31}P{^{1}H} NMR spectrum (CD_2Cl_2, RT) of complex [Pt(CN-*o*-tol)(MeCN)(PPh_3)](ClO_4) (**30**).

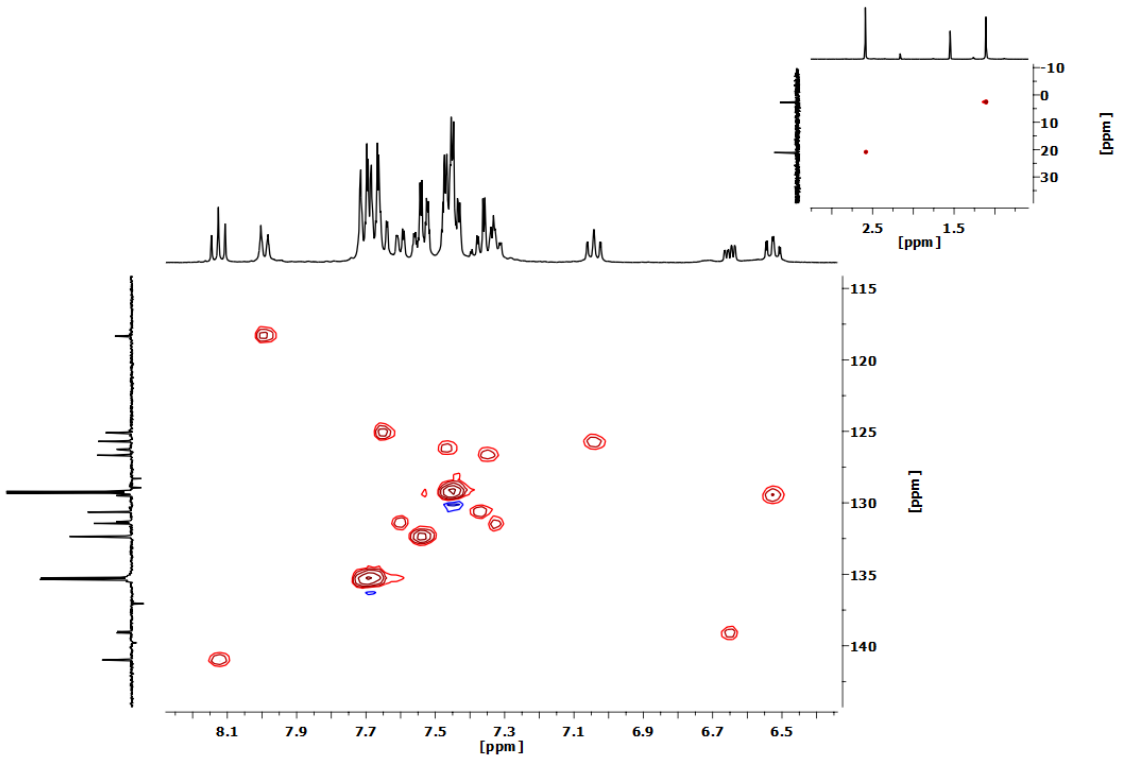

Figure S3.21. ^{1}H-^{13}C HSQC NMR spectrum (CD_2Cl_2, RT) of complex [Pt(CN-*o*-tol)(MeCN)(PPh_3)](ClO_4) (**30**).

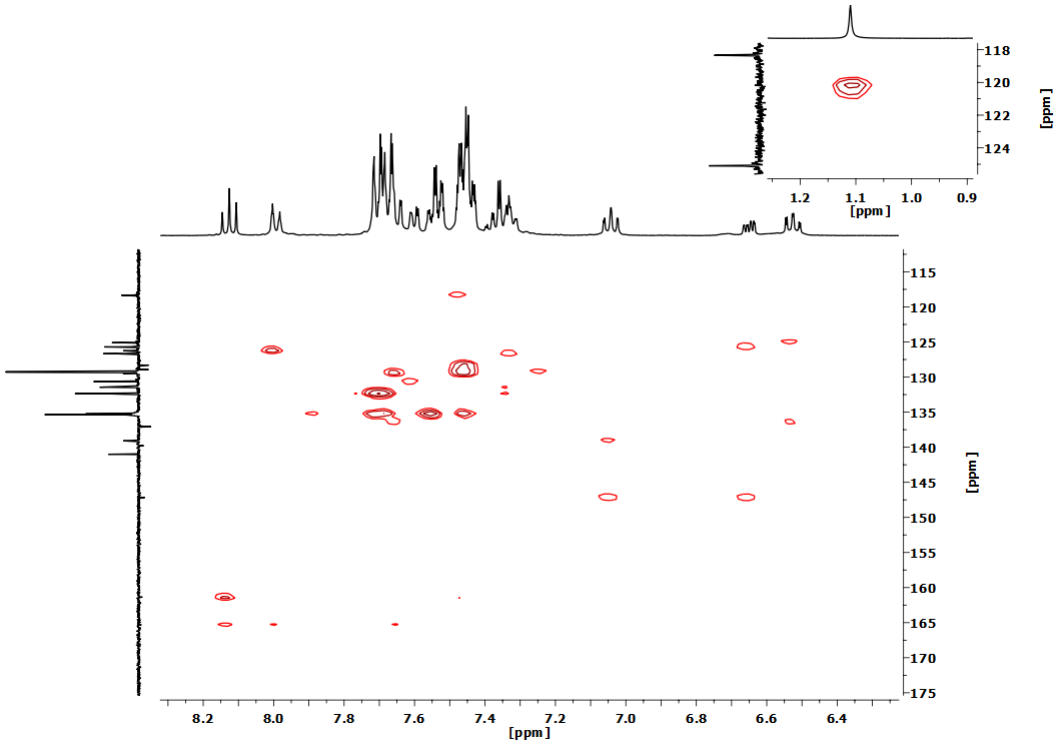

Figure S3.22. ^{1}H-^{13}C HMBC NMR spectrum (CD_2Cl_2, RT) of complex [Pt(CN-*o*-tol)(MeCN)(PPh_3)](ClO_4) (**30**).

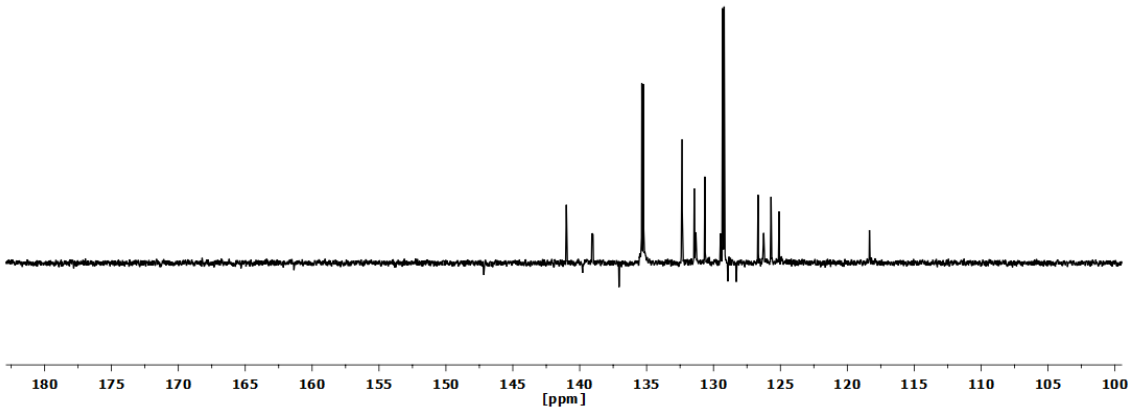

Figure S3.23. APT $^{13}C\{^{1}H\}$ NMR spectrum (CD_2Cl_2, RT) of complex [Pt(CN-*o*-tol)(MeCN)(PPh_3)](ClO_4) (**30**).

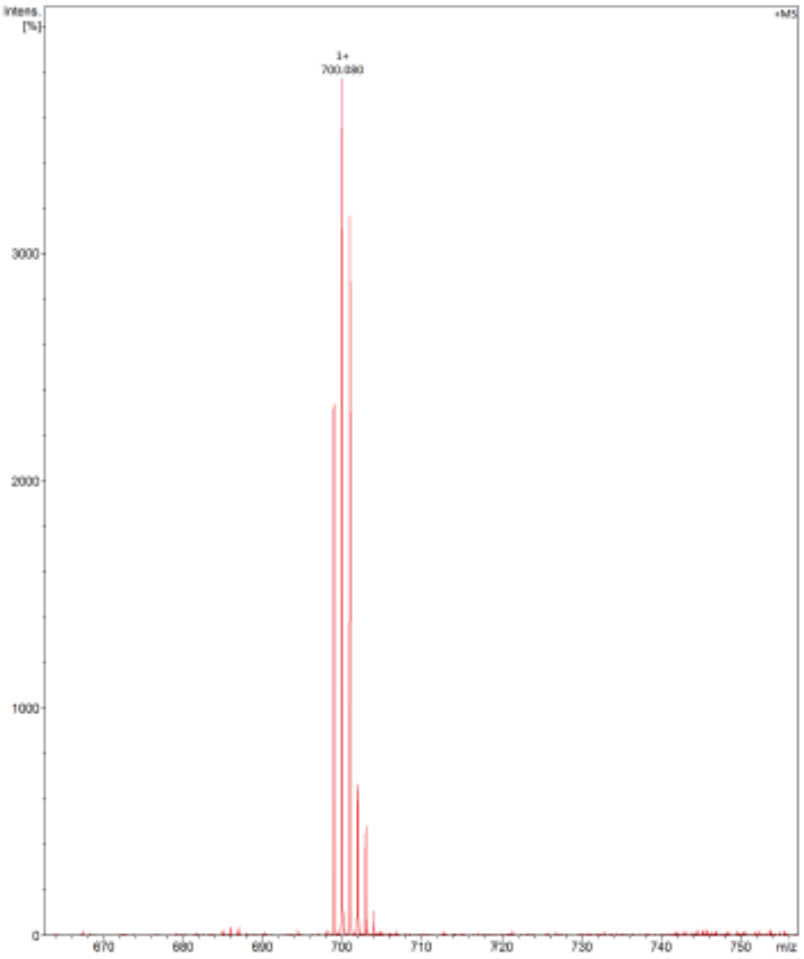

Figure S3.24. MS (MALDI+ DCTB) selected peak of complex [Pt(CN-*o*-tol)(MeCN)(PPh_3)](ClO_4) (**30**).

2.4. Spectra of complex [Pt(CNC-Me)(PPh$_3$)] (32).

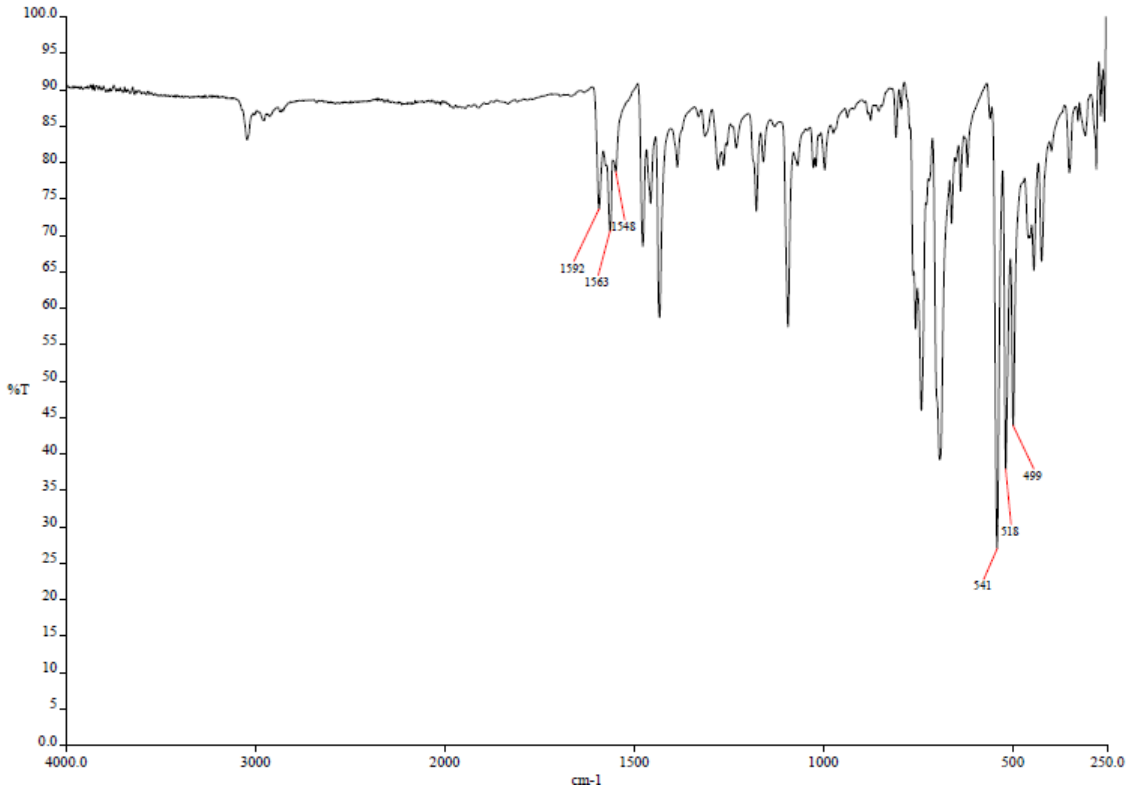

Figure S3.25. IR spectrum of complex [Pt(CNC-Me)(PPh$_3$)] (**32**).

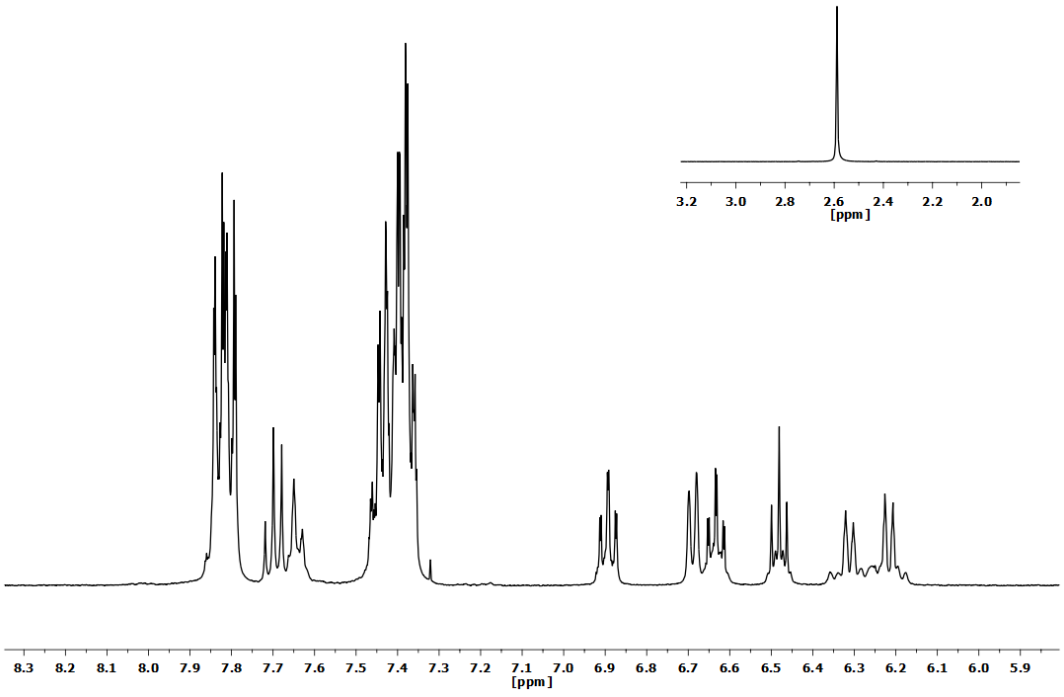

Figure S3.26. ^{1}H NMR spectrum (CD_2Cl_2, RT) of complex [Pt(CNC-Me)(PPh$_3$)] (**32**).

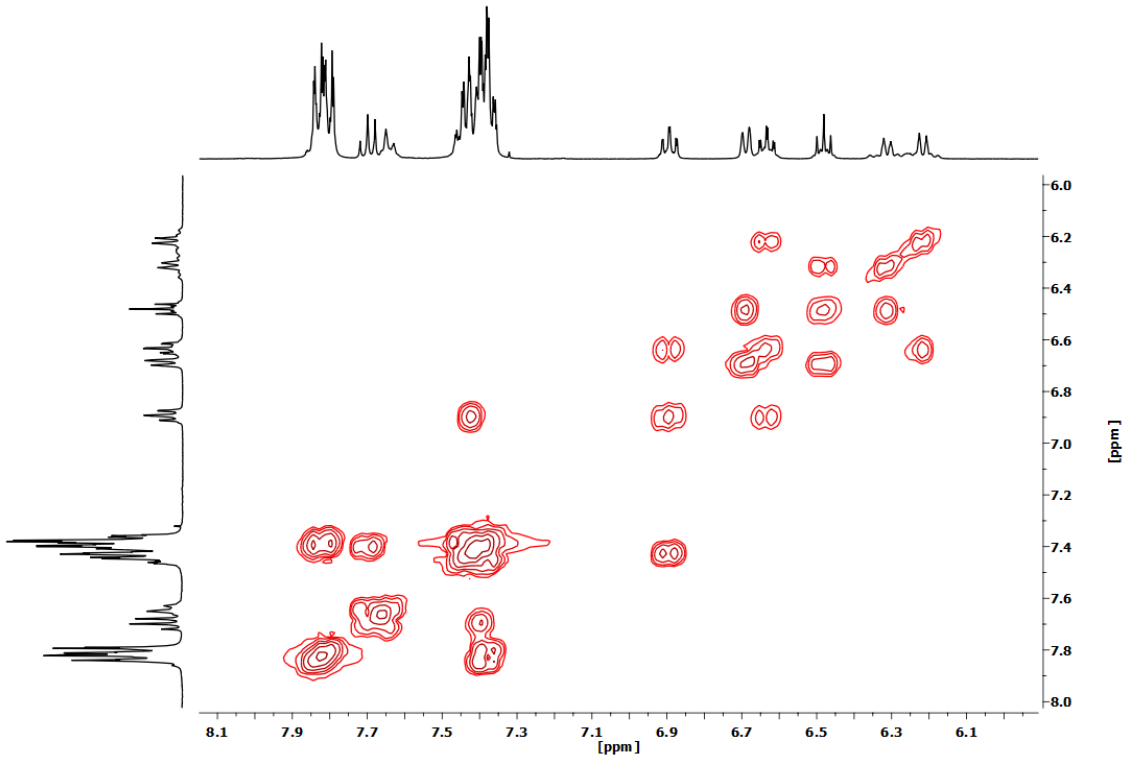

Figure S3.27. ^{1}H-^{1}H COSY NMR spectrum (CD_2Cl_2, RT) of complex [Pt(CNC-Me)(PPh_3)] (**32**).

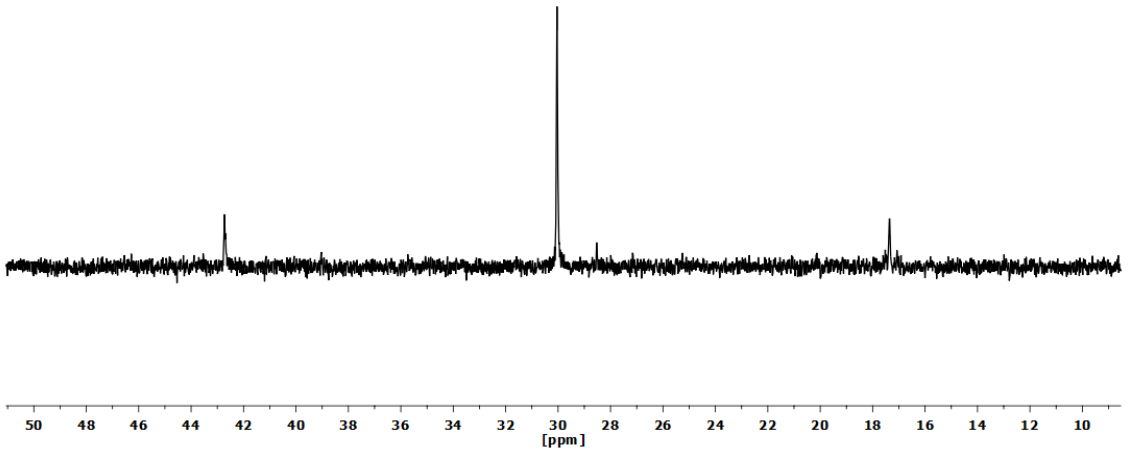

Figure S3.28. $^{31}P\{^{1}H\}$ NMR spectrum (CD_2Cl_2, RT) of complex [Pt(CNC-Me)(PPh_3)] (**32**).

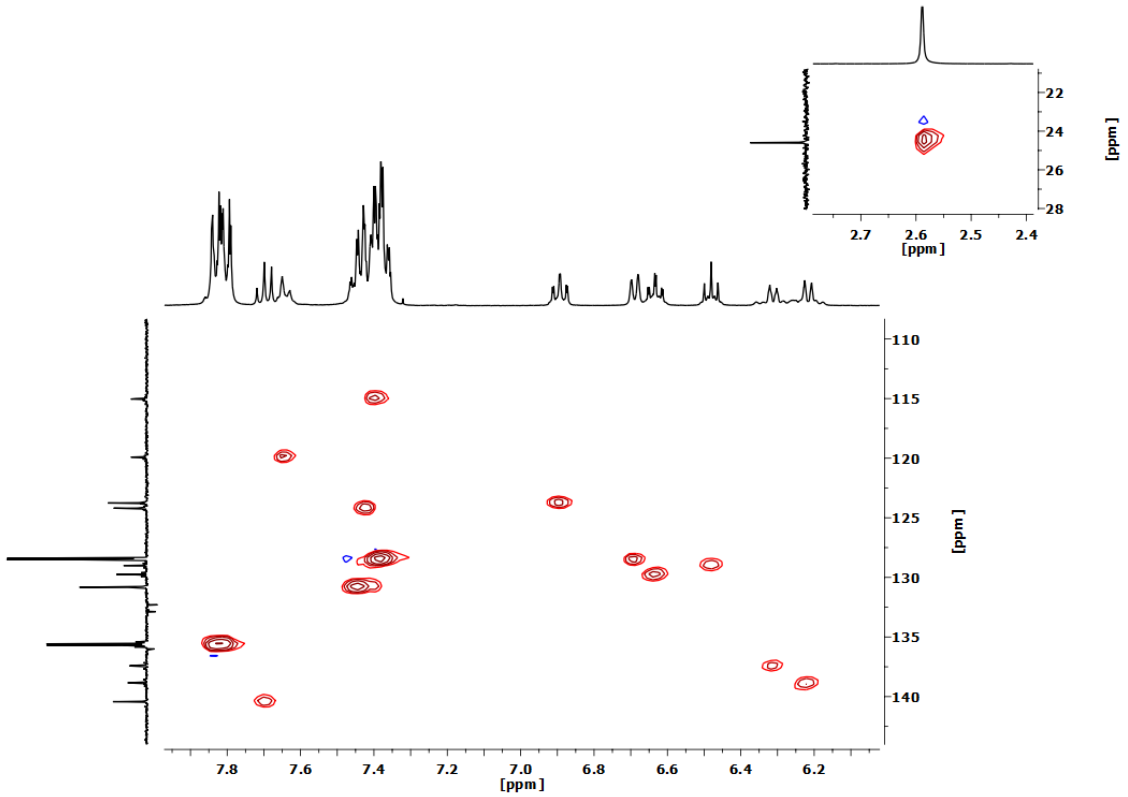

Figure S3.29. ^{1}H-^{13}C HSQC NMR spectrum (CD_2Cl_2, RT) of complex [Pt(CNC-Me)(PPh_3)] (**32**).

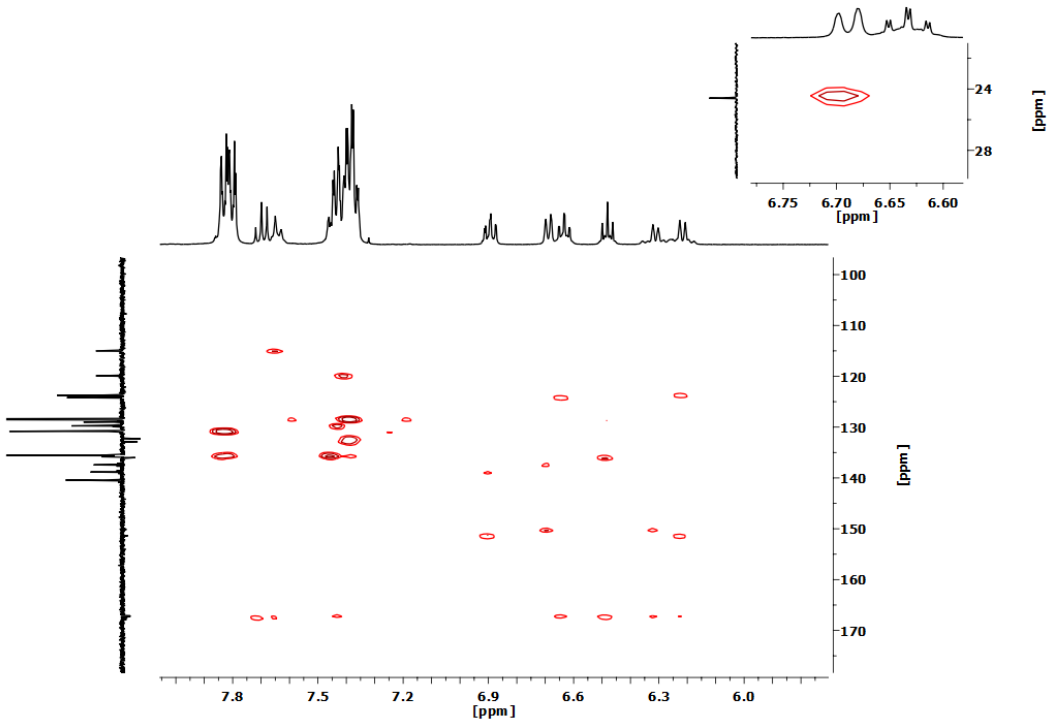

Figure S3.30. ^{1}H-^{13}C HMBC NMR spectrum (CD_2Cl_2, RT) of complex [Pt(CNC-Me)(PPh_3)] (**32**).

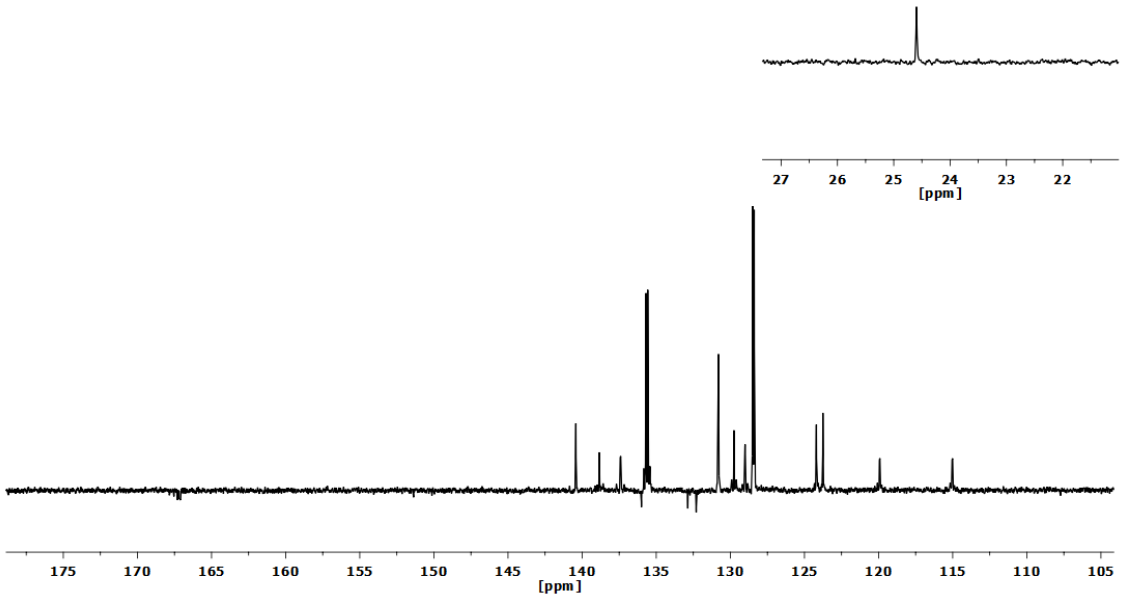

Figure S3.31. APT $^{13}C\{^{1}H\}$ NMR spectrum (CD_2Cl_2, RT) of complex [Pt(CNC-Me)(PPh_3)] (**32**).

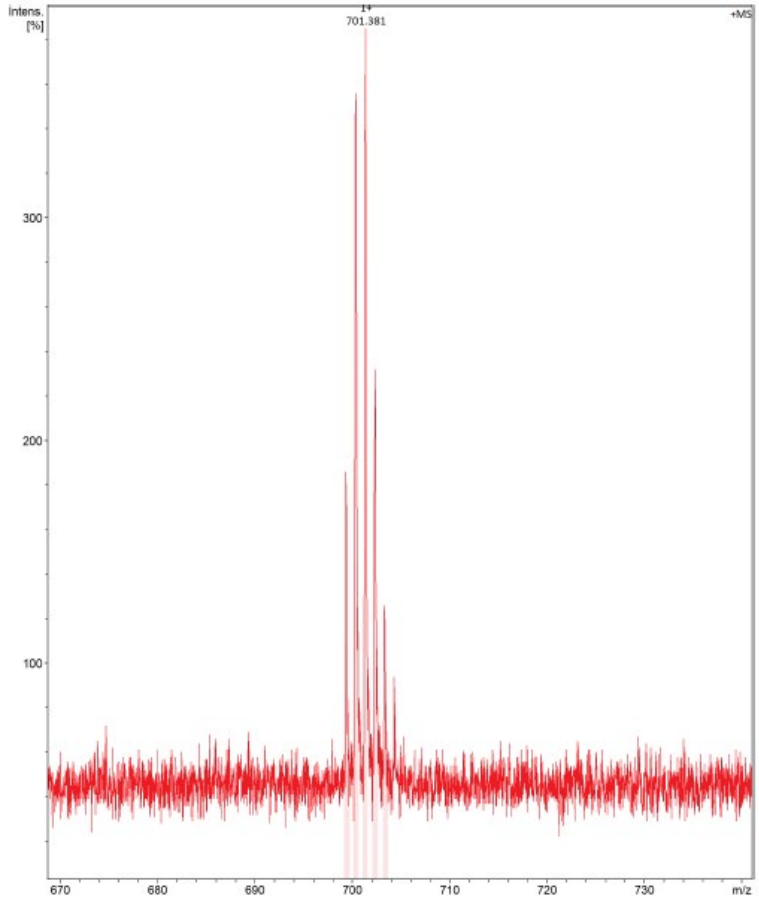

Figure S3.32. MS (MALDI+ DCTB) selected peak of complex [Pt(CNC-Me)(PPh_3)] (**32**).

2.5. Spectra of complex [Pt(CN-2,6-xyl)I(PPh$_3$)] (33).

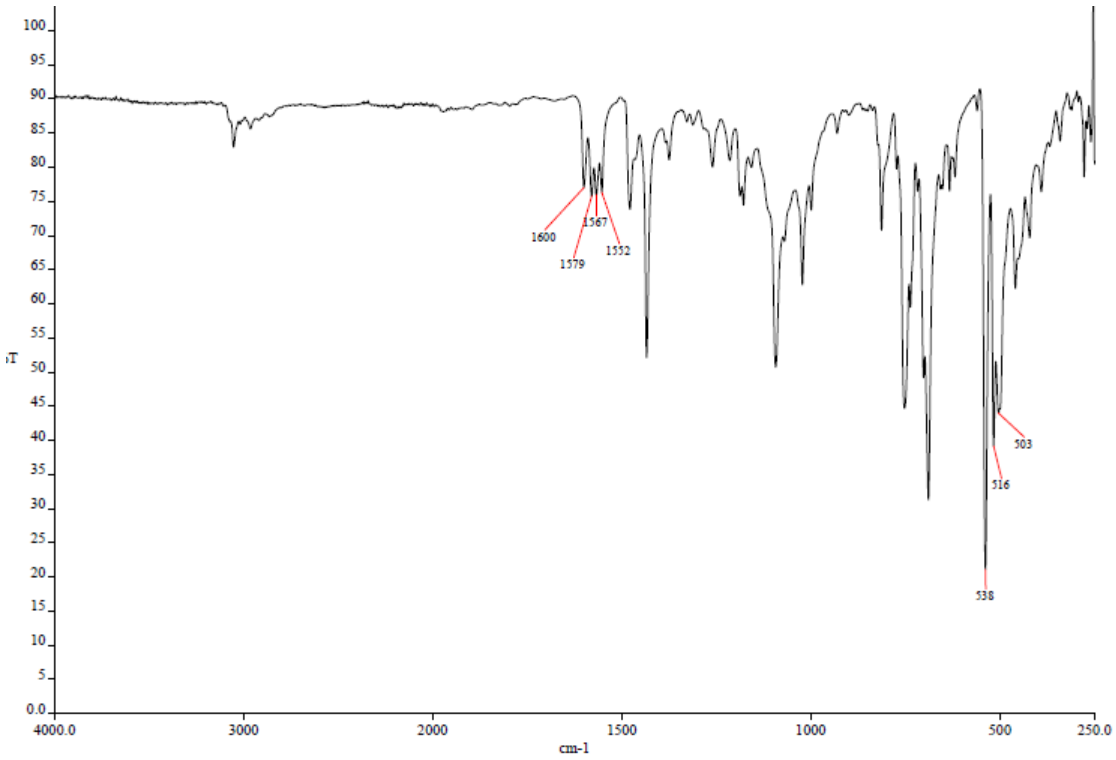

Figure S3.33. IR spectrum of complex [Pt(CN-2,6-xyl)I(PPh$_3$)] (**33**).

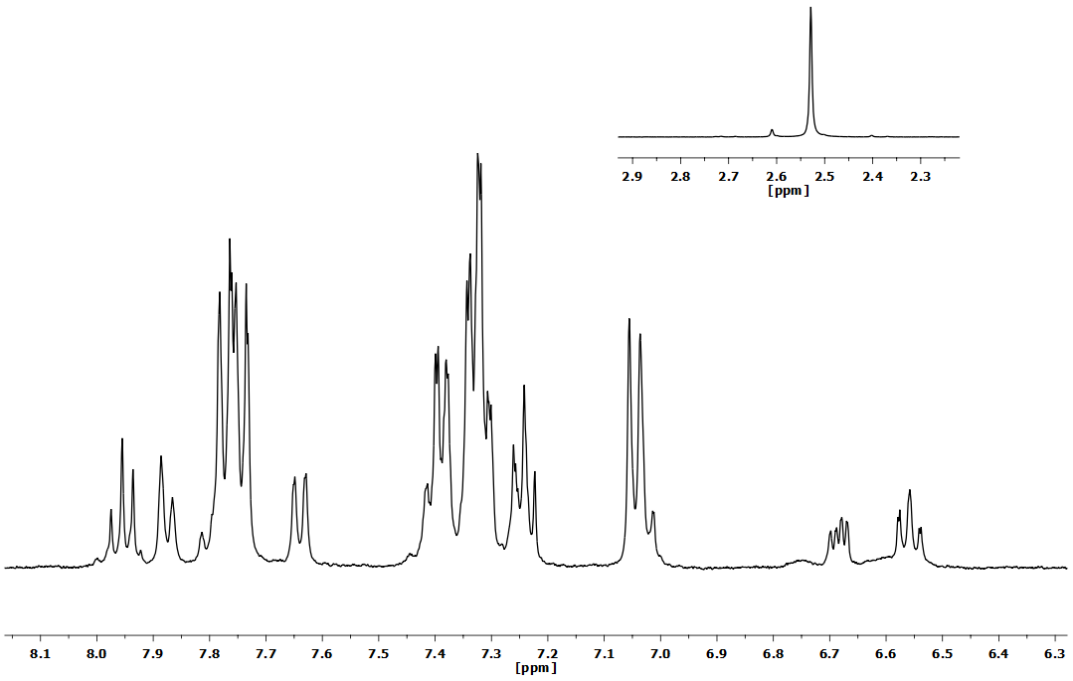

Figure S3.34. ^{1}H NMR spectrum (CD_2Cl_2, RT) of complex [Pt(CN-2,6-xyl)I(PPh$_3$)] (**33**).

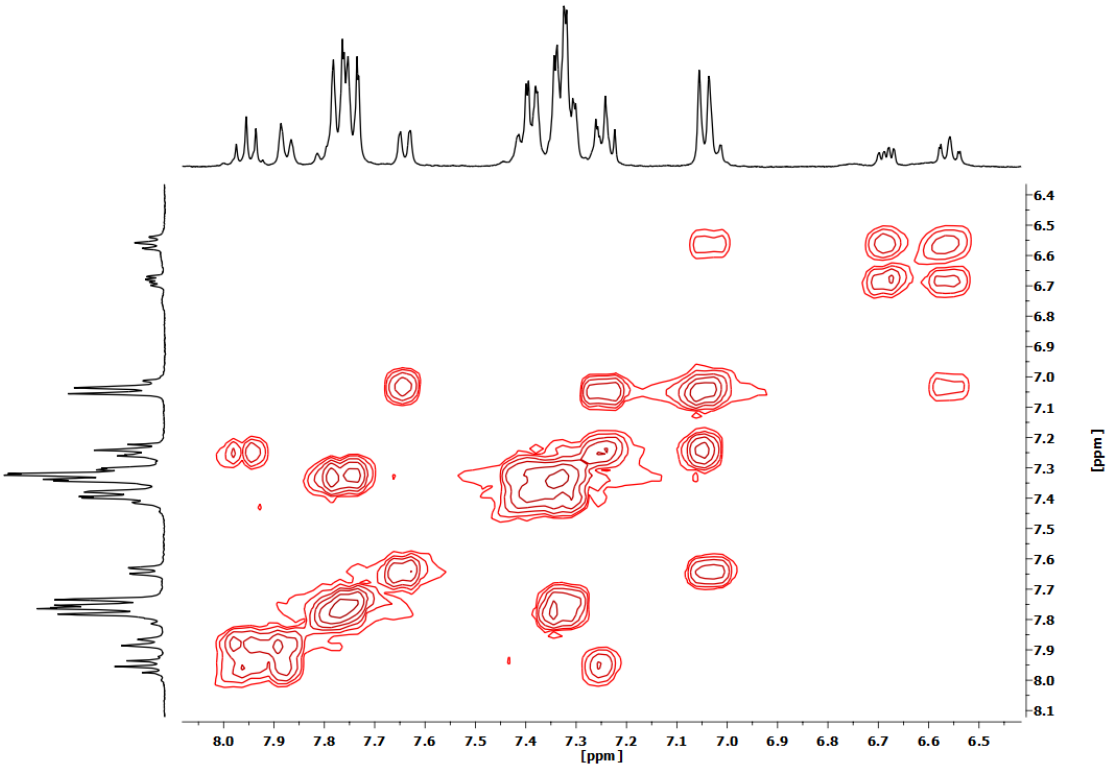

Figure S3.35. ^{1}H-^{1}H COSY NMR spectrum (CD_2Cl_2, RT) of complex [Pt(CN-2,6-xyl)I(PPh_3)] (**33**).

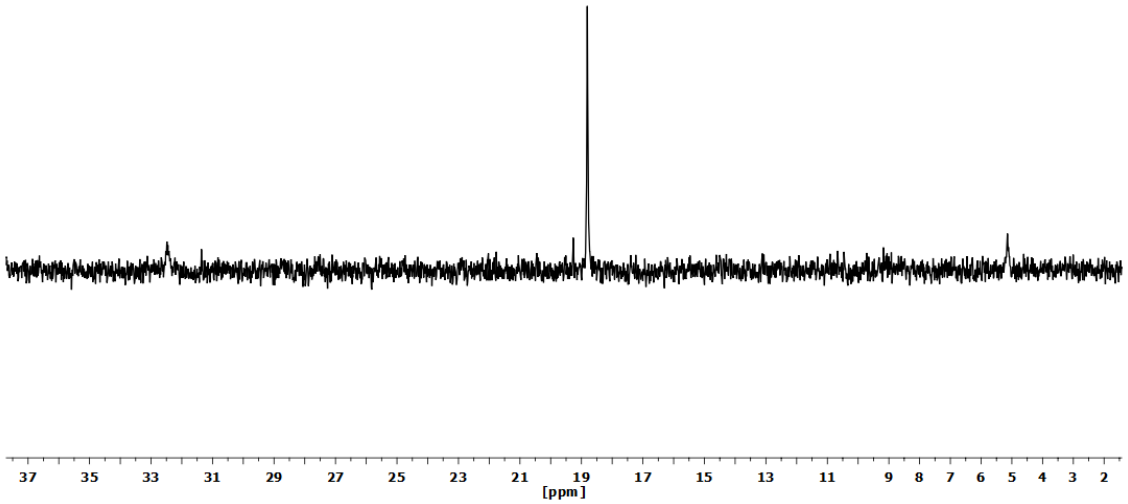

Figure S3.36. ^{31}P{^{1}H} NMR spectrum (CD_2Cl_2, RT) of complex [Pt(CN-2,6-xyl)I(PPh_3)] (**33**).

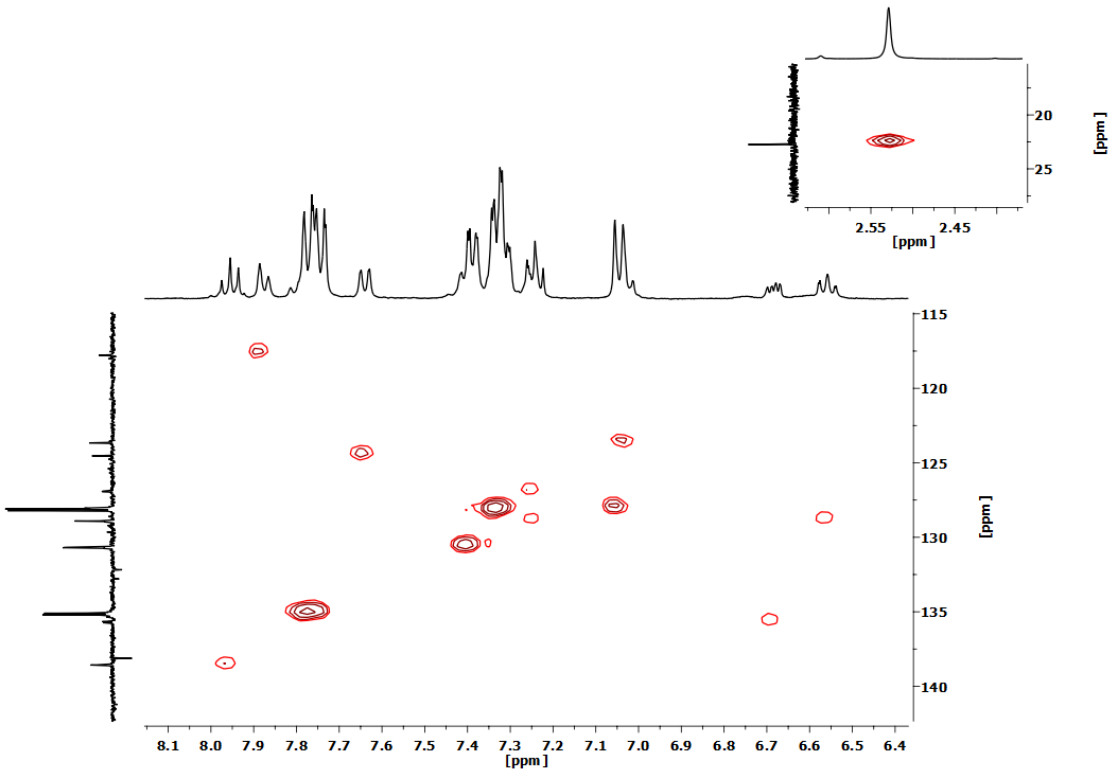

Figure S3.37. ^{1}H-^{13}C HSQC NMR spectrum (CD_2Cl_2, RT) of complex [Pt(CN-2,6-xyl)I(PPh_3)] (**33**).

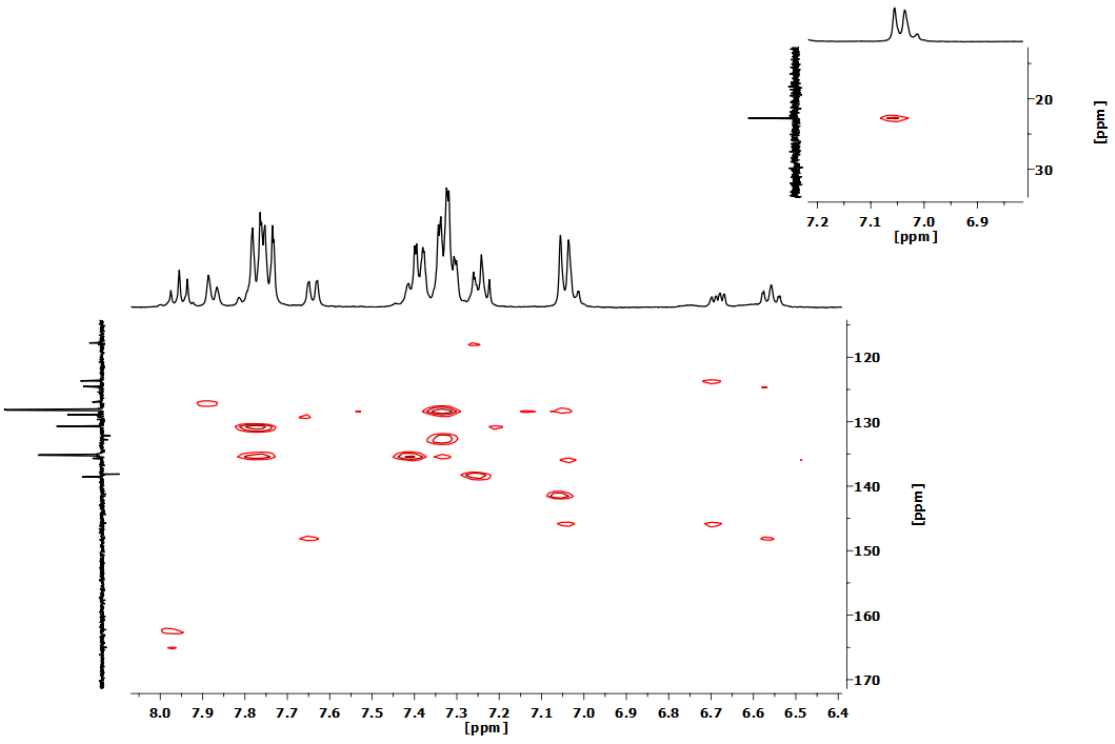

Figure S3.38. ^{1}H-^{13}C HMBC NMR spectrum (CD_2Cl_2, RT) of complex [Pt(CN-2,6-xyl)I(PPh_3)] (**33**).

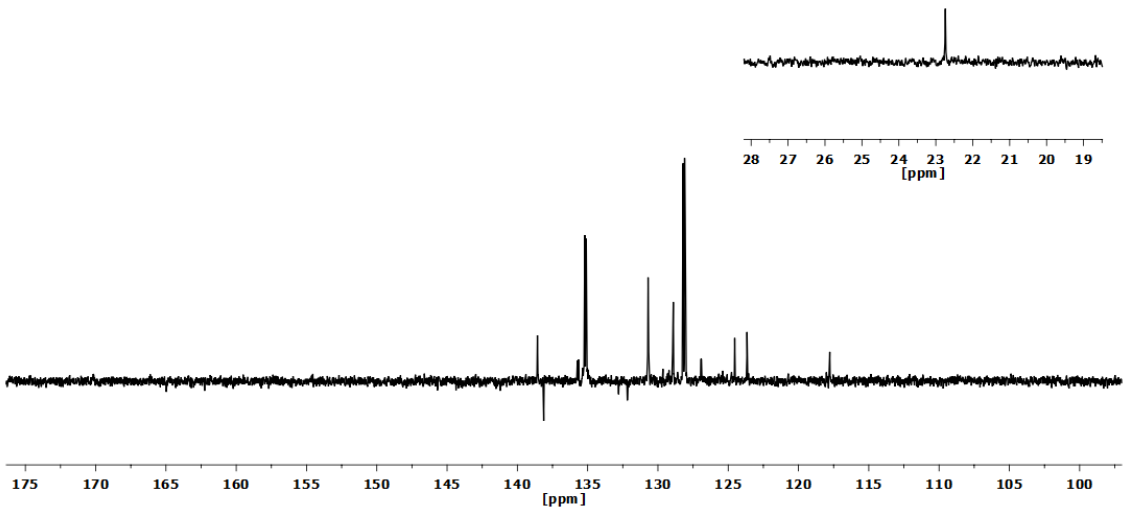

Figure S3.39. APT $^{13}C\{^{1}H\}$ NMR spectrum (CD_2Cl_2, RT) of complex [Pt(CN-2,6-xyl)I(PPh_3)] (**33**).

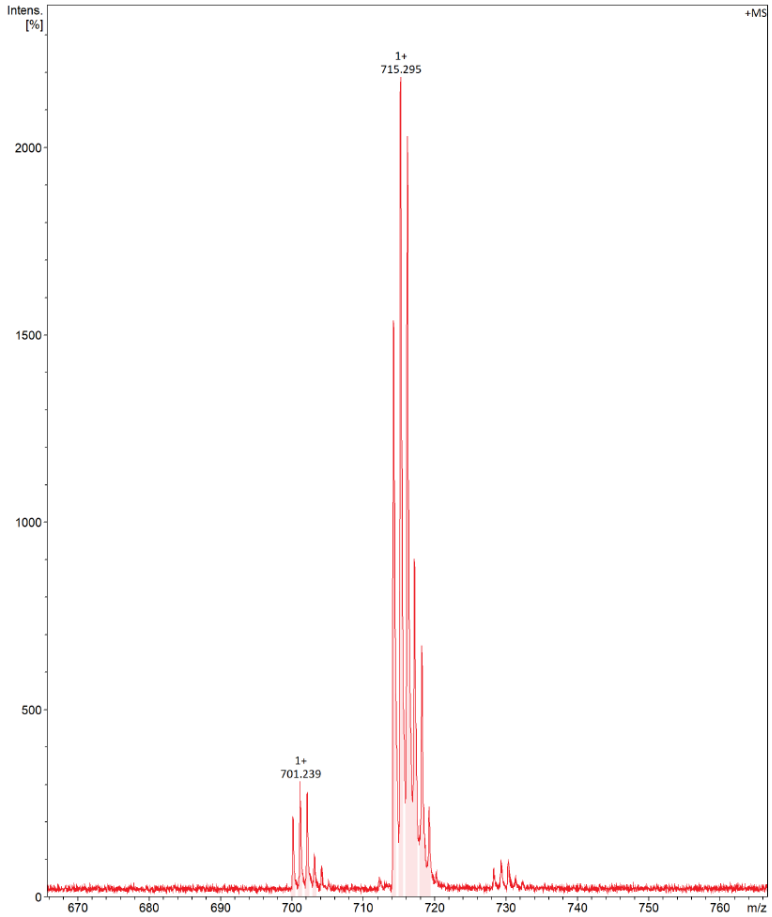

Figure S3.40. MS (MALDI+ DCTB) selected peak of complex [Pt(CN-2,6-xyl)I(PPh_3)] (**33**).

2.6. Spectra of complex [Pt(CN-*o*-tol)Cl(PPh$_3$)] (35).

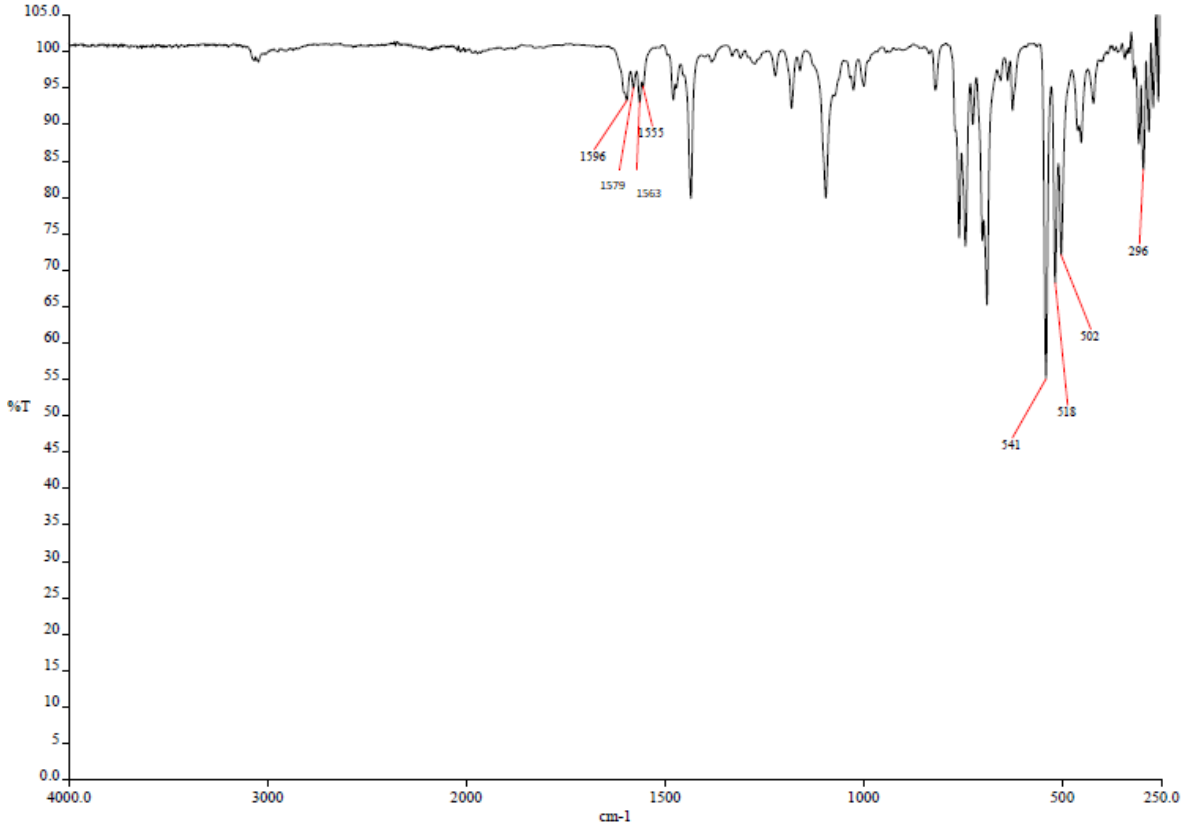

Figure S3.41. IR spectrum of complex [Pt(CN-*o*-tol)Cl(PPh$_3$)] (**35**).

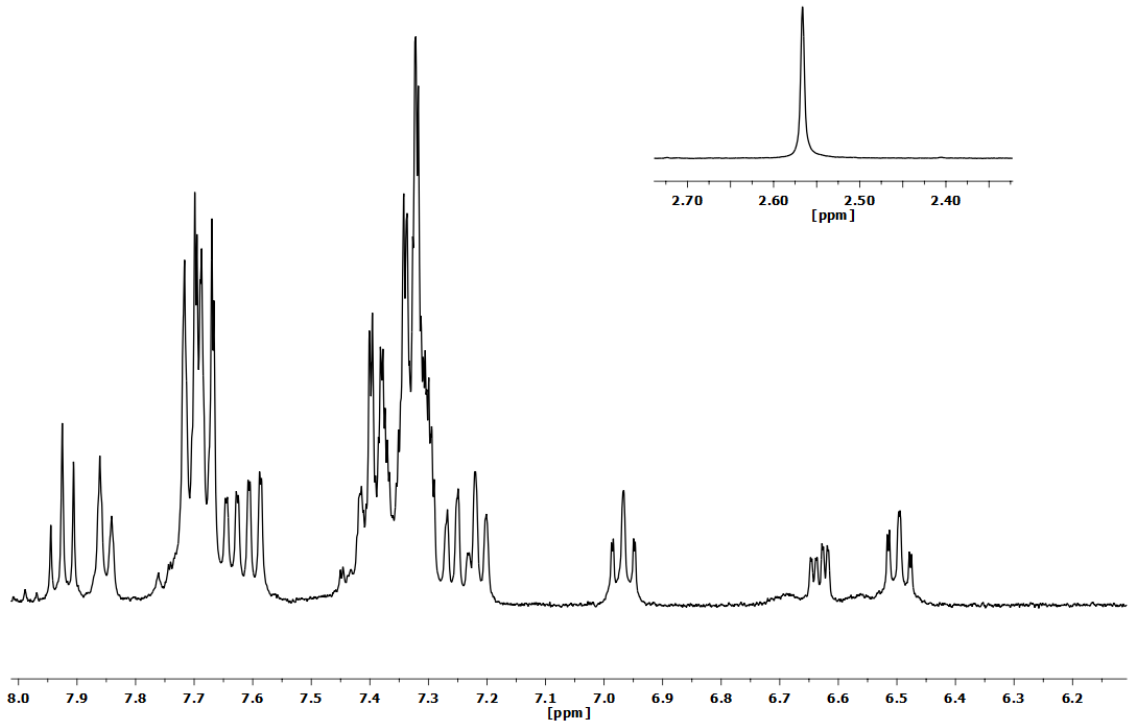

Figure S3.42. ^{1}H NMR spectrum (CD_2Cl_2, RT) of complex [Pt(CN-*o*-tol)Cl(PPh_3)] (**35**).

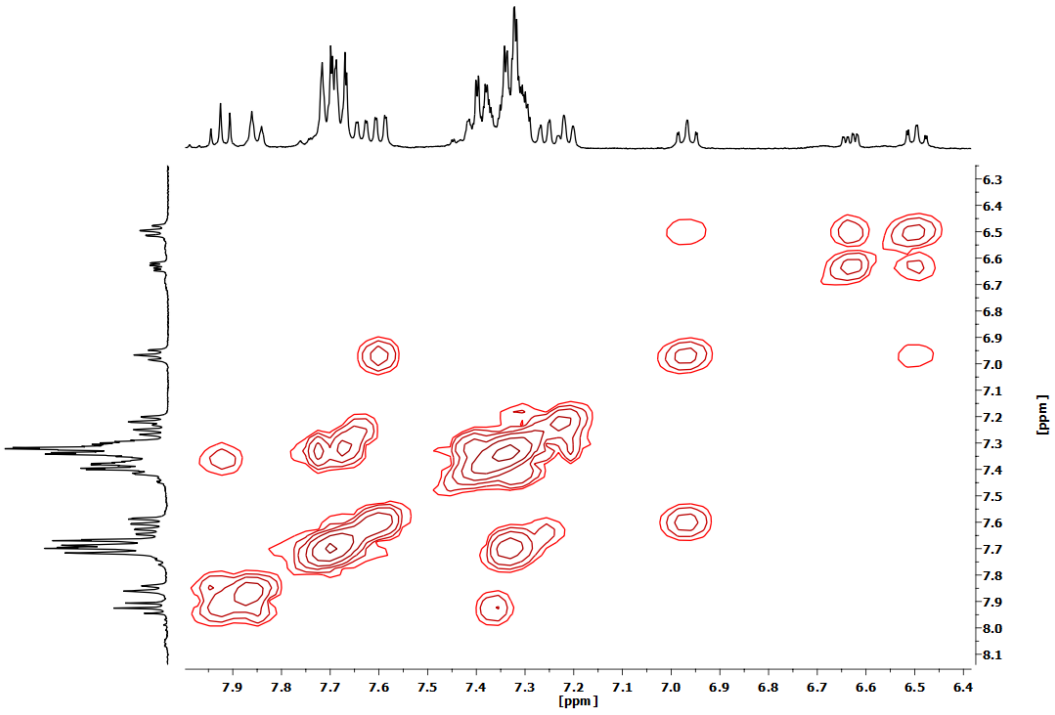

Figure S3.43. ^{1}H-^{1}H COSY NMR spectrum (CD_2Cl_2, RT) of complex [Pt(CN-*o*-tol)Cl(PPh_3)] (**35**).

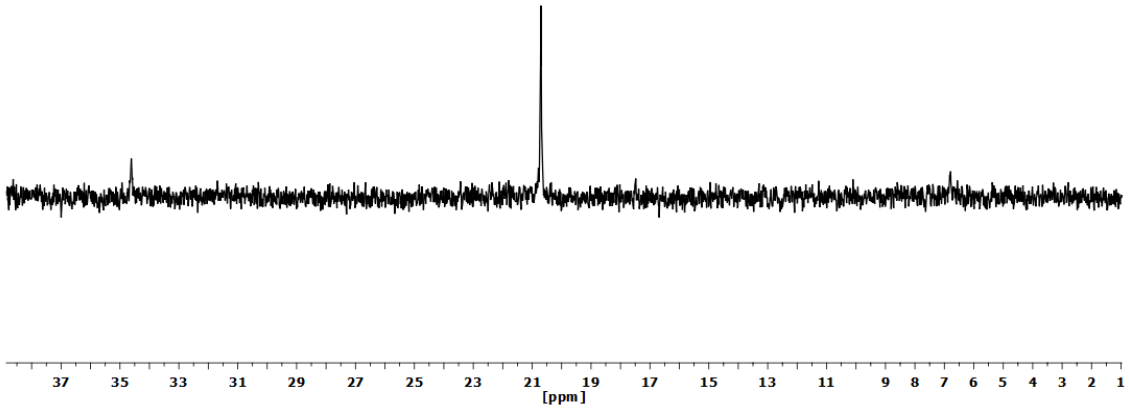

Figure S3.44. $^{31}P\{^{1}H\}$ NMR spectrum (CD_2Cl_2, RT) of complex [Pt(CN-*o*-tol)Cl(PPh_3)] (**35**).

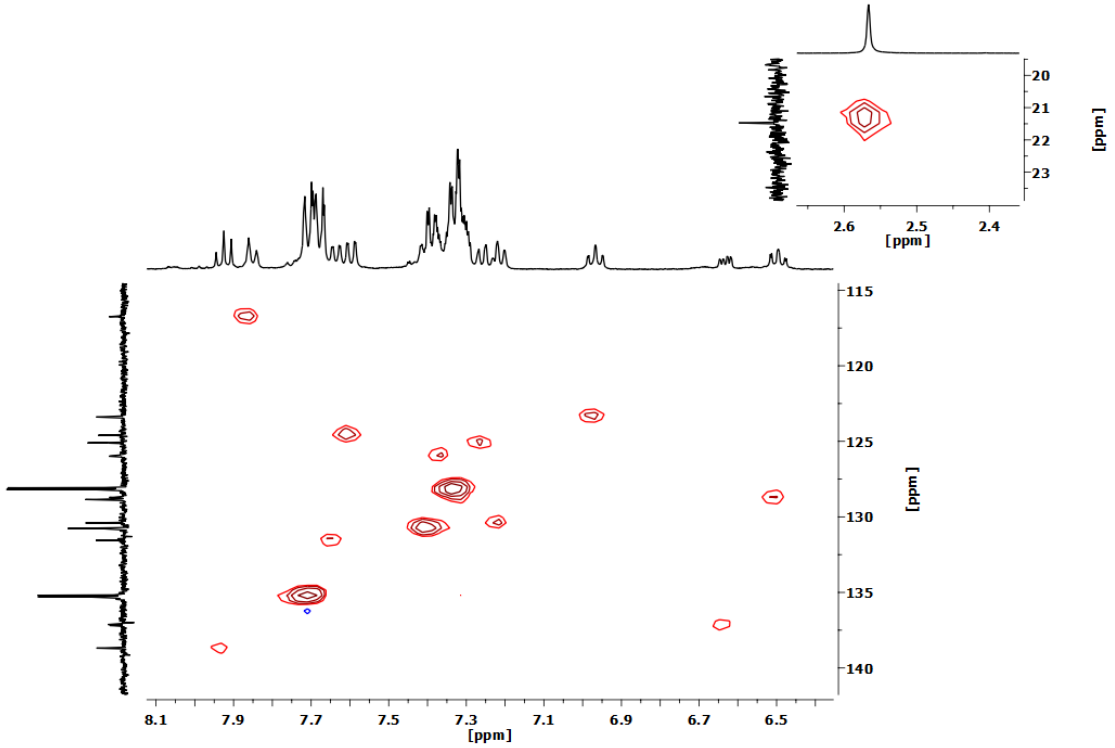

Figure S3.45. ^{1}H-^{13}C HSQC NMR spectrum (CD_2Cl_2, RT) of complex [Pt(CN-*o*-tol)Cl(PPh_3)] (**35**).

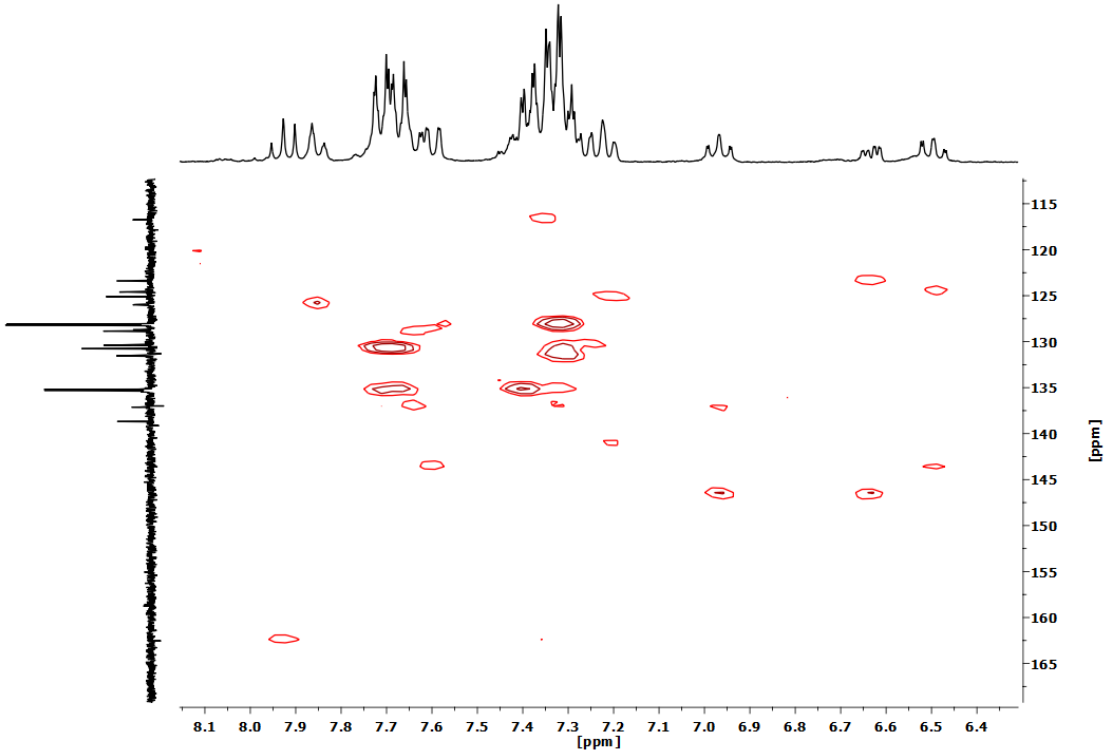

Figure S3.46. ^{1}H-^{13}C HMBC NMR spectrum (CD_2Cl_2, RT) of complex [Pt(CN-*o*-tol)Cl(PPh_3)] (**35**).

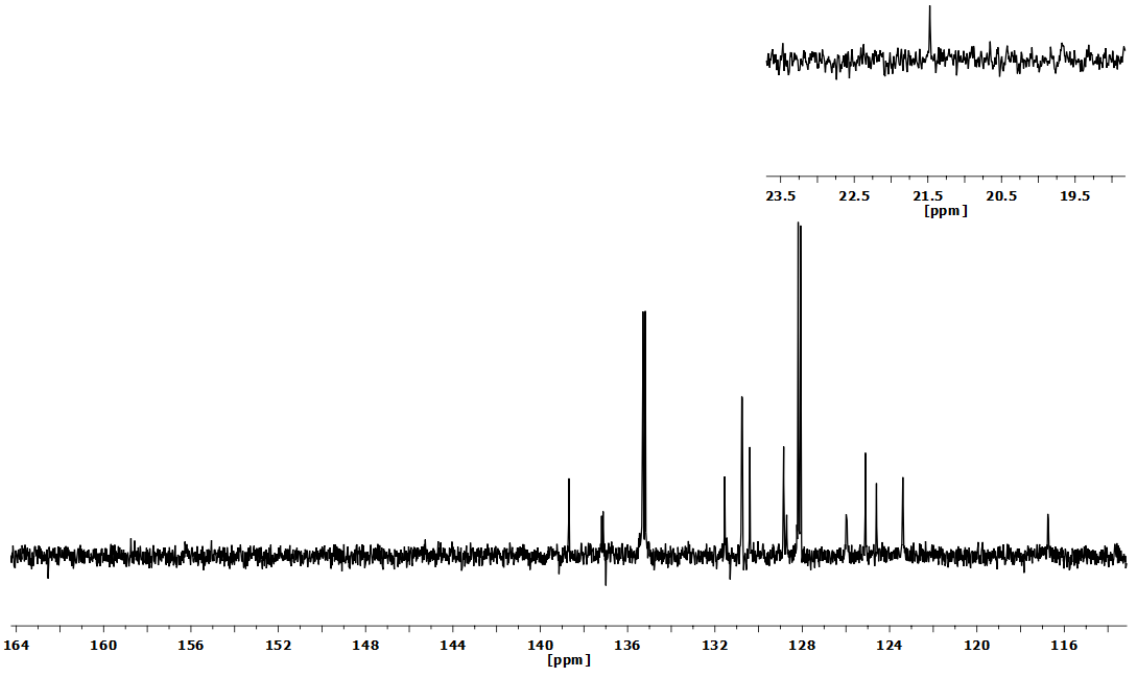

Figure S3.47. APT $^{13}C\{^{1}H\}$ NMR spectrum (CD_2Cl_2, RT) of complex [Pt(CN-*o*-tol)Cl(PPh_3)] (**35**).

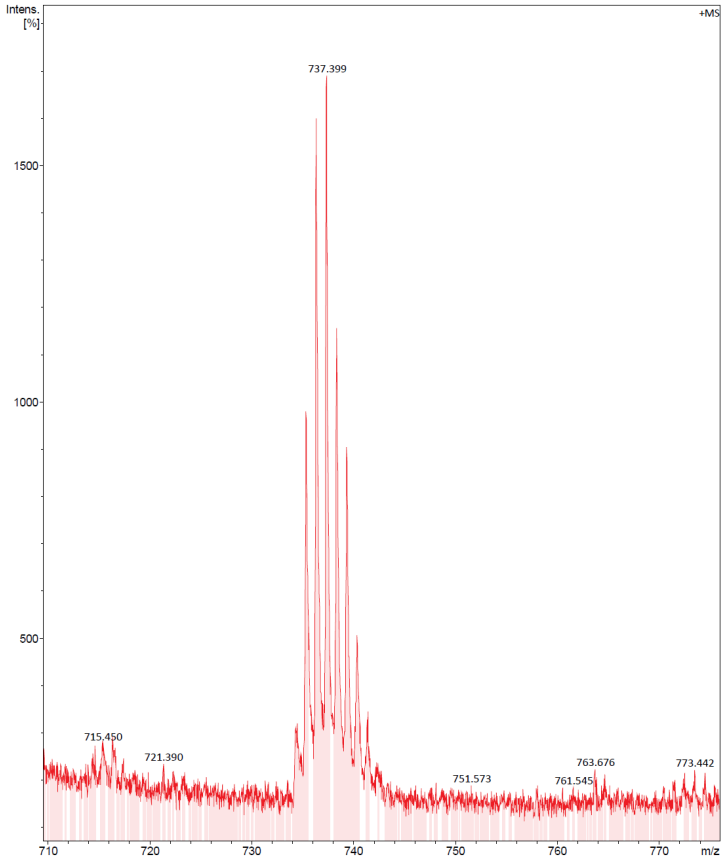

Figure S3.48. MS (MALDI+ DCTB) molecular peak of complex [Pt(CN-*o*-tol)Cl(PPh_3)] (**35**).

3. Computational details

Density Functional Theory (DFT) calculations were carried out with the Gaussian 16[3] suite of programs, using the BP-86 density functional[4] together with Grimme's D3 dispersion correction.[5] The ECP-60-mwb pseudopotential[6] was used for platinum, the ECP-46-mwb pseudopotential was used for iodine,[6] and the 6-31G(d)[7] basis set was used for all other atoms. Geometry optimizations were performed without any symmetry constraint, either in CH_2Cl_2 or CH_3CN by using the solvation model based on density (SMD)[8] or in the gas phase. Stationary points were characterized by calculating the Hessian matrix analytically to confirm that all species are minima (no imaginary frequencies) or transition states (one single imaginary frequency) on the potential energy surface. Conceptual DFT post analysis was performed from the optimized geometry obtained from Gaussian 16, using the Multiwfn package.[9] Atomic coordinates (x, y, z) for the optimized structures are included in a separate file (***DFT-chapter3.xyz***).

4. References

(1) CrysAlis Pro 1.171.39.44a, Rigaku Oxford Diffraction **2018**.

(2) Sheldrick, G. M. *Acta Crystallogr.* **2015**, *A71*, 3-8.

(3) Frisch, M. J.; Trucks, G.W.; Schlegel, H. B.; Scuseria, G. E.; Robb, M. A.; Cheeseman, J. R.; Scalmani, G.; Barone, V.; Petersson, G. A.; Nakatsuji, H.; Li, X.; Caricato, M.; Marenich, A. V.; Bloino, J.; Janesko, B. G.; Gomperts, R.; Mennucci, B.; Hratchian, H. P.; Ortiz, J. V.; Izmaylov, A. F.; Sonnenberg, J. L.; Williams-Young, D.; Ding, F.; Lipparini, F.; Egidi, F.; Goings, J.; Peng, B.; Petrone, A.; Henderson, T.; Ranasinghe, D.; Zakrzewski, V. G.; Gao, J.; Rega, N.; Zheng, G.; Liang, W.; Hada, M.; Ehara, M.; Toyota, K.; Fukuda, R.; Hasegawa, J.; Ishida, M.; Nakajima, T.; Honda, Y.; Kitao, O.; Nakai, H.; Vreven, T.; Throssell, K.; Montgomery Jr., J. A.; Peralta, J. E.; Ogliaro, F.; Bearpark, M. J.; Heyd, J. J.; Brothers, E. N.; Kudin, K. N.; Staroverov, V. N.; Keith, T. A.; Kobayashi, R.; Normand, J.; Raghavachari, K.; Rendell, A. P.; Burant, J. C.; Iyengar, S. S.; Tomasi, J.; Cossi, M.; Millam, J. M.; Klene, M.; Adamo, C.; Cammi, R.; Ochterski, J. W.; Martin, R. L.; Morokuma, K.; Farkas, O.; Foresman, J. B.; Fox, D. J. *Gaussian 16 Rev. C.01*, Wallingford, CT, **2016**.

(4) a) Becke, D. *Phys. Rev. A* **1988**, *38*, 3098-3100 b) Perdew, J. P. *Phys. Rev. B* **1986**, *33*, 8822-8824.

(5) Grimme, S.; Antony, J.; Ehrlich, S.; Krieg, H. *J. Chem. Phys.* **2010**, *132*, 154104.

(6) Andrae, D.; Häußermann, U.; Dolg, M.; Stoll, H.; Preuß, H. *Theor. Chim. Acta* **1990**, *77*, 123−141.

(7) a) Ditchfield, R.; Hehre, W. J.; Pople, J. A. *J. Chem. Phys.* **1971**, *54,* 724-728. b) Hariharan, P. C.; Pople, J. A. *Theor. Chim. Acta* **1973**, *28*, 213-222.

(8) Marenich, A. V.; Cramer, C. J.; Truhlar, D. G. *J. Phys. Chem. B* **2009**, *113*, 6378-6396.

(9) Lu, T.; Chen, F. *J. Comput. Chem*. **2012**, *33*, 580-592.